Final Report on the I-129 Missouri River Bridge Deck Condition Assessment Using Non-Destructive Testing Methods

Bridge No. 9700.0S129, Sioux City, IA

Sponsored by the Iowa Department of Transportation

and

the Federal Highway Administration

Disclamer Notice

The contents of this report reflect the views of the authors, who are responsible for the facts and the accuracy of the information presented herein. The opinions, findings, and conclusions expressed in this publication are those of the authors and not necessarily of the sponsors.

The sponsors assume no liability for the contents or use of the information contained in this document. This report does not constitute a standard, specification, or regulation.

The sponsors do not endorse products or manufacturers. Trademarks or manufacturer's names appear in this report only because they are considered essential to the objectives of the document.

Statement of Non-Discrimination

Federal and state laws prohibit employment and/or public accommodation discrimination on the basis of age, color, creed, disability, gender identity, national origin, pregnancy, race, religion, sex, sexual orientation or veteran's status. If you believe you have been discriminated against, please contact the Iowa Civil Rights Commission at 800-457-4416 or Iowa Department of Transportation's affirmative action officer. If you need accommodations because of a disability to access the Iowa Department of Transportation's services, contact the agency's affirmative action officer at 800-262-0003.

1. Report No. # SPR 90-00-RB20-011	**2. Government Accession No.** Not Required	**3. Recipient Catalog No.** Not Required
4 Title and Subtitle I-129 Missouri River Bridge Deck Condition Assessment Using Non-Destructive Testing Methods. Subtitle not required.		**5 Report Date** November 5, 2012 **6 Performing Organization Code** Optional
7. Author(s) James P. Donnelly, Associate Principal and Project Manager John S. Lawler, Senior Associate Nathaniel S. Rende, Associate III Paul D. Krauss, Principal Jonah C. Kurth, Associate III Remy D. Lequesne, Associate II		**8 Performing Organization Report No.** Optional
9 Performing Organization Name and Address Wiss, Janney, Elstner Associates, Inc. 330 Pfingsten Road Northbrook, IL 60062		**10 Work Unit No. (TRAIS)** Not Required **11 Contract or Grant No.** Not Required
12 Sponsoring Organization Name and Address Iowa Department of Transportation 800 Lincoln Way Ames, IA 50010 and Federal Highway Administration		**13 Type of Report and Period Covered** Final Report **14 Sponsoring Agency Code** IA-DOT
15 Supplementary Notes Optional		

16 Abstract

Field testing using various non-destructive testing (NDT) methods was performed on the reinforced concrete deck of the I-129 Bridge over the Missouri River in Sioux City, Iowa to provide a basis for comparing the NDT techniques and characterizing the current condition of the deck. The NDT techniques employed included visual inspections and sounding, infrared (IR) thermography, ground penetrating radar (GPR), impact echo (IE), and half-cell potential testing. The actual damage in the deck that was used to evaluate the NDT methods was estimated based on the mechanical sounding surveys, with core sampling to confirm these findings. In addition to confirming the NDT testing, core samples were also collected to determine chloride concentrations through the deck thickness. Based on this data and extensive measurements of concrete cover depths obtained using GPR, service life predictions were developed using a statistical model built on a finite difference-based approach for modeling chloride movement through the multi-layer deck of this bridge, which included a low-slump concrete overlay.

Delaminations and spalls were observed in 1 to 2 percent of the deck top surface area; this damage was concentrated around transverse cracks and was typically caused by chloride-induced corrosion of the reinforcing steel. The low-slump overlay has effectively protected the reinforcing steel in the deck from chloride infiltration away from cracks, and service life analysis suggests that the service life extension provided by the highly impermeable low-slump concrete may be as high as 80 years when compared to typical bridge deck concrete alone. Repairs for this deck should focus on preventing further chloride ingress at cracked regions and on repairing existing damage.

None of the survey techniques employed was wholly accurate. Aside from visual and sounding techniques, the two most accurate techniques, as applied to this bridge, were IE and IR thermography. IE testing was sensitive to misidentifying delaminations, in part due to the epoxy injection work performed previously on this bridge deck. IR thermography is inherently dependent on conducive weather, but was also adversely affected by epoxy residue on the deck top surface.

17 Key Words Non-Destructive Testing Concrete Bridge Deck		**18 Distribution Statement** No restrictions. This document is available to the public through the National Technical Information Service, Springfield, Virginia 22161	
19 Security Classification (of this report) Unclassified	**20 Security Classification (of this page)** Unclassified	**21 No. of pages** Optional	**22 Price** Not Required

Form DOT F 1700.7 (8-72)

Final Report
I-129 Missouri River Bridge
Deck Condition Assessment Using Non-Destructive Testing Methods
Bridge No. 9700.0S129, Sioux City, IA

November 5, 2012

James P. Donnelly
Associate Principal and Project Manager

John S. Lawler
Senior Associate

Nathaniel S. Rende
Associate III

Paul D. Krauss
Principal

Jonah C. Kurth
Associate III

Remy D. Lequesne
Associate II

Wiss, Janney, Elstner Associates, Inc.
330 Pfingsten Road
Northbrook, IL 60062
Tel: 847.272.7400
Fax: 847.291.9599
e-mail: jdonnelly@wje.com
jlawler@wje.com
nrende@wje.com
jkurth@wje.com

Sponsored by the Iowa Department of Transportation
and
the Federal Highway Administration

WJE ENGINEERS ARCHITECTS MATERIALS SCIENTISTS

TABLE OF CONTENTS

WJE ENGINEERS ARCHITECTS MATERIALS SCIENTISTS

I-129 MISSOURI RIVER BRIDGE
Deck Condition Assessment Using Non-Destructive Testing Methods

Bridge No. 9700.0S129, Sioux City, IA

0.0 EXECUTIVE SUMMARY

Field testing using various NDT methods was performed to evaluate the condition of the reinforced concrete bridge deck of the I-129 Bridge over the Missouri River in Sioux City, Iowa. This bridge deck, constructed in 1976 and consisting of an 8 in. deck with conventional uncoated reinforcing bars and a low-slump concrete overlay, is in very good condition for its age overall, although several conventional patch repairs and multiple epoxy injection repairs have been performed in the past. The NDT techniques employed to evaluate this bridge deck included visual inspections and sounding, infrared (IR) thermography, ground penetrating radar (GPR), impact echo (IE), and half-cell potential testing. To gain further understanding of the capabilities and effectiveness of non-destructive testing (NDT) for assessing bridge decks, each of these techniques was evaluated for ease of use, speed of data collection, and accuracy. Additionally, the current condition and possible future performance of this concrete bridge deck was characterized to aid in planning for future maintenance and rehabilitation activities.

The field testing began with an overall survey of one traffic lane (right lane) and the associated shoulder for nearly the entire length of both the eastbound and westbound lanes using conventional visual and sounding survey methods. In addition to providing a more complete characterization of the condition of the full bridge deck, the findings of this overall survey were used as the basis for selecting six in-depth study areas where the NDT methods were evaluated. Each in-depth study area was 200-ft long and 18- to 22-ft wide, and was located where significant deterioration was present.

At the in-depth study areas, the best estimate of actual damage was determined based on detailed sounding (chain drag and hammer) surveys conducted twice in each area by different operators, with core sampling to confirm these findings. Then each of the NDT methods was used to determine a separate projection of deck damage. For comparison between techniques, ***maps of delaminations identified by each NDT method and by sounding were superimposed on the plan drawings given as an appendix to this report.*** To provide a quantifiable measure of the accuracy of the survey methods, the maps of the delaminated areas identified by the NDT methods and by sounding were compared, and two metrics were calculated: 1) the amount of overlapping area between the findings of the two methods, interpreted as *correctly* identified delaminated areas; and 2) the amount of area identified by the NDT method that the sounding determined was not delaminated, i.e. not overlapping, interpreted as *incorrectly* identified delaminated areas or "false positives".

In addition to the NDT testing in the in-depth study areas, a half-cell potential survey and GPR-based cover surveys were conducted over the right lane and shoulder of nearly the entire length the bridge in each direction. Additional core sampling intended to determine chloride concentrations through the deck were also collected outside of the study areas. The cores extracted from the bridge deck were analyzed in

the laboratory to determine the chloride ion concentration, carbonation depth, condition of the reinforcing steel, and, by petrographic analysis, the concrete quality. Acid-soluble chloride concentrations up to nearly 7000 ppm were identified near the deck surface, and levels more than sufficient to initiate corrosion were measured at the depths of reinforcing steel in some locations. The carbonation depth was limited to approximate 1/8 in. or less, and while the petrographic analysis found that some aggregate particles susceptible to alkali-silica reaction (ASR) are present in the deck slab concrete, this does not appear to be a major contributor to the existing damage.

Service life predictions were developed using a statistical model built on a finite difference-based approach for modeling chloride movement through the multi-layer deck concrete. This model determines the amount of bridge deck area affected by chloride-initiated corrosion based on the statistical distribution of key parameters considered to govern corrosion initiation, including cover, exposure to chlorides, ability of the concrete to resist chloride ingress, and cracking, across the bridge deck.

The conclusions made about the overall condition of the I-129 bridge deck based on this condition survey are summarized as follows:

- The overall survey of the bridge deck identified damage consisting of delaminations and spalls of 1.1 percent and 2.0 percent of the top deck surface in the areas surveyed in the westbound and eastbound lanes, respectively. Damage on the westbound lanes was concentrated in two spans, while damage in the eastbound lanes was most common in the shoulder of three spans.
- The damage was concentrated around transverse cracks and was typically caused by corrosion of the reinforcing steel as a result of locally elevated chloride concentrations. Away from cracks and delaminations, the chloride content in the deck slab concrete has not reached concentrations where corrosion could be expected at the typical bar depth.
- The low-slump overlay has remained well-bonded to the deck slab, and based on the measured chloride concentrations in the deck slab, has effectively protected the reinforcing steel in the deck from chloride infiltration away from cracks. The median diffusion coefficient of the overlay concrete was approximately 1/15th of that seen by WJE in 2010 in the typical deck concrete of other bridge decks in Iowa. Service life analysis based on these differences suggests that the service life extension provided by the installation of the highly impermeable low-slump concrete may be as high as 80 years when compared to the performance of a deck with similar total cover concrete over the reinforcing steel and with properties assumed to be equal to those of typical Iowa bridge deck slab concrete.
- The service life model developed for this bridge suggests that additional damage away from cracks may not develop until the bridge age reaches 80 years or more. However, delaminations and spalls initiating at cracks may disrupt the cover concrete in adjacent areas of the deck, resulting in corrosion-related deterioration that develops and grows in a self-propagating process well before 80 years.
- Repairs for this deck should focus on preventing further chloride ingress at cracked regions and on repairing existing damage. Existing cracks without detectable damage should be sealed, and areas with existing damage should be repaired using appropriate concrete repair techniques. If repairs to the transverse cracks had been successfully executed soon after the cracks formed, the extent and concentration of the corrosion-related deterioration that currently exists at the cracks most likely would have been significantly reduced, and the service life of the bridge deck at the deck cracks extended close to that predicted for the uncracked areas.

- Replacement of the overlay need not be considered at this time. None of the chloride contents measured in the uncracked deck slab concrete meet the corrosion threshold, even where taken above the reinforcing. Service life modeling of the bridge deck indicates that widespread corrosion-related deterioration in uncracked areas of the bridge deck may not begin to occur until the bridge deck is at least 80 years old. Therefore, the replacement of the existing overlay may be of limited benefit for another 15 to 25 years. Additional chloride content testing should be performed in approximately 10 to 15 years to verify this finding.

The conclusions made about the effectiveness of the NDT approaches evaluated in this study based on the comparison of these methods are summarized as follows:

- The accuracy of the testing methods, assessed by quantitatively comparing the extent and location of areas identified as delaminated by each method relative to sounding and to the findings from the core sampling, varied widely. None of the survey techniques employed, including sounding, was found to be perfectly accurate. Highly sensitive techniques (those most likely to indicate the presence of a delamination with minor indications of damage) were more likely to correctly identify a larger percentage of the areas found to be delaminated by sounding methods, but also were more likely to misidentify large areas as delaminated. This trend is demonstrated by the two most accurate techniques, IE (which demonstrated high sensitivity) and IR thermography (which demonstrated low sensitivity), as applied to this bridge. IE correctly identified 69 percent of the combined delaminated area and misidentified 94 percent, while IR thermography correctly identified 37 percent of the combined delaminated area but misidentified only 42 percent.
- While slow, labor-intensive and highly operator-dependent, visual and sounding techniques were demonstrated to still be highly effective for evaluating this bridge deck. Of all methods, this combination of techniques provides the fullest, most accurate picture of the condition of the bridge deck.
- As implemented for this deck, IE testing was among the most accurate of the methods evaluated, but was sensitive to misidentifying delaminations. Detection of surface delaminations is based on a user-selected threshold applied to the measured signal, and the technique's resolution is equipment-dependent. Improved calibration of thresholds may increase the accuracy of this method. Additionally, the epoxy resin present on many localized areas of this bridge resulted in a significant portion of the mis-identified locations; the accuracy of this method may be greatly improved for bridge decks without this or other material contaminants on its surface.
- IR thermography-based deck surveys can be executed rapidly, but this method is inherently dependent on conducive weather. Features of the I-129 deck, including high (approximately 4-in.) cover, varied deck surface color, and epoxy resin spills, limited the effectiveness of IR thermography in this instance. Despite these drawbacks, IR thermography was still among the most accurate techniques considered in this study. IR thermography may be better suited to decks with lower cover that have not seen extensive previous repairs. Therefore, additional evaluation of this technique in such a setting is recommended.
- GPR does not identify delaminations directly but identifies areas of probable delamination by detecting features associated with corrosion, such as locally elevated moisture content, chloride concentration, and corrosion by-products that affect the reflection of electromagnetic radar pulses from the top mat of the reinforcing bars. This technique was relatively easy to implement; however, the accuracy of this technique for both of the antennas used was poor.

- Half-cell potential testing does not directly identify delaminations, and the areas identified as corroding with this technique far exceeded the actual areas of delamination. However, HCP testing does provide information about the extent of corrosion in the bridge deck and can be used to predict areas of future delamination.

1.0 INTRODUCTION

Many different techniques are available for the evaluation of the condition of bridge decks. The Iowa Department of Transportation requested this study to gain further understanding of the capabilities and effectiveness of various non-destructive testing (NDT) techniques for assessing bridge decks. During this study, field testing of various NDT techniques was performed to evaluate the present condition of the reinforced concrete bridge deck of the I-129 bridge over the Missouri River in Sioux City, Iowa, with the goal of identifying the most effective test methods for acquiring the necessary data to make repair decisions. The various techniques were evaluated for ease of use, speed of data collection, and accuracy. Additionally, the data collected during this study can be used by the Iowa Department of Transportation to characterize the current condition of this concrete bridge deck and as an indication of possible future performance in order to direct maintenance and rehabilitation activities.

1.1 Description of Structure

The bridge deck selected for this study is the I-129 bridge across the Missouri River on the south side of Sioux City, Iowa. This bridge deck is an 8 inch thick reinforced concrete slab with a 2 inch low slump concrete overlay and is typical of a number of other decks constructed in the mid-1970s. The bridge was constructed in 1976 and is reinforced with conventional uncoated reinforcing steel. The overlay was installed in 1976 prior to opening the bridges to traffic. Recent work on this bridge deck includes injecting the deck delaminations with epoxy in 2008, and a survey in 2009 that identified additional delaminations in the concrete deck. It is our understanding that the epoxy injection work performed in 2008 was intended to re-bond areas of delaminated concrete in order to inhibit spalling on the wearing surface. Iowa DOT has indicated that the majority of delaminations addressed during the 2008 epoxy injection work were believed to be at the interface between the overlay concrete and the deck concrete. Therefore, these delaminations were most likely associated with debonding of the overlay, and were not at the level of the reinforcing steel as would be expected for a delamination that formed due to corrosion of the embedded deck reinforcing.

The design drawings for this bridge contain various dates from 1973, and were prepared by Richardson, Gordon and Associates. These drawings indicate that the reinforcing was to be composed of either Grade 40 or Grade 60 ASTM A615 steel, with only Grade 40 bars used where field-bending was to be performed. The bridge deck was to be cast with Standard Iowa DOT Class D concrete, for which the applicable Iowa Standard Specifications required a water-cement ratio of 0.41, a cement content of 7 1/2 sacks per cubic yard, and an entrained air content of 6.0 percent, with the coarse aggregate meeting AASHTO 57 grading requirements, which would correspond to a nominal maximum size of 1 inch. A separate set of design documents was prepared for the installation of the overlay which indicate that the work was to be done following the requirements of the Iowa DOT Supplemental Specifications, and that a typical Iowa low-slump concrete was to be used to cast the overlay. The Iowa DOT supplemental specifications for low-slump concrete overlays in effect at the time of construction required a water-cement ratio of 0.33, an entrained air content of 6.0 percent in the hardened concrete, a cement content of 8-3/4 sacks per cubic yard, and a nominal maximum coarse aggregate size of 1/2 inch.

1.2 Investigation Approach

This bridge deck was surveyed using a combination of soundings, infrared thermographic surveys, ground penetrating radar, visual inspections, impact echo, half cell testing, and deck coring to determine the condition of the bridge deck and to identify areas of deck delamination and debonding. Initially, a significant portion of one lane and the adjacent shoulder from both the eastbound and westbound lanes were surveyed visually and by sounding (chain drag). This initial overall survey was conducted on May 3

and 4, 2011. Based on the findings from this initial survey, three in-depth testing areas were identified in each direction, for a total of six in-depth test areas. Within the in-depth testing areas, various NDT techniques were utilized, and the findings compared. To calibrate and confirm the data gathered, a delamination survey involving chain drag and hammer sounding techniques, along with coring of selected areas of the bridge decks, were performed. The in-depth studies using the NDT techniques and the core sampling was performed during the week of June 20 to 24, 2011.

2.0 VISUAL INSPECTION, MECHANICAL SOUNDING, AND CORE SAMPLING

2.1 Introduction

An overall condition survey of the deck was performed during the initial survey work using conventional visual and mechanical sounding techniques to determine the condition of the accessible portions of the bridge deck. In addition to providing a more complete characterization of the condition of the full bridge deck, the findings of this overall survey were used as the basis for selecting the in-depth study areas evaluated using the NDT techniques identified above. The findings from the visual and mechanical sounding surveys were supplemented by conventional core sampling of the bridge deck performed during the in-depth studies. The details and findings of the conventional surveys and core sampling are presented in this chapter.

2.2 Background

Conventional deck survey techniques include visual inspection, mechanical sounding, and core sampling. Visual inspection relies on the ability of the inspector to discern features significant to the durability of the bridge, but is otherwise self-explanatory. Mechanical sounding is standardized as ASTM D4580-03(2007) *Standard Practice for Measuring Delaminations in Concrete Bridge Decks by Sounding.* Delaminations are detected by the inspector who listens for ringing or hollow sounds while dragging a chain across the surface of the concrete deck. Core sampling provides a means for confirming, at a limited number of discrete locations, the presence of delaminations, and for obtaining samples for later laboratory analysis, including the assessment of bar conditions and chloride contents within the concrete.

2.3 Overall Deck Survey

The overall deck survey consisted of visual inspection, mechanical sounding, and core sampling.

2.3.1 Investigation

A visual examination of one traffic lane (right lane) and the associated shoulder was conducted for the entire length of the eastbound and westbound lanes, with the exception of ramps that remained open during the survey work. The area of the bridge deck that was surveyed is shown in Figure 2.1. In conjunction with the visual survey, a delamination survey was conducted using conventional chain dragging and hammer sounding methods (see Figure 2.2). The location and estimated area or length of observed distress, including delaminations, spalls, cracks, and patches, were documented on plan views of the bridge deck. Typical crack widths were measured, and the crack density (ft/ft^2) was calculated by dividing the total length of the cracks identified by the surface area of the deck area that was surveyed. The quantities and approximate distribution of delaminations and spalls, patches, and cracks identified during this survey, as well as the crack densities and the percentage of the deck surface exhibiting damage calculated from this data, are shown in Tables 2.1 and 2.2 for the westbound and eastbound lanes, respectively.

A total of forty-six 3-3/4-inch diameter core samples were cut from the deck using water-cooled diamond tipped bits, with twenty-five extracted from the westbound lanes and twenty-one taken from the eastbound lanes. A typical view of the coring process is shown in Figure 2.3. The cores were taken from the right shoulder, and from both the right wheel path and the left wheel path of the right travel lane. The cores were taken at both representative locations of the deck, as well as at locations of deterioration. As a result, some cores were taken at delaminations, some were taken at edges of delaminated concrete, and some were taken away from delaminations. Also, some cores were taken at locations of high and low

cover over the reinforcing steel to permit calibration of the GPR equipment. Twenty-four of the cores were taken from areas of the deck that contained cracks or delaminations, and eighteen of the cores included a section of reinforcing steel. The locations of the cores are listed in Table 2.3. Each core hole was patched with a rapid-setting repair material. The laboratory testing program performed with the core samples is discussed in Chapter 8.0.

2.3.2 Findings

The deck exhibited transverse cracking, and delaminations and spalls likely associated with corrosion of the reinforcing steel (see Figure 2.4). In nearly all cases, the delaminations and spalls coincided with deck cracks as shown in Figure 2.4 or with construction joints in the overlay as shown in Figure 2.5. While the delaminations typically were found on both sides of the cracks, some delaminations occur on only one side of the crack, as shown in Figure 2.6. The observed deck cracks typically range in width from 0.010 to 0.030 in., whereas the construction joints in the overlay were generally tighter in width (0.010 in. or less). The observed cracks are likely related to early age shrinkage or thermal contraction of the deck concrete that occurred soon after construction of the deck but prior to casting of the overlay. Where relative movement occurred at such deck cracks after the overlay was cast, those cracks would have reflected through the overlay and been visible during our inspection. However, some of the observed cracking may have been caused by differential shrinkage or thermal contraction between the overlay and deck concrete, in which case they would be limited to the depth of the overlay.

Some of the areas where delaminated concrete was identified may actually be associated with debonding of the overlay from the underlying deck slab concrete. Debonding of the overlay would be more likely to occur adjacent to construction joints in the overlay or at cracks, where the stresses in the bond line due to drying shrinkage of the overlay and thermal changes are increased because of the discontinuity in the overlay concrete. However, such debonding along the construction joints in the overlay was found to be limited in this study, implying that most of the delaminations adjacent to cracks are associated with corrosion of the reinforcing steel at the crack.

Several conventional patch repairs (see Figure 2.7) and the remains of multiple epoxy injection repairs (see Figure 2.8) were visible on the deck surface. It appears that the epoxy injection may have been used to treat cracks as well as to fill delaminations. In some cases, delamination continues to occur around the periphery of numerous delaminations injected previously with epoxy. However, it appears that the epoxy injection was reasonably successful at re-establishing bond at some locations where delaminations were present in 2008, and may also have reduced the quantity of delaminations that progressed to spalls.

Damage was observed immediately adjacent to the modular expansion joint seal systems installed over Pier Nos. 7 and 10, and at the east and west abutments, as shown in Figure 2.9. The delaminations and spalling in these areas may be due to corrosion of the steel joint components, not the reinforcing steel. Similar damage was not observed around the finger joint at Pier 4.

Based on the findings of the visual and sounding surveys, which are summarized in Tables 2.1 and 2.2, the condition of the deck slab varied along the length and between the two sides of the bridge. The corrosion-related damage (areas with delaminations/spalls or patches) on the westbound lanes was generally less severe than on the eastbound lanes. The damage as a percentage of the area surveyed measured 1.1 percent and 2.0 percent in the westbound and eastbound lanes, respectively. Approximately three-fourths of the damage on the westbound lanes was concentrated in two regions of the deck: between Pier Nos. 4 and 5 and between Pier Nos. 6 and 7. In the eastbound lanes, the deterioration was

concentrated in the shoulder, as shown in Figure 2.10. Approximately three-fourths of the damage identified in the eastbound lanes occurs between Pier Nos. 6 and 7 and between Pier Nos. 1 and 3.

Throughout the bridge, the observed cracking was generally oriented transverse to the span direction (typical of early-age thermal and shrinkage cracking), with no longitudinal cracking noted. The calculated crack density (ratio of crack length to area, excluding construction joints) was relatively low for both sides of the bridge, but was lower on the westbound lanes (0.012 ft/ft^2) as compared to the eastbound lanes (0.021 ft/ft^2). It is interesting to note that the relative ratio of calculated crack density and corrosion-related damage is almost identical for the eastbound and westbound lanes, with the westbound lanes having approximately 55% of the cracking and damage of that exhibited by the eastbound lanes.

Detailed information regarding the cores, including the core location and length; the measured overlay thickness; whether cracks, delaminations, or epoxy were present; and the cover and condition of any reinforcing bars sampled; are listed in Table 2.3. Figure 2.11 gives an example of a core taken at a delamination, showing the corrosion of the reinforcing bar in the deck slab.

2.4 In-Depth Study Areas

Based on the overall condition survey, six areas were selected for in-depth study with the various NDT methods mentioned previously, including three such areas each for the westbound and eastbound lanes. These areas were chosen to include larger concentrations of damage, and were intended to provide a basis for evaluating the effectiveness of the NDT approaches.

2.4.1 Investigation

The location and extent of the in-depth study areas are shown in Figure 2.1. The three areas selected on the eastbound lanes were labeled EB-1, EB-2, and EB-3, while those on the westbound side of the bridge were labeled WB-1, WB-2, and WB-3. Each in-depth study area was 200-ft long, and generally varied in width from 18 to 22 ft in order to encompass the right shoulder and the majority of the right traffic (travel) lane. A 2-ft grid was established on the deck surface in each of these areas by spray-painting dots. The study areas of the deck were sounded, and delaminations identified and marked twice by different members of WJE's team, and the grid was used to produce a detailed map of the delaminations, spalls, and existing patches for each area and to provide reference points for the results obtained with the various NDT techniques.

2.4.2 Findings

In general, the in-depth study areas contained all of the various types of distress identified in Section 2.3.2 above. The condition of the deck in each of these in-depth study areas is summarized in Table 2.4, which gives the areas of delaminations and spalls, of patches, and of deck surface covered with epoxy injection resin. In the in-depth study areas, the damage ranged from 0.9 to 6.8 percent of the surveyed area, and the crack density ranged from 0.039 to 0.108 ft/ft^2. The distribution of these features, and the locations of cores, is shown on plan views in Appendix A.

Each approximately 20-ft wide in-depth study area required about 90 minutes to perform a visual survey and a delamination survey once. The duration of the surveys performed by sounding varied depending on deck condition, and was significantly slower if a large number of delaminations requiring delineation were identified.

Twenty-nine cores were taken within the six in-depth study areas, and 17 of these cores were through delaminated concrete. Sounding of the deck correctly identified that a delamination was present at or immediately adjacent to 13 of the 17 delaminated locations (76 percent). Sounding correctly identified sound concrete in all 12 locations where cores were taken through intact concrete, giving sounding a 86 percent accuracy rate where checked with cores.

2.5 Discussion

The conventional survey techniques described in this chapter (visual inspection, chain dragging, and core sampling) have been used for many years for bridge deck evaluation (Manning & Bye, 1983) (New York State Department of Transportation, 1992). Studies have been conducted that suggest there can be large variations in the findings of sounding surveys of deck delaminations depending on the individual teams performing the work (Graybeal, Rolander, Phares, Moore, & Washer, 2001). Delamination surveys can also be sensitive to weather conditions and traffic, since wind and traffic noise can interfere with the ability of the inspector to hear the subtle variations in sound that indicate damage. This ability to hear subtle sound variations will also vary between inspectors. The presence of well-bonded epoxy filled delaminations, as may have been present in the I-129 deck, would be essentially undetectable by sounding, since no hollow sounding vibrations would be produced when the surface is impacted by a hammer or chain. This technique is also sensitive to the depth of the delamination. Shallower damage produces an easily detectable, high frequency sound, but delamination planes deeper than 4 in. below the surface are generally not possible to detect with a chain drag. Sounding with a hammer can detect slightly deeper delaminations, but this technique is not practical for large areas such as a bridge deck. Finally, chain dragging is a labor-intensive process that requires full traffic control.

Despite these potential drawbacks, the sounding surveys performed here were considered an accurate method for identifying the deck delaminations, in part because each of the in-depth study areas was sounded twice, with a different member of WJE's team performing the second sounding survey. Therefore, the findings from the sounding survey were used as the primary basis for comparing the effectiveness of the other techniques evaluated in this study.

3.0 INFRARED THERMOGRAPHY

3.1 Background

Infrared (IR) thermography uses specialized camera equipment to measure the infrared radiation emitted by objects, which can be correlated with the temperature of the object. IR data is commonly presented in the form of thermograms, which are color-coded photographs showing the temperature of the objects within the field of view. The technology behind IR thermography is well established, and the construction industry has made use of infrared technology as a NDT method for identifying variations in structural conditions for at least 20 years. More recently, it has become more common to use IR thermography for identifying delaminations in bridge decks.

IR thermography can be used for quickly evaluating the presence of delaminations on bridge decks (Maser & Roddis, 1990). Delaminations are detectable as temperature differences because the thin layer of concrete above a delamination responds to changing environmental conditions at a different rate than the surrounding concrete. Therefore, delaminated concrete warms more quickly than the surrounding deck when exposed to solar radiation during the day and cools more quickly when exposed to cooling ambient air at night. This is because trapped air in the delamination acts as an insulator preventing heat energy transmission between the delaminated concrete surface and sound underlying concrete.

Application of IR thermography to bridge decks is standardized as ASTM D4788-03(2007) *Standard Test Method for Detecting Delaminations in Bridge Decks Using Infrared Thermography*. If an automated collection system is used, IR thermography allows faster data collection than sounding. Although the quality of data collected can vary widely depending on environmental conditions, IR thermography-based delamination detection is generally less operator-dependent than sounding techniques. This is because IR thermographic data collection is standardized, although the interpretation of the data still relies somewhat on the subjective evaluation of the operator. IR thermography of bridge decks can be challenging, because surface temperature differences between intact and delaminated deck areas are typically small (less than about 5ºF). Other interferences include moisture on the deck, changes in surface color or texture, and shadows on the deck from adjacent structures, barriers, signs, and trees. Additionally, when environmental conditions are relatively stable or do not permit significant differences in thermal conditions to develop, such as on cloudy or windy days, this technique most likely will not be able to identify surface temperature differences representative of delaminations.

3.2 Investigation

The evaluation of IR thermography at the I-129 bridge was conducted in two ways: 1) data was collected at a stationary location in an area including a delamination present at various depths to assess the effects of changing environmental conditions throughout multiple days on the ability of IR thermography to detect this delamination, and 2) a mobile system was used to collect both optical and infrared video of the in-depth study areas. To monitor ambient environmental conditions in order to determine their impact on the thermographic data, a weather station was installed and monitored throughout the field work.

3.2.1 Weather Station

The weather station was installed in the shoulder of the westbound lane near the center of the bridge to monitor local weather conditions (see Figure 3.1). The weather station continuously recorded wind speed, ambient air temperature, solar radiance and relative humidity. The weather station was installed adjacent to a known delamination, and thermocouples were installed in the sound and delaminated concrete at

depths of approximately 0, 0.875, 2.25, and 3.25 in. to measure the temperature of the deck at multiple depths.

3.2.2 Infrared and Optical Video Collection and Analysis

To obtain both infrared and optical video of the deck surface, two cameras were mounted on a rig attached to the rear of a truck, as shown in Figure 3.2. The rig allowed the cameras to be positioned perpendicular to the deck surface to avoid distortion of the images caused by filming the deck surface at an angle and to permit an approximately 10-ft wide field of view. The infrared camera (FLIR SC660) used for capturing the infrared data has a sensitivity of 0.05°F and an accuracy of ±1.8°F. The resolution of the IR camera was 640 x 480 pixels, so one pixel represents approximately 0.2 x 0.2 in. of the deck area. A high-definition webcam was mounted beside the IR camera to collect optical video, which is important for identifying features, such as debris on the deck surface, that produce temperature variations in the IR data unrelated to deck delaminations or distress. Two laptop computers were used to control the instrumentation from the back of the field truck and to synchronously record the thermographic and optical video.

During mobile scanning, it is necessary to associate each infrared and optical scan with the location on the bridge. This was accomplished with an optical encoder fixed to a wheel behind the truck (see Figure 3.2), and by using the 2-ft grid painted on the deck surface in the in-depth study areas. This grid was supplemented with reflective indicators demarcating 10-ft intervals and proved useful for not only measuring position, but also for aligning images of the deck surface.

The optical video scans of the bridge deck documented the visual condition of the deck surface, and the infrared video identified the associated variations in temperature. To present this information in terms of location and size relative to the deck area, each type of video was decomposed into a series of images and assembled into a map of the deck surface.

The infrared videos were filtered using appropriate bounds (the highest and lowest temperature considered) and an appropriate color palette (the array of colors that is used to map the temperature distribution between the bounds). Figure 3.3 shows the same image of the deck surface filtered using a rainbow palette and a sepia palette. In both images, the upper and lower bounds of the filter differ by approximately 18°F (10°C). These images show localized regions that are warmer than the surrounding deck surface, for example the whitish area at the lower left of both images. If the corresponding optical image did not show any corresponding surface anomaly (e.g. discolorations or changes in texture), then it is likely that these “hot spots” indicate sub-surface delaminations of the bridge deck. Figure 3.4 shows the same image, but filtered using the sepia palette with upper and lower bounds that differ by only 7.2°F (4°C). As can be seen in this comparison, delaminations were more easily identified in images processed using the sepia palette and a temperature range of 7.2°F (4°C), so these settings were used for the analysis presented in the remainder of this document. An example of a sequence of IR images filtered in this way is shown in Figure 3.5. This map represents the shoulder and the adjacent traffic lane over approximately 40 ft of bridge deck. Various features, including delaminations, epoxy on the deck surface, wheelpaths, lane markers and variations in deck surface color, can be differentiated in this image.

3.2.3 Tests Performed

3.2.3.1 Interaction of Deck Temperature and Ambient Conditions. Data at the weather station was recorded for the 5-day period during which scans of the bridge surface were performed. Infrared and optical scans of the delamination near the weather station were performed at regular intervals during the

one sunny day of investigation (between 4 pm on Thursday, June 23, and 12 noon on Friday, June 24). The resulting scans were then plotted relative to the ambient air temperature and solar radiance (the intensity of sunlight) measured throughout that time period.

3.2.3.2 Effect of Delamination Depth. To determine the effect that the thickness of concrete above the delamination has on the ability of IR thermography to correctly identify delaminated regions, two regions known to be delaminated were closely investigated. At each of these two locations, multiple holes were drilled through the delamination to determine the distance between the surface and the horizontal crack separating the delamination from the sound concrete below. Multiple IR scans were then performed at each of the delaminated regions at different times of day.

3.2.3.3 Survey of In-depth Study Areas. The six in-depth study areas of the bridge deck identified in Chapter 2.0 and shown in Figure 2.1 were surveyed using both the infrared and optical video equipment. For each in-depth study area, two scans were required to capture the approximate 20-ft width. To perform a survey of a test area, the survey truck was driven slowly (approximately 5 mph) from one end of the study area to the other, then reversed and the process repeated over the other half of the study area. Multiple scans were performed for each study area at different times of day and in different weather conditions. This data was then processed to generate a detailed map identifying areas with patches, surface discolorations, and suspected delaminations.

3.3 Findings

3.3.1 Interaction of Deck Temperature and Ambient Conditions

3.3.1.1 Results. The weather data (ambient air temperature, relative humidity, solar radiance, and wind speed) recorded for the period of June 20-24, 2011 are plotted in Figure 3.6. The temperatures ranged between approximately 60°F at night and 65 to 85°F in the day. The high humidity recorded throughout the week is a result of the rain that occurred June 20 to 22. The recorded solar radiance indicates that bright sunlight was only recorded early in the afternoon on June 20, briefly on June 21, and then steadily throughout June 23 and 24. Wind speeds generally varied between 6-12 mph, and did not exceed the 30 mph limit given in ASTM D4788 at any time during this period**.**

The temperatures measured at depths of 0, 0.875, 2.25, and 3.25 in. in the sound and delaminated concrete regions adjacent to the weather station are shown in Figure 3.7. In this location, the horizontal crack causing the delamination occurred at approximately 1 in. from the deck surface. In general, the temperatures of the sound and delaminated regions follow similar trends. The temperature of the concrete at and near the surface varies more greatly and changes more quickly than the temperatures deeper in the concrete deck. One notable difference between the distribution of temperatures in the sound and delaminated concrete regions are the temperatures measured at a depth of 0.875 in. For the sound concrete, the temperature at 0.875 in. is midway between the temperatures at the surface and at 2.25 in., whereas in the delaminated region, the temperature at 0.875 in. is generally similar to the temperature at the surface. This difference is a result of the horizontal separation (delamination) 1 in. below the deck surface.

The variations in temperature resulting from the delamination are further illustrated in Figure 3.8, which shows the difference between the temperatures measured at all depths and the temperature of the sound concrete at a depth of 3.25 in. for both the delaminated and sound concrete. When plotted this way, it is clear that the differences between the temperatures at 0.875 in. and 2.25 in. are greater in the delamination

than in the sound concrete, because the delamination separates the two zones of concrete represented by these measurements. In addition, the difference between the internal temperatures in the bulk of the deck (at depths of 2.25 and 3.25 in.) varied less than 5°F throughout the 5-day period in both the sound and delaminated regions.

These temperatures through the thickness of the deck illustrate the phenomenon that leads to the "hot spots" visible in an infrared thermograph; however, IR scanning for delaminations relies on differences in surface temperature. The temperatures of the surface of the delamination and of the surface of the adjacent sound concrete are plotted in Figure 3.9, along with their difference (where a positive difference indicates the delamination is warmer). With the exception of short periods (less than 1 hr) on two days, the surface temperatures in the delaminated and sound concrete generally do not differ by more than 3°F. Additionally, the temperature differences noted in the evening when the deck is cooling after sunset are 2°F or less. This means that, to be effective at identifying delaminations, the IR system must be sensitive to variations in temperature of this magnitude or smaller. It is likely that deeper delaminations may exhibit even less variation in surface temperature compared to the surrounding concrete, so deeper delaminations may be more difficult to detect, as discussed further in Section 3.3.2.

The influence of the time of day on the effectiveness of IR thermography was also examined over a period of approximately 20 hours of clear, sunny weather during this investigation. The IR thermograph of the delaminated region, captured each hour, is shown in Figure 3.10, along with the ambient air temperature and the measured solar radiance. The temperature measured on the surface of the delamination is indicated on each individual image. In general, the delamination was hotter than the surrounding concrete until around 8 pm when the sun set. At sunset, the delamination and the surrounding concrete had similar temperatures, and the delamination was difficult to discern. After sunset, the delamination again became visible, because it cooled faster than the surrounding concrete. By around 11 pm, the temperature of the delamination and surrounding deck again converged, concealing the delamination. All of the images taken between 9 and 11 am on the following sunny day show the delamination is noticeably warmer than the surrounding concrete and clearly discernible.

3.3.1.2 Discussion. The concept of using surface temperature variations for identifying bridge deck delaminations was proven to be effective through both demonstration using IR thermography and through direct (thermocouple) measurement of the concrete temperatures. It was demonstrated that IR thermography is most effective for bridge deck delamination detection in the morning and early afternoon of a sunny day. In the periods when conditions were conducive to IR data collection during this investigation (when rain did not interfere), a delamination that is approximately 1 in. deep could be identified in the afternoon until an hour before sunset as a hot-spot, and for about 2 hours after sunset as a cool-spot on the bridge deck. Measurements of the surface temperature of the 1 in. delamination over a 5-day period indicate that the surface of a 1 in. deep delamination may not differ from the surface of surrounding sound concrete by more than 3°F, except for brief periods of time**.**

This suggests a dry deck surface and sunny/partly sunny weather is required for infrared thermography to be effective. The presence of solar radiation (sun) is required to drive the differential heating of the deck surface that leads to identifiable delaminations. Moisture on the deck surface will mask delaminations, and moisture within the delaminations may cause cooling of the area, leading to delaminated areas appearing cooler than the surrounding deck.

3.3.2 Effect of Delamination Depth

3.3.2.1 Results. The results of the study of delamination depth performed on a delamination on the westbound side of the bridge are shown in Figure 3.11. The top image shows the delamination and the surrounding concrete with the depth of the delamination (as determined by drilling) noted. The depth of the delamination varied from approximately 4 in. near the crack to 0.5 in. at the edge of the delamination. There is dark discoloration on the surface of the concrete caused by epoxy residue also visible in the upper portion of this photo. The middle image, which shows an IR thermograph of this region taken at 9:30 am, shows the thin parts of the delamination and the dark epoxy as bright hot-spots. The part of the delamination that is approximately 2 in. or deeper is noticeably cooler than the rest of the deck. It is possible that water has entered through the crack and infiltrated below the delamination and is acting to keep this region cool while the surrounding deck is warmed by the sun. A second scan at 10:30 am, shown at the bottom of Figure 3.11, shows that the deeper portion of the delamination has warmed and is similar in temperature to the surrounding deck, making the infrared image only effective at identifying the darker epoxy patch at the top of the image and the portion of the delamination that is less than about 1.5 in. deep.

A similar inability to identify deeper damage was observed at a delamination located on the eastbound side of the bridge, shown in Figure 3.12. Regardless of the time of day the scan was performed, the only identifiable portion of the delamination is the region that was measured to be approximately 1 in. deep. The temperature changes associated with the delaminated areas that are 2.75 and 3 in. deep, if measureable, are obscured by other variations in the temperature of the bridge deck.

3.3.2.2 Discussion. The clearly discernible hot-spot associated with portions of both delaminations (with depths less than 1.5 in.) confirm the effectiveness of this method for identifying shallow delaminations. However, the dim appearance of the portions of the delaminations deeper than approximately 1.5 in. suggests that this method may not be effective for systematically identifying delaminations deeper than about 1.5 in. Bridge decks with top reinforcement closer to the surface than I-129 bridge will tend to produce shallower delaminations and may be more suited for analysis using infrared thermography.

These thermographic images also show that other factors, beyond the presence of delaminations, can influence surface temperature. The middle portion of the delamination in Figure 3.11 shows up cooler than the surrounding deck, even though, as a delamination, it might be expected to be warmer. Water could be present inside the delamination, a condition that could be present with some regularity on bridge decks, which may explain the slower warming of the surface. When examining infrared scans of bridge decks, both hot- and cold-spots may indicate potentially delaminated regions, so both were used throughout this study to identify delaminations.

Further, IR thermography will not be able to identify delaminations below regions whose surface temperature is dominated by surface variations. The dark epoxy discoloration in Figure 3.12 is the warmest region of the image, which illustrates the obstructive effect that surface discolorations may have on this method. Variations in texture and seemingly minor variations in color, such as differences between wheelpaths in the traffic lanes, where the concrete surface has been abraded so that the white limestone aggregate is exposed, and the darker surrounding concrete (see Figure 3.13) can influence deck temperatures measured by the IR system. This effect is clearly visible in the thermographs shown in Figure 3.5. These examples demonstrate the importance of obtaining optical video in parallel with the IR data, so that surface features can be identified and their influence evaluated.

3.3.3 Survey of Test Areas

3.3.3.1 Results. Mosaics of the bridge deck were created from the optical and IR video collected in each of the in-depth study areas, and each mosaic was analyzed. Visible surface discolorations, including paint, debris, and epoxy on the surface, shadows, and patch repairs, were identified in the optical maps and used to develop a plan of these features that was superimposed on the IR maps. The resulting maps were then examined, and hot- and cold-spots were identified as possible concrete delaminations. To evaluate the accuracy of IR thermography, the resulting maps of identified delaminations were superimposed on a map showing the location and extent of features identified during the visual and sounding surveys. Plan views showing this information for each in-depth study area are given in Appendix B.

Examination of these plan drawings shows that there was generally a reasonably good coincidence between delaminations identified with sounding and IR thermography techniques. Deterioration was identified by IR thermography in approximately the same location as the majority of larger delaminations found by sounding, but the IR thermography typically identified only a portion of the region otherwise determined to be delaminated. In some cases, especially for study areas where a large amount of damage was present, such as EB-1 and WB-2, delaminations identified by sounding under or in close proximity to epoxy on the surface were not identified by IR thermography. As discussed in Section 2.4.2, 29 cores were taken within the six in-depth study areas, and 13 of these cores were through delaminated concrete. IR thermography correctly identified that a delamination was present at 6 of the 13 delaminated locations (46 percent). IR thermography correctly identified sound concrete in 15 of 16 locations (94 percent) where cores were taken through undelaminated concrete. Therefore, the findings from the IR thermography were confirmed by coring at 72 percent of the core locations.

The location of the epoxy on the deck surface was accurately mapped with the optical video captured as part of the IR thermography effort. By comparison, mapping the many isolated spots of epoxy on the deck surface during the visual survey was not practical due to the amount of field time required.

The surface areas of deck where deterioration was identified by the IR surveys are summarized in Table 3.1. Each row of this table represents one of the six in-depth study areas shown in Figure 2.1, with the analysis of WB-2 repeated at 11 pm to evaluate a scan performed at night. For each in-depth study area, the total area of delaminations, patches, and surface discolorations identified by analysis of the optical and infrared maps are shown. Actual areas of delamination and epoxy injection repairs identified by the visual/sounding survey are also given for each area for comparison.

To quantify the accuracy of the survey methods, maps of the delaminated areas identified by the NDT methods and by sounding were compared and two metrics were calculated: 1) the amount of overlapping area between the findings of the two methods, interpreted as *correctly* identified delaminated areas; and 2) the amount of area identified by the NDT method that the sounding determined was not delaminated, i.e. not overlapping, interpreted as *incorrectly* identified delaminated areas or "false positives". The process by which these areas were determined is illustrated in Figure 3.14, which first shows images of the area identified as delaminated by sounding alone and by IR thermography alone. Below this, an image of the area identified as delaminated by both methods (the overlapped areas) is shown. At the bottom of Figure 3.14 is an image of the area identified as delaminated by IR thermography but not by sounding (the not overlapped areas or "false positives").

The area of overlapped and not overlapped areas for IR thermography are given in Table 3.2 as a percentage of the total area surveyed and as a percentage of the area identified as delaminated by sounding. IR thermography, based on the averages, correctly identified 37 percent of the delaminated area in each in-depth study area and incorrectly identified as delaminated an area equal to 42 percent of the area identified as delaminated by sounding. The rate of identification of false positives ranged between 5 and 138 percent, and is an area of concern for this method. Although IR thermography identified a total delaminated area that was somewhat similar to the total area identified by deck sounding, the actual locations of delaminations did not necessarily coincide with the true areas of delamination.

Each approximately 20-ft wide in-depth study area was surveyed in two passes, each of which took about 2 minutes. Surveying an entire in-depth study area, including reversing the truck and restarting data collection, required about 15 minutes. The duration of the survey was consistent regardless of the amount of damage.

3.3.3.2 Discussion. The series of bridge deck scans reported herein provided mixed results with regards to the accuracy of IR thermography for identifying deck deterioration. The optical scans were highly effective at identifying the location and extent of surface discolorations, epoxy, lane markings, patches, and surface damage (such as potholes). The IR scans, however, generally identified a smaller area of delamination than the mechanical sounding, and incorrectly identified as delaminated an area of sound concrete equal to 42 percent of the total delaminated concrete area by combined average.

Some of this inaccuracy is likely due to the depth of the delaminations and the conditions on the surface obscuring the delaminations. Further, more sophisticated data analysis may reduce the inaccuracy somewhat. Infrared thermography as used in this study was shown by the studies of effectiveness versus depth described previously to be unreliable for identifying delaminations deeper than about 1.5 in. Based on the observed delamination depths, and given the overlay construction of this deck and the typically high concrete cover over the reinforcing (averaging 3.97 in. as reported in Section 8.1), it is expected that many potential delaminations occurring in this deck due to conventional corrosion of the top reinforcing mat will be at least at the depth of the reinforcing steel, almost 4 in. As a result, it is quite likely that those delaminations would not be detectable by IR thermography as used in this study.

The accuracy of the identification of delaminations was also somewhat affected by the epoxy injection work performed previously on this deck. Locations where residual epoxy resin was present on the deck top surface tended to show up as the warmest regions of the images produced by IR thermography. Because such locations were discounted during the processing of the data from the IR thermography, those delaminations identified by sounding under or in close proximity to epoxy on the surface would not be identified by IR thermography. No effect of the epoxy was identified in those locations that had been injected but that did not have epoxy on the surface, as there were few such locations.

Small variations in surface temperature at a delamination (on the order of 3°F or less according to the weather station data) are the only indication detectable by IR thermography that damage is present, and similar variations may be measured on the deck surface due to other sources. For example, the wheel paths in each lane stand out because exposed aggregate, worn down by traffic, reflects more solar radiation and is cooler than the less worn portions of roadway. Therefore, inaccurate results obtained using IR thermography may be due to surface conditions including shadows, debris, and surface discolorations that cause variations in deck surface temperature that do not correspond to the subsurface condition of the deck. In and around these areas, variations in temperature due to delaminations are masked and thus are very difficult to identify by IR thermography.

The primary driving force for the detectable temperature differentials that indicate delaminated regions of concrete is exposure to the sun. For a large part of a sunny day, and especially around a peak time late in the morning, delaminations are identifiable as a hot-spot on the deck surface. However, near sunset, most of the deck and the delaminations are approximately the same temperature, rendering IR detection ineffective. IR scans can also be performed in the first few hours after sunset as the delaminated regions cool faster than the surrounding deck; however, evening scans are likely to be less accurate than scans conducted during the day because the temperature differences between sound and delaminated concrete are expected to be less in magnitude and shorter in duration.

As demonstrated during this study, a key advantage of IR thermography is its ability to rapidly test large areas of deck. Performing the scans in these relatively small in-depth study areas was accomplished in minutes, and it would likely be possible to scan the entire deck surface in just a few hours of actual time on the deck.

3.4 Discussion

In general, it was shown that infrared scanning may be an effective method for quickly scanning bridge decks to estimate the total area and location of delaminated concrete, provided the weather is conducive and that the delaminations are not deep. The accuracy of the method was shown to be negatively impacted by cloudy, rainy weather and certain deck conditions. Measurements taken at the weather station indicated that the temperature of the surface of delaminations may not differ from the temperature of surrounding concrete by more than 2 to 3°F, which makes identification of delaminations susceptible to minor variations in surface temperature caused by differing surface texture or color. The method will be most useful for bridge decks that have relatively minor surface discolorations or contaminants (e.g. no epoxy injection-related residue), have few shadows projected onto the deck, and have relatively thin cover over the top reinforcement. This smaller distance between top reinforcement and the deck top surface will generally lead to shallower delaminations, which are more reliably identified by IR thermography. Even if conditions are not ideal, IR thermography can be effective for quickly obtaining a general picture of deck conditions. While all work reported here was done with a full lane closure, IR thermography could be conducted using a rolling lane closure, which would provide lower impact on traffic than the other NDT techniques evaluated in this study. If used for comparing the condition of multiple bridge decks, IR thermography will be most accurate when the compared road surfaces have relatively similar conditions.

4.0 GROUND PENETRATING RADAR

4.1 Background

Ground-Penetrating Radar (GPR), also known as pulsed radar, is a geophysical nondestructive testing technique for the evaluation of structural elements and materials. The method involves using electromagnetic waves to assess the internal characteristics of the material. GPR surveys performed on structural concrete elements allow for the detection and location of embedded objects (such as mild steel reinforcement, prestressing/post-tensioning strand, metal and plastic conduit), assessment of member thickness and element geometry, identification of internal conditions (such as poor consolidation and flaws), and assessment of material interfaces (such as a slab to sub-base interface).

The technique involves the use of a high-frequency radar antenna that transmits electromagnetic radar pulses along a discrete longitudinal scan at the surface of a structural element or geological material. Electromagnetic signals are reflected from material interfaces of differing dielectric properties along the propagation path of the waves. Signals are collected by the antennae, amplified, and displayed for subsequent interpretation. GPR antennas with different operating frequencies provide for GPR surveying at various depths into the substrate. Additionally, post-processing software integrating signal filtering and visualization functions allows for subsequent analysis of the GPR scans collected. The principles of GPR and general guidelines for the use of GPR for the evaluation of structural concrete and subsurface assessment are provided in ACI 228.2R *Nondestructive Test Methods for Evaluation of Concrete in Structures* (ACI Committee 228, 1998) and in ASTM D6432 *Standard Guide for Using the Surface Ground Penetrating Radar Method for Subsurface Investigation*.

The use of GPR to evaluate top surface delamination of concrete bridge decks is based on one of two accepted GPR data processing methodologies, both of which rely on the analysis of reflection amplitudes and are presented in ASTM D6087 *Standard Test Method for Evaluating Asphalt-Covered Concrete Bridge Decks Using Ground Penetrating Radar*. The first method, known as the bottom deck reflection attenuation technique, calculates deterioration by evaluating the relative reflection amplitudes from the bottom of the concrete bridge deck. The second method, known as the top reinforcing reflection attenuation technique, calculates deterioration by evaluating the relative reflection amplitudes from the upper layer of reinforcing steel. GPR signal attenuation in concrete varies with moisture content and chloride concentration, since these material properties affect the dielectric constant and conductivity of the concrete. Because the reflection amplitudes are affected by the presence of moisture and high chloride concentration, which normally accompany reinforcing steel corrosion and delamination, the variations in these amplitudes can be assessed and used as an indicator of corrosion and corrosion-related damage. The principle of measurement is based on comparing relative reflection amplitudes within the deck and applies whether or not an overlay is present.

Work by others (Gucunski, Feldmann, Romero, Kruschwitz, Abu-Hawah, & Dunn, 2009) (Parrillo, Roberts, & Haggan, 2006) (Scott, Rezaizadeh, Santos, Moore, Graybeal, & Washer, 2003) (Romero, Roberts, & Roberts, 2000) has shown that these evaluation approaches, especially the top reinforcing reflection attenuation technique, can provide a reliable estimate of the percentage of a bridge deck that is delaminated, depending on the type of GPR system and antenna used, specific data collection parameters, and the selection of appropriate amplitude thresholds.

Air-coupled (horn) antennas, which can be mounted above the deck or pavement, can provide for rapid GPR data collection without the need for lane closures; however, air-coupled antennas have been found to provide lower resolution data than surface-coupled antennas and are not readily available in the US for

the frequencies required for accurate assessment. Surface-coupled antennas, which remain in contact with the surface during data collection, have been found to provide adequate signal penetration on both asphalt-overlaid, concrete-overlaid, and non-overlaid bridge decks, and better resolution of top reinforcing layers for delamination assessment. Generally, broadband surface-coupled GPR antennas with center frequencies of 1600 to 3000 MHz have been found to provide adequate signal penetration and optimum resolution for the evaluation of top reinforcing layers. Note that effective application of the top reinforcing reflection attenuation technique requires that the upper-most reinforcing layer be oriented in the transverse direction, that is, perpendicular to the direction of measurement.

To identify areas in which the reflection amplitude from the top reinforcing layer indicates probable delamination, reflection amplitude values are typically plotted as a contour map over the survey area. Since high (more positive) reflection amplitudes are indicative of sound concrete and low (more negative) reflection amplitudes are indicative of features associated with corrosion, amplitude thresholds can be selected and applied to large data sets to identify areas most likely to be delaminated. Areas with reflection amplitudes below the chosen threshold are considered potentially delaminated. A threshold value of -10 dB is recommended by the Federal Highway Administration (Longstreet); however, this threshold value is not normalized to the data set from a specific bridge deck, and has been shown to overestimate the percentage of delaminations in some cases. A more refined approach, outlined in ASTM D6087, identifies probable areas of delamination based on an amplitude threshold set relative to the maximum reflection amplitudes recorded throughout the survey area. For the purpose of this investigation, two amplitude thresholds were used: 1) an upper amplitude threshold 6 dB below the average of the maximum 10 percent of the collected data in each in-depth study area, and 2) a lower amplitude threshold 8 dB below the average of the maximum 10 percent of the collected data in each in-depth study area.

4.2 Investigation

4.2.1 Survey of Test Areas

To assess the effectiveness of GPR at detecting concrete deck delaminations using the top reinforcing reflection attenuation technique with a surface-contact antenna, detailed surveys of the six in-depth study regions, where delaminated areas were known to exist, were performed.

For this investigation, a Sir-3000 GPR control unit manufactured by Geophysical Survey Systems, Inc. (GSSI) was used in combination with two broadband surface-coupled antennas: a 1.6 GHz center-frequency antenna with a signal penetration depth of approximately 12 to 15 in., and a 2.6 GHz center-frequency antenna with a signal penetration depth of approximately 8 to 10 in. Each antenna was mounted in a four-wheeled data collection cart with an integrated distance encoder. Data was collected using an antenna transmission rate of 100 kHz, a sample rate of 512 samples per scan, and a scan resolution of 24 to 32 scans per foot. All data post-processing was completed using software developed by GSSI, commercially known as Radan.

For each in-depth study area, GPR scans were collected longitudinally (parallel to the lanes) at an approximate spacing of 1 ft on center, with individual scans alternating in direction. Data collection in each in-depth study area was completed in roughly 30 minutes. This process, shown in Figure 4.1, was repeated using each of the two antennas. To provide for accurate depth assessment of the top reinforcing bars, three calibration drill locations were selected at reinforcing bars in each in-depth study area. The depths of these reinforcing bars were measured directly and used to determine an average GPR wavespeed within each in-depth study area.

4.2.2 Data Processing and Plotting

All raw GPR data was initially reviewed, uploaded, and retained. A sample of the raw data collected with the 1.6 GHz antenna within Study Area WB-2 is provided in Figure 4.2. A similar sample of the raw data collected with the 2.6 GHz antenna is provided in Figure 4.3. In these images, each bar is resolved as a hyperbolic trace, the top of which coincides with the location of the bar. While the top reinforcing layer of the deck is identifiable in the image generated from data collected using either antenna, the 2.6 GHz antenna provides slightly better resolution. Initial review of the raw data files also indicated that delaminated areas as identified by sounding affected signal resolution and reflection amplitude from the top reinforcing area, as indicated by areas of less sharply defined and darker bar traces in Figure 4.2 and Figure 4.3.

To assess reinforcing spacing and depth and to extract the reflection amplitude from the top reinforcing layer for delamination assessment, additional data analysis was performed using the Radan data processing software. For each of the in-depth study areas, the individual GPR scans collected with each antenna were combined based on the scan locations to create two-dimensional representations of the collected data within the in-depth study area. Data post-processing of the combined file consisted of vertical position adjustment, signal filtering using vertical and horizontal Finite Impulse Response (FIR) filters, signal gain adjustment, and two-dimensional velocity migration. The peak positive reflection from each individual reinforcing bar was identified using a semi-automated reflection selection tool within the Bridge Assessment Module that is a part of the Radan software. An example of processed data collected with the 1.6 GHz and 2.6 GHz antennas within Study Area WB-2 is provided in Figure 4.4 and Figure 4.5, respectively. The x- and y- coordinates (ft), reflection time (ns), approximate depth (in.), and amplitude (normalized dB), for each identified reinforcing bar within the post-processed data files was determined.

Detailed contour maps identifying areas with low amplitude reflections from the top reinforcing layer were generated. Per the recommendation of ASTM D6087, reflection amplitude thresholds of 6 dB (upper threshold) and 8 dB (lower threshold) below the average of the maximum 10 percent of the collected data in each in-depth study area were also established and used to identify regions within the contour map where the measured amplitude was indicative of damage in the deck. Note that the lower threshold is more selective than the upper threshold and will result in smaller areas of the deck being judged to be potentially delaminated. The resulting maps were then compared to field survey maps of the bridge deck generated by traditional sounding of the deck to provide a measure of the effectiveness of surface-coupled GPR at identifying delaminated regions.

4.3 Findings

4.3.1 GPR Testing Results

The results of the GPR assessment using the 1.6 GHz antenna and 2.6 GHz antennas are summarized in Table 4.1. For each detailed study area, Table 4.1 provides the average cover and standard deviation of the top transverse reinforcing bars, the upper and lower delamination threshold amplitudes, and the percentage of the data points that indicate probable delamination based on the reflection amplitude thresholds. Reinforcing depth data is based on the average GPR wavespeed determined at the locations within each in-depth study area where bars were exposed by drilling. As shown in the tabular summary of the GPR data collected with each antenna, the average transverse reinforcing cover ranged from 3.5 in. to 4.4 in., which includes the current thickness of the concrete overlay and the original concrete cover

provided in the structural deck slab. The standard deviation of cover measured $^{1}/_{4}$ to $^{3}/_{8}$ in., indicating relatively uniform top transverse bar placement within the deck at each in-depth study area.

Due to differences in initial signal amplitude and signal attenuation with each antenna, the average of the top 10 percent of reflection amplitudes, and therefore the calculated upper and lower amplitude thresholds, were slightly greater using the 1.6 GHz antenna. The variation in the average of the top 10 percent of reflection amplitudes observed between in-depth study areas is likely due to minor differences in moisture and the conductivity of the concrete deck and overlay at each in-depth study area. Variations in reflection amplitude between the areas surveyed did not appear to correlate closely with average reinforcing cover, indicating that variations in the depth of the transverse reinforcing bars did not have a significant effect on reflection amplitude for the conditions present.

In order to further evaluate the data from the GPR testing, contour plots of the reflection amplitude from the top reinforcing bars were compiled and compared for each in-depth study area. A sample of the contour plots for portions of selected in-depth study areas for each antenna are shown in Figure 4.6. The contour scales for these plots were designed to highlight in red to yellow the areas with reflection amplitudes below the delamination thresholds, which are based on the maximum reflection amplitudes measured with each antenna. Therefore, the contour scales differ slightly between the 1.6 GHz and the 2.6 GHz data.

The contour plots indicated areas of reduced amplitude located generally along the edge of the bridge deck near the shoulder barrier (at the bottom of the plot for each in-depth study area) and which extended in thin strips toward the center of the bridge as shown in Figure 4.6. These thin strips of low amplitude reflections generally corresponded to one to four top reinforcing bars (see Figure 4.2 and Figure 4.3) and often coincided with transverse cracking and relatively narrow areas of delamination observed on the top surface of the deck. Large areas of lower amplitude data were generally not observed, suggesting that large areas indicative of planar delamination and deterioration were not present within the areas surveyed. The areas of reduced amplitude located along the edges of the bridge deck that were identified with the 1.6 GHZ antenna (see Figure 4.6a) do not appear to coincide with delaminations identified in the bridge deck by sounding and also were not identified with the 2.6 GHz antenna. As a result, these readings were presumed to be indicative of more moisture and/or chlorides in the deck concrete, and were therefore discounted as areas of actual delamination.

The contour plots for each in-depth study area were then used to develop plan drawings showing areas in which reflection amplitudes were below the lower and upper delamination thresholds. These drawings are provided in Appendix C for each antenna and each in-depth study area, and include a representation of the actual areas of delamination and epoxy injection repairs identified by sounding and visual observations within each area surveyed. A summary of the total areas identified as potentially delaminated based on the upper and lower delamination thresholds using GPR and by traditional visual/sounding techniques is provided in Table 4.2 for the 1.6 GHz and 2.6 GHz antennas.

Comparison of the GPR and sounding findings indicates mixed results regarding the accuracy and effectiveness of the GPR surveys. For a majority of the individual delaminated areas, at least some part of the delamination was identified successfully using GPR with either antenna frequency. GPR, however, typically identified only a small percentage of the delaminated area identified by sounding. In many instances where larger delaminations were present, only thin strips of potential delaminations coinciding with cracking were found using GPR.

In general, the total areas identified as potentially delaminated using the 2.6 GHz antenna were two to three times as large as the areas identified by the 1.6 GHz antenna, regardless of which threshold was used. Additionally, the total areas identified as potentially delaminated based on the upper threshold were two to three times as large as the areas based on the lower threshold.

To further explore the accuracy of the GPR assessment, the areas identified as potentially delaminated by GPR based on the more-inclusive, upper threshold were then compared to the delaminated areas identified by sounding using a procedure similar to that outlined in Section 3.3.3.1. In this procedure, the area of overlap between the delaminated areas identified by both the sounding and GPR surveys is determined, and the delaminated areas identified by GPR that do not overlap with delaminated areas identified by sounding are identified. A schematic of this procedure is shown in Figure 4.7, and the results are summarized in Table 4.3.

GPR conducted with the 1.6 GHz antenna, on averages, correctly identified 20 percent of the delaminated area in each in-depth study area and incorrectly identified as delaminated an area equal to 35 percent of the area identified as delaminated by sounding. GPR conducted with the 2.6 GHz antenna, on average, correctly identified 29 percent of the delaminated area in each in-depth study area but incorrectly identified as delaminated an area equal to 92 percent of the area identified as delaminated by sounding.

No clear difference in response was observed in areas that were previously repaired by epoxy injection compared to unrepaired areas of the deck, indicating that the top reinforcing amplitude assessment method cannot distinguish between the repaired and unrepaired conditions. This may be because conditions affecting the amplitude of reflection from the top reinforcing layer, including corrosion product, loss of steel area, and high chloride content, are not addressed by epoxy injection.

4.4 Discussion

The concept of identifying features in the GPR wave reflections that correspond to delaminations was shown to be valid during this study of the I-129 bridge deck, both through review of individual GPR scans and through contour plotting of full in-depth study areas. However, the effectiveness of using ground-penetrating radar for bridge deck delamination assessment was found to be highly dependent on the GPR antenna used and on the selection of amplitude thresholds during data processing and interpretation. In general, the higher frequency (2.6 GHz) antenna in combination with the upper threshold identified the largest amount of deck area as potentially delaminated.

Comparisons with the results of visual/sounding methods indicate that a majority of existing delaminations were partially identified; however, large delaminated areas were present that the GPR scanning did not identify as potentially delaminated. The areas judged to be potentially delaminated based on the combination of the 2.6 GHz antenna and upper threshold overlapped the largest amount of actual delamination, but also incorrectly identified large areas and the highest overall quantity of sound concrete as potentially delaminated. The errors in identification of potential delaminations may be partially due to the deterioration mechanism of this particular bridge deck, which consists of crack-induced corrosion resulting in narrow, non-planar delaminations. This mechanism affects a limited number of reinforcing bars at or directly adjacent to the original crack. The delamination plane resulting from this damage extends upward from the corroding bar(s) toward the deck surface, passing over but not intersecting adjacent reinforcing bars. As a result, only a portion of the area of deteriorated concrete at any given damage site would be captured using the top reinforcing amplitude assessment technique.

Although performing the scans required access to the bridge deck and setup of a testing grid, continuous scans could be collected fairly quickly in each in-depth study area to provide high resolution data. The method for processing the data can be largely automated, making this method relatively straight-forward to implement.

The following items have been identified as factors that limit the accuracy and feasibility of using ground-penetrating radar for evaluating corrosion-related delaminations in bridge decks.

- The top reinforcing reflection attenuation technique reported herein represents an indirect approach to assessing the presence of delaminations. Damage is assumed to be associated with the presence of moisture and high chloride concentration, which affect signal attenuations and reduces the reflection amplitude from embedded elements and interfaces. The presence of moisture and high chloride concentrations may or may not accompany corrosion of reinforcing steel, cracking or delaminations in concrete. For example, debonding of an unreinforced overlay, as apparently has occurred in small areas of this bridge deck, would not be detected by this technique.
- Natural signal attenuation must be considered when evaluating the reflection amplitudes in bridge decks with large variations in top reinforcing depth. Normalization of amplitude data to depth can typically account for natural signal attenuation and provide more accurate identification of features associated with delaminations, but requires additional analysis.
- The top reinforcing reflection attenuation technique is efficient for decks with topmost reinforcing bars oriented in the transverse direction, allowing for data collection longitudinally along the bridge and eliminating interference of longitudinal bars. The technique may work for longitudinal top bars, but modifications to the testing procedures, e.g. scanning runs oriented transverse to the deck, would be necessary.
- Resolution of the GPR results is dependent on the spacing of top reinforcing bars, since amplitude assessment is performed at each reinforcing bar.
- Depending on the type of repair, the dielectric and conductive properties of existing repairs may differ from those of the original concrete deck and can affect reflection amplitudes and identification of delaminations. However, little effect from the epoxy injection repairs and from the residual epoxy on the surface was observed on the I-129 bridge deck.
- Surface-coupled antennas have been shown to provide more accurate and reliable results than air-coupled antennas; however, surface-coupled antennas require contact with the surface of the bridge deck during data collection. Recent advances in GPR systems and scanning carts designed specifically for bridge deck evaluation have led to improvements in the scanning rates, but GPR data collection using surface-coupled antennas requires lane closures and several hours of setup and data collection on the bridge deck.
- GPR testing is unlikely to identify areas where debonding of the overlay has occurred. Interpretation of GPR scans for bridge deck delamination assessment is based on the analysis of variations in the amplitude of the signal reflection from the top transverse reinforcing bars. Factors that may impact that reflection (moisture, local concrete cracking, corrosion product, section loss of rebar) are generally assumed to be associated with corrosion-related damage, including delaminations. In the absence of moisture or a large air gap, debonding of the concrete overlay may have a slight effect on reflection amplitude from the top reinforcing layer, but this effect would likely be small compared to the effect of corrosion-related delaminations. Therefore,

GPR data, analyzed using the procedure outlined in this report, is unlikely to reveal debonding between the overlay and deck slab.

- GPR testing is also not expected to reveal delaminations in the deck slab that occur beneath the top layer of reinforcing. Because only the signal reflection from the top bars is typically assessed in studies of bridge deck delamination using GPR and in this study, no data from below the top reinforcing bars is even being considered. This is because the signal reflection from bars lower in the deck is often affected by the presence of the top mat of reinforcing, particularly where the top bars are closely-spaced, as is the case in most bridge decks, or are placed in the same vertical plane as the lower bars. This can make it difficult to reliably detect variations in the signal reflections from the lower bars due to the presence of corrosion, and therefore difficult to detect delaminations at that elevation in the deck.

5.0 IMPACT ECHO

5.1 Background

Impact-echo (IE) testing is an ultrasonic non-destructive testing (NDT) technique based on the propagation and reflection of stress waves within an elastic medium. For a concrete bridge deck evaluation, IE testing is performed on the top or bottom surface of the deck to identify the presence of internal concrete flaws, such as planar cracking, delaminations, or debonding of layered and repair systems.

The IE method requires that a short pulse of mechanical energy be imparted to the surface of the deck. The resulting energy pulse travels through the concrete as compressive P-waves, which reflect at flaws and discontinuities due to changes in acoustic impedance and are measured at the surface using a displacement transducer positioned near the impact point. With knowledge of the propagation velocity through the material, the received waveforms can be analyzed to determine the depth to internal flaws or the thickness of the deck. The analysis of reflected waves is typically performed by assessing the amplitude and attenuation of the wave in the time domain. Additionally, dominant reflection frequencies can be identified in a frequency spectral plot obtained by performing a Fast Fourier Transform (FFT) analysis of the received waveforms. If the wave propagation velocity through the material is known, the frequency spectrum plot can be used to identify the depth to internal discontinuities or external boundaries based on Eq. 5.1:

$$T = C_P/2f \qquad \text{Eq. 5.1}$$

where *T* is the thickness of the element (in.), Cp is the compression wave velocity in the medium (in/s), and *f* is the frequency (Hz). For unflawed plate-like structures, such as a non-deteriorated bridge deck, a majority of the compressive waves will reflect from the bottom surface at approximately the same dominant frequency, which can be easily identified on a frequency spectrum plot. Damage in the deck can is indicated by response frequencies either higher or lower than the dominant frequency associated with the deck thickness. A planar delamination below the near surface will result in a higher frequency response coinciding with the depth to the delamination. However, a comparatively thin, near surface delamination will produce a lower frequency modal response, resulting from the excitation of the delamination itself.

A schematic diagram of the test setup is shown in Figure 5.1 along with a frequency spectrum plot representing the data from a typical test. The principles of IE and general guidelines for the use of IE for the evaluation of structural concrete are provided in *Nondestructive Test Methods for Evaluation of Concrete in Structures* (ACI Committee 228, 1998) and in ASTM C1383 *Standard Test Method for Measuring the P-Wave Speed and the Thickness of Concrete Plates Using the Impact-Echo Method*.

Work by others (Gucunski, Slabaugh, Weng, Fang, & Maher, 2008) (Gucunski, Feldmann, Romero, Kruschwitz, Abu-Hawah, & Dunn, 2009) (Sansalone, 1993) (Sansalone & Streett, 1997) (Scott, Rezaizadeh, Santos, Moore, Graybeal, & Washer, 2003) has shown that this evaluation approach can be used to identify bridge deck delaminations at various stages of deterioration if testing and data analysis is performed carefully. Although IE testing is typically performed using a single transducer unit on a discrete testing grid, new advances in equipment and data processing have resulted in the development of impact-echo equipment capable of semi-continuous scanning. Scanning impact-echo, also known as rolling impact-echo, consists of wheel assemblies with multiple, integrated impactors and displacement

transducers, which efficiently collect data by conducting discrete IE tests as the wheel is rolled over the tested surface. Multiple wheels can be used simultaneously to collect data over a distance perpendicular to the direction of scanning. To evaluate the effectiveness of the IE method for identifying delaminations, IE surveys were conducted on the I-129 bridge deck using both a single-transducer IE system and a scanning IE system.

5.2 Investigation

5.2.1 Scanning Impact-Echo

Olson Engineering (Olson), of Wheat Ridge, Colorado was subcontracted to conduct detailed surveys of the bridge using a proprietary two-wheel scanning impact-echo (IE) system. These surveys were performed at the six in-depth study areas of the bridge deck previously discussed. A detailed description of the scanning IE data collection parameters, data-processing procedures, and testing results was provided by Olson in a report entitled *Non-Destructive Bridge Deck Evaluation; Bridge Deck Scanner - Impact Echo Testing of Concrete Deck*, which is included in Appendix H. A summary of the testing is provided below.

5.2.1.1 Testing Procedures. The rolling testing equipment used by Olson, referred to as the Bridge Deck Scanner Impact Echo (BDS IE) system, consisted of two wheels spaced 1 ft apart, each with embedded IE sensors spaced at 6 in. around the circumference of the wheel, as shown in Figure 5.2. For each in-depth study area, individual IE scans were collected longitudinally (parallel to the lanes) at an approximate spacing of 2 ft on center based on a rough testing grid set up within each test area. Starting 1 ft from the barrier wall, data was collected by walking the unit from one end of the in-depth study area to the other end. Each subsequent scan was collected in the opposite direction. As dictated by the wheel and sensor spacing, individual IE tests were collected every 6 in. longitudinally and every 1 ft transversely. Data collection in each in-depth study area was completed in roughly 45 minutes.

5.2.1.2 Data Processing and Plotting. For each IE test, a record of the wave response at the surface, measured by the embedded displacement transducer, was recorded in the time domain. A FFT analysis was performed to obtain the frequency spectrum of the received waveform and to identify the dominant reflection frequencies (or peaks) at each individual test location. The recorded peak frequencies were then used to determine the thickness of the deck or to identify potential delaminations at each testing point.

Results of the scanning IE testing within each of the in-depth study areas were interpreted by Olson and translated onto color-coded maps. An example of one of these maps, taken from Olson's report, is shown in Figure 5.3, which shows the delaminations detected in Study Area EB-1. The plots present the ratio of the resultant thickness measured by IE to the design thickness of the deck (10 in.). Theoretically, a perfectly sound deck would return a ratio of 1.0. However, because variability in the results and the deck can be expected, ratios within 20 percent of 1.0 (between 0.8 and 1.15) were assumed by Olson to indicate a sound deck. Shallow delaminations are typically characterized by a low frequency response because the mechanical energy pulse tends to excite flexural modes of vibration. This produces a resultant thickness ratio greater than 1.0 at shallow delaminations. Resultant ratios of greater than 1.30 were identified by Olson as 'top shallow delaminations' and are shown as red in the color-coded maps. Areas at which the resultant ratio measured 1.15 to 1.30 were identified by Olson as 'incipient delaminations' and were reported to be areas of internal damage or cracking that will likely become a delamination in the future. The incipient delaminations are highlighted in yellow in the color-coded maps. Additionally, areas in which the resultant ratio measured less than 0.80 were identified by Olson as potential areas containing

'bottom delaminations' or 'internal cracking', since these ratios would indicate a reflection from an internal interface located closer to the surface than the deck underside. Bottom delaminations are not detectable using the other NDT methods employed in this study. For the purposes of comparison with other methods, only the areas designated as top shallow delaminations, which are highlighted in red, were considered.

5.2.2 Single-Transducer Impact-Echo

To corroborate the results reported by Olson, WJE performed limited surveys of areas of the deck using single-transducer IE testing equipment. Results of the single-transducer IE testing were intended to provide confirmation of the analysis and interpretation procedures employed by Olson to identify potential delaminations using scanning IE and to provide a qualitative assessment of the accuracy and repeatability of IE surveys with different IE testing equipment.

5.2.2.1 Testing Procedures. WJE selected three test areas within the full in-depth study areas where limited IE testing would be performed using the single-transducer IE unit. The approximate locations and sizes of the test areas are provided in Table 5.1. Each test area consisted of a grid of testing points starting 2 ft from the barrier wall, with IE testing conducted on a point-by-point basis using the 2-ft grid. Figure 5.4 shows the collection of IE data using the single-transducer IE testing unit. Several individual tests were conducted at each test grid location and a representative result was retained for each point.

5.2.2.2 Data Processing and Plotting. Analysis of results of IE testing includes an assessment of both the received waveform, plotted in the time domain, and the frequency spectral plot obtained from the FFT function. An example of an individual IE testing results at a location at which no internal flaws were identified is provided in Figure 5.5. The upper plot in Figure 5.5 shows the time domain for the longitudinal stress wave received by the displacement transducer. The time domain plot, which displays the signal amplitude on the y-axis and time along the x-axis, represents the sinusoidal waveform received after reflection from any internal interfaces, in this case from the bottom of the deck. The lower portion of Figure 5.5 displays the spectral plot, which displays the occurrence of each frequency at which the received waveform occurs. Each dominant frequency peak corresponds to a thickness at which a possible internal interface occurs. At this test location, the only predominant frequency occurs at 6.8 kHz; indicative of the nominal 10.5 in. thick concrete deck. Testing at areas of potentially unsound concrete, internal cracking, or shallow delaminations results in variations in the time signal and frequency spectrum observed. Shallow delaminations, for instance, typically result in erratic, high amplitude time signals and low frequency peaks in the spectral plot. Figure 5.6 shows an IE test result at a shallow delamination. Deeper internal cracks and planar delaminations typically result in irregular, multiple frequency time signals which may identify dominant frequencies coinciding with the approximate flaw depths. Testing results at each test area were analyzed in this manner and were compared with results of the visual/sounding survey and with the scanning IE.

5.3 Findings

5.3.1 Scanning Impact-Echo

To provide a comparison between the results from scanning IE surveys and the other methods included in this study, the delamination maps provided by Olson were further analyzed by WJE. Plan drawings that identify areas in which scanning IE identified shallow delaminations within each in-depth study area are provided in Appendix D. These drawings also include a representation of the actual areas of delamination

and epoxy injection repairs identified by sounding and visual observations within each in-depth study area.

Table 5.2 shows the total area of top shallow delaminations identified through scanning IE surveys, as calculated by WJE, based on maps of the in-depth study areas provided by Olson. For comparison, the total area of delaminated concrete that was identified by WJE using traditional visual inspection and sounding techniques is also given in the table.

The areas identified as top shallow delaminations by scanning IE testing were then compared to the delaminated areas identified by sounding using a procedure similar to that outlined in Section 3.3.3.1. The results are summarized in Table 5.3, which shows the areas of overlap between the delaminated areas identified by sounding and by scanning IE surveys, and the areas identified by scanning IE that do not overlap with areas identified by sounding. A schematic of what these values represent for IE is shown in Figure 5.7.

Scanning IE, based on the weighted averages, correctly identified approximately 69 percent of the delaminated area in the in-depth study areas and incorrectly identified as delaminated an additional area approximately equal to 94 percent of the area identified as delaminated by sounding.

5.3.2 Single-Transducer Impact-Echo

Results of IE testing using the single-transducer unit within the selected test areas identified in Table 5.1 were compared with the plots of shallow delaminations identified using the scanning IE method and conventional sounding. At each discrete testing point, the time and spectral frequency plots were analyzed to identify probable delaminations. Results at each testing point provides the approximate thickness of the deck, the approximate depth to a delamination, if present, or an indication of a shallow delamination, represented by a low frequency dynamic response. To provide a comparison with results of the scanning IE, test locations that are clearly delaminated were identified in plan for each of the selected testing areas.

Results of the single-transducer IE testing were overlaid onto portions of the plan view drawings provided in Appendix D. Testing results at Station 1572 to 1588 within Study Area EB-2 are shown in Figure 5.8. In the figure, areas of shallow delaminations identified by scanning IE are hatched red and discrete test points identified as delaminated by the single-transducer IE testing are shown as dark crosses. In each of the three selected test areas, results of the IE testing using the single-transducer unit correlated well with the areas of shallow delaminations identified with scanning IE.

5.4 Discussion

The concept of identifying internal flaws and planar delaminations using both the single-transducer and the scanning Impact-Echo testing methods was shown to be valid during this study of the I-129 bridge deck. Comparisons of plots of delaminations identified using scanning IE results and visual/sounding methods indicate that a majority of existing delaminations (identified via sounding) were at least partially identified. Quantitative assessment of the IE results indicated that 69 percent of the delaminated area was correctly identified.

Results of the scanning IE assessment also, on average, incorrectly identified areas of sound concrete (not identified as delaminated via sounding) equal to 94 percent of the delaminated concrete area. This error is an indication that Olson's IE surveys may have been overly sensitive to variations in deck properties that did not correspond to deck surface delaminations. For example, some areas of sound concrete (by

sounding survey) incorrectly identified as delaminated by scanning IE corresponds to locations where epoxy residue was present on the deck surface. These comparisons are based on delamination maps produced through the sounding surveys, and it should be recognized that the sounding surveys are potentially influenced by site conditions and human error. However, two of the cores taken in supposedly sound areas of the deck (as determined by sounding) found relatively deep delaminations at 3.7 and 5.0 in. below the deck surface that were in areas indicated as having top shallow delaminations by scanning IE. This indicates that sounding techniques will have difficulty identifying deeper delaminations, whereas impact echo techniques theoretically should be able to identify deeper delaminations with appropriate evaluation of the raw data. Nonetheless, for the purposes of this study, it is assumed that sounding methods provide the most accurate maps of delaminated areas. Likely sources of inaccuracies in the IE results include unanticipated deck properties, measurement variability, effects from epoxy on the deck surface, and assumptions made extrapolating the point-by-point results.

The effectiveness of the IE methods is not limited by the presence of epoxy repairs conducted to bond delaminations to the deck. As discussed, top shallow, i.e., near-surface, delaminations are identified by IE methods as lower frequency flexural vibrations occurring in the delaminated concrete. If the repaired delaminations are well-bonded, such vibrations will not develop. However, if the concrete is delaminated, the presence of residual epoxy on the deck surface will have limited effect on these vibrations. For the I-129 deck, the IE methods were generally capable of differentiating delaminated areas that were successfully repaired from areas that may not have been fully repaired or had subsequently delaminated. However, some locations of sound concrete with residual epoxy on the surface were mis-identified as delaminated.

Limited testing using the single-transducer IE unit confirmed that the testing procedures and fundamental analysis methods used for scanning IE testing and data processing were consistent with more traditional IE testing. Although the use of a single-transducer system provides for more careful data collection and analysis at discrete testing points, data collection using this method is considerably more time consuming. Additionally, testing resolution is limited to the grid spacing during single-transducer testing. Identifying smaller delaminations or accurately defining the extent of larger delaminations is difficult if testing resolution is poor. Scanning IE was shown to provide comparable testing results with better testing resolution and a much faster data collection speed.

Although performing the IE scans required access to the bridge deck and the setup of a testing grid, continuous scans could be collected fairly quickly in each in-depth study area to provide high resolution data. Also, the technique was not sensitive to weather, solar radiation, or moisture on the deck surface. The method for processing the data can be largely automated, making this method relatively straight-forward to implement.

6.0 HALF-CELL POTENTIAL

6.1 Background

Half-cell potential (HCP) testing provides an indication of corrosion risk for reinforcing steel in concrete. Corrosion of reinforcing steel in concrete is caused by the breakdown of a normally passive layer created by the highly alkaline environment of the concrete pore solution. Typically, this breakdown is caused by either chloride ions at the bar level (which act as a catalyst for corrosion) or by a reduction in pH of the concrete pore solution due to carbonation.

In corrosion micro- and macro-cells, the two halves of the corrosion reaction are made of anodic and cathodic reactions (Equation 6.1 and 6.2, respectively). At the anodic reaction, the steel is oxidized, resulting in the generation of electrons and more negative charges; in contrast, electrons are consumed by the cathodic reaction. For the corrosion reactions to occur, the anode and cathode sites must be connected with both an electron path (the reinforcing steel) and an electrolytic path (concrete pore solution). This system is represented by the sketch in Figure 6.1.

$$Fe \rightarrow Fe^{++} + 2e^{-} \qquad \text{Eq. 6.1}$$

$$H_2O + \frac{1}{2}O_2 + 2e^{-} \rightarrow 2OH^{-} \qquad \text{Eq. 6.2}$$

Half-cell potential testing measures relative potential changes on the concrete surface to detect anodic and cathodic regions. The two halves of the reaction generating the potential measured by this testing technique are the reference half-cell (typically a copper rod in saturated copper-sulfate solution) and the reinforcing steel immersed in the concrete pore solution. Similar to the anodic reaction for corrosion, these two halves of the corrosion reaction participate in reversible reactions shown below in Equation 6.3 and 6.4. The two halves of the corrosion reaction are connected by an electron path (through the reinforcing) and an electrolytic path (through the concrete pore solution to a wet sponge on the moist concrete surface). Once connected, the potential difference between them is measured by a digital voltmeter. Figure 6.2 provides a comparison of this testing technique to an equivalent battery cell.

$$Cu \Leftrightarrow Cu^{++} + 2e^{-} \qquad \text{Eq. 6.3}$$

$$Fe \Leftrightarrow Fe^{++} + 2e^{-} \qquad \text{Eq. 6.4}$$

Standard procedures for half-cell potential testing and interpretation are outlined by ASTM C876 *Standard Test Method for Half-Cell Potentials of Uncoated Reinforcing Steel in Concrete,* and the general guidelines for interpretation of the data per ASTM C876 are shown in Table 6.1. However, findings from FHWA RD-86-93, (Pfeifer, Landgren, & Zoob, 1987), showed a bilinear relationship between half-cell potential and corrosion current, where potentials more negative than -250 mV versus a copper-copper sulfate reference electrode (CSE) indicate active corrosion (see Figure 6.3). For the purposes of evaluating the effectiveness of half-cell potentials as an NDT technique for indicating deck damage, a threshold of -250 mV has been used in this study, with the ASTM C876 threshold of -350 mV also provided for comparison.

Due to the nature of the measurements, half-cell potentials do not directly locate spalls, delaminations, repair areas, or other damage sites. However, these regions are often anodic and corroding, and thus coincide with more negative potential readings. Additionally, anodic regions that have not yet caused

delaminations or spalls are also measured by this technique, and thus can be used as a leading indicator of regions likely to become damaged by corrosion in the near future.

6.2 Investigation

Half-cell potential surveys were performed by establishing an electrical connection (ground) to the reinforcement and placing a copper-copper sulfate reference electrode (CSE) on the surface of the concrete. The half-cell potentials between the reinforcement and the CSE were measured using instrumentation with a 10 M-ohm or greater internal impedance. Connections to the reinforcing steel were made by drilling through the concrete to expose individual reinforcing bars. Before commencing half-cell potential measurements, electrical continuity was verified between such connections.

Half-cell potentials were measured on a 20-ft width of the available lane closure for both east- and west-bound lanes. Two different types of equipment were used to take measurements: 1) a rolling cart with five CSEs attached to a datalogger (see Figure 6.4), and 2) a single rolling wheel attached to a datalogger (Proceq Canin+, see Figure 6.5).

The rolling cart was used to measure half-cell potentials for both in-depth study areas and other areas of the lane closure. The electrodes were placed in contact with deck and allowed to equilibrate for approximately 5 seconds before the voltages at each location were logged. For the in-depth study areas, measurements were taken on a 4-ft (transverse) by 2-ft (longitudinal) grid; for other areas, measurements were taken on a 4-ft (transverse) by 2.5-ft (longitudinal) grid.

The single rolling wheel equipment was also used to measure half-cell potentials in Study Area EB-1 for comparison. Multiple grid spacings were used to determine the influence of grid spacing on sensitivity to smaller areas of corrosion activity. The grid spacing longitudinally along the deck ranged from 3 inches to 1 foot, and grid spacing transversely ranged from 1 to 2 feet.

6.3 Findings

For the in-depth study areas, measured half-cell potentials more negative than -250 mV vs. CSE were plotted on contour maps containing the sounding survey results. These contour maps are shown in Appendix E. Only measured potentials more negative than -250 mV vs. CSE, indicative of some risk of corrosion, are shown on the maps. In general, areas with potentials more negative than -250 mV vs. CSE corresponded with delaminated and spalled regions identified by the visual and sounding survey. However, some areas not identified as delaminated are shown with corrosion potentials more negative than -250 mV vs. CSE. Many of these regions correspond with cracks observed in the deck, and may indicate corrosion is occurring that has not yet resulted in detectable damage.

Additionally, the areas of the deck with potentials more negative than -250 mV vs. CSE [moderate probability of corrosion based on the FHWA-RD-86-93 study (Pfeifer, Landgren, & Zoob, 1987)] and more negative than -350 mV vs. CSE (high probability of corrosion based on ASTM C876) were calculated. These areas for each in-depth study area are provided in Table 6.2. The areas more negative than -250 mV vs. CSE ranged from 1.1 to 3.8 times the damaged (spalled and delaminated) areas identified by the visual and sounding surveys. However, the surface areas more negative than -350 mV vs. CSE were much smaller, ranging from 0.1 to 0.7 times the damaged areas identified by the visual and sounding survey. Figure 6.6 shows a plot of the surface areas determined by the half-cell thresholds versus the damaged areas identified by sounding. A strong correlation was identified between the -250 mV vs. CSE threshold and the delaminated areas determined by sounding.

The areas marked by the -250 mV vs. CSE threshold were then compared to the delaminated areas identified by sounding using the procedure similar to that outlined in Section 3.3.3.1, and the results are summarized in Table 6.3. This table shows the area of overlap between the delaminated areas identified by sounding and half-cell potential surveys, and the area identified by half-cell potential surveys that does not overlap with areas identified by sounding. A schematic of what these values represent is shown in Figure 6.7. Based on the weighted average, 44 percent of the delaminated areas were also identified by the -250 mV vs. CSE half-cell potential threshold. However, the additional area identified by the -250 mV vs. CSE threshold that did not overlap with the area identified by sounding was approximately 1.6 times the area identified by sounding.

The two types of half-cell potential testing equipment measured similar values when compared on a point by point basis. However, the contour maps generated by the two data sets differed slightly, as shown in Sheet E.1b of Appendix E. This difference was primarily attributable to the smaller grid spacing used by the rolling wheel equipment. The contour mapping algorithm interpolates between data points; consequently, if small areas with more negative or positive potentials exist between measured grid points, these differences are not resolved in the contour maps.

The effect of this difference in the grid spacing is demonstrated in Figure 6.8. In the figure, half-cell potentials are plotted from 0 to -600 mV vs. CSE for the west end of Study Area EB-1. Core #40 was extracted from a delaminated region in this study area. Because this delamination was relatively large, both the wider grid spacing (4-ft by 2-ft) of the cart and the narrower grid spacing of the rolling wheel (2-ft by 1-ft) identified a region of highly negative corrosion potentials at this delamination. However, Core #43 was extracted from a smaller delaminated region. Only the narrower grid spacing (2-ft by 1-ft) detected more negative corrosion potentials around this location, because the points of the wider spaced grid landed on either side of the delaminated area.

For the cart, each in-depth study area was surveyed in a single pass, which took approximately 30 minutes. Additional time spent locating, drilling, and creating electrical connections to reinforcing totaled approximately 15 minutes per study area, so the total time required to survey one study area was 45 minutes.

6.4 Discussion

The -250 mV threshold appeared to be more appropriate for identifying areas of corrosion activity than the -350 mV threshold on this bridge. In part because the half-cell senses the onset of corrosion, the areas defined by the -250 mV threshold were larger than the surveyed damaged areas. This may be because the bars outside of but immediately adjacent to damaged regions were corroding, but had not yet resulted in damage to the concrete.

The delaminations identified during this study can be attributed to two different mechanisms, delamination within the concrete due to corrosion of the embedded deck reinforcing steel, and debonding of the overlay concrete from the deck concrete. Because a large percentage of delaminations identified by sounding coincided with anodic regions (more negative than -250 mV) identified by the half-cell survey, most of the damage on the deck appears to be corrosion-related. This is further confirmed by the core samples, of which only two exhibit debonding at the overlay/deck concrete interface. The delaminated areas not identified by the -250 mV threshold could have been missed for a few reasons. First, if the delaminated concrete was not in intimate contact with the concrete below and the rust products oxidized,

the electrolytic pathway would have been disrupted and ferrous ions would have been taken out of solution, leading to erroneous half-cell determinations. Second, delaminations not caused by corrosion (i.e. debonding of the overlay only), would not have resulted in more negative half-cell potentials. Third, anodic regions and associated delaminations smaller than the grid spacing used would not have been detected if occurring between grid points.

Half-cell measurements can be limited by adverse field conditions. Extremely dry concrete surfaces add resistance to the electrolytic path between the half-cell and reinforcing, thereby affecting measured values. As a result, dry surfaces may require additional pre-wetting prior to taking readings. Furthermore, standing water on the surface causes "shorts" between grid points. Ideally, moisture conditions for half-cell readings should consist of a saturated-surface-dry concrete surface. Also, half-cell measurements cannot be performed if the electrolytic path between the half-cell and the reinforcing is interrupted. This can be caused by sub-freezing conditions or if electrically insulating materials, such as epoxy on the deck surface or polymeric or bituminous overlays, are present.

Epoxy injected into cracks or delaminations may locally shift potentials slightly in the positive direction. However, provided that an electrical connection to the concrete surface can be made and the affected area is limited in size, it is expected that this type of repair would generally have limited effect on half-cell measurements. While the electrolytic path to portions of individual bars may be broken by the insulating epoxy, some alternate path from the surface to most reinforcing bars is likely present that would still allow the corrosion cell between the reference cell and bar to develop and generate potentials indicative of corrosion, if corrosion was present. In fact, in areas where the deck has delaminated, it is likely that an alternate electrolytic path was already considered for the half-cell measurement.

7.0 COMPARISON OF NDT METHODS

Field testing using visual inspections and sounding, IR thermography, GPR, IE, and half-cell testing was performed to gain further understanding of the capabilities and effectiveness of NDT for assessing the condition of the I-129 bridge deck. In this chapter, the accuracy and speed of data collection for these techniques are compared, and the advantages and limitations of each technique are discussed.

7.1 Accuracy

To quantify the accuracy of the survey methods, the delaminated or potentially delaminated areas identified by each NDT method and by sounding were compared. As discussed in Section 3.3.3.1, the overlap area (interpreted as delaminated areas correctly identified) and the not overlapped area (interpreted as incorrectly identified delaminated areas, i.e. "false positives") were calculated for each NDT technique for all six in-depth study areas. To illustrate the variability in performance of the evaluated NDT methods, Figures 7.1 and 7.2 were prepared to show these results calculated independently for each method and each in-depth study area. To provide a basis for comparing overall performance, the combined overlapped and non-overlapped areas for all six in-depth study areas as a percentage of the combined delaminated areas identified by sounding are given in Table 7.1.

None of the evaluated methods was in close agreement with the results of the deck sounding. While this may be partially influenced by the inaccuracies of sounding and documenting the exact location of each delamination, the sounding surveys were conducted twice by different members of the survey team, and the results of the sounding has been considered the basis for evaluating the other survey methods. In general, highly sensitive NDT methods (those most likely to indicate the presence of a delamination with minor indications of damage) that produced a large percentage of overlap with the actual delamination areas also produced large percentages of not overlapped, i.e. incorrectly identified, areas.

The IR surveys, which correctly identified 37 percent of the delaminations and falsely identified as delaminated an area of sound concrete equal to 42 percent of the delaminated area, showed a reasonable balance of correct and incorrect identification, when compared with the other methods. However, this method may not be well-suited to the conditions embodied in this bridge deck, namely the presence of areas of epoxy on the surface and the concrete cover averaging nearly 4 in. over the bars. IR has the potential to perform better on conventional decks with minimal repairs, a more moderate amount of concrete cover, and under more favorable site conditions.

The GPR survey conducted using the 1.6 GHz antenna correctly identified an area of potentially delaminated concrete that was only approximately 20 percent the actual area of delaminated concrete, with an area of incorrectly identified delaminations equal to 35 percent of the actual delaminated area. Use of the 2.6 GHz antenna modestly improved these results, correctly identifying an area of delaminated concrete of 29 percent of the actual delaminated area. However, the GPR survey using the 2.6 GHz GPR antenna incorrectly identified as delaminated an area of sound concrete equal to 92 percent of the delaminated area. These results indicate that GPR was not highly accurate at identifying delaminated concrete in this deck.

Scanning IE correctly identified an average of 69 percent of the delaminated area, which was the highest percentage of any technique, but also incorrectly identified as delaminated an area of sound concrete equal to 94 percent of the delaminated area. Although this level of accuracy may not be adequate for locating specific repair locations and dimensions, it indicates that IE may be the most accurate of the

methods considered for identifying damage in this bridge deck. The apparent accuracy of this method may be improved by modification of the threshold used for interpreting this data.

The half-cell testing identified approximately 44 percent of the delaminated concrete as potentially corroding. A large area of apparently sound concrete equal to 166 percent of the delaminated concrete area was also classified as potentially corroding. While these results show that this method is not well suited for directly identifying delaminations, it is important to note that this is not the normal objective of half-cell testing. Instead, these results suggest that sizeable areas of reinforcing steel distributed across the deck surface may be corroding, which may lead to future delaminations. Further development of the half-cell method is promising given that threshold values and gradients might be established to identify both delaminated and actively corroding locations, providing additional information compared to the other techniques. It is also the least expensive of the NDT techniques evaluated relative to the chain drag.

7.2 Speed

The amount of time required to collect delamination-related data at one 200 ft by approximately 20 ft in-depth study area using each of the deck assessment methods presented in this report are summarized in Table 7.2. Note that the main focus of this effort was not to maximize efficiency, and possible modifications to the methods that could speed up data collection were not employed here. Additionally, this table does not reflect the time required to process the field data, which can be significant for some of the NDT methods studied. Nevertheless, this table, which reports the duration of methods using the test equipment and parameters (e.g. grid spacing) discussed above, gives some idea about the relative speed of each method. Each of the methods evaluated collected data on the deck much faster than chain drag method, with IR Thermography requiring the least time, although the time to process the field data was higher for each NDT method than for the chain drag method.

7.3 Advantages and Limitations

The following items have been identified as advantages and limitations of the various NDT methods utilized in this study for evaluating bridge decks, excluding comments regarding accuracy, which were provided above.

Summary of Visual/Sounding (Chain Drag) Surveys Advantages and Limitations

Advantages	Limitations
▪ Low equipment cost ▪ Not affected by weather conditions or time of day, except for the case of freezing conditions and snow/ice covering the deck ▪ Accuracy is not affected by repairs, discolorations, or surface variations, because the user can make adjustments based on field observations ▪ Deck features (e.g., repairs, delaminations, cracks, drains) that may be important to future performance of deck can be captured ▪ High resolution	▪ Slowest method ▪ Requires full lane closures ▪ Accuracy is user dependent ▪ Accuracy diminished by ambient noise (e.g., passing traffic, trains, wind) ▪ Time for processing of field data is negligible ▪ Will not identify delaminations very deep in the deck (>4 in.)

Summary of IR Thermography Advantages and Limitations

Advantages	Limitations
▪ Rapid method for surveying large areas of deck. ▪ Testing can be performed with rolling lane closures or possibly at moderate traffic speeds. ▪ Deck features (e.g., repairs, delaminations, cracks, drains) that may be important to future performance of deck can be captured ▪ Less operator dependent than sounding techniques.	▪ Only effective at identifying delaminations that are less than approximately 1.5 in. deep. Deeper delaminations may not be identified by this method unless conditions are optimum. ▪ Conducive (sunny/partly sunny) weather conditions and a dry road surface are required for infrared thermography to be effective. ▪ Testing effective only from mid-morning to mid-afternoon, and shortly after sunset. (Note: night scans are likely to be less accurate than scans conducted during the day.) ▪ Surface discoloration (e.g., epoxy, pooling water, surface abrasion, paint, debris) will result in surface temperatures that do not correspond to the bridge deck conditions, and can mask underlying deterioration. ▪ Condition of existing repairs may not be assessed, since color difference can produce temperature variation. ▪ Specialized equipment required to detect the small temperature difference (2 to 3°F) associated with delaminations. ▪ Evaluation of findings somewhat operator dependent.

Summary of Surface-Coupled Ground-Penetrating Radar (GPR) Advantages and Limitations

Advantages	Limitations
▪ Less operator bias than sounding techniques ▪ Not influenced by surface coloration or lighting conditions ▪ Not affected by time of day ▪ Measurements can be performed through impermeable overlays (polymeric, asphaltic, etc.) ▪ Data collection is relatively fast with equipment specifically developed for bridge deck assessment ▪ May be capable of detecting corroding areas that have not yet caused damage ▪ Reinforcing cover is not an issue	▪ Indirect approach, actually measuring signal attenuation due to moisture, chlorides, and corrosion by-products ▪ Lane closure required for survey ▪ Data collection and results affected by weather conditions - should not be performed if raining, or snow/ice/water/debris present on deck surface ▪ Condition of existing repairs cannot be reliably assessed, since existing conditions affect reflection amplitudes ▪ Data post-processing and analysis is extensive and requires training and experience ▪ GPR scan direction dependent on top reinforcing orientation ▪ Resolution of the GPR results is dependent on the spacing of top reinforcing bars ▪ Significant variations in cover could affect reflection amplitudes, but can be addressed with additional analysis ▪ Different frequency antennas and different amplitude thresholds produce different results ▪ May underestimate the width of delaminated areas due to the inclination of the delamination plane towards the deck surface ▪ Not effective at detecting damage below the top mat of reinforcing or overlay debonding

Summary of Scanning Impact-Echo (IE) Advantages and Limitations

Advantages	Limitations
▪ Less operator bias than sounding techniques ▪ Not influenced by surface coloration or lighting conditions ▪ Not affected by time of day or weather conditions, except for the case of snow/ice covering the deck ▪ Condition of existing repairs can be reliably assessed ▪ Data collection is relatively fast with equipment specifically developed for bridge deck assessment ▪ Results comparable to single-transducer method but with better resolution and much faster data collection ▪ Can identify deeper delaminations than sounding or thermography	▪ Lane closure required for survey ▪ Layer of material on surface, such as epoxy resin, adversely affects measurement accuracy ▪ Not capable of detecting corroding areas that have not yet caused damage ▪ Data post-processing and analysis is extensive and requires training and experience ▪ Scanning IE equipment not commercially available

Summary of Half-Cell Potential Advantages and Limitations

Advantages	Limitations
▪ Capable of detecting corroding areas that have not yet caused damage ▪ Less operator bias than sounding techniques ▪ Not influenced by surface coloration or lighting conditions ▪ Data analysis can be done with simple spreadsheet or plotting programs ▪ Low equipment costs	▪ Lane closure required for survey ▪ Does not detect damage directly, and non-corrosion-related damage (debonding) is not identified ▪ Requires drilling and patching to create connections to embedded reinforcing ▪ Testing cannot be done while raining or in sub-freezing conditions ▪ Measurements cannot be performed through non-conductive (e.g., polymeric, asphaltic) overlays and coatings ▪ Resolution of measurement limited by spacing of discrete test locations ▪ Delaminations not in direct contact with sound concrete below can produce erroneous readings

7.4 Summary of NDT Delamination Study

The accuracy of the NDT approaches evaluated by this study, which was assessed by quantitatively comparing the extent and location of the areas identified as delaminated by each method relative to sounding, varied widely. None of the methods employed, including sounding, were completely accurate at locating delaminations. However, while slow, labor-intensive, and highly operator-dependent, visual and sounding techniques were found to be highly effective for evaluating the condition of this bridge deck. Of all the methods evaluated, this provided the fullest picture of the deck condition. Of the NDT techniques evaluated, the two most accurate techniques were IE and IR thermography.

As implemented for this deck, IE testing was probably the most accurate of the NDT methods evaluated, but was susceptible to misidentifying delaminations. This method detects surface delaminations as low-frequency flexural resonances that are distinguished from signal reflections based on a user-selected threshold. Based on this study, the thickness at which the primary indication of a delamination changes from the low-frequency flexural resonance resulting from a shallow delamination to a reflected signal as in the case of a deeper delamination was not clear. The technique's resolution is limited to the spacing of the discrete measurement points, which is dictated by the equipment. Nevertheless, this technique was among the most robust of those evaluated and was successfully conducted during rainy weather using equipment dedicated for use in bridge decks. Improved calibration of thresholds may increase the accuracy of this method.

IR thermography was found to be a rapid method for identifying delaminations, effective for surveying large deck areas, but is inherently weather-dependent. Features of the I-129 bridge deck, including high concrete (approximately 4-in.) cover, varied deck surface color, and epoxy resin spills, limited the effectiveness of IR thermography in this instance. Despite these drawbacks, IR thermography was still among the most accurate of the techniques considered in this study. IR thermography may be better suited to decks with lower cover that have not seen extensive previous repairs. Therefore, additional evaluation in such a setting is recommended.

GPR does not identify delaminations directly but identifies areas of probable delamination by detecting features associated with corrosion, such as locally elevated moisture contents and chloride concentrations, that affect the reflection of electromagnetic radar pulses from the top mat of reinforcing bars. This technique was relatively easy to implement, and the data reduction was automated. However, the accuracy of this technique for both tested antennas was poor.

Half-cell potential testing does not directly identify delaminations, instead identifying areas of relatively high corrosion potential. The areas identified as corroding with this technique far exceeded the actual areas of delamination. This may indicate that corrosion is likely to occur or may already be occurring at a significant quantity of areas that are not currently delaminated, but nonetheless this technique significantly overestimates the quantity of delaminated concrete. However, HCP testing does provide information about the extent of corrosion in the bridge deck and can be used to predict areas of future delamination. With dedicated equipment, this technique can be executed relatively quickly over large areas.

8.0 OVERALL CONDITION ASSESSMENT OF I-129 BRIDGE DECK

In addition to the evaluation of the NDT Methods described in the preceding chapters, the overall condition of the I-129 bridge deck was assessed. The field investigation included the brief visual survey and the delamination and crack mapping surveys of the entire bridge deck performed during the initial survey, and the sampling of cores for laboratory study, all of which were discussed in Chapter 2.0. The overall deck condition evaluation also included a half-cell potential survey and a cover survey performed for the entire bridge deck. The cores extracted from the bridge deck were analyzed in the laboratory to determine the chloride ion concentration, carbonation depth, condition of the reinforcing steel, and the concrete quality.

8.1 Field Studies

8.1.1 Visual and Delamination Survey

The findings of the visual and delamination survey (by sounding) were summarized in Section 2.3.2.

8.1.2 Cover Survey

GPR was used to locate and determine the concrete cover of the reinforcing bars. Two scans parallel to the deck centerline were taken in both the eastbound and westbound lanes of the deck for the full length of the lane closure, with one scan in the right shoulder and one in the left wheelpath of the travel lane. The depths of the top reinforcing bars indicated by the GPR scans were calibrated to actual depth measurements of the top reinforcing bars taken at core and drill hole locations.

The average and standard deviation of the measured cover for each line of data collection and for all data combined is given in Table 8.1. The cumulative distribution of the individual cover measurements is shown in Figure 8.1. As can be seen from this plot, the cover at the shoulder was somewhat less than the cover at the travel lane examined, especially in the eastbound lanes. This may partially explain the concentration of damage along the shoulders. Additionally, the typical cover in the westbound lanes is slightly greater than in the eastbound lanes.

8.1.3 Half-Cell Potential Survey

Half-cell potentials (HCP) were measured to investigate the corrosion potential of the reinforcing bars for the full length of the bridge deck within the lane closures. This work was performed in accordance with ASTM C876 *Standard Test Methods for Half-Cell Potentials of Uncoated Reinforcing Steel in Concrete*. Further description of this testing method is provided in Chapter 6. This survey was performed using the previously described rolling cart that holds five reference electrodes spaced 4 ft. apart. The rolling cart was advanced in 2.5-ft. intervals and the electrodes were placed in contact with deck and allowed to equilibrate for approximately 5 seconds before the voltages at each location were logged.

Electrical connections to the reinforcing bars were made at approximately 200-ft. intervals. Before commencing HCP measurements, an electrical continuity test was performed within each section of the deck (length of continuous deck between expansion joints) to verify the electrical continuity between electrical connections to the reinforcing steel within the section.

The measured half-cell potentials were tabulated for each 100 ft. of length. These readings are shown in Tables 8.2 and 8.3 for the eastbound and westbound lanes, respectively, summarized by the percentage of readings that were more negative than -200 and -350 mV versus CSE. These are the thresholds defined

by ASTM C876 for moderate and high probability of corrosion, respectively. The percentages summarized by this method differed slightly from the method described previously in Chapter 6 for the in-depth study areas, since a different threshold (-250 mV per FHWA RD-86-93) was used to generate the contour maps and corresponding areas of deck damage stated in Chapter 6. For the eastbound lanes, an average of 16.8 and 2.5 percent of readings were less than -200 and -350 mV versus CSE, respectively. For the westbound lanes, an average of 13.6 and 1.5 percent of readings were less than -200 and -350 mV versus CSE, respectively. This compared to an average of 2.3 and 1.1 percent damaged areas (delaminated and repaired) for the eastbound and westbound lanes, respectively, as measured by the visual and sounding survey.

8.2 Laboratory Studies

All of the cores removed from the bridge decks were transported to WJE's laboratory, photographed, and assessed. Some of the cores contained a segment of a reinforcing bar from the top mat of reinforcing, including a few with both a longitudinal and a transverse reinforcing bar. Each of the bar segments was extracted from the cores and was visually examined for corrosion.

In-depth laboratory analysis of the cores was performed, consisting of petrographic examination, chloride content testing, and carbonation depth measurement of selected cores. Nine cores were selected for carbonation depth measurement, two cores were selected for petrographic examination, and twelve cores were selected for chloride content testing. The methods and results for each of the analyses are described below.

8.2.1 Carbonation Depth

8.2.1.1 Background. Carbonation is a process that lowers the high pH of the concrete paste and disrupts the protective passive layer that inhibits corrosion of reinforcing steel in concrete, allowing corrosion to initiate in the presence of sufficient moisture and oxygen. Carbon dioxide in the air is a primary cause of carbonation as it diffuses slowly into the concrete, mainly through air-filled pores of the cement paste. The progression of carbonation is influenced by moisture and relative humidity (RH), surface finish, cement composition, porosity and density of the concrete, and the availability of carbon dioxide.

8.2.1.2 Methods. The depth of carbonation was tested by applying a phenolphthalein indicator solution onto freshly broken surfaces of the extracted cores. Phenolphthalein solution induces a pink color on the surface of the concrete if the concrete has a pH greater than 9, while a treated area of the concrete that does not undergo a color change has a pH below 9 and is considered carbonated. The distance from the exterior surface of the core to the color change boundary was measured to determine carbonation depth. A representative photograph of a core with phenolphthalein indicator applied to a freshly cracked surface is shown in Figure 8.2. Because the protective passive layer on the reinforcing steel may be disrupted when the pH is 9.5 to 11, carbonation-induced corrosion may initiate at slightly greater depths than the carbonation depth indicated by phenolphthalein testing.

8.2.1.3 Findings. The depth of carbonation was measured in both the overlay and base concrete for the selected cores. The measured carbonation depths for each core are provided in Table 8.4. As shown in the table, the average depth of carbonation was 0.13 inch for the overlay and 0.01 inch for the base concrete.

The measured depth of carbonation in the overlay is relatively minimal, although the amount is not unusual for a high quality concrete of this age and consistency. Additionally, it appears that the overlay has effectively prevented the progression of carbonation in the base concrete.

8.2.2 Petrographic Examination

8.2.2.1 Methods. A petrographic analysis was performed to characterize the overall quality and nature of the concrete, as outlined in ASTM C856-04 *Standard Practice for Petrographic Examination of Hardened Concrete*. The petrographic analysis included microscopic evaluation of the selected core samples to assess the characteristics of the air void system, the cement paste, the soundness of the aggregate, the water-cement ratio, and the depth of carbonation.

8.2.2.2 Findings. Core 6 and Core 42 from the westbound and eastbound lanes, respectively, were selected for petrographic examination.

Core 6 was located on a transverse crack in the bridge deck adjacent to a delamination. Horizontal and vertical cracking was detected in the overlay portion of this core, and vertical cracking was present in the deck slab concrete of Core 6. The cause of the cracking in the overlay was likely the adjacent delamination, which presumably was caused by reinforcing corrosion. The cause of the cracking in the deck slab portion of the same core was likely stresses produced by restrained early age drying shrinkage and thermal contraction. This core also exhibited debonding at the interface between this overlay and the deck structural slab. Only 3 of the 46 cores exhibited debonding at this interface, indicating that in general the overlay is well bonded.

Core 42 was located in a delaminated region. The overlay portion of Core 42 did not exhibit any cracking, but the deck slab concrete exhibited major cracking throughout. Most of these cracks were transverse to the core length but some were also randomly oriented. Two severely corroded bars were observed in the deck slab concrete at the level of the cracks transverse to the core length, and corrosion staining was present on the cracked surfaces and within the surrounding cement paste. The deck slab concrete of Core 42 also contained reactive sandstone coarse aggregate particles that had cracked the surrounding paste, and a large reactive siliceous lump of industrial waste, probably a contaminant, was embedded in the bottom of the core. Abundant alkali-silica reaction (ASR) gel was found on crack surfaces and in air voids of this layer. The cracking within Core 42 was judged to be due to two factors: corrosion of the embedded steel and ASR. Most of the ASR was due to the presence of a reactive contaminant lump, but some was attributed to reactive sandstone particles within the coarse aggregate. It was unknown if the corrosion-related cracking or ASR-related cracking occurred first.

Alkali-silica reactive particles were also detected within fine aggregates in both layers of both cores. These reactive particles were mainly shale particles containing siliceous elements that had reacted with alkalis within the cement paste. Some potentially reactive coal and chert particles were also found in the fine aggregates of the overlay concrete in both cores. Because these particles are all small sizes of fine aggregate, they tend to be too small to exert sufficient pressure on the surrounding paste to cause cracking.

The cement paste was of good quality in all layers of both cores. The water-cement ratios (w/c) were estimated at 0.42±0.05 in the overlay and at 0.42±0.03 in the deck slab concrete. The cement contents were estimated at 6-1/2 ± 1/2 bags per cubic yard of concrete for the overlay and 5 ± 1/2 bags per cubic yard for the deck slab concrete. Pozzolans were not detected in any of the layers. The measured properties

of the overlay do not conform to the specifications, which called for a w/c of 0.33 and a cement content of 8-3/4 bags per cubic yard. The w/c of the deck slab concrete does appear consistent with specification, which called for a w/c of 0.41, but the observed cement content is lower than the specified 710 lbs. per cubic yard (approximately 7-1/2 bags per cubic yard).

Air entrainment was lacking (less than 3.5 percent) in the overlay of Core 42, but was adequate (approximately 5 percent) in the remaining layers of both cores. No evidence of freeze-thaw related damage was found in any of the layers.

The carbonation of the cement paste in the two cores examined petrographically was minimal (3/32 inch maximum) in all layers. This is comparable to the carbonation depths measured on other cores and reported in Table 8.4.

8.2.3 Chloride Content

8.2.3.1 Background. For corrosion to initiate on reinforcing steel that is embedded in sound concrete, chloride ions must accumulate to a sufficient concentration, known as the chloride threshold, to break down the naturally occurring protective film that develops on a steel surface in the highly alkaline environment within concrete. The onset of corrosion is governed by the time required for chloride to penetrate through the concrete cover over the steel and build up at the bar depth to the chloride threshold value. The chloride threshold is dependent on a number of conditions within the concrete, including cement content and chemistry, moisture conditions, and steel chemistry and surface conditions, but can be assumed to be approximately 350 ppm for uncoated bars in uncarbonated concrete (Bentur, Diamond, & Berke, 1997), (Pfeifer, Landgren, & Zoob, 1987).

8.2.3.2 Chloride Content Testing Method. To evaluate the current distribution of chloride ions within the deck and to permit estimates of chloride concentrations in the future, the chloride concentration profiles with depth were determined for twelve cores, including six from each travel direction. The top approximately 1/8-in. of each of the concrete cores was removed before testing, and both the overlay and deck slab portions of the cores were sectioned to obtain samples at various depths below the deck surface. In cores taken away from cracks, four 1/8-in. slices of the full core cross-section were taken from both the overlay concrete and the deck slab concrete for a total of eight slices per core. The slices were centered at approximately the following depths in inches from both the top surface of the overlay and from the bond interface: 3/16, 7/16, 13/16, 1-5/16. For cores taken at cracks that parallel reinforcing bars (as was the case with all cracks), the cores were first cut vertically on either side of the crack to obtain a 3/4-in. wide block extending from the surface of the core to the bar. This block was then cut into 1/2-in. slices to provide sufficient material for testing. The purpose of this modified cutting process was to more accurately represent the chloride concentration to which a bar at a crack will be exposed. All slices were pulverized for acid-soluble chloride content analysis essentially according to ASTM C1152-04 *Standard Test Method for Acid-Soluble Chloride in Mortar and Concrete*.

8.2.3.3 Findings. In this report, chloride concentrations are given in terms of acid-soluble chloride, which represents nearly all chloride contained in the concrete sample, including any chloride chemically bound within the aggregate. The measured chloride contents versus depth are shown in Figure 8.3 through Figure 8.5. The figures show data from cores with sound concrete (uncracked and without delaminations), cores with delaminations, and cores with through-thickness vertical cracks, respectively. The cores contained moderate levels of background chloride (approximately 100 ppm), which is identified by uniform chloride levels over a range of depths beyond where significant surface-applied chlorides would be expected to have penetrated. The laboratory data from the chloride testing is provided in Appendix G.

Where present, background chlorides, i.e. chloride present from when the concrete is batched, are often due to chloride-containing aggregate, or to salts admixed in the deck concrete to accelerate hydration. In a study performed for the Iowa Department of Transportation in 2010 (Donnelly, Krauss, & Lawler, 2011), levels of elevated background chlorides in similar bridges were determined to be from bound chloride in the limestone coarse aggregates. Such chloride is generally unavailable to promote corrosion.

For Cores 9, 12, 28, and 35, the chloride content at typical bar depths (approximately 4 inches) exceeded 350 ppm, the assumed chloride-induced corrosion threshold. These cores were all located at cracked and delaminated areas. Cracks wider than 10 mils bisected Cores 9, 28, and 35, and Core 12 was located only approximately 1 inch from a crack.

For the other cores, chloride contents at typical bar depths did not exceed 350 ppm. Furthermore, measured chloride contents did not exceed 350 ppm at any depth in the deck slab concrete, indicating that chloride penetration into the deck slab concrete was minimal away from cracks.

8.2.4 Discussion

Based on cores from both uncracked and sound regions, the overlay appears to have protected the deck slab from carbonation and nearly all chloride ingress. The average measured depth of carbonation in the deck slab concrete was very small (0.01 inch), and measured chloride contents were less than 350 ppm.

However, the overlay has not prevented chloride ingress into the deck slab concrete in the immediate vicinity of cracks, or in delaminated regions, which generally correspond to locations of deck cracking. Cracks, many of which extend to the reinforcing steel, have allowed chloride to penetrate deep into the deck slab and to collect at elevated levels (greater than 350 ppm at the bar level), sufficient to cause corrosion of reinforcing, providing that sufficient moisture and oxygen is available, which generally is the case at a crack.

Additionally, the petrographic examination identified some ASR-related distress in a core from a delaminated region. Although the ASR-related distress was attributed primarily to a contaminant in the coarse aggregate, some other ASR was detected in the sandstone coarse aggregate and in those fine aggregates consisting of shale, coal, and chert. Damage due to cracking and delaminations likely allowed elevated moisture contents to build up, which accelerated the ASR. In contrast, minimal ASR-related distress was observed in the core from an uncracked, sound region.

8.3 Service Life Modeling

Based on the findings of the field survey and the laboratory analysis, the primary distress-causing mechanism for the I-129 bridge deck is chloride-induced corrosion of the deck reinforcement. As a consequence, the extent of the service life of the deck is expected to be primarily controlled by the time

for corrosion–related damage to develop. To determine the expected remaining service life of the I-129 bridge deck and to study the effect of the existing low-slump overlay on deck service life, a service life model based on corrosion–related deterioration was developed and applied to both the overall bridge deck and to each individual in-depth study area.

As previously discussed in Section 8.2.3.1, for corrosion to initiate in reinforcing steel embedded in sound concrete, chloride ions must accumulate to sufficient concentration, known as a chloride threshold, to break down the naturally-occurring passive film protecting the steel. Although multiple factors (cement content and chemistry, moisture conditions, steel chemistry, etc.) affect the influence of chloride concentration on corrosion, the chloride content at the bar level was assumed to be the primary factor responsible for corrosion initiation in the I-129 bridge deck and that a single, fixed chloride threshold was applied throughout the deck.
The time required for corrosion-related damage to occur at any point on the deck can be conceptually separated into two time periods: the corrosion initiation time (t_i) and the corrosion propagation time (t_p). Figure 8.6 illustrates this corrosion sequence (Tuutti, 1982). The initiation time is the time required for the chloride to penetrate through the concrete and accumulate to a specified chloride threshold concentration. The propagation time is the time during which corrosion products build up to a sufficient volume to create tensile stresses in the surrounding concrete capable of causing cracking or delamination. These two periods were considered individually and then combined to model the time before deterioration at a given location becomes apparent.

The service life of the deck is defined as the time until the amount of damaged area (i.e., the percentage of locations where the sum of corrosion initiation and propagation time has passed) exceeds some level of acceptability. This limit can be based on the maximum amount of damage that may be permitted before structural capacity is diminished, or can be based on concerns regarding serviceability or appearance. Previous research indicates that a limit of 10 to 12 percent is often considered the maximum allowable damaged area for bridge decks before rehabilitation, such as the installation or replacement of an overlay, is performed (Koch et. al, 2002) (Krauss, Lawler, & Steiner, 2009). A threshold of 10 percent was adopted for this study, assuming that at this level of damage, some maintenance action is needed to address the resulting decreases in ride quality, and considering the time necessary to plan, coordinate, and implement a repair program.

8.3.1 Method and Bases for Analysis

8.3.1.1 Description of Probabilistic Model. An established statistical model developed by Sagüés (Sagüés, 2003) was used as the basis for the service life model. This model determines the amount of bridge deck area affected by chloride-initiated corrosion based on the statistical distribution of key parameters considered to govern corrosion initiation. This model also recognizes the fact that corrosion in bridge decks is a local process that develops at multiple locations over time. For this investigation, initiation of corrosion was considered to be governed largely by the following properties:

- prevalence of cracking
- exposure conditions (i.e., severity of deicing salt application)
- ability of the overlay and deck slab concretes to resist chloride ingress
- concrete cover (overlay and deck slab thickness)

- chloride threshold of reinforcing steel in concrete

Corrosion initiation was defined as the time required for chloride content to exceed the corrosion threshold value at a given bar depth. The Sagüés approach considers time-to-corrosion initiation as a probabilistic variable, influenced by the combinations of independent random variables assumed to interact to govern chloride accumulation at the reinforcing, and thus corrosion initiation and subsequent damage. This process can be described mathematically as follows (Bastidas-Arteaga, Chateauneuf, Sanchez-Silva, Bressolette, & Schoefs, 2011).

Corrosion initiation time is governed by a joint probability distribution, which is a function dependent on four deck properties:

$$f(\underline{x}) = f(chloride\ exposure,\ \ concrete\ permeability,\ \ cover,\ \ overlay\ thickness) \quad \text{Eq. 8.1}$$

where $\underline{x}$ represents the vector of random variables, and $f(\underline{x})$ represents a function of their joint probability distribution. Corrosion initiates when chloride concentrations at a particular bar depth and time exceed the chloride-induced corrosion threshold. The initiation time at a given location is then defined by a limit state function:

$$g(\underline{x},t) = C_t - C(\underline{x},t,d), \qquad where \quad \begin{cases} g(\underline{x},t) \le 0, & corrosion\ initiation \\ g(\underline{x},t) > 0, & no\ corrosion \end{cases} \quad \text{Eq. 8.2}$$

where C_t represents the corrosion threshold, and $C(\underline{x},t,d)$ is the chloride concentration where t represents the age of the deck, and d represents the depth of cover. Combining the two statements, the probability that the reinforcing steel at any point in the deck has started to corrode is calculated by integrating over the failure domain:

$$p_f = \int_{g(\underline{x},t)\le 0} f(\underline{x}) d\underline{x} \quad \text{Eq. 8.3}$$

The probability of failure with respect to a single location can then be abstracted to the performance of the deck as a whole. If the deck is of sufficient size for multiple, independent locations of corrosion-related damage to develop, the deck can be discretized into a large number of segments with properties defined by the statistical distributions measured or assumed for the specific deck. The cumulative probability of the deck segments exhibiting damage through a given time then can be used to determine the percent damaged area of the deck versus time.

Once corrosion initiates, the rate of corrosion is determined by other factors not captured in the initiation model, including cathode-anode effects, temperatures, oxygen availability, etc. As a result, the propagation time was also considered as a random variable, and the time-to-damage is a combination of initiation time t_i and the propagation time t_p.

$$t_{damage} = t_i + t_p \quad \text{Eq. 8.4}$$

Because of the complexity of the required analysis, a Monte Carlo simulation was run to account for the interaction between considered variables. Latin Hypercube Sampling was used to reduce the number of segments requires for model convergence (Wyss & Jorgenson, 1998).

In the following sections, the processes by which statistical distributions describing the interacting factors that govern corrosion initiation and propagation were determined for the I-129 bridge deck are presented.

8.3.1.2 Influence of Cracking. Crack lengths and orientation were measured during the visual field survey, with the cracking observed oriented transverse to the bridge span. Transverse bridge deck cracking has been studied extensively (Krauss & Rogalla, 1996), (French, Le, Eppers, & Hajjar, 1999), (Saadeghvaziri & Hadidi, 2002), and is generally related to stresses caused by thermal gradients related to hydration and drying shrinkage. Previous work by Fanous et al. (Fanous, Wu, & Pape, 2000) reported a strong influence of cracking on bar corrosion for epoxy-coated reinforcing in similar Iowa bridge decks.

A crack-affected width (i.e., the width of the area around each crack where damage is assumed to be affected by that crack) of 12 inches was determined to apply to the I-129 deck based on the width of delaminations and spalls oriented along cracks as observed during the field studies. While the great majority of deck damage was oriented parallel to and associated with cracks, only approximately 50 percent of the observed crack lengths had measurable damage.

Crack widths ranged from 10 to 30 mils; further examination of extracted cores indicated that the cracks narrowed to 1/3 or less of the surface width as they approached the bar depth (Figure 8.7). For the purposes of modeling and based on the findings of the field investigation, crack width was estimated to be log-normally distributed, with a median value of 5 mils and a coefficient of variation of 60 percent.

8.3.1.3 Chloride Ion Transport. Chloride ion transport in concrete is complex and may occur through diffusion (caused by chloride ion concentration gradient), capillary absorption (wetting and drying), and permeation (driven by pressure gradients) (Stanish, Hooton, & Thomas, 1997). Chloride transport may also be slowed by chemical binding of the chlorides with aluminate phases in the cement, or by physical absorption or trapping of chloride ions in pores. Despite the potential complexity of the chloride penetration process in concrete, it is commonly assumed that diffusion plays the largest role. Therefore, describing chloride transport by using a mathematical representation of diffusion, quantified based on an "apparent" diffusion coefficient calculated from chloride concentration profiles measured in the actual structure, is judged to be a reasonable representation of this process accounting for other influences (Sohanghpurwala, 2006).

The driving force behind the diffusion process is the chloride exposure, or the amount of chloride applied to the concrete surface. This is quantified in terms of the effective surface chloride concentration, C_s.

Chloride diffusion in concrete, driven by a concentration gradient, can be described by Fick's Second Law of Diffusion:

$$\frac{\partial C}{\partial t} = D_a \frac{\partial^2 C}{\partial x^2} \qquad \text{Eq. 8.5}$$

where C is the chloride concentration at a depth of x from the concrete surface at time t, and D_a is the chloride diffusion coefficient.

If the surface chloride concentration C_s and D_a are assumed to be constants, the concentration $C(x, t)$ through a uniform medium at depth of x and time t is given by the following solution (Crank, 1956):

$$C(x,t) = C_s - (C_s - C_0) \times \text{erf}\left(\frac{x}{2\sqrt{D_a t}}\right) \qquad \text{Eq. 8.6}$$

where erf() is the Gaussian error function, and C_0 is the background or original chloride concentration.

The suitability of the solution above for describing chloride movement in the I-129 bridge deck is limited by the presence of the overlay and associated dual-layer diffusion behavior. A more applicable solution for an overlay and a relatively thick deck slab is given by the following solution for chloride concentration in a semi-infinite composite medium (Mejlbro & Poulsen, 2006):

$$C(x,t) = C_0 \sum_{n=0}^{\infty} \alpha^n \left[\frac{(2n+1)l + x}{2\sqrt{D_{a1}t}} - \alpha * \text{erfc}\frac{(2n+1)l - x}{2\sqrt{D_{a1}t}}\right] \quad \text{for } -l < x < 0 \text{ (the overlay)} \qquad \text{Eq. 8.7}$$

$$C(x,t) = \frac{2kC_0}{k+1} \sum_{n=0}^{\infty} \alpha^n * \text{erfc}\frac{(2n+1)l + kx}{2\sqrt{D_{a1}t}} \quad \text{for } 0 < x < \infty \text{ (the deck slab)} \qquad \text{Eq. 8.8}$$

where

$k = \sqrt{\frac{D_{a1}}{D_{a2}}}$ and $\alpha = \frac{1-k}{1+k}$

where l represents the thickness of the overlay, and the interface between overlay and deck slab is taken as x=0.

The closed-form solution above is not readily adaptable for modeling variations of exposure or material properties with time. Consequently, a finite difference solution for determining chloride concentration with depth over time applicable to a multi-layer system was used. This solution is based on a Crank-Nicholson discretization of Equation 8.5, for which the general form is provided below (Chapra & Canale, 2002). A complete derivation of the finite difference solution is provided in Appendix I.

$$D_a[V_{i+1} - 2(D_a + K)V_i] + D_a V_{i-1} = -D_a U_{i+1} + 2(D_a - K)U_i - D_a U_{i-1}$$

where
i = current slice
D_a = apparent diffusion coefficient
U = concentration at timestep j
V = concentration at timestep j+1
$K = \frac{(\Delta X)^2}{\Delta T}$, where X = depth and T = time

Eq. 8.9

8.3.1.4 Chloride Exposure. Values of C_s are strongly influenced by the exposure conditions (i.e., severity of deicing salt application). Based on studies of bridge decks in northern states conducted by WJE, C_s can range from greater than 0.80 percent by weight of concrete in New York to 0.15 percent by weight of concrete in Virginia (Lee & Krauss, 2003). Exposure conditions may be characterized as follows based on C_s (Krauss, Lawler, & Steiner, 2009):

- mild: up to 0.25 percent by weight of concrete
- moderate: 0.25 to 0.45 percent by weight of concrete
- severe: 0.45 percent by weight of concrete or higher

For the I-129 bridge deck, values of C_s were determined based on the chloride concentration profiles determined by laboratory analyses as described previously. The exposure was assumed to be bi-linear, such that the surface concentration was equal to zero in the first year and built up to a level that was constant after the fifth year. This exposure versus time relationship is represented in Figure 8.8. With this assumption, a non-linear least-squares error fitting algorithm was used to find C_s based on diffusion as represented by the finite difference discretization.

8.3.1.5 Apparent Diffusion Coefficients. For the purpose of the model, apparent diffusion coefficients (Da) were considered separately for uncracked and cracked regions, in recognition of the fact that chloride transport is likely to occur more rapidly through cracks. Areas treated as cracked and uncracked concrete in these analyses are based on the calculated average crack densities previously reported, and on the treatment of cracking discussed in Section 8.3.1.2.

For typical bridge deck concretes, apparent diffusion coefficients in uncracked concrete may be categorized as very low to high, when they range from 0.05 in.^{2}/yr. to 0.30 in.^{2}/yr., respectively (Krauss, Lawler, & Steiner, 2009). In the overlay, apparent diffusion coefficients were determined based on a least-squares error fit of the finite difference discretization to measured chloride content data from cores, an example of which is shown in Figure 8.9.

In uncracked cores from the I-129 bridge deck, a minimal amount of chloride had penetrated through the overlay to the deck slab concrete below the overlay. As a result, meaningful apparent diffusion coefficients for the deck slab concrete could not be calculated. Therefore, for the purposes of the modeling, the distribution of the apparent diffusion coefficient for this concrete was assumed to be similar to that measured in the deck concrete during a previous study conducted by WJE in 2010 of eight bridge decks in Iowa (Donnelly, Krauss, & Lawler, 2011).

The average of the apparent diffusion coefficients determined for the overlay was approximately 0.008 in.^{2}/yr., which is a very low diffusion rate. A previous study by Fanous et al. (Fanous, Wu, & Pape, 2000), reported an average apparent diffusion coefficient of 0.018 in.^{2}/yr. for three bridges with similar low-slump overlays. In contrast, apparent diffusion coefficients used for the deck slab concrete were assumed to be approximately 0.120 in.^{2}/yr. In uncracked regions, the very low value of the apparent diffusion coefficient of the overlay concrete can be expected to result in relatively slow chloride ion penetration. In this study, the apparent diffusion coefficients for the overlay and deck slab are identified as D_{a1} and D_{a2}, respectively.

In cracked regions, the apparent diffusion coefficient was determined based on an effective crack width determined as discussed in Section 8.3.1.2 and in Equation 8.10 below. The equations below reflect research by others showing that apparent diffusion coefficients for crack widths greater than 3 mil approach the diffusion coefficient of chloride in plain water (Djerbi, Bonnet, Khelidj, & Baroghel-bouny, 2007). This effectively allows chloride to penetrate through cracks to typical bar depths in a matter of days.

$$D_{cr}(w_{cr}), in.^2/yr. = 24.9 * w_{cr} - 19.6 \qquad w_{cr} < 3.1 \text{ mils} \qquad \text{Eq. 8.10}$$
$$D_{cr}(w_{cr}), in.^2/yr. = 58.7 \qquad w_{cr} > 3.1 \text{ mils}$$

8.3.1.6 Concrete Cover and Overlay Thickness. The distribution for concrete cover was determined based on the GPR measurements reported in Table 4.1 for the in-depth study areas and Table 8.1 for the overall bridge deck. Cover was assumed to be normally distributed, and is tabulated for each in-depth study area and the bridge overall in these two tables.

The distribution of the overlay thickness was determined based on measurements of the overlay thickness at the cores taken during this study. Due to the limited number of samples in each in-depth study area, the same distribution of overlay thickness was assumed to apply for all in-depth study areas and for the overall bridge deck.

8.3.1.7 Corrosion Threshold and Propagation Time. Studies have shown that concentrations of freely available chloride of 350 ppm by weight of concrete or greater can promote corrosion of embedded steel in non-carbonated concrete (Pfeifer, Landgren, & Zoob, 1987), (Bentur, Diamond, & Berke, 1997). Background chloride was assumed to be inherent to the aggregates in the concrete, and not available for participation in corrosion activity, as previously discussed in Section 8.2.3.3.

Previous research by others identified that the propagation time (time-to-cracking) is dependent on cover depth, properties of the concrete and steel/concrete interface, type of corrosion products, size of reinforcing, and corrosion rate (Liu & Weyers, 1998), (Vu, Stewart, & Mullard, 2005). Although typical time-to-corrosion cracking for uncoated bars is commonly assumed to be about 5 years, the deeper cover on the I-129 deck (3 to 4 inches) and generally impermeable nature of the overlay may slow corrosion rates and increase time-to-cracking. Application of the work by Liu and Weyers and by Vu, Stewart, and Mullard indicates that for structures with good cover (3 inches) and a moderate water/cementitious materials ratio (w/cm) (0.45), propagation times for 10-mil cracks resulting from corrosion are 20 to 30 years (Stewart & Mullard, 2007). Consequently, propagation time was considered to be a random variable with a log-normal distribution. Based on field observations that 50 percent of the observed cracks exhibit damage, the median (50th percentile) propagation time was set to be 30 years (equal to the 35 year age of the bridge minus 5 years to account for chloride build up) to represent the existing condition of the deck. Additionally, a coefficient of variation of 60 percent was assumed for the propagation time, which allowed the model output to more closely match the actual observed conditions.

8.3.1.8 Summary of Considered Deck Properties. Tables 8.5 and 8.6 list the random variables considered in the performance model and the associated statistical distributions assumed to apply both uniformly across the structure and varying for each in-depth study area, respectively. The bases for these values were quantified for modeling purposes based on field observations and laboratory testing, as discussed above.

8.3.2 Results

8.3.2.1 Projected Service Life. The service life model results, in terms of predicted damage (area of deck exhibiting corrosion-related delamination or spalling) versus time, for the entire deck on average and for each of the in-depth study areas are plotted in Figure 8.10. In the figure, solid lines indicate the predicted damage versus time for the I-129 bridge as constructed, which includes the beneficial effects of the low-permeability overlay. Also shown on this figure as single points are the actual damage areas observed to date for the entire deck and for each of the in-depth study areas.

The actual predicted damage versus observed damage through 35 years is plotted for the entire deck and in-depth study areas in Figure 8.11. A diagonal line is provided for reference on the plot, which would indicate a perfect match between predicted and observed values. The plot shows that, although predicted values vary somewhat from observed values, the model predicts observed damage quite well.

Considering the as-built condition, the damage curves for the bridge have three distinct periods: an initial increasing phase lasting 10 to 20 years; a plateau ranging from 20 to 80 years; and a second increasing damage phase starting at 80 to 100 years. The initial phase of damage predicted by the model is strongly related to the crack density and is controlled by the assumed rapid rate of chloride ingress through cracks. The plateau is a stable period that occurs after damage related to cracking has occurred but before chloride penetrating through the uncracked concrete causes additional corrosion at sites away from deck cracks. The initiation of this additional corrosion results in the third period.

Considering that the bridge as-surveyed is in the second phase of the damage curve, the currently observed damage should strongly correlate with the observed crack density, since that controls the extent of damage in the first phase of the damage curve. Figure 8.12 illustrates this linear relationship between crack density and currently observed damage.

The start of the third phase of the damage curve (second increase), caused by chloride penetration through the uncracked regions of the deck, is marked by an inflection point in the damage curve. This indicates that, in uncracked areas of the I-129 bridge deck, the overlay effectively delayed chloride from reaching the deck slab reinforcing bars for approximately 80 to 100 years.

As projected by this model and considering a 10 percent damage threshold for the deck, the total service life for the I-129 bridge deck is estimated to range from 110 to 140 years. At or before the time that the bridge reaches this age, some repair programs will be needed.

This long service life is largely a result of the predicted length of the second phase of the damage curve (the plateau). However, the predicted length of the second phase as modeled is somewhat uncertain, because the compounding effects of damage have not been considered. Damage areas, i.e. cracking or spalling caused by corrosion, allow chloride to penetrate into the concrete, negating the effects of concrete cover and protective overlay.

There is additional uncertainty related to the true nature of the corrosion process, which is simplified for the purpose of the model and is assumed to begin uniformly wherever chloride concentrations exceed the threshold. For example, macro-cell corrosion in the deck can result in cathodic regions, partnering with anodic regions, that might not result in rust formation and damage even at high chloride concentrations. As a consequence, the predicted service life grows more uncertain at older ages and higher damage levels.

8.3.2.2 Comparison between Performance With and Without Overlay. To provide a basis of quantifying the benefits provided by the overlay, a similar analysis to that reported above was performed based on the assumption that the chloride penetration resistance of the overlay was the same as that assumed for the deck slab (i.e., the same apparent diffusion coefficient). This represents the condition where the full deck was constructed homogenously without an overlay. The predicted damage versus time curves for the bridge based on these assumptions, with all other variables kept the same, are shown as the dotted lines in Figure 8.10.

The modeled performance with and without the overlay show similar damage levels through the first 10 years due to the early incidence of damage at cracked regions. In this phase, the first phase of the damage curve, the permeability of the overlay has minimal discernible effect on reducing damage because it does little to reduce chloride penetration at cracks, where most of the chloride penetration and deck damage occurs in the early life of a bridge deck. This influence is best illustrated by the following comparison of the corrosion initiation time for each segment of the bridge deck, as defined in Section 8.3.1.1. Each such segment was assigned properties defined by the statistical distributions measured or assumed for the specific deck. Figure 8.13 and Figure 8.14 plot corrosion initiation time for each segment versus apparent diffusion coefficient for both the as-built and no-overlay conditions, respectively. The apparent diffusion coefficients in cracked regions are generally greater than 1 $in.^2/yr.$ regardless of whether or not an overlay is present, and have corresponding low corrosion initiation times generally less than 5 years for both conditions. For uncracked regions, initiation time correlates with the apparent diffusion coefficients of the upper zone of concrete in the deck (D_{a1}), which is a low-permeability concrete in the case with the overlay and ordinary concrete in the case without the overlay. When the low permeability of the overlay is considered, corrosion initiation times are generally greater than 60 years, as shown in Figure 8.13. However, when the overlay permeability is no greater than the deck slab concrete, initiation times still correlate with D_{a1}, but are reduced and generally range between 5 and 60 years (see Figure 8.14).

No difference in trends for the other considered variables (concrete cover, overlay thickness, C_s) was identified between the overlay and non-overlay conditions.

Based on the above analysis, the inclusion of the low-permeability overlay has greatly delayed corrosion initiation time for the uncracked regions of the deck. However, no significant difference in performance was predicted by the model in cracked regions. Based on comparisons of the deck modeled with and without a low-permeability overlay, considering the observed crack density and a 10 percent damage threshold, the service life extension provided to this deck through the use of the overlay is estimated to be 80 to 100 years.

8.4 Discussion and Recommendations

Comparison of findings from the visual and sounding surveys, half-cell surveys, and service life modeling show that cracking has played a large role in the damage seen to date on the bridge. Observations from cores showed that the top transverse bars tended to align with the cracks, which allow for rapid penetration of chloride to the bar depth.

The visual survey identified a number of cracked and delaminated areas that had been epoxy-injected. These existing epoxy repairs appeared to have had some success preventing further damage to the deck in areas that were already delaminated by rebonding delaminations to prevent spalls. However, additional delaminated areas were observed beyond the edge of many epoxy-injection sites. Furthermore, the half-

cell survey identified highly negative potentials at most epoxy-injected areas that coincided with delaminations, indicating that corrosion activity was continuing.

The effect of epoxy repairs on cracked but sound regions of the deck was not definitive. Based on the half-cell potential contours provided, some epoxy repairs at cracks did not show elevated half-cell potentials. Similarly crack locations without epoxy repairs were present that did not show elevated half-cell potentials. However, small regions of elevated half-cell potentials were observed at some epoxy repairs without delaminations, indicating that corrosion activity may still be occurring near the cracked region.

The low-permeability overlay has been effective at preventing chlorides from penetrating to the bar depth in uncracked regions. In all uncracked cores, the chloride concentration exceeds chloride-induced corrosion threshold only at depths was less than 1-1/2 inches. Considering a mean overlay depth of 2-1/4 inches, the overlay has substantial service life remaining before replacement is prudent.

Although some aggregates susceptible to ASR were identified during petrographic examination of the cores, most of the ASR gel identified appears to be associated with a contaminant and with reactive fine aggregate particles. As a result, ASR is not anticipated to result in widespread damage to the deck slab concrete. However, there are some ASR-reactive sandstone particles in the coarse aggregate of the deck concrete, so minimizing the penetration of moisture at cracks is advisable.

If no further maintenance is performed on the structure, the service life predictions for the deck are likely to be unconservative. Regions with existing damage at the time of the survey will continue to corrode and encourage corrosion in adjacent areas, and this compounding effect of damage is not considered by the model. However, appropriate repairs at damaged locations should reduce this effect.

Repairs for the bridge deck should focus on preventing further chloride and moisture ingress at cracked regions and repairing existing damage. Existing cracks without detectable damage should be sealed or injected with a low viscosity epoxy resin, methacrylate, or other crack sealer. Areas with existing damage (such as delaminations and spalls) should be repaired using appropriate concrete repair techniques. ICRI Publication Nos. 320.1R-1996 and 320.2R-2009 provide guidance for appropriate concrete repair methods.

9.0 CONCLUSIONS

To gain further understanding of the capabilities and effectiveness of non-destructive testing (NDT) for assessing bridge decks, field testing was performed using various NDT methods to evaluate the condition of the reinforced concrete bridge deck of the I-129 bridge over the Missouri River in Sioux City, Iowa. The techniques employed included visual inspections and sounding, infrared thermography, ground penetrating radar, impact echo, and half-cell testing, and each of these was evaluated for ease of use, speed of data collection, and accuracy. Additionally, the current condition and possible future performance of this concrete bridge deck was characterized to aid in planning for future maintenance and rehabilitation activities.

This deck was constructed in 1976 and included a low-slump overlay, resulting in an average concrete cover over the uncoated reinforcing bars of nearly 4 in. Several conventional patch repairs and multiple epoxy injection repairs have been performed in the past, but overall the bridge deck is in very good condition for its age.

An overall survey of one traffic lane (right lane) and the associated shoulder was performed for nearly the entire length of the eastbound and westbound lanes using conventional visual and sounding survey methods. Additionally, the various NDT techniques selected for this study were evaluated in six in-depth study areas, each of which was 200-ft long and 18- to 22-ft wide and was located where significant deterioration was present.

The conclusions made about the condition of the I-129 bridge deck based on this condition survey are summarized as follows:

- The overall survey of the bridge deck identified damage consisting of delaminations and spalls of 1.1 percent and 2.0 percent of the top deck surface in the areas surveyed in the westbound and eastbound lanes, respectively. Damage on the westbound lanes was concentrated in two spans, while damage in the eastbound lanes was most common in the shoulder of three spans.
- The damage was concentrated around transverse cracks and was typically caused by corrosion of the reinforcing steel as a result of locally elevated chloride concentrations. Away from cracks and delaminations, the chloride content in the deck slab concrete has not reached concentrations where corrosion could be expected at the typical bar depth.
- The low-slump overlay has remained well-bonded to the deck slab, and based on the measured chloride concentrations in the deck slab, has effectively protected the reinforcing steel in the deck from chloride infiltration away from cracks. The median diffusion coefficient of the overlay concrete was approximately 1/15th of that seen by WJE in 2010 in the typical deck concrete of other bridge decks in Iowa. Service life analysis based on these differences suggests that the service life extension provided by the installation of the highly impermeable low-slump concrete may be as high as 80 years when compared to the performance of a deck with similar total cover concrete over the reinforcing steel and with properties assumed to be equal to those of typical Iowa bridge deck slab concrete.
- Service life predictions were developed using a statistical model built on a finite difference-based approach for modeling chloride movement through the multi-layer deck concrete, and which considers the observed variability in corrosion-governing properties across the bridge deck. This model suggests that additional damage away from cracks may not develop until the bridge age reaches 80 years or more. However, delaminations and spalls initiating at cracks

may disrupt the cover concrete in adjacent areas of the deck, resulting in corrosion-related deterioration that develops and grows in a self-propagating process well before 80 years.

- Repairs for this deck should focus on preventing further chloride ingress at cracked regions and on repairing existing damage. Existing cracks without detectable damage should be sealed, and areas with existing damage should be repaired using appropriate concrete repair techniques. If repairs to the transverse cracks had been successfully executed soon after the cracks formed, the extent and concentration of the corrosion-related deterioration that currently exists at the cracks most likely would have been significantly reduced, and the service life of the bridge deck at the deck cracks extended close to that predicted for the uncracked areas.
- Replacement of the overlay need not be considered at this time. None of the chloride contents measured in the uncracked deck slab concrete meet the corrosion threshold, even where taken above the reinforcing. Service life modeling of the bridge deck indicates that corrosion-related deterioration of the bridge deck in uncracked areas may not begin to occur until the bridge deck is at least 80 years old. Therefore, the replacement of the existing overlay may be of limited benefit for another 15 to 25 years. Additional chloride content testing should be performed in approximately 10 to 15 years to verify this finding.

The conclusions made about the effectiveness of the NDT approaches evaluated in this study based on the comparison of these methods are summarized as follows:

- The accuracy of the testing methods, assessed by quantitatively comparing the extent and location of areas identified as delaminated by each method relative to sounding and the core sample conditions, varied widely. None of the survey techniques employed, including sounding, were perfectly accurate. Highly sensitive techniques (those most likely to indicate the presence of a delamination with minor indications of damage) were more likely to correctly identify as delaminated a larger percentage of the areas found to be delaminated by sounding methods, but also were more likely to misidentify large areas as delaminated. This trend is demonstrated by the two most accurate techniques, IE (which demonstrated high sensitivity) and IR thermography (which demonstrated low sensitivity), as applied to this bridge. IE correctly identified 69 percent of the combined delaminated area and misidentified 94 percent, while IR thermography correctly identified 37 percent of the combined delaminated area but misidentified only 42 percent.
- While slow, labor-intensive and highly operator-dependent, visual and sounding techniques were demonstrated to still be highly effective for evaluating this bridge deck. Of all methods, this combination of techniques provides the fullest, most accurate picture of the condition of the bridge deck.
- As implemented for this deck, IE testing was among the most accurate and robust of the methods evaluated, but was sensitive to misidentifying delaminations. Detection of surface delaminations is based on a user-selected threshold applied to the measured signal, and the technique's resolution is equipment-dependent. Improved calibration of thresholds may increase the accuracy of this method. Additionally, the epoxy resin present on many localized areas of this bridge resulted in some mis-identified locations, indicating that the accuracy of this method may be improved for bridge decks without this or other material contaminants on its surface.
- IR thermography-based deck surveys can be executed rapidly, but this method is inherently dependent on conducive weather. Features of the I-129 deck, including high (approximately 4-

in.) cover, varied deck surface color, and epoxy resin spills, limited the effectiveness of IR thermography in this instance. Despite these drawbacks, IR thermography was still among the most accurate techniques considered in this study. IR thermography may be better suited to decks with lower cover that have not seen extensive previous repairs. Therefore, additional evaluation of this technique in such a setting is recommended.

- GPR does not identify delaminations directly but identifies areas of probable delamination by detecting features associated with corrosion, such as locally elevated moisture content, chloride concentration, and corrosion by-products that affect the reflection of electromagnetic radar pulses from the top mat of the reinforcing bars. This technique was relatively easy to implement; however, the accuracy of this technique for both of the antennas used was poor.
- Half-cell potential testing does not directly identify delaminations, and the areas identified as corroding with this technique far exceeded the actual areas of delamination. However, HCP testing does provide information about the extent of corrosion in the bridge deck and can be used to predict areas of future delamination.

10.0 BIBLIOGRAPHY

ACI Committee 228. (1998). *Nondestructive Test Methods for Evaluation of Concrete in Structures (ACI 228.2-98) (reapproved 2004).* Farmington Hills, MI: American Concrete Institute.

Bastidas-Arteaga, E., Chateauneuf, A., Sanchez-Silva, M., Bressolette, P., & Schoefs, F. (2011). A Comprehensive Probabilistic Model of Chloride Ingress in Unsaturated Concrete. *Engineering Structures, 33*, 720-730.

Bentur, A., Diamond, S., & Berke, N. (1997). *Steel Corrosion in Concrete: Fundamentals and Civil Engineering Practice.* London: St Edmundsbury Press.

Chapra, S. C., & Canale, R. P. (2002). *Numerical Methods for Engineers* (4th ed.). McGraw-Hill.

Crank, J. (1956). *The Mathematics of Diffusion.* Oxford: Clarendon Press.

Djerbi, A., Bonnet, S., Khelidj, A., & Baroghel-bouny, V. (2007). Influence of Traversing Crack on Chloride Diffusion into Concrete. *Cement and Concrete Research, 38*, 877-883.

Donnelly, J. P., Krauss, P. D., & Lawler, J. S. (2011). *Performance Evaluation of Iowa Bridge Decks Constructed with Epoxy-Coated Reinforcing Bars.* Northbrook, Illinois: Wiss, Janney, Elstner Associates, Inc.

Fanous, F., Wu, H., & Pape, J. (2000). *Impact of Deck Cracking on Durability.* Iowa State University, Center for Transportation Research and Education, Ames.

French, C., Le, Q., Eppers, L., & Hajjar, J. (1999). *Tranverse Cracking in Bridge Decks: Summary Report.* University of Minnesota. St. Paul: Minnesota Department of Transportation.

Graybeal, B. A., Rolander, D. D., Phares, B. M., Moore, M. E., & Washer, G. A. (2001). Reliability and Accuracy of In-Depth Inspection of Highway Bridges. *Transportation Research Record,* 93-99.

Gucunski, N., Feldmann, R., Romero, F., Kruschwitz, S., Abu-Hawah, A., & Dunn, M. (2009). Multimodal Condition Assessment of Bridge Decks by NDE and Its Validation. *Proceedings of the 2009 Mid-Continent Transportation Research Symposium.* Ames, IA: Iowa State University.

Gucunski, N., Slabaugh, G., Weng, Z., Fang, T., & Maher, A. (2008). Visualization and Interpretation of Impact Echo Data from Bridge Deck Testing. *Transportation Research Record 2050,* 11-121.

Krauss, P. D., & Rogalla, E. A. (1996). *NCHRP Report 380 - Transverse Cracking in Newly Constructed Bridge Decks.* Washington, DC: Transportation Research Board - National Research Council.

Krauss, P. D., Lawler, J. S., & Steiner, K. A. (2009). *Guidelines for Selection of Bridge Deck Overlays, Sealers and Treatments, NCHRP Project 20-07, Task 234.* Washington, D.C.: National Cooperative Highway Research Program.

Lee, S. K., & Krauss, P. (2003). *Service Life Extension of Northern Bridge Decks Containing Epoxy-Coated Reinforcing Bars.* Northbrook, IL: Wiss, Janney, Elstner Associates, Inc.

Liu, Y., & Weyers, R. (1998). Modeling the Time-to-Corrosion Cracking in Chloride Contaminated Reinforced Concrete Structures. *ACI Materials Journal, 95*(6), 675-681.

Longstreet, W. (n.d.). *SHRP Product 2015: Ground-Penetrating Radar for Bridge Deck Evaluations*. Retrieved November 10, 2011, from AASHTO Innovative Highway Technologies: http://leadstates.transportation.org/car/SHRP_products/2015.stm

Manning, D. G., & Bye, D. H. (1983). *Bridge Deck Rehabiliation Manual.* Downsview, Ontario: Ontario Ministry of Transportation and Communications.

Maser, K. R., & Roddis, M. (1990). Principles of Thermography and Radar for Bridge Deck Assessment. *Journal of Transportation Engineering*, 583-590.

Mejlbro, L., & Poulsen, E. (2006). *Diffusion of Chloride in Concrete: Theory and Application.* London: Taylor and Francis.

New York State Department of Transportation. (1992). *Bridge Deck Evaluation Manual.* Albany, NY: New York State Department of Transportation.

Parrillo, R., Roberts, R., & Haggan, A. (2006). Bridge Deck Condition Assessment Using Ground Penetrating Radar. *European Federation for Non-Destructive Testing (ECNDT).* Berlin, Germany: German Society for Non-Destructive Testing.

Pfeifer, D. W., Landgren, J. R., & Zoob, A. (1987). *Protective Systems for New Prestressed and Substructure Concrete, FHWA-RD-86-193.* McLean, Virginia: Federal Highway Administration.

Romero, F., Roberts, G., & Roberts, R. (2000). Evaluation of GPR Bridge Deck Survey Results Used for Delineation of Removal/Maintenance Quantity Boundaries on Asphalt-Overlaid, Reinforced Concrete Deck. In S. Alampalli (Ed.), *Structural Materials Technology IV (NDT Conference),* (pp. 23-30). Lancaster, PA: Technomic Pub.

Saadeghvaziri, M., & Hadidi, R. (2002). *Cause and Control of Transverse Cracking in Concrete Bridge Decks.* New Jersey Institute of Technology. NJDOT.

Sagüés, A. A. (2003). Modeling the Effects of Corrosion on the Lifetime of Extended Reinforced Concrete Structures. *Corrosion, 59*(10), 854-866.

Sansalone, M. J. (1993). Detecting Delaminations in Concrete Bridge Decks With and Without Asphalt Overlays Using an Automated Impact-Echo Field System. *NDT in Civil Engineering* (pp. 807-820). Liverpool: British Institute of Non-Destructive Testing.

Sansalone, M. J., & Streett, W. B. (1997). *Impact-Echo Nondestructive Evaluation of Concrete and Masonry.* Ithica, NY: Bullbrier Press.

Scott, M., Rezaizadeh, A., Santos, C. G., Moore, M., Graybeal, B., & Washer, G. (2003, June). Comparison of Nondestructive Evaluation Methods For Bridge Deck Assessment. *NDT and E International, 36*(4), 245-255.

Sohanghpurwala, A. A. (2006). *NCHRP Report 558: Manual on Service Life of Corrosion-Damaged Reinforced Concrete Bridge Superstructure Elements.* Washington, D.C.: Transportation Research Board.

Stanish, K. D., Hooton, R. D., & Thomas, M. D. (1997). *Testing the Chloride Penetration Resistance of Concrete: A Literature Review, FHWA Contract DTFH61-97-R-00022.* Toronto, Ontario, Canada: University of Toronto.

Stewart, M., & Mullard, J. (2007). Spatial Time-dependent Reliability Analysis of Corrosion Damage and the Timing of First Repair for RC Structures. *Engineering Structures, 29*, 1457-1464.

Tuutti, K. (1982). *Corrosion of Steel in Concrete.* Stockholm, Sweden: Swedish Cement and Concrete Research Institute.

Vu, K., Stewart, M., & Mullard, J. (2005). Corrosion-Induced Cracking: Experimental Data and Predictive Models. *ACI Structural Journal, 102*(5), 719-726.

Wyss, G. D., & Jorgenson, K. H. (1998). *A User's Guide to LHS: Sandia's Latin Hypercube Sampling Software.* Sandia National Laboratories, Risk Assessment and Systems Modeling Department, Albuquerque.

Tables

Table 2.1. Summary of Findings from Overall Visual and Mechanical Sounding Surveys of Westbound Lanes

Distance from East Abutment (ft.)		Pier No.	Width of Survey (ft)	No. of Delams./Spalls	Area of Delams./Spalls (ft^2)	No. of Repairs	Area of Repairs (ft^2)	Crack Length (ft)	Damage[1] (%)	Crack Density (ft/ft^2)
0	100	14	0[2]	-	-	-	-	-	-	-
100	200	13	10	2	9	0	0	10	1.0	0.010
200	300	12	20	1	10	0	0	20	0.5	0.010
300	400	11	25	5	39	0	0	60	1.6	0.024
400	500	10	25	6	35	0	0	5	1.4	0.002
500	600	-	22	0	0	0	0	0	0.0	0.000
600	700	9	22	0	0	0	0	0	0.0	0.000
700	800	8	22	1	3	0	0	22	0.1	0.010
800	900	7	22	6	14	0	0	0	0.6	0.000
900	1000	-	25	8	32	0	0	69	1.3	0.028
1000	1100	-	25	5	35	2	9	98	1.8	0.039
1100	1200	6	25	7	23	3	35	42	2.3	0.017
1200	1300	-	25	5	34	0	0	43	1.4	0.017
1300	1400	-	25	1	3	0	0	0	0.1	0.000
1400	1500	-	25	2	29	0	0	25	1.2	0.010
1500	1600	5	25	3	26	0	0	0	1.0	0.000
1600	1700	-	25	6	60	3	48	114	4.3	0.046
1700	1800	-	25	9	93	2	20	125	4.5	0.050
1800	1900	4	25	2	10	0	0	0	0.4	0.000
1900	2000	-	25	1	2	0	0	25	0.1	0.010
2000	2100	3	25	1	4	0	0	12	0.2	0.005
2100	2200	-	22	0	0	0	0	0	0.0	0.000
2200	2300	2	22	1	3	0	0	14	0.1	0.006
2300	2400	-	25	1	35	0	0	25	1.4	0.010
2400	2500	1	25	4	18	0	0	23	0.7	0.009
2500	2590	-	25	1	4	0	0	0	0.2	0.000
Average for Total Survey Area									**1.1**	**0.012**

[1] Includes delaminated/spalled and repaired areas

[2] Area not surveyed (throat for entrance ramp)

Table 2.2. Summary of Findings from Overall Visual and Mechanical Sounding Surveys of Eastbound Lanes

Distance from West Abutment (ft)		Pier No.	Width of Survey (ft)	No. of Delams./Spalls	Area of Delams./Spalls (ft^2)	No. of Repairs	Area of Repairs (ft^2)	Crack Length (ft)	Damage[1] (%)	Crack Density (ft/ft^2)
0	100	-	25	3	8	3	5	24	0.5	0.010
100	200	1	25	8	40	1	6	87	1.8	0.035
200	300	-	25	7	56	2	11	113	2.7	0.045
300	400	2	25	10	55	0	0	75	2.2	0.030
400	500	-	25	8	28	7	70	118	3.9	0.047
500	600	3	25	7	28	4	19	59	1.9	0.024
600	700	-	25	9	39	2	10	29	2.0	0.012
700	800	4	22	1	3	0	0	6	0.1	0.003
800	900	-	25	6	43	0	0	76	1.7	0.030
900	1000	-	25	3	25	1	3	15	1.1	0.006
1000	1100	5	15	2	14	0	0	25	0.9	0.017
1100	1200	-	0[2]	-	-	-	-	-	-	-
1200	1350	-	0[2]	-	-	-	-	-	-	-
1350	1400	-	22	5	41	3	27	22	6.2	0.020
1400	1500	6	25	7	32	1	7	34	1.6	0.014
1500	1600	-	25	12	156	1	6	167	6.5	0.067
1600	1700	-	25	12	74	0	0	95	3.0	0.038
1700	1800	7	25	9	48	0	0	8	1.9	0.003
1800	1900	8	25	3	7	0	0	10	0.3	0.004
1900	2000	9	25	16	77	0	0	36	3.1	0.014
2000	2100	-	25	9	47	0	0	43	1.9	0.017
2100	2200	10	25	8	24	0	0	20	1.0	0.008
2200	2300	11	22	2	6	0	0	8	0.3	0.004
2300	2400	12	15	4	24	0	0	18	1.6	0.012
2400	2500	13	0[2]	-	-	-	-	-	-	-
2500	2605	14	0[2]	-	-	-	-	-	-	-
Average for Total Survey Area									**2.0**	**0.021**

[1] Includes delaminated/spalled and repaired areas

[2] Area not surveyed (throat for exit ramps)

WJE ENGINEERS ARCHITECTS MATERIALS SCIENTISTS

Table 2.3a. Summary of Cores - Westbound Lanes

Core No.	Study Area	Station (ft) [1]	Distance to Barrier	Core Length (in.)	Overlay Thickness (in.)	Vertical Cracking				Horizontal Cracking (Delaminations)				Reinforcing		
						Present in or near core?	Surface Width (mil) [2]	Epoxy Present?	Epoxy Bonded?	Cause (Debonding or Corrosion) [3]	Depth (in.)	Epoxy Present?	Epoxy Bonded?	Size	Depth	Corrosion Condition
1	-	472	9' 2"	6.25	2.4	-	-	-	-	-	-	-	-	-	-	-
2	-	616	14'-0"	6.5	1.9	-	-	-	-	-	-	-	-	-	-	-
3	-	743	14'-0"	6	2.3	-	-	-	-	-	-	-	-	-	-	-
4	-	819	3'-7"	6	2.8	-	-	-	-	-	-	-	-	-	-	-
5	-	942	10'-8"	5.2 to 6.5	2.3	-	-	-	-	Corrosion	2	N	-	-	-	-
6	-	1028	15'-6"	6.5 to 6.7	2.2	-	-	-	-	Debonding	2.25	N	-	-	-	-
7	-	1324	27'-2"	5.5 to 6.5	2.5	-	-	-	-	-	-	-	-	-	-	-
8	-	1513	2'-8"	6.0 to 6.5	3.4	-	-	-	-	-	-	-	-	-	-	-
9	-	2002	3'-10"	5.3 to 6.6	2.3	4” from core	30	n.a.	n.a.	Corrosion	2 to 4	Y	Y	-	-	-
10	-	2177	13'-3"	6.3 to 6.5	2.5	-	-	-	-	-	-	-	-	-	-	-
11	WB-2	1613	10'-6"	6 to 6.0	2.3	-	-	-	-	-	-	-	-	-	-	-
12	WB-2	1656	14'-0"	6.7	2.4	4” from core	15	n.a.	n.a.	Corrosion	4	N	-	-	-	-
13	WB-2	1727	17'-8"	6.5	2.4	-	-	-	-	-	-	-	-	-	-	-
14	WB-2	1743	6'-3"	5.7 to 6.6	2.2	-	-	-	-	-	-	-	-	-	-	-
15	WB-2	1757	11'-9"	6.9	2	4” from core	25	n.a.	n.a.	Corrosion	2 to 4	Y	Y	-	-	-
16	WB-3	2353	7'-0"	6.7 to 7.0	2.3	18” from core	35	n.a.	n.a.	Debonding	2	Y	Y	-	-	-
17	WB-3	2411	12'-5"	5.3 to 6.3	2.2	-	-	-	-	-	-	-	-	-	-	-
18	WB-3	2462	8'-6"	5.7 to 6.3	2.3	-	-	-	-	-	-	-	-	-	-	-
19	WB-3	2473	8'-6"	6.8 to 7.0	2.1	-	-	-	-	-	-	-	-	-	-	-
20	WB-3	2538	16'-4"	6 to 6.7	2.5	-	-	-	-	-	-	-	-	-	-	-
21	WB-1	253	7'-10"	6.1 to 6.4	2.7	12” from core	n.a. (overlay c. j.)	n.a.	n.a.	-	-	-	-	-	-	-
22	WB-1	328	14'-2"	7	1.8	-	-	-	-	-	-	-	-	-	-	-
23	WB-1	339	9'-10"	7	1.7	8” from core	25 to 30	n.a.	n.a.	Unclear	0.5	N	-	#6	3.3	minor
24	WB-1	389	6'-1"	7	2	4” from core	15 to 20	n.a.	n.a.	Unclear	1.5	N	-	-	-	-
25	WB-1	435	12'-6"	6.5	2.4	-	-	-	-	-	-	-	-	-	-	-

n.a. = not available, c.j. = construction joint

[1] From East Abutment

[2] 1,000 mil = 1 in.

[3] Debonding = cracking judged to initiate at interface between overlay and deck slab concretes; Corrosion = inclined cracking in overlay or deck slab likely originating at corroding reinforcing bar

Table 2.3b. Summary of Cores - Eastbound Lanes

Core No.	Study Area	Station (ft) [1]	Distance to Barrier	Core Length (in.)	Overlay Thickness (in.)	Vertical Cracking				Horizontal Cracking (Delaminations)				Reinforcing		
						Present in or near core?	Surface Width (mil) [2]	Epoxy Present?	Epoxy Bonded?	Cause (Debonding or Corrosion) [3]	Depth (in.)	Epoxy Present?	Epoxy Bonded?	Size	Depth	Corrosion Condition
26	-	1798	6'-4"	6.8	2.2	through core	20	Y	N	-	-	-	-	#6	4	severe
27	-	1788	6'-5"	6.4	2	-	-	-	-	-	-	-	-	#6	3.9	none
28	EB-2	1635	7'-5"	5.5	2.8	through core	35	Y	N	Corrosion	4.5	N	-	#6	4.6	severe
29	EB-2	1615	4'-4"	6	2.6	6” from core	15 to 20	n.a.	n.a.	Corrosion	2 to 3	N	-	#6	4.2	minor
30	EB-2	1576	8'-6"	6.7	2.5	through core	25 to 30	Y	N	Corrosion	4	N	-	#6	4	severe
31	EB-2	1535	4'-5"	6 to 6.5	2.3	6” from core	30 to 35	n.a.	n.a.	Corrosion	1 to 2	N	-	#6	4.7	minor
32	-	426	12'-7"	6.8	2	through core	30 (over deck c. j.)	N	-	-	-	N	-	-	-	-
33	-	438	12'-6"	5.7	1.9	through core	10	Y	Y	-	-	-	-	#6	3.7	minor
34	-	444	12'-5"	6.5	1.8	-	-	-	-	-	-	-	-	-	-	-
35	EB-2	1564	3'-2"	6.7	2.4	through core	15	N	-	Corrosion	4.5	N	-	#6	4.4	severe
36	EB-3	1887	16'-0"	4.7 to 5.7	2.2	-	-	-	-	-	-	-	-	#6	4.5	none
37	EB-3	1891	3'-6"	5.5 to 6.0	2	6” from core	n.a.	n.a.	n.a.	Corrosion	1.5 to 2	Y	N	-	-	-
38	EB-3	1925	16'-0"	6.6	2.1	-	-	-	-	-	-	-	-	#6	3.9	none
39	EB-3	2026	5'-0"	7	1.7	6” from core	15	n.a.	n.a.	Corrosion	3.25	N	-	#6	3.3	minor
40	EB-1	175	4'-0"	4.2	2	12” from core	15 to 20	n.a.	n.a.	Corrosion, Corrosion	0.5; 3.25	N	-	#6	3.3	moderate
41	EB-1	212	8'-0"	7	2	through core	20	N	-	Corrosion	3.5	N	-	#6	3.7	severe
42	EB-1	325	6'-6"	5.2 to 6.5	2.3	5” from core	40	n.a.	n.a.	Corrosion	3.5	N	-	#6	3.6	severe
43	EB-1	151	2'-0"	6.5	2.3	through core	15 to 20	Y	Y	Corrosion	3.5	N	-	#6	3.7	severe
44	EB-1	266	13'-6"	6.5-6.9	1.5	-	-	-	-	-	-	-	-	#6	3	none
45	-	797	2'-9"	6.3-6.7	3.4	-	-	-	-	-	-	-	-	-	-	-
46	-	820	3'-0"	5.3-5.9	3.3	through core	20 to 25	Y	Y	Corrosion	5.5	N	-	no bar	5.6	stain on core

n.a. = not available, c.j. = construction joint

[1] From West Abutment

[2] 1,000 mil = 1 in.

[3] Debonding = cracking judged to initiate at interface between overlay and deck slab concretes; Corrosion = inclined cracking in overlay or deck slab likely originating at corroding reinforcing bar

Table 2.2. Summary of Findings from Visual and Mechanical Sounding Surveys of In-Depth Survey Areas

Study Area	Area of Survey	Delaminations/ Spalls		Patches		Epoxy on Deck		Crack Length	Damage[1]	Crack Density
	(ft^2)	(ft^2)	(%)	(ft^2)	(%)	(ft^2)	(%)	(ft)	(%)	(ft/ft^2)
EB-1	3200	83	2.6	17	0.5	300	9.4	262	3.1	0.082
EB-2	3200	216	6.8	0	0.0	34	1.1	345	6.8	0.108
EB-3	3200	77	2.4	0	0.0	29	0.9	126	2.3	0.039
WB-1	3200	29	0.9	0	0.0	4	0.1	131	0.9	0.041
WB-2	3600	166	4.6	13	0.4	295	8.2	325	5.0	0.090
WB-3	3200	50	1.6	0	0.0	44	1.4	170	1.6	0.053
Average[2]		-	3.2	-	0.2	-	3.6	-	3.3	0.069

[1] Sum of delaminated/spalled and patched areas.

[2] Average is weighted based on area of survey to account for differently sized survey areas

Table 3.1. Comparison Between Delaminated Areas Identified by IR Thermography and Visual/Sounding Surveys

Study Area	Area of Survey (ft^2) [1]	Time of Scan	Delaminated Area Identified by IR Scans (ft^2)			Delaminated/Spalled Area Identified by Sounding (ft^2)
			Delamination	Patch	Epoxy on Surface	
EB-1	3200	12:30	133	17	115	83
EB-2	3200	13:00	144	0	21	216
EB-3	3200	13:15	76	0	10	75
WB-1	3200	11:20	26	0	0	29
WB-2	2400	11:40	60	10	51	140
WB-2[2]	2400	23:15	32	10	51	140
WB-3	3200	11:50	28	0	49	50

[1] Each survey method captured slightly different areas of deck surface. This table considers only the overlapping area common to all survey methods.

[2] Scan performed at night.

Table 3.2. Summary of Percentage of Overlap Between Areas Identified by IR Thermography and Areas Identified by Sounding Surveys

Study Area	Area of Delamination by IR (% of total)	Overlap With Sounded Area (% of total area)[1]	Area Not Overlapped with Sounded Area (% of total area)[2]	Overlap With Sounded Area (% of delaminated area by sounding)[3]	Area Not Overlapped with Sounded Area (% of delaminated area by sounding)[4]
EB-1	4.2	0.6	3.6	21.9	137.5
EB-2	4.5	2.8	1.7	41.5	25.0
EB-3	2.4	0.9	1.5	39.1	62.4
WB-1	0.8	0.3	0.5	28.8	55.6
WB-2	2.5	2.2	0.3	38.4	5.1
WB-3	0.9	0.7	0.2	41.9	14.6
Average	2.5[5]	1.2[5]	1.3[5]	37.2[6]	41.5[6]

[1] Area identified as delaminated by both sounding and IR thermography, divided by the survey area

[2] Area identified as delaminated by IR thermography but not by sounding, divided by the survey area

[3] Area identified as delaminated by both sounding and IR thermography, divided by the delaminated area identified by sounding

[4] Area identified as delaminated by IR thermography but not by sounding, divided by the delaminated area identified by sounding

[5] Average is weighted based on area of survey to account for differently sized survey areas

[6] Average is weighted based on percent of delaminated area identified by sounding to account for variation in observed damage in the in-depth study areas. This average is calculated as ratio of the sum of areas identified as overlapping or not overlapping to sum of area identified by sounding for all in-depth study areas

Table 4.1. Summary of GPR Assessment

In-Depth Study Area	Reinforcing Cover (in.)		Average of Top 10% of Amplitude (dB)	Upper Delamination Threshold (dB)[1]	Percentage Delaminated: Upper Threshold	Lower Delamination Threshold (dB)[2]	Percentage Delaminated: Lower Threshold
	Average	Std. Dev.					
1.6 GHz Antenna							
EB-1	3.63	0.22	-18.98	-24.98	2.19%	-26.98	1.02%
EB-2	4.32	0.36	-20.27	-26.27	5.83%	-28.27	2.83%
EB-3	3.76	0.28	-20.30	-26.30	0.67%	-28.30	0.27%
WB-1	3.57	0.26	-20.34	-26.34	0.26%	-28.34	0.13%
WB-2	3.93	0.28	-20.91	-26.91	2.80%	-28.91	1.46%
WB-3	4.40	0.31	-21.80	-27.80	2.19%	-29.80	0.88%
2.6 GHz Antenna							
EB-1	3.54	0.21	-22.78	-28.78	4.47%	-30.78	2.96%
EB-2	4.09	0.32	-24.34	-30.34	11.80%	-32.34	5.60%
EB-3	3.55	0.29	-23.75	-29.75	1.65%	-31.75	0.81%
WB-1	3.56	0.27	-25.25	-31.25	0.86%	-33.25	0.40%
WB-2	3.70	0.26	-26.89	-32.89	3.93%	-34.89	2.17%
WB-3	4.31	0.29	-27.45	-33.45	3.90%	-35.45	1.75%

[1] Upper Delamination Threshold (dB) represents 6 dB below the average amplitude of the top 10% of the data per ASTM D6087

[2] Lower Delamination Threshold (dB) represents 8 dB below the average amplitude of the top 10% of the data per ASTM D6087

Table 4.2. Comparison Between Areas of Delaminated Concrete Identified by Ground Penetrating Radar (GPR) and Visual/Sounding Surveys

In-Depth Study Area	Area of Survey (ft^2)	Visual/Sounding Delaminations (ft^2)	GPR Potential Delaminations	
			Upper Delamination Threshold [1] (ft^2)	Lower Delamination Threshold [2] (ft^2)
1.6 GHz Antenna				
EB-1	3200	83	50	18
EB-2	3200	216	164	51
EB-3	3200	75	7	1
WB-1	3200	29	10	3
WB-2	2400	140	38	14
WB-3	3200	50	60	17
2.6 GHz Antenna				
EB-1	3200	83	146	76
EB-2	3200	216	337	158
EB-3	3200	75	31	10
WB-1	3200	29	22	13
WB-2	2400	140	67	20
WB-3	3200	50	112	47

[1] Upper Delamination Threshold (dB) is 6 dB below the average amplitude of the top 10% of the data per ASTM D6087

[2] Lower Delamination Threshold (dB) is 8 dB below the average amplitude of the top 10% of the data per ASTM D6087

Table 4.3. Summary of Percentage of Overlap Between Areas Identified by GPR Based on the Upper Threshold, and Areas Identified by Sounding Surveys

Study Area	Area of Potential Delamination by GPR (% of total)	Overlap With Sounded Area (% of total area)[1]	Area Not Overlapped with Sounded Area (% of total area)[2]	Overlap With Sounded Area (% of delaminated area by sounding)[3]	Area Not Overlapped with Sounded Area (% of delaminated area by sounding)[4]
1.6 GHz Antenna					
EB-1	1.5	0.6	1.0	22.0	37.3
EB-2	5.1	1.7	3.4	25.1	50.2
EB-3	0.2	0.1	0.1	5.2	3.7
WB-1	0.3	0.1	0.1	15.7	14.4
WB-2	1.6	1.1	0.5	18.5	9.0
WB-3	1.8	0.3	1.4	20.0	92.6
Average	1.8[5]	0.6[5]	1.1[5]	19.7[6]	34.6[6]
2.6 GHz Antenna					
EB-1	4.6	1.2	3.4	44.6	130.0
EB-2	10.5	2.3	8.2	34.3	121.4
EB-3	1.0	0.4	0.6	15.8	24.8
WB-1	0.7	0.3	0.4	37.4	46.1
WB-2	2.8	0.9	1.8	16.1	31.1
WB-3	3.5	0.5	3.0	30.8	193.7
Average	3.9[5]	0.9[5]	3.0[5]	29.0[6]	91.5[6]

[1] Area identified as delaminated or potentially delaminated by both sounding and GPR, divided by the survey area

[2] Area identified as delaminated or potentially delaminated by GPR but not by sounding, divided by the survey area

[3] Area identified as delaminated or potentially delaminated by both sounding and GPR, divided by the delaminated area identified by sounding

[4] Area identified as delaminated or potentially delaminated by GPR but not by sounding, divided by the delaminated area identified by sounding

[5] Average is weighted based on area of survey to account for differently sized survey areas

[6] Average is weighted based on percent of delaminated area identified by sounding to account for variation in observed damage in the in-depth study areas. This average is calculated as ratio of the sum of areas identified as overlapping or not overlapping to sum of area identified by sounding for all in-depth study areas

Table 5.1. Selected Testing Areas for Single-Transducer IE Testing

Test Location	In-Depth Study Area	Station (ft)	Size of Test Grid
1	EB-1	314 to 330	9x7 (2 ft o.c. grid)
2	EB-2	1572 to 1588	9x8 (2 ft o.c. grid)
3	WB-1	334 to 346	7x7 (2 ft o.c. grid)

Table 5.2. Comparison Between Areas of Delaminated Concrete Identified by Scanning Impact-Echo (IE) and Visual/Sounding Surveys (all areas in ft^2)

In-Depth Study Area	Area of Survey (ft^2)[1]	Delaminated Area Identified by IE	Delaminated Area Identified by Sounding
EB-1	3200	174	83
EB-2	3200	337	216
EB-3	3200	120	75
WB-1	3200	77	29
WB-2	2400	180	140
WB-3	3200	78	50

[1] Each survey method captured slightly different areas of deck surface. This table considers only the overlapping area surveyed by all methods.

Table 5.3. Summary of Percentage of Overlap Between Areas Identified by Impact-Echo (IE) and Areas Identified by Sounding Surveys

Study Area	Area of Delamination by IE (% of total)	Overlap With Sounded Area (% of total area)[1]	Area Not Overlapped with Sounded Area (% of total area)[2]	Overlap With Sounded Area (% of delaminated area by sounding)[3]	Area Not Overlapped with Sounded Area (% of delaminated area by sounding)[4]
EB-1	5.4	1.9	3.5	72.6	135.5
EB-2	10.5	5.2	5.3	77.2	78.4
EB-3	3.7	1.5	2.3	62.1	97.1
WB-1	2.4	0.4	1.9	48.2	217.7
WB-2	7.5	3.7	3.8	63.4	65.5
WB-3	2.4	1.0	1.4	65.9	90.6
Average	5.2[5]	2.3[5]	3.0[5]	69.0[6]	93.5[6]

[1] Area identified as delaminated by both sounding and IE, divided by the survey area

[2] Area identified as delaminated by IE but not by sounding, divided by the survey area

[3] Area identified as delaminated by both sounding and IE, divided by the delaminated area identified by sounding

[4] Area identified as delaminated by IE but not by sounding, divided by the delaminated area identified by sounding

[5] Average is weighted based on area of survey to account for differently sized survey areas

[6] Average is weighted based on percent of delaminated area identified by sounding to account for variation in observed damage in the in-depth study areas. This average is calculated as ratio of the sum of areas identified as overlapping or not overlapping to sum of area identified by sounding for all in-depth study areas

Table 6.1. Half-Cell Potential Corrosion Risk (ASTM C876)

Half-Cell Potential vs. CSE	Corrosion Risk
> -200 mV	low - 10% probability of corrosion
-200 to -350 mV	moderate - increasing probability of corrosion
< -350 mV	high - 90% probability of corrosion

Table 6.2. In-Depth Study Area Corrosion Risk Area Comparison

Study Area	Equipment	Measured Area	Area < -250 mV	Area < -350 mV	Delaminated Areas by Sounding
		sq. ft.	sq. ft.	sq. ft.	sq. ft.
EB-1	cart	3200	210	30	83
EB-2	cart	3200	410	14	216
EB-3	cart	3200	85	6	75
WB-1	cart	3200	85	4	29
WB-2	cart	2400	264	38	140
WB-3	cart	3200	190	13	50

Table 6.3. Summary of Percentage of Overlap Between Areas Identified by Half Cell Potential (HCP) and Areas Identified by Sounding Surveys

Study Area	Area < -250 mV by HCP (% of total)	Overlap With Sounded Area (% of total area)[1]	Area Not Overlapped with Sounded Area (% of total area)[2]	Overlap With Sounded Area (% of delaminated area by sounding)[3]	Area Not Overlapped with Sounded Area (% of delaminated area by sounding)[4]
EB-1	6.5	1.3	5.2	49.8	200.3
EB-2	12.9	3.8	9.1	55.9	134.4
EB-3	2.7	0.8	1.9	31.9	82.4
WB-1	2.6	0.1	2.5	7.4	283.8
WB-2	11.0	2.4	8.6	42.0	146.8
WB-3	5.9	0.4	5.5	27.6	354.2
Average	6.8[5]	1.4[5]	5.3[5]	44.0[6]	165.6[6]

[1] Area identified as delaminated by sounding and as having a potential < -250 mV by HCP, divided by the survey area

[2] Area identified as having a potential < -250 mV by HCP but as not delaminated by sounding, divided by the survey area

[3] Area identified as delaminated by sounding and as having a potential < -250 mV by HCP, divided by the delaminated area identified by sounding

[4] Area identified as having a potential < -250 mV by HCP but as not delaminated by sounding, divided by the delaminated area identified by sounding

[5] Average is weighted based on area of survey to account for differently sized survey areas

[6] Average is weighted based on percent of delaminated area identified by sounding to account for variation in observed damage in the in-depth study areas. This average is calculated as ratio of the sum of areas identified as overlapping or not overlapping to sum of area identified by sounding for all in-depth study areas

Table 7.1. Comparison of NDT Techniques Based on Percentage of Overlapping Delaminated Areas

NDT Survey Method	Average[1] Overlap[2] With Sounded Area (% of delaminated area by sounding)	Average[1] NDT Area Not Overlapped[3] with Sounded Area (% of delaminated area by sounding)
IR	37.2	41.5
GPR, 1.6 GHz Antenna[4]	19.7	34.6
GPR, 2.6 GHz Antenna[4]	29.0	91.5
IE	69.0	93.5
Half-Cell Potential	44.0	165.6

[1] Average is weighted based on percent of delaminated area identified by sounding to account for variation in observed damage in the in-depth study areas. This average is calculated as ratio of the sum of areas identified as overlapping or not overlapping to the sum of areas identified as delaminated by sounding for all in-depth study areas

[2] Area identified as delaminated by both sounding and the NDT method

[3] Area identified as delaminated by the NDT method but not by sounding

[4] Calculated based on upper threshold

Table 7.2. In-Depth Study Area Survey Time for Each Method as Performed

NDT Survey Method	Time to survey one in-depth study area [1] (min.)
Conventional Sounding	90
IR Thermography	15
GPR	30
IE (performed by Olson Eng.)	45
Half-Cell Potential	45

[1] Dimension: 200 ft x approximately 18 ft

Table 8.1. Summary of GPR Cover Survey

Location	Average Cover (in.)	Standard Deviation of Cover (in.)
Westbound - 6 ft from Barrier	3.98	0.38
Westbound - 2 ft N. of Lane Line	4.08	0.40
Eastbound - 2 ft S. of Lane Line	3.94	0.32
Eastbound - 3 ft from Barrier	3.75	0.38
All	3.97	0.39

Table 8.2. Summary of Findings from Overall Visual, Sounding, and Half-Cell Potential Surveys of Eastbound Lanes

Distance from West Abutment (ft.)		Pier No.	Width of Survey (ft)	Damage[1] (%)	Measured Half-Cell Potentials (%)		
					Number of Readings	< -200 mV (%)	< -350 mV (%)
0	100		25	0.5	195	8.2	1.0
100	200	1	25	1.8	225	14.2	3.1
200	300		25	2.7	250	23.2	4.8
300	400	2	25	2.2	225	6.7	0.9
400	500		25	3.9	200	16.0	2.5
500	600	3	25	1.9	200	11.5	2.5
600	700		25	2.0	200	10.0	0.5
700	800	4	22	0.1	195	15.9	6.2
800	900		25	1.7	45	22.2	2.2
900	1000		25	1.1	0 [2]	-	-
1000	1100	5	15	0.9	0 [2]	-	-
1100	1200		0[2]	-	0 [2]	-	-
1200	1350		0[2]	-	0 [2]	-	-
1350	1400		22	6.2	80	21.3	3.8
1400	1500	6	25	1.6	200	17.0	2.0
1500	1600		25	6.5	250	36.8	2.4
1600	1700		25	3.0	250	33.6	2.4
1700	1800	7	25	1.9	200	28.0	5.5
1800	1900	8	25	0.3	225	4.0	1.8
1900	2000	9	25	3.1	250	9.6	0.4
2000	2100		25	1.9	225	9.3	0.9
2100	2200	10	25	1.0	0 [2]	-	-
2200	2300	11	22	0.3	0 [2]	-	-
2300	2400	12	15	1.6	0 [2]	-	-
2400	2500	13	0[2]	-	0 [2]	-	-
2500	2605	14	0[2]	-	0 [2]	-	-
Average for Total Survey Area				2.0		16.8	2.5

[1] Includes delaminated and repaired areas identified by visual and sounding survey

[2] Area not surveyed (open to traffic)

Table 8.3. Summary of Findings from Overall Visual, Sounding, and Half-Cell Potential Surveys of Westbound Lanes

Distance from East Abutment (ft.)		Pier No.	Width of Survey (ft)	Damage[1] (%)	Measured Half-Cell Potentials (%)		
					Number of readings	< -200 mV (%)	< -350 mV (%)
0	100	14	0 [2]	-	0 [2]	-	-
100	200	13	10	1.0	0 [2]	-	-
200	300	12	20	0.5	130	3.8	1.5
300	400	11	25	1.6	250	10.8	1.6
400	500	10	25	1.4	220	10.5	2.3
500	600		22	0.0	200	1.5	0.0
600	700	9	22	0.0	198	1.5	0.0
700	800	8	22	0.1	198	2.0	0.5
800	900	7	22	0.6	193	9.3	0.5
900	1000		25	1.3	198	40.4	5.1
1000	1100		25	1.8	198	42.4	3.5
1100	1200	6	25	2.3	200	31.0	3.5
1200	1300		25	1.4	188	9.0	0.5
1300	1400		25	0.1	160	3.1	1.3
1400	1500		25	1.2	179	2.2	1.1
1500	1600	5	25	1.0	200	1.0	0.0
1600	1700		25	4.3	255	19.6	1.6
1700	1800		25	4.5	250	32.8	3.2
1800	1900	4	25	0.4	195	8.7	3.6
1900	2000		25	0.1	200	3.5	1.0
2000	2100	3	25	0.2	200	5.5	0.5
2100	2200		22	0.0	200	2.0	0.0
2200	2300	2	22	0.1	199	15.1	0.0
2300	2400		25	1.4	225	15.6	0.9
2400	2500	1	25	0.7	249	16.9	0.8
2500	2590		25	0.2	209	24.4	1.9
Average for Total Survey Area				2.0		13.6	1.5

[1] Includes delaminated and repaired areas by visual and sounding survey

[2] Area not surveyed (open to traffic)

Table 8.4. Measured Depth of Carbonation in Cores

Core	Comments	Depth of Carbonation (in.)	
		Overlay	Base
3	-	0.16	0.00
10	-	0.20	0.00
11	-	0.20 to 0.35	0.04
18	-	0.04 to 0.08	0.04
22	-	0.16	0.00
34	-	0.04	0.00
38	-	0.12	0.04
41	Vertical crack in core	0.04	0.00
44	-	0.08	0.00
Average		0.13	0.01

Table 8.5. Parameters Relating to Service Life Model Assumed Uniform for Entire Bridge

Parameter	Distribution	Mean or Median [1]	COV
Crack width (mil)	log-normal	5	60%
Overlay (in.)	log-normal	2.29	17%
Cs (ppm)	normal	5892	25%
Da_1 (in.^{2}/yr.)	log-normal	0.008	47%
Da_2 (in.^{2}/yr.)	log-normal	0.118	83%
tp (yr.)	log-normal	35	60%

[1]. Mean for normal distribution. Median for log-normal distribution.

Table 8.6. Parameters Relating to Service Life Model - Assumed to Vary in Each In-depth Study Area

Parameter	Distribution	Property	Study Area					
			EB-1	EB-2	EB-3	WB-1	WB-2	WB-3
Crack density (ft/ft^2)	-	measured value	0.082	0.108	0.039	0.041	0.090	0.053
Cover (in.) [1]	normal	Mean	3.63	4.32	3.76	3.57	3.93	4.40
		COV	6%	8%	7%	7%	7%	7%

[1] Based on GPR data obtained using the 1.6 GHz antenna

WJE ENGINEERS ARCHITECTS MATERIALS SCIENTISTS

Figures

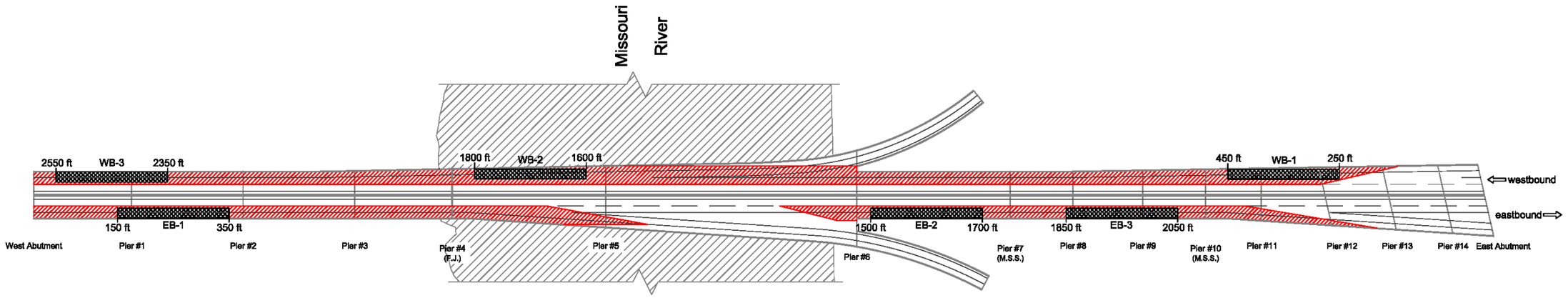

Figure 2.1. Plan of I-129 Missouri River Bridge.

Figure 2.2. Mechanical sounding.

Figure 2.3. Removal of concrete core sample.

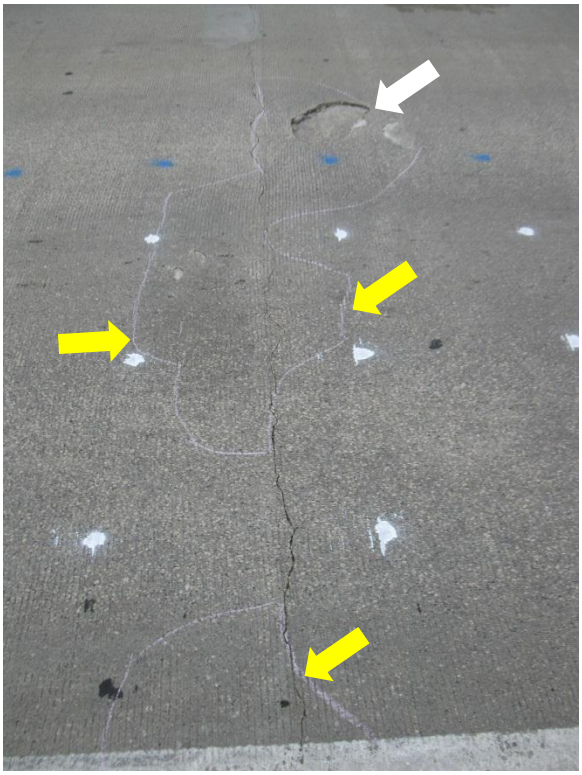

Figure 2.4. Typical delamination (highlighted with chalk) of concrete at a crack. Surface spalling is also visible (white arrow).

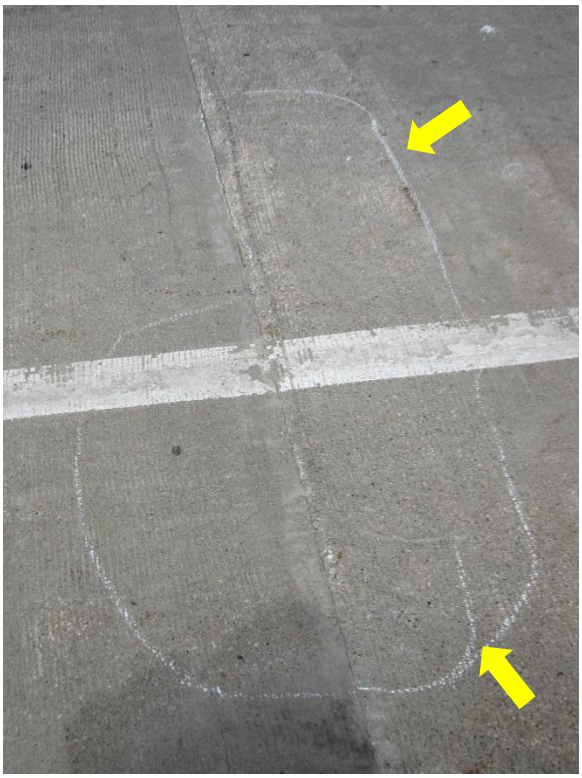

Figure 2.5. Delamination (highlighted with chalk) of concrete at a construction joint in overlay.

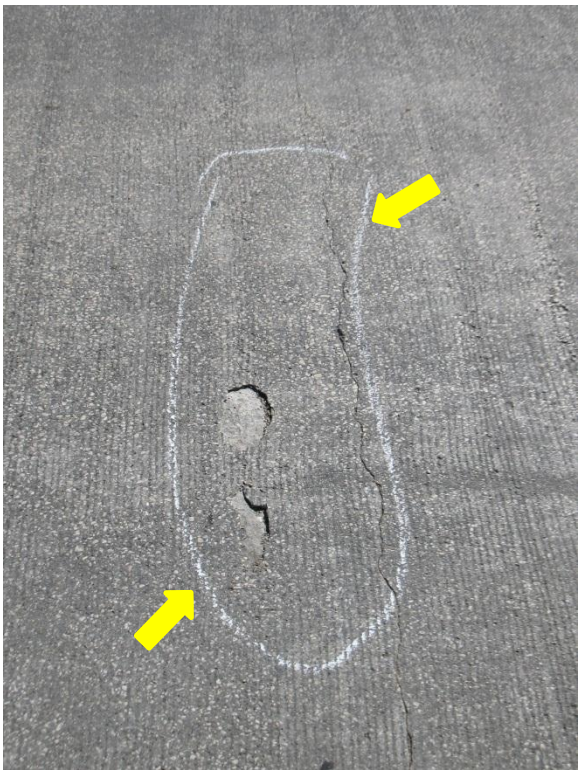

Figure 2.6. Delamination (highlighted with chalk) of concrete on one side of crack.

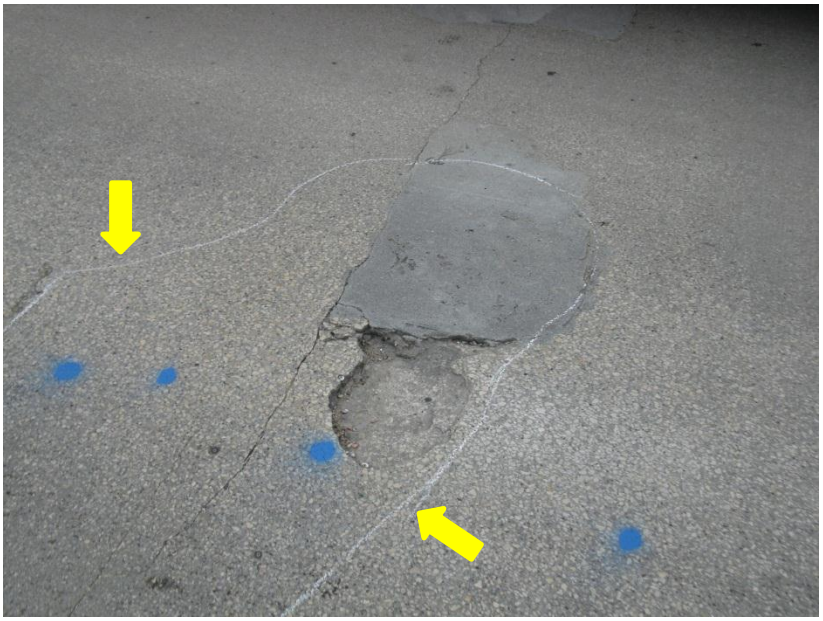

Figure 2.7. Existing concrete patch repair and cracking of deck. Note adjacent spall and new delamination (arrows) outlined in chalk.

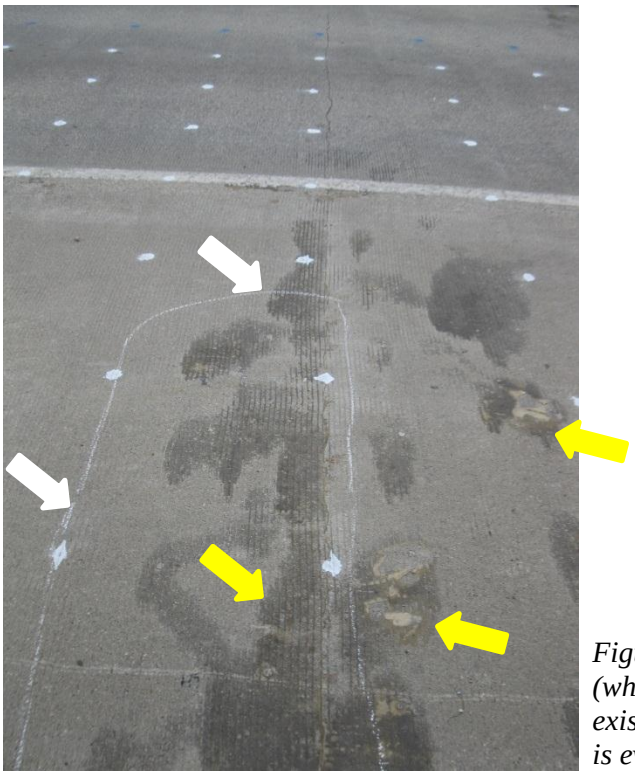

Figure 2.8. Delamination of surface concrete (white arrows) along crack where evidence of existing epoxy injection repairs (yellow arrows) is evident.

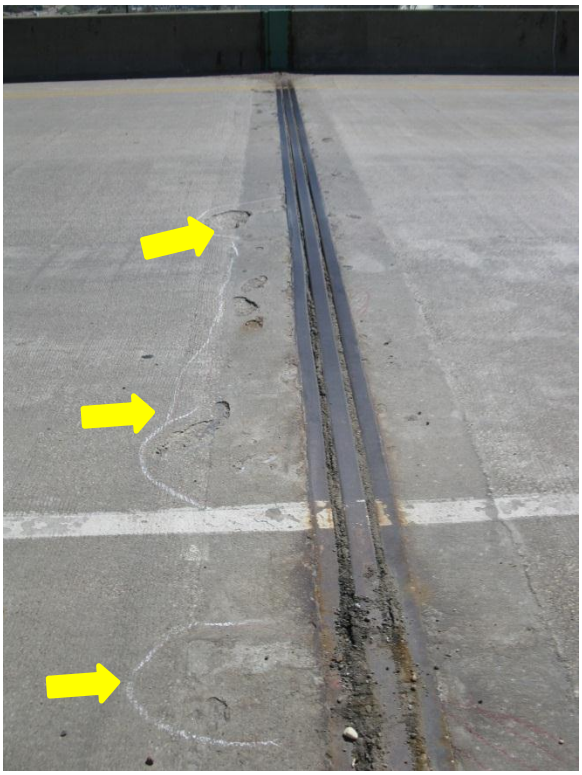

Figure 2.9. Typical delamination of concrete deck surface (highlighted in chalk) near a modular expansion joint seal system.

Figure 2.10. Delamination in shoulder (highlighted in chalk). Note epoxy injection resin on the surface.

Core sections separated to show both faces of core at delamination plane.

Core positioned upside

Figure 2.11. Core sample with evidence of horizontal cracking/delamination along the plane of reinforcement due to corrosion of the reinforcing. Note smaller coarse aggregate in overlay visible in bottom photograph.

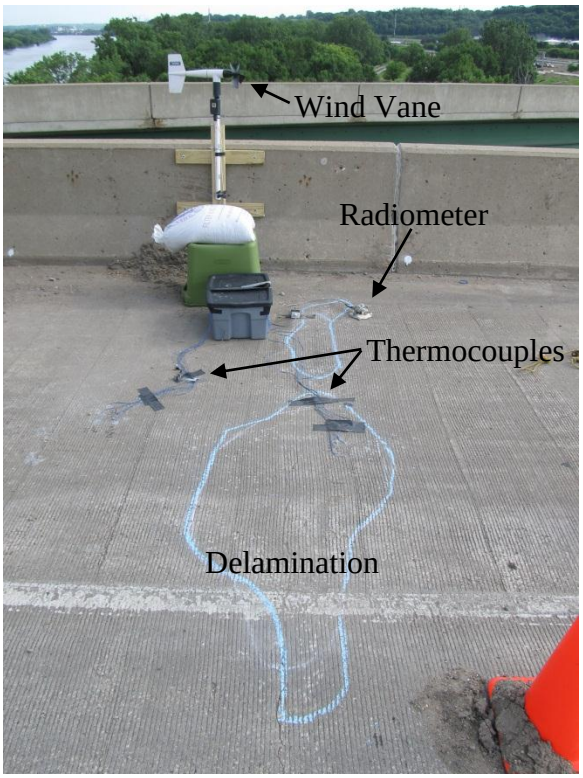

Figure 3.1. Weather station installed at a known delamination for monitoring local weather conditions.

Figure 3.2. Truck equipped with infrared camera, optical camera, and encoder wheel for measuring distance travelled.

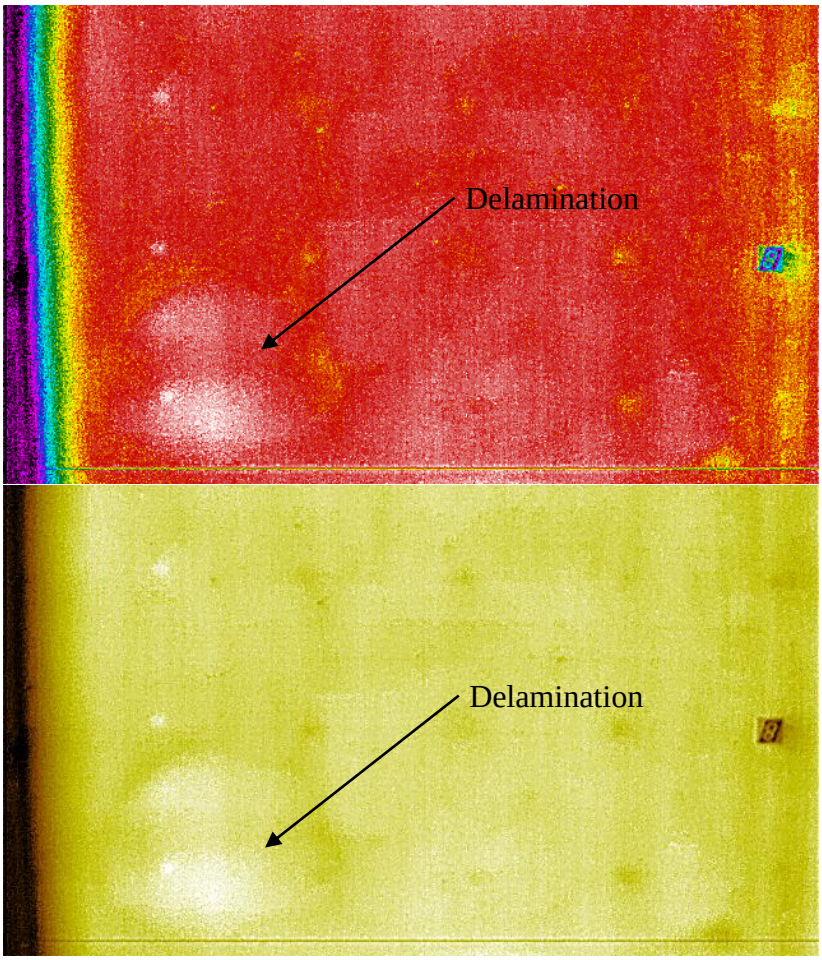

Figure 3.3. Sample infrared image, filtered using the rainbow (top) and sepia (bottom) palettes with upper and lower temperature bounds separated by 18°F (10°C). A delamination is present in the lower left corner of the image (arrow).

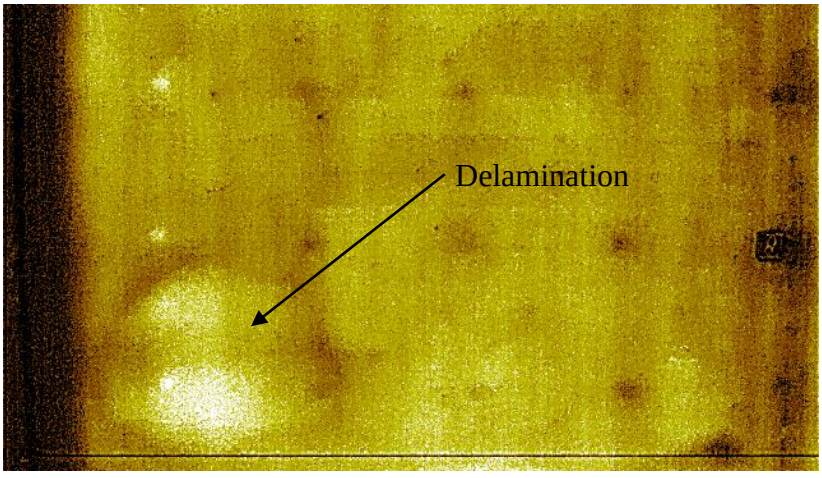

Figure 3.4. Same infrared data as shown in Figure 3.3, filtered using the sepia palette with upper and lower temperature bounds separated by 7.2°F (4°C).

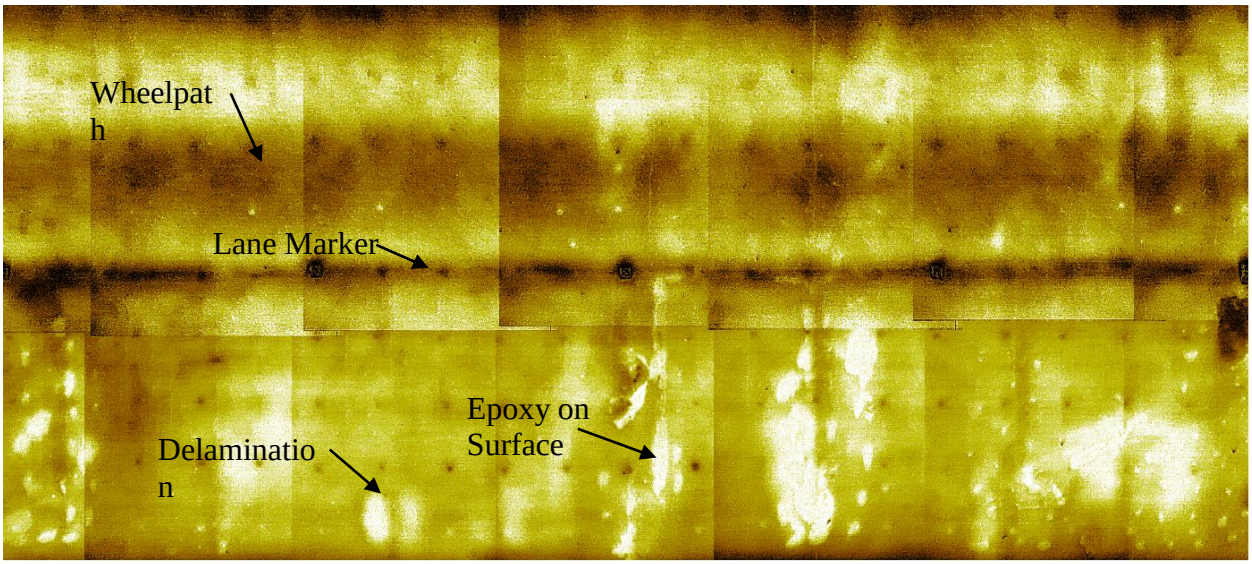

Figure 3.5. Sample bridge deck map of a 40-ft length of the shoulder (bottom) and right-most lane of the eastbound traffic direction. Bright, white spots are indicative of higher temperature resulting from delaminations, epoxy on the deck surface, or other variations in the color of the deck surface. Dark areas are indicative of wheelpaths, lane markers, and other light-colored areas of the deck.

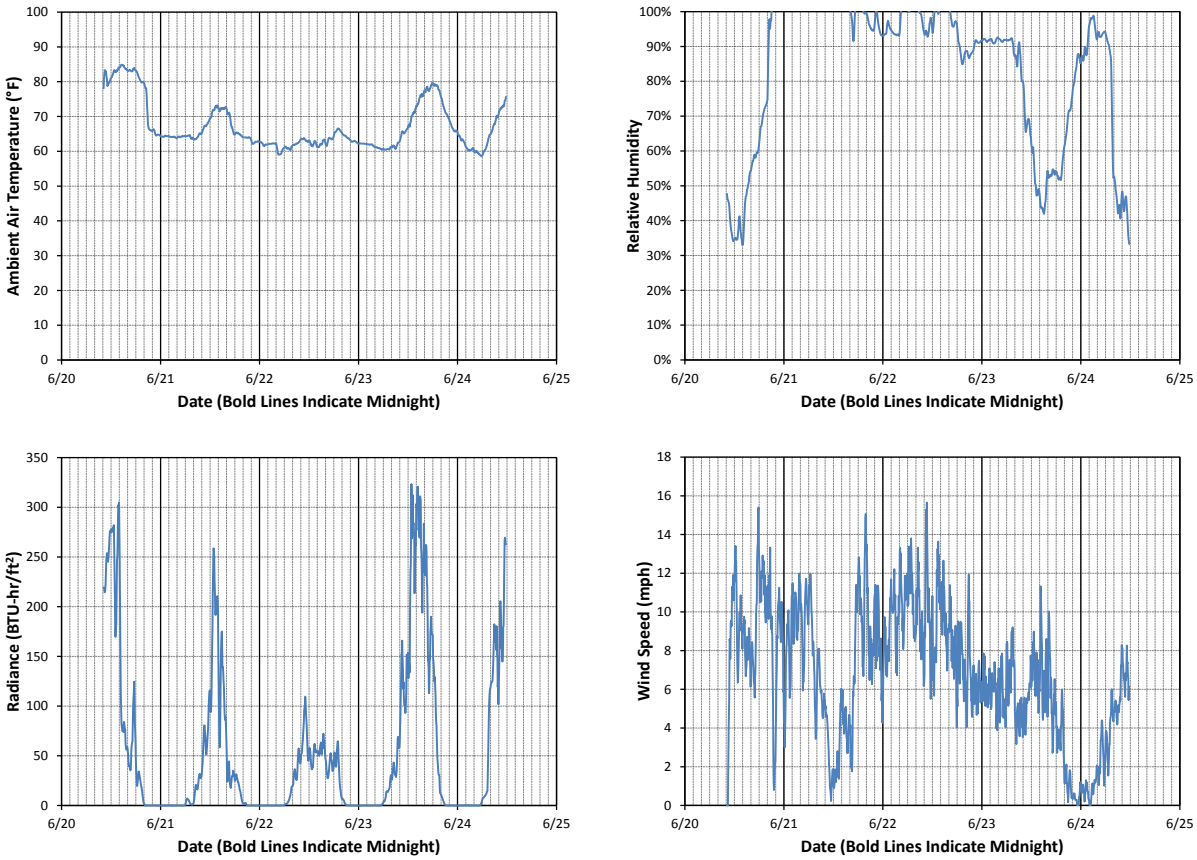

Figure 3.6. Local weather conditions recorded by the installed weather station for June 20-24, 2011.

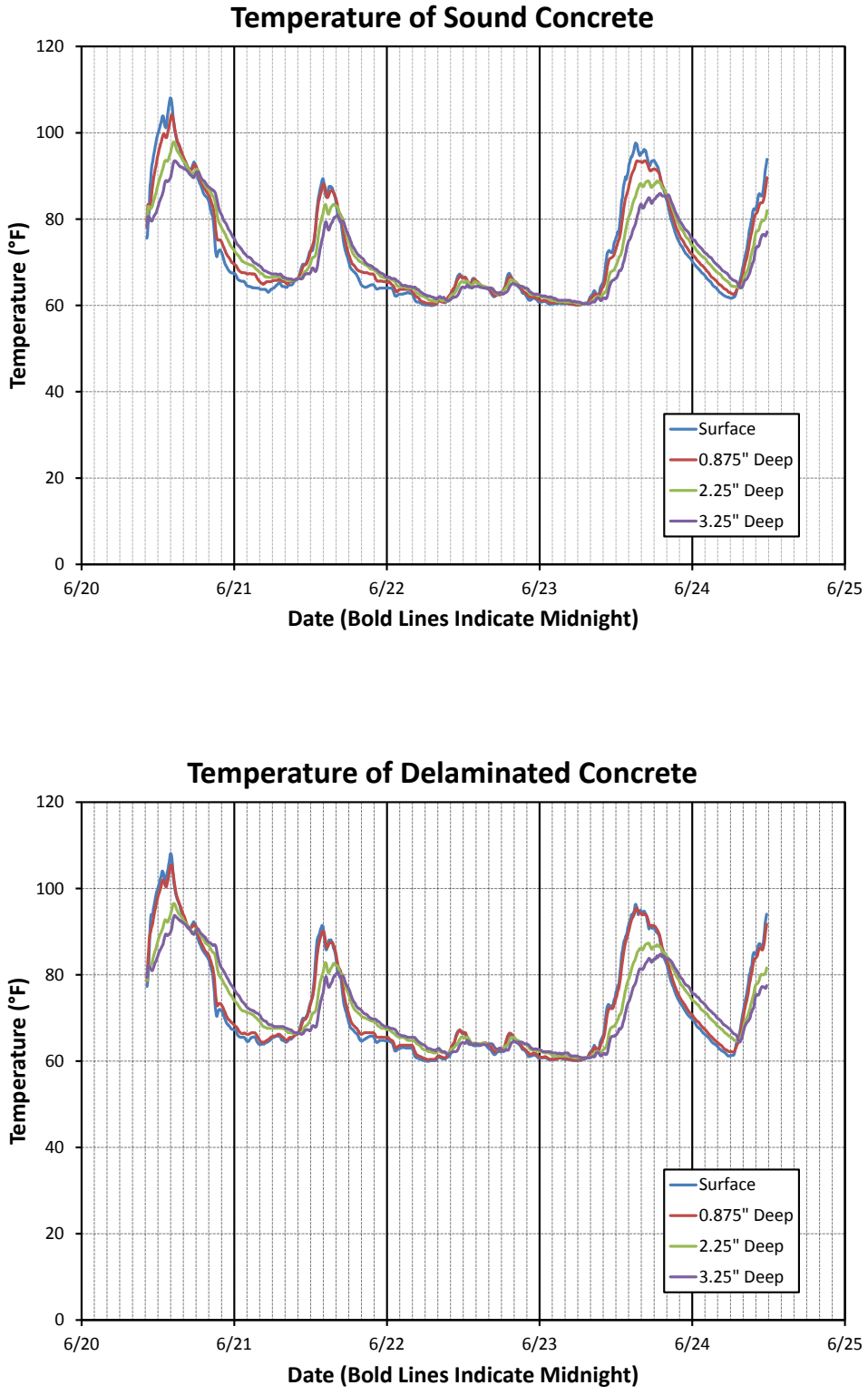

Figure 3.7. Temperature of sound (top) and delaminated (bottom) concrete at the surface and at various depths. The delamination is approximately 1 in. thick at the location of temperature measurement.

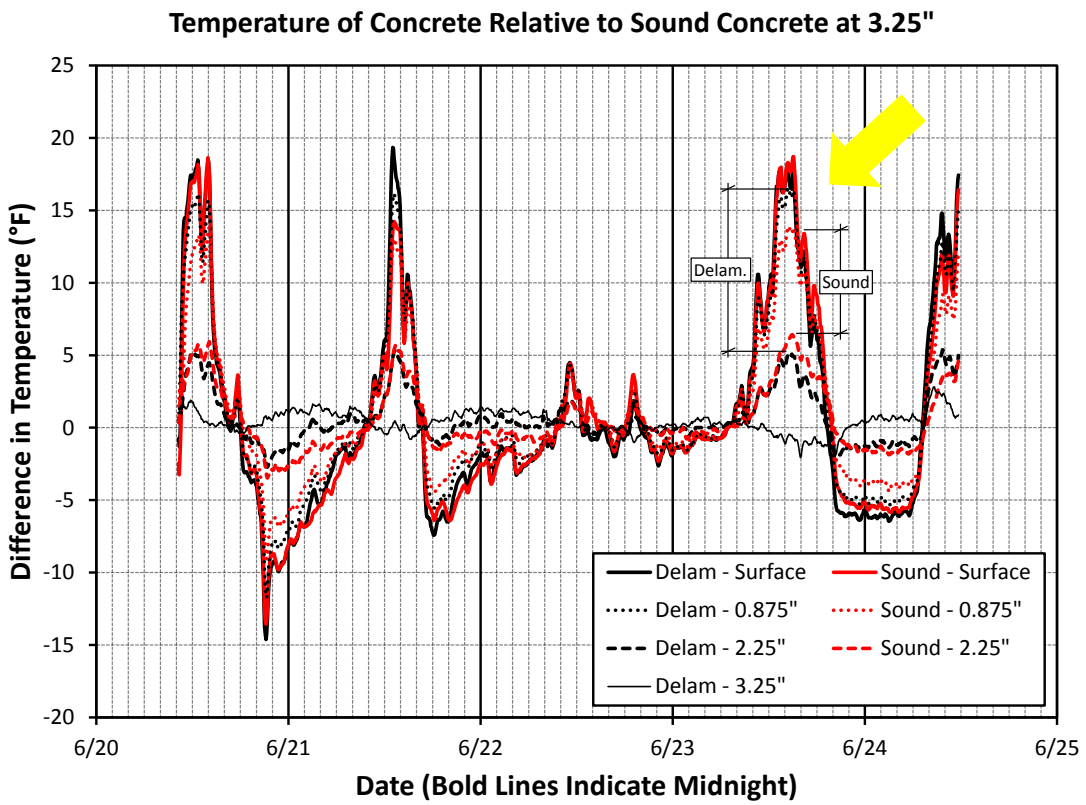

Figure 3.8. Difference between concrete temperatures measured at various depths in the sound and delaminated concrete compared to the temperature of the sound concrete at a depth of 3.25 in. The variance between the temperature differences in the sound and delaminated concrete at 0.875 in. and 2.25 in. on the afternoon of June 23 is specifically called out; the larger difference in the delaminated concrete is typical.

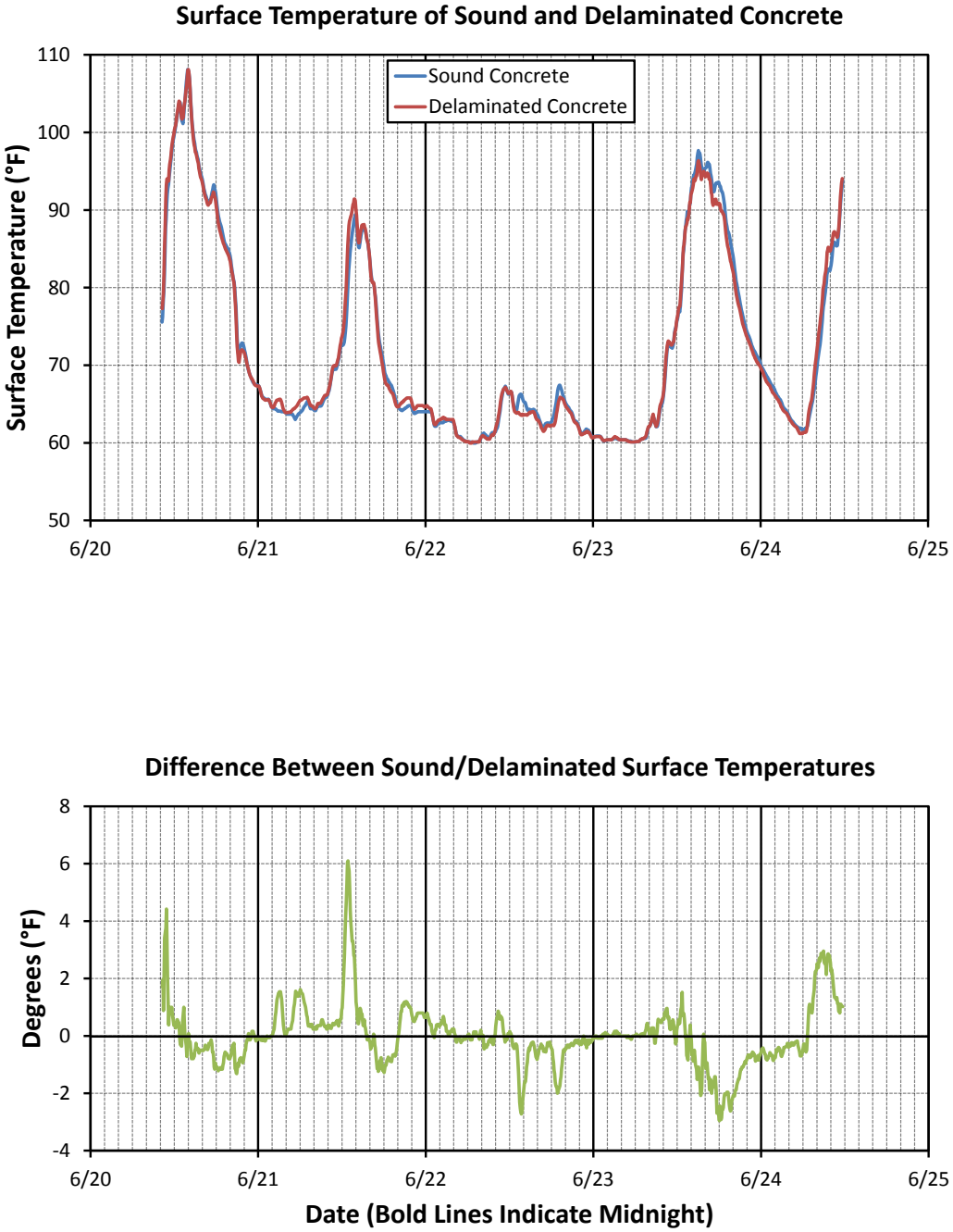

Figure 3.9. Surface temperature of sound and delaminated concrete (top); difference between the surface temperature of the sound and delaminated concrete (bottom).

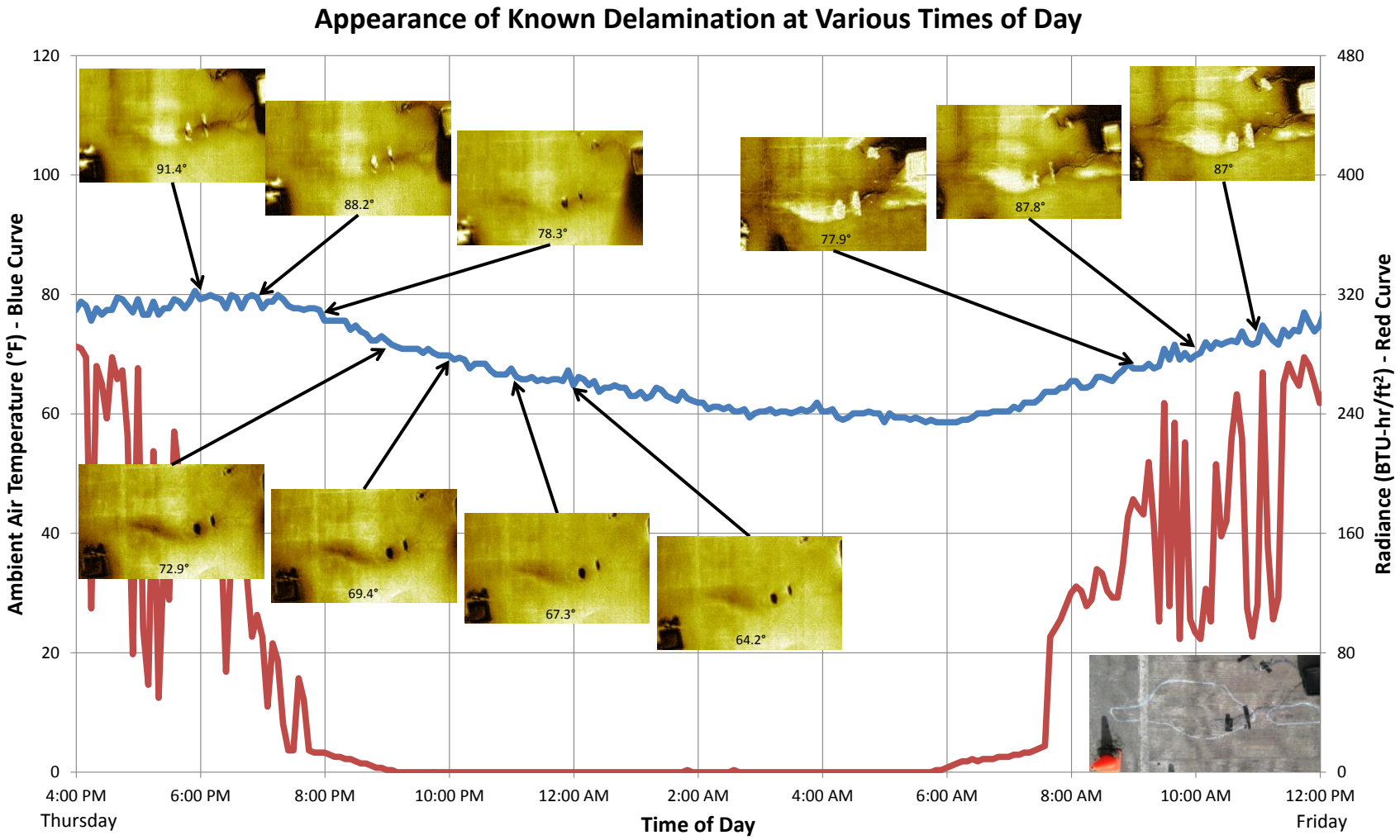

Figure 3.10. Appearance of known delamination at the installed weather station over a 20-hour period, plotted with ambient air temperature and solar radiance. The temperature of the surface of the delamination is indicated on each image. The visual appearance of the delamination outlined in blue chalk is shown in the lower right. Some of the dark or light features in the image result from items on the deck, such as a traffic cone and tape fixing the thermocouple wires in place.

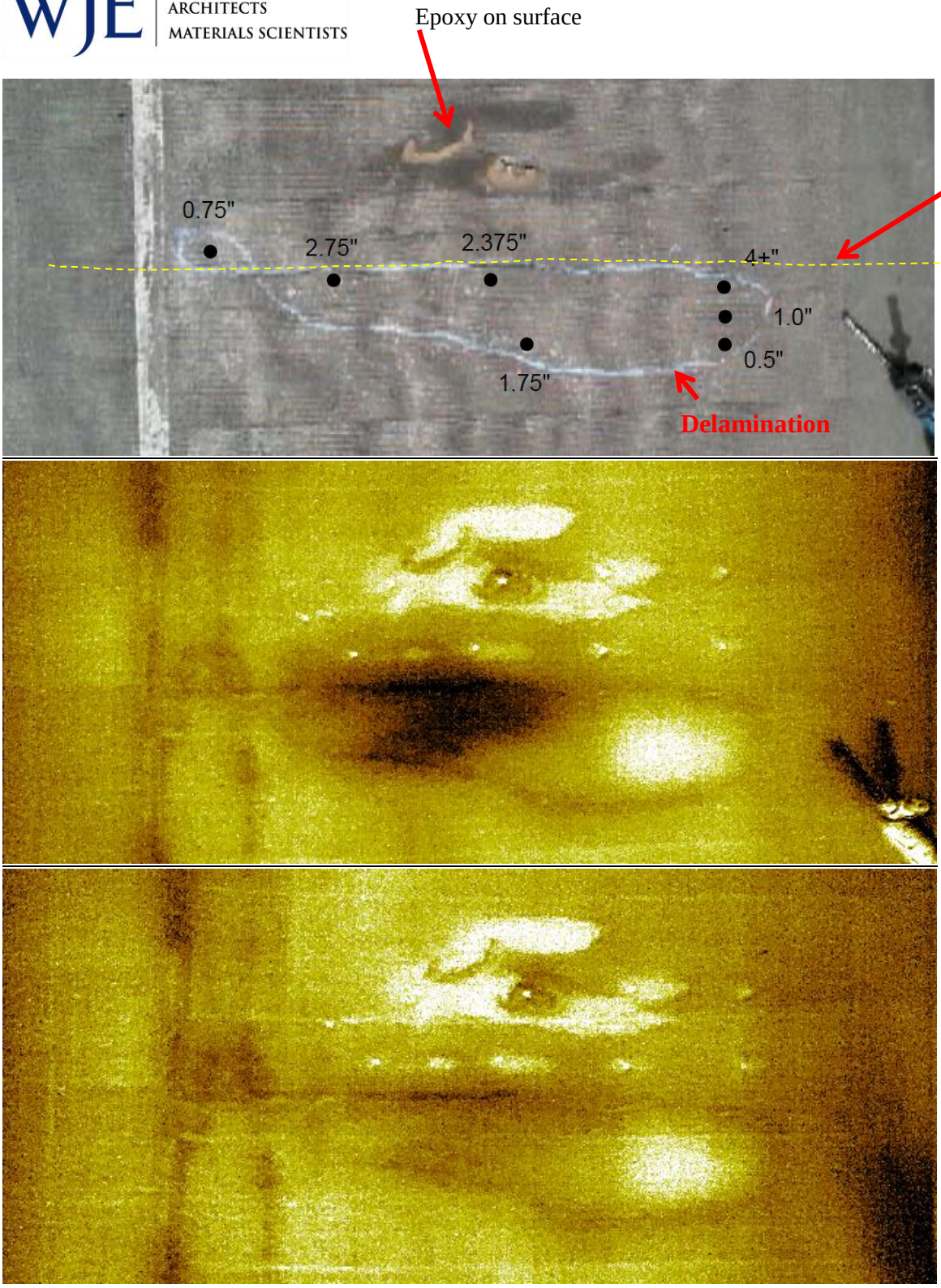

Figure 3.11. Study of depth of delamination in westbound lanes: photo of marked delamination with results from drilling indicating depth of delamination and crack location (highlighted in yellow); infrared image taken at 9:30 am on June 24; infrared image taken at 10:30 am on June 24 (top to bottom).

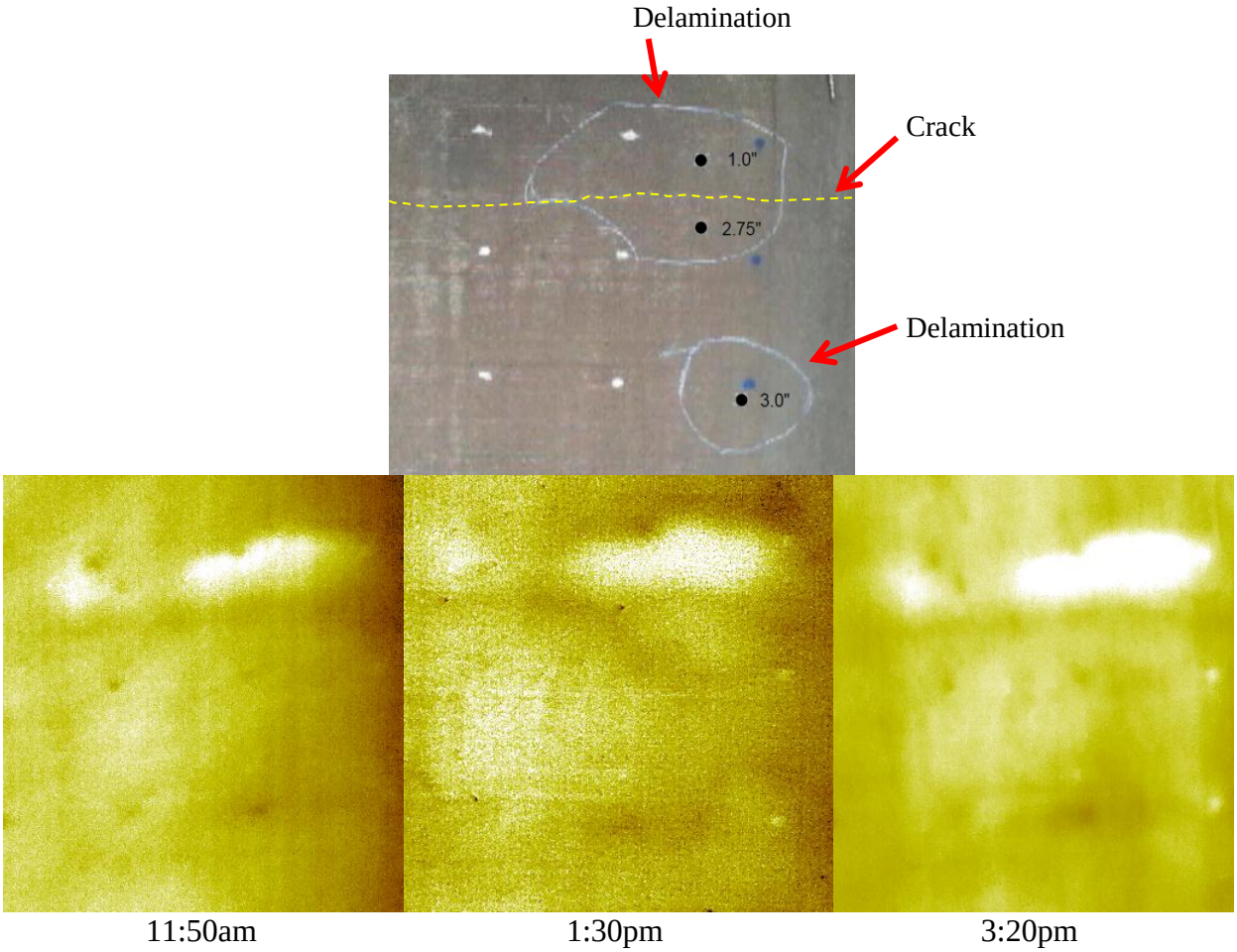

Figure 3.12. Study of depth of delamination in eastbound lanes: photo of marked delamination with results from drilling indicating the depth of the delamination and crack location (highlighted in yellow, top); infrared images taken at the times shown (bottom). The bright spot observed in the top left of the infrared image is not associated with a delamination, but with a dark spot on the deck surface.

Figure 3.13. Deck surface showing surface texture and color variation between wheelpaths and surrounding deck.

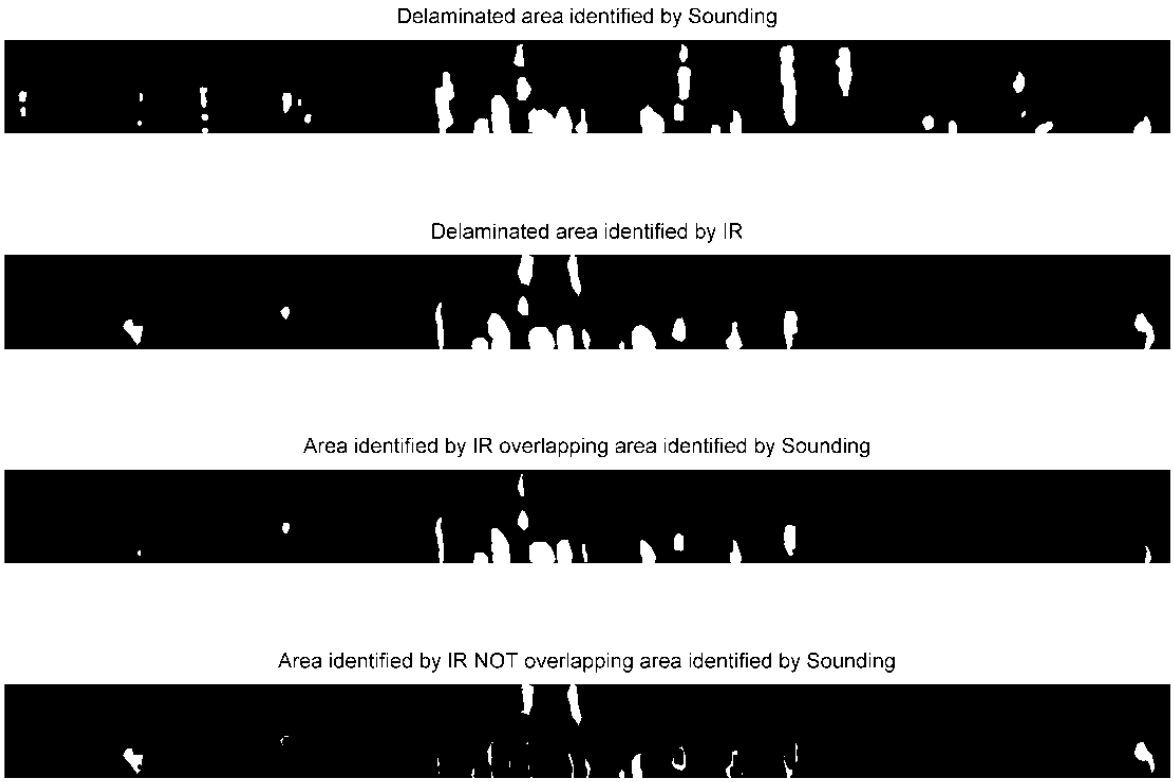

Figure 3.14. Images used to calculate the overlapped and not overlapped area between the delaminated areas identified by IR thermography and sounding surveys (example from Study Area EB-2).

Figure 4.1. GPR data collection within the WB-2 study area using the GSSI Bridgescan system.

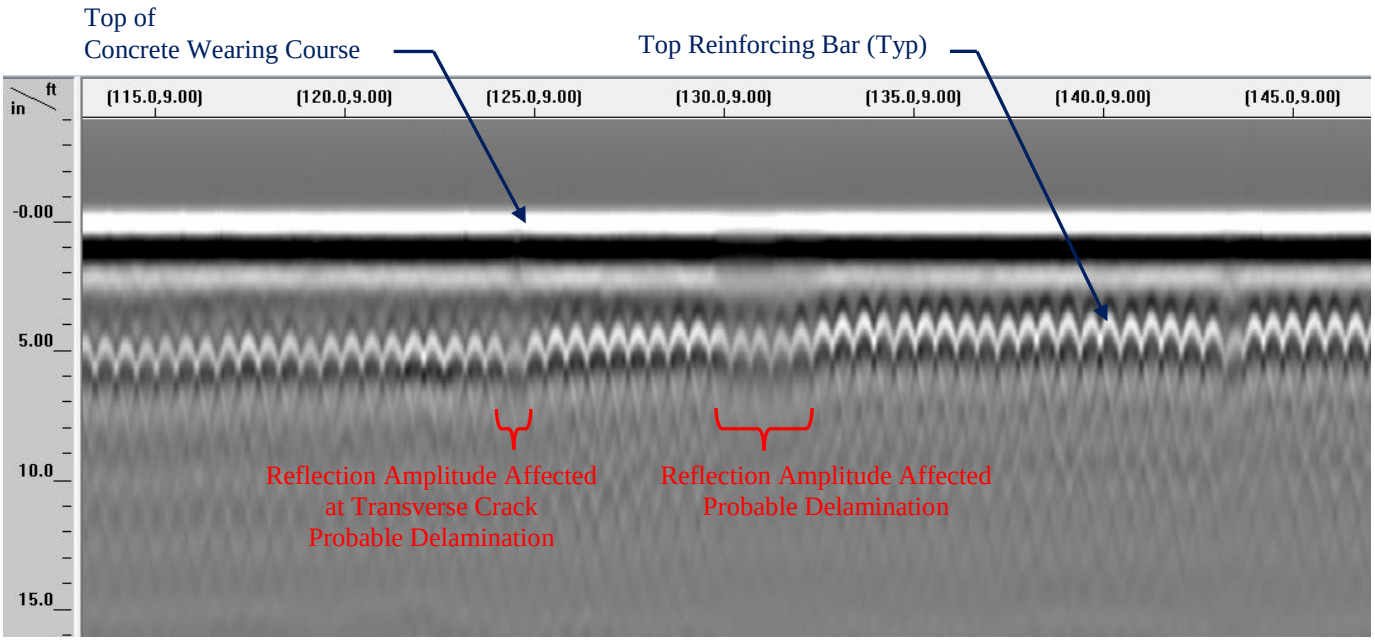

Figure 4.2. Portion of raw GPR data collected within WB-2 study area using 1.6 GHz ground-coupled antenna.

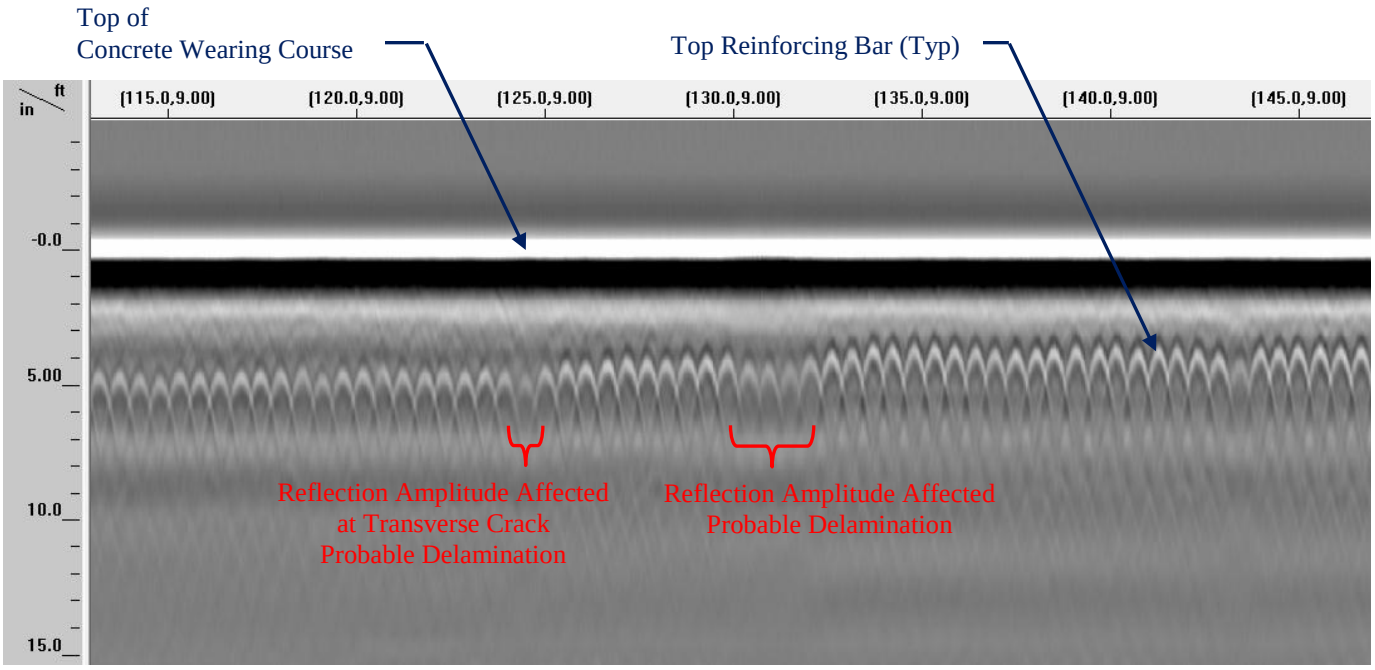

Figure 4.3. Portion of raw GPR data collected within WB-2 study area using 2.6 GHz ground-coupled antenna.

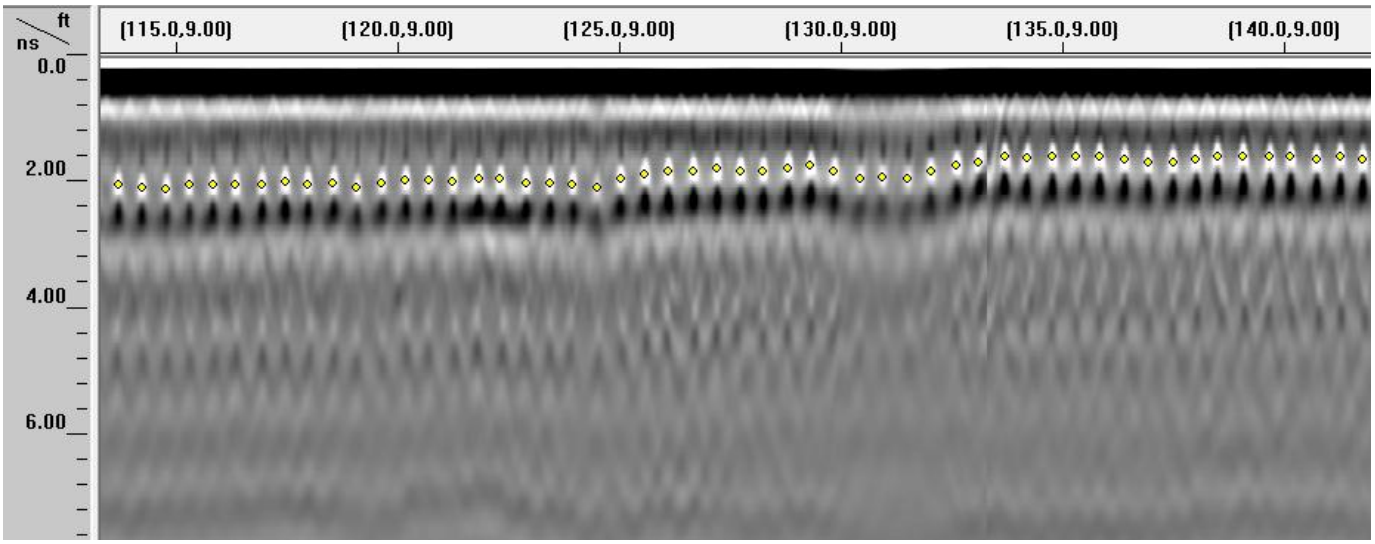

Figure 4.4. GPR data after post-processing and selection of top reinforcing bars. Data collected within WB-2 study area using 1.6 GHz ground-coupled antenna.

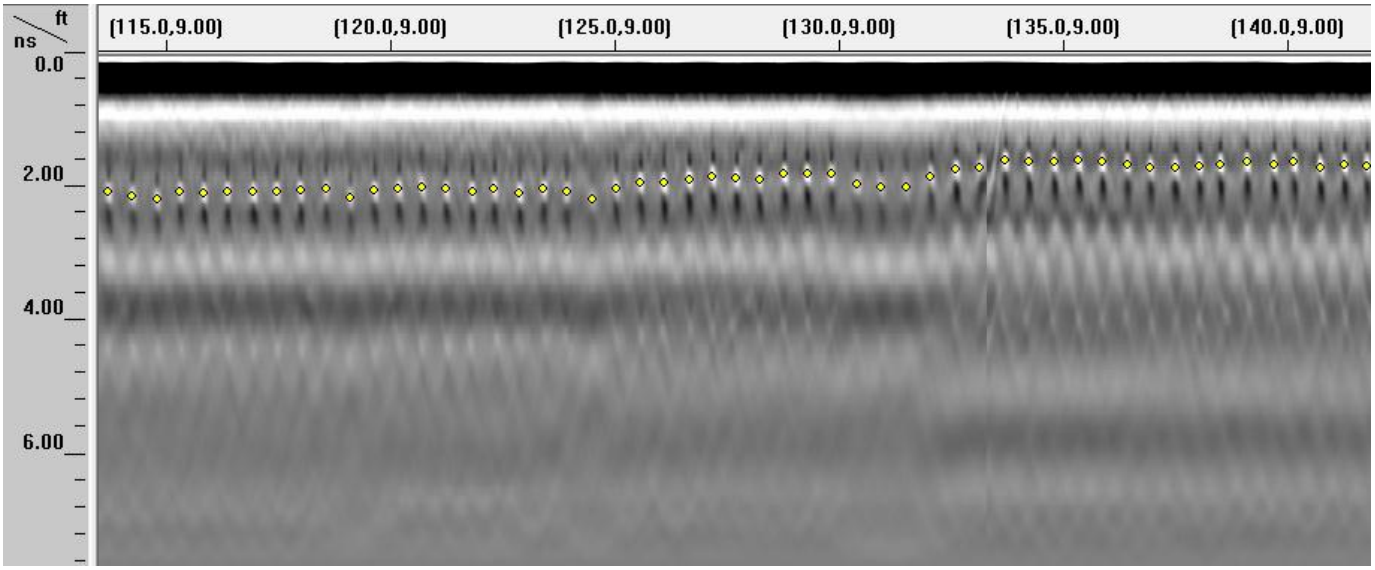

Figure 4.5. GPR data after post-processing and selection of top reinforcing bars. Data collected within WB-2 study area using 2.6 GHz ground-coupled antenna.

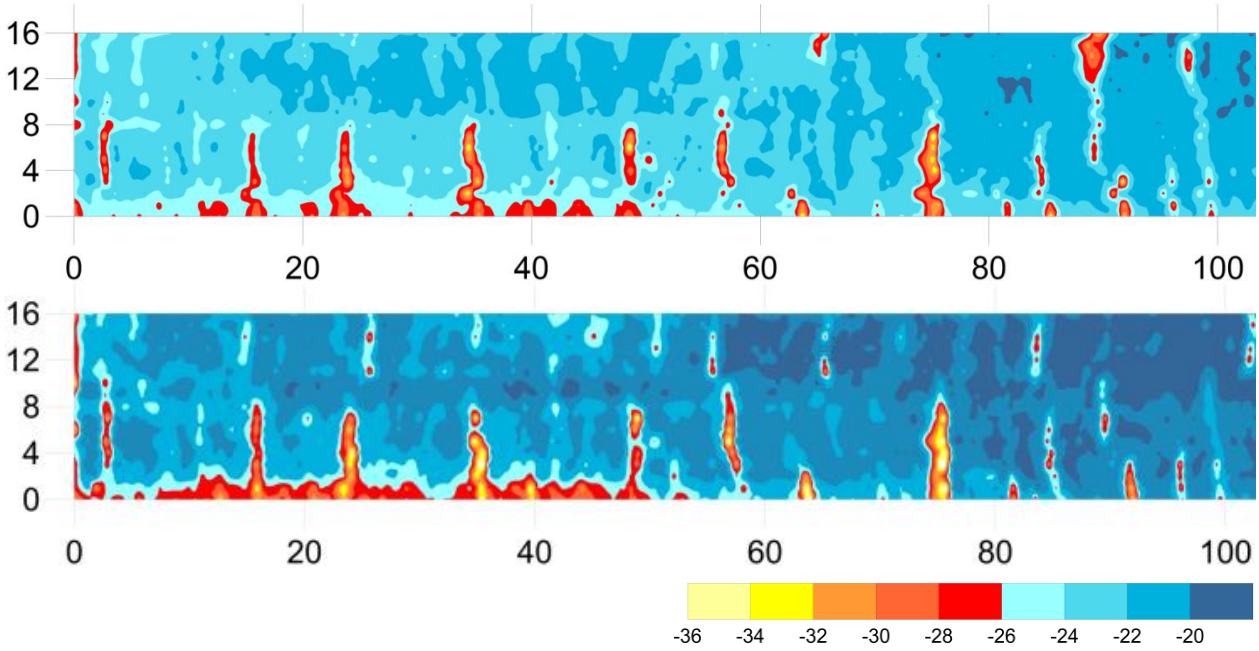

a) Portions of Study Area EB-2; 1.6 GHz Antenna (top) and 2.6 GHz Antenna (bottom)

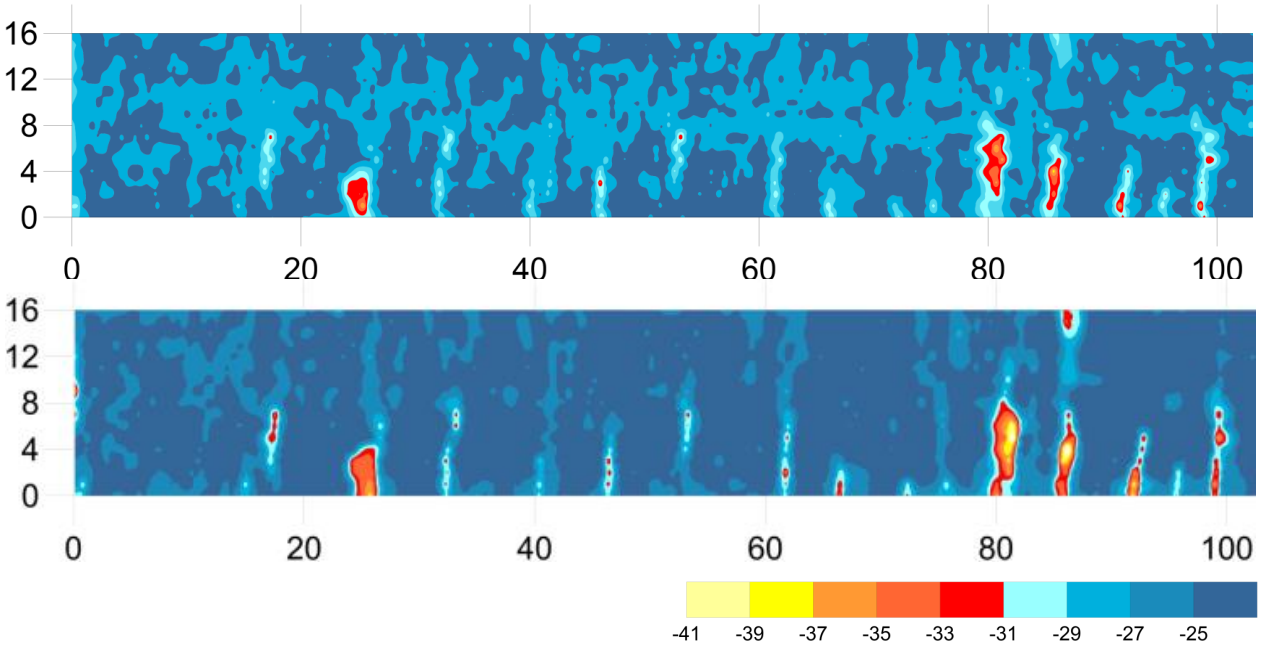

b) Portions of Study Area EB-1 1.6 GHz Antenna (top) and 2.6 GHz Antenna (bottom)

Figure 4.6. Contour plots of reflection amplitude of top transverse reinforcing for portions of Study Areas EB-1 (Figure 4.6a) and EB-2 (Figure 4.6b) using the 1.6 GHz and 2.6 GHz antennas.

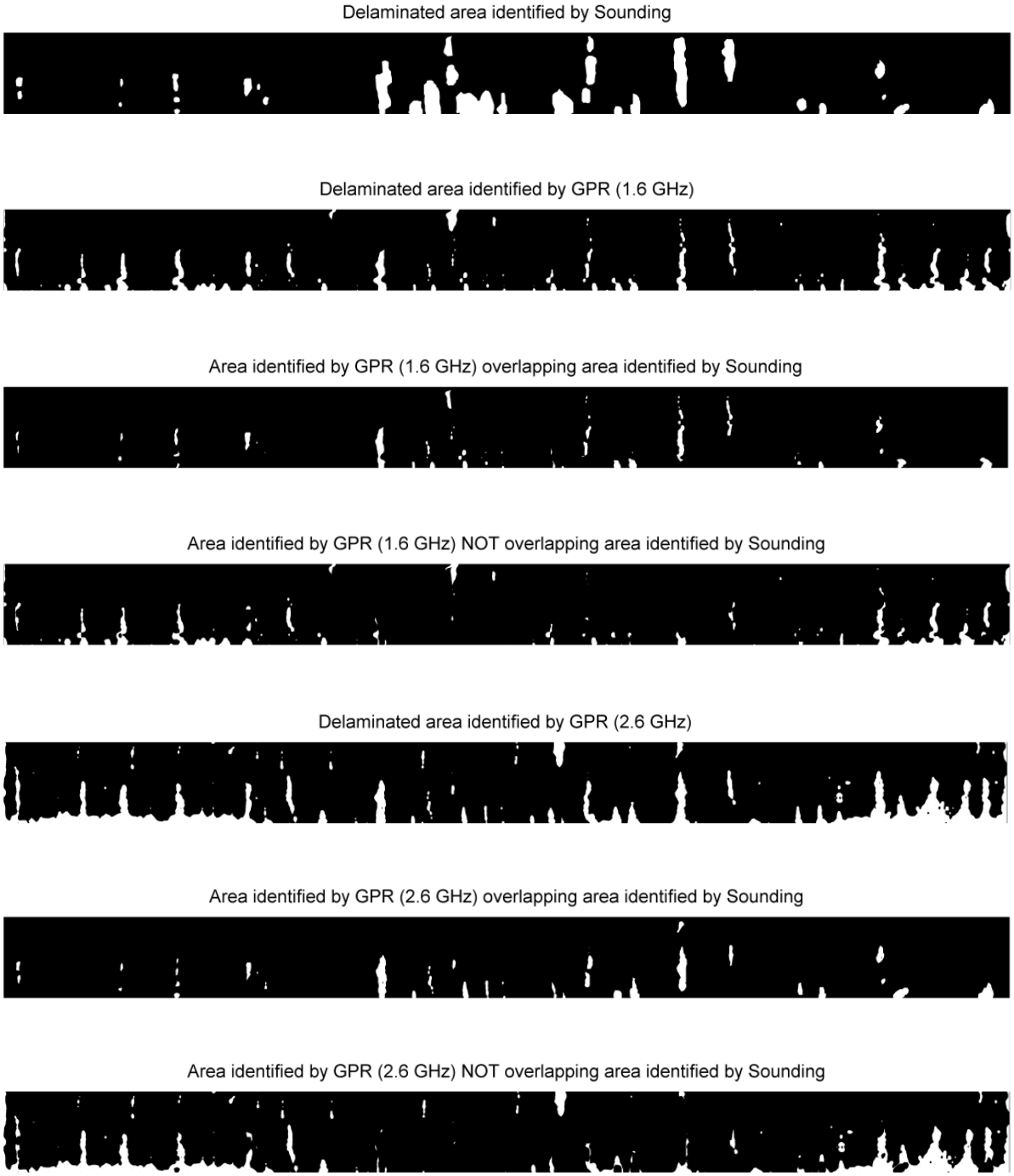

Figure 4.7. Images used to calculate the overlapped and not overlapped area between the delaminated areas identified by GPR based on upper threshold and sounding surveys (example shown from Study Area EB-2).

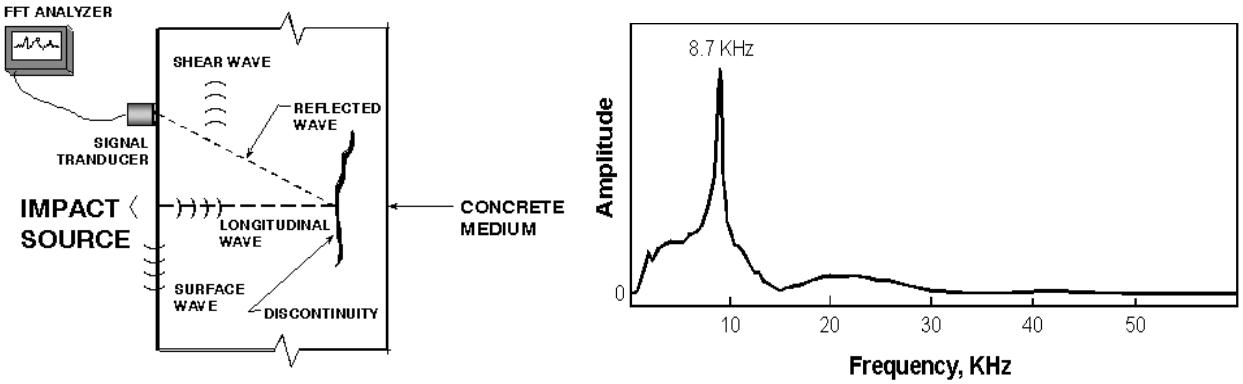

Figure 5.1. Schematic of the Impact-Echo method. The general basis of the method is on the left, and a typical frequency spectrum plot is on the right. The dominant (resonant) frequency is then correlated with deck thickness or delamination depth.

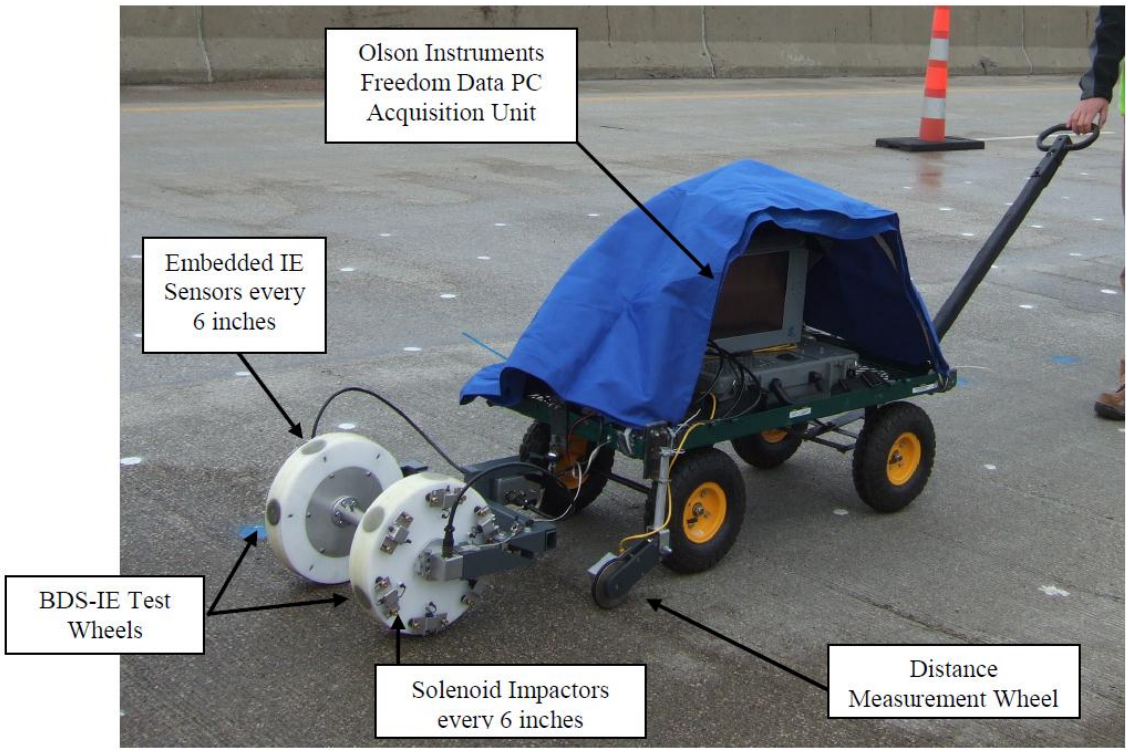

Figure 5.2. Photograph of Olson Engineering's mobile impact-echo system. The data acquisition system was covered with a tarp due to rain.

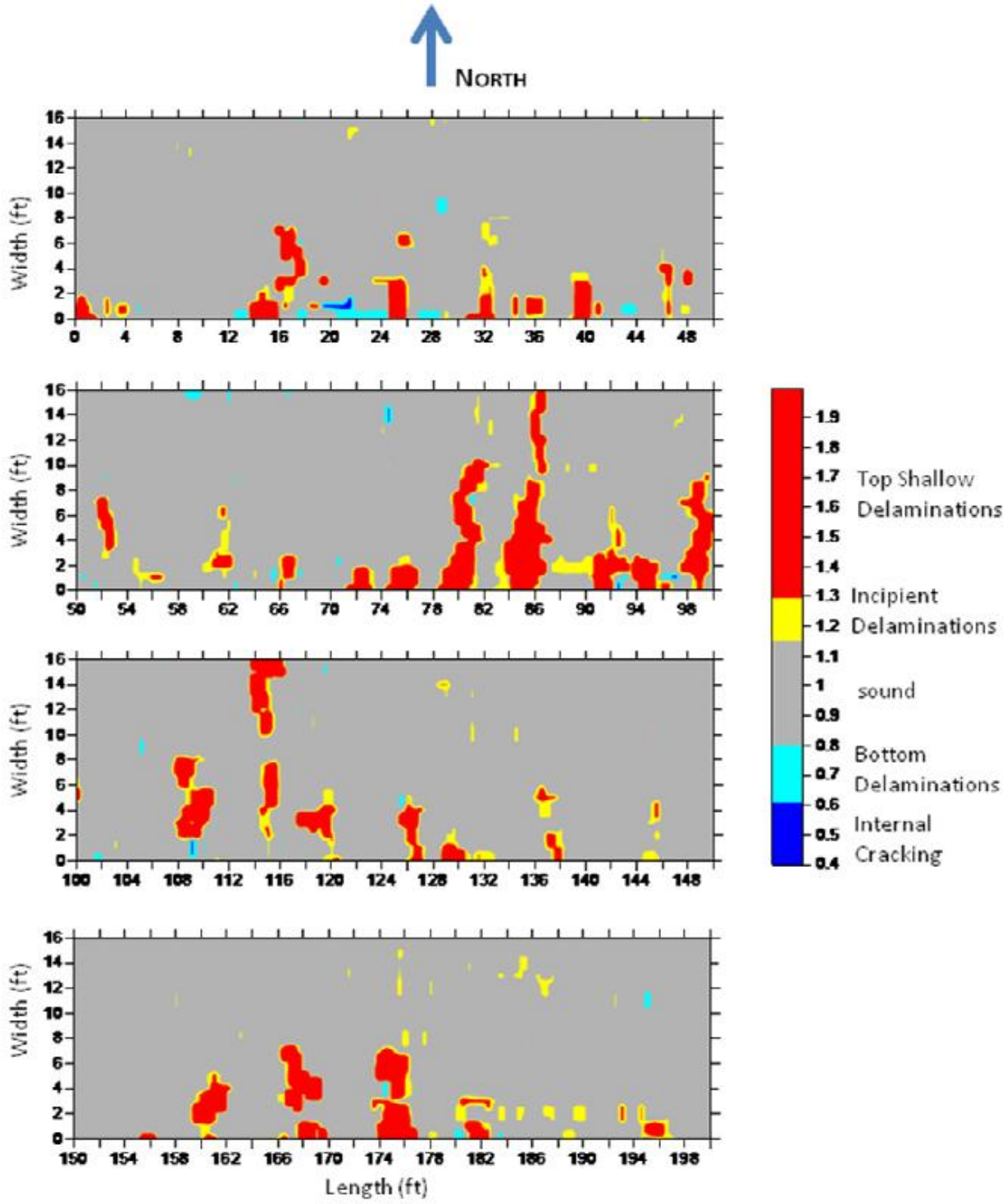

Figure 5.3. Result from Olson scan of in-depth Study Area EB-1, showing areas of concrete delamination near the top deck surface in red.

Figure 5.4. Collection of Impact-Echo data at distinct testing points using single-transducer IE unit.

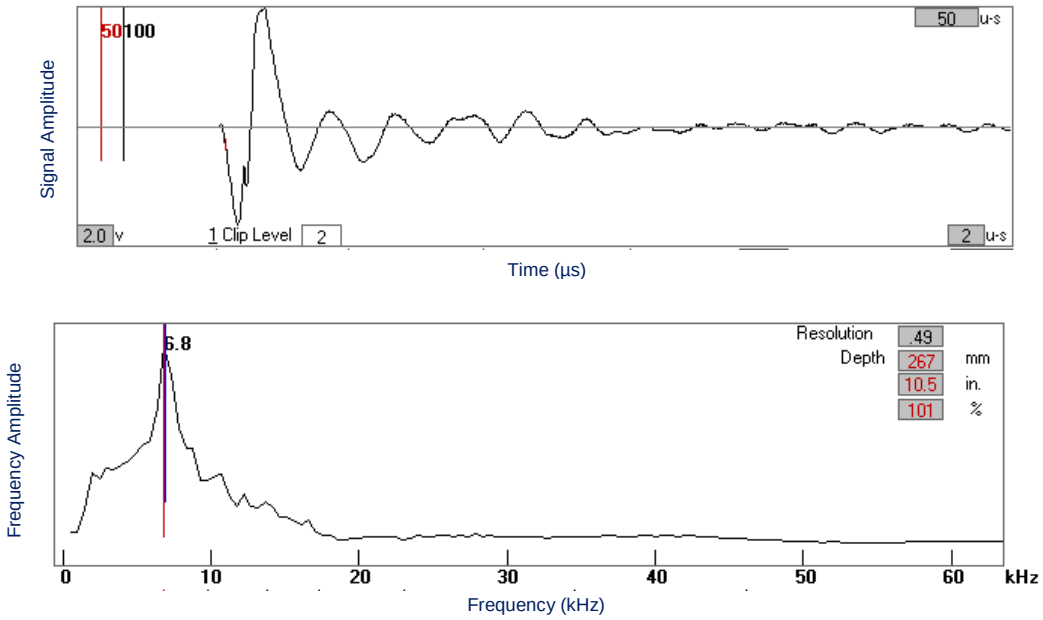

Figure 5.5. IE test result showing a reflection from the bottom of the deck at a depth of 10.5 in. (Study Area EB-1; Station 314).

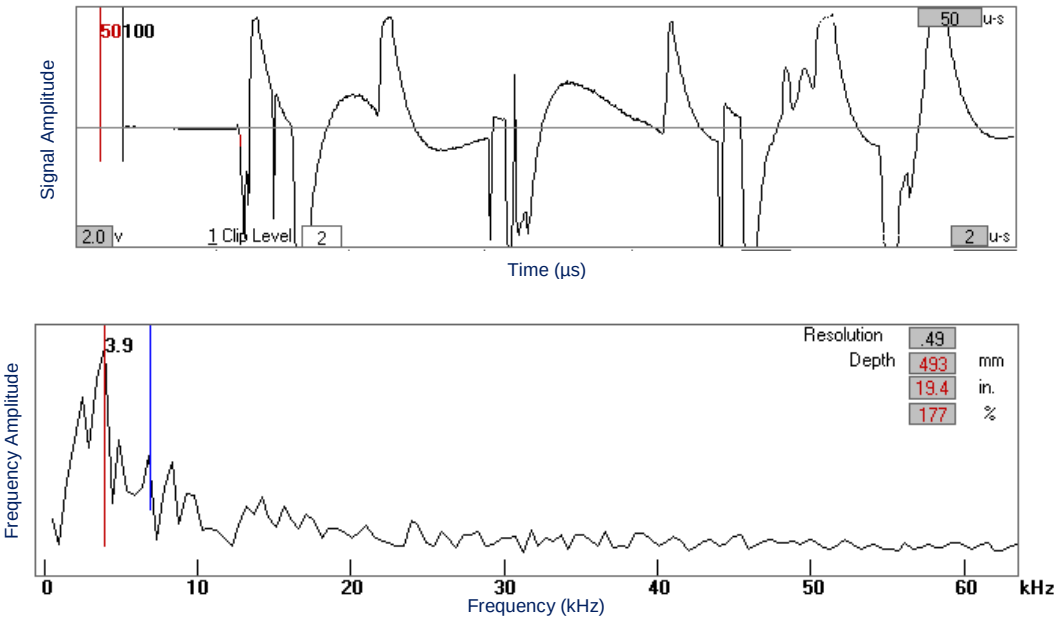

Figure 5.6. IE test result showing a shallow delamination (Study Area EB-1; Station 318).

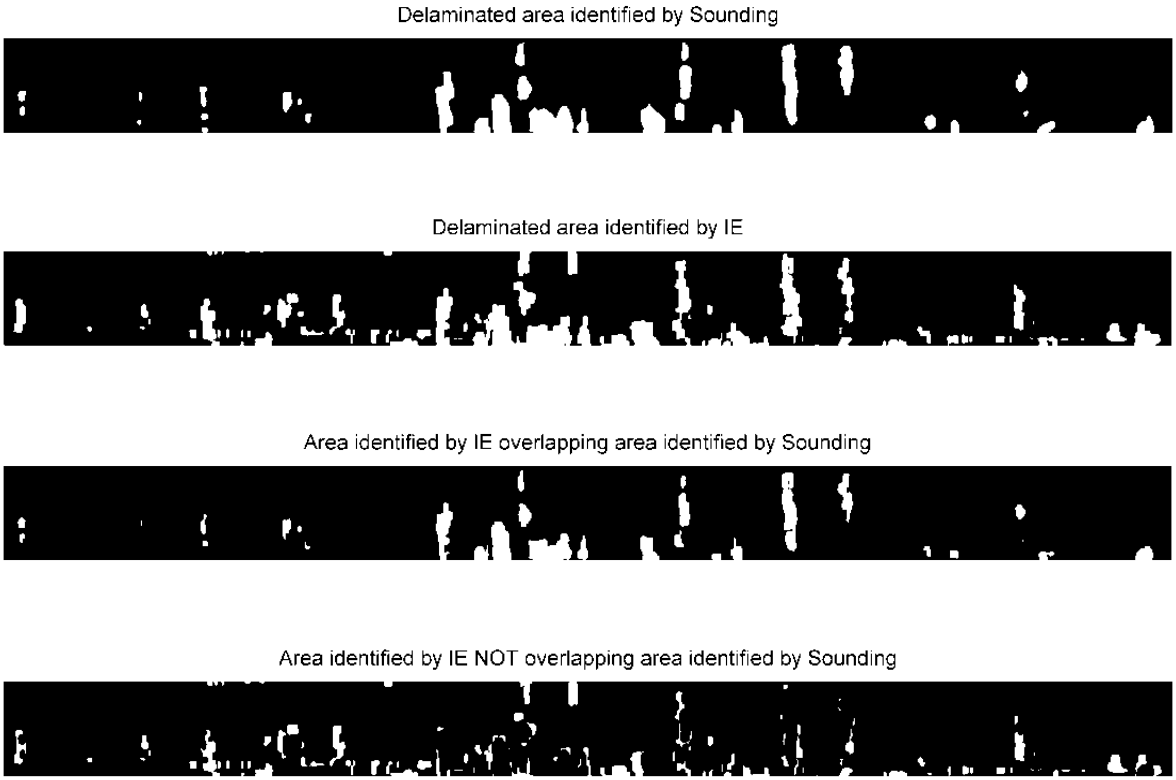

Figure 5.7. Images used to calculate the overlapped and not overlapped area between the delaminated areas identified by Scanning IE and by sounding surveys (example from Study Area EB-2).

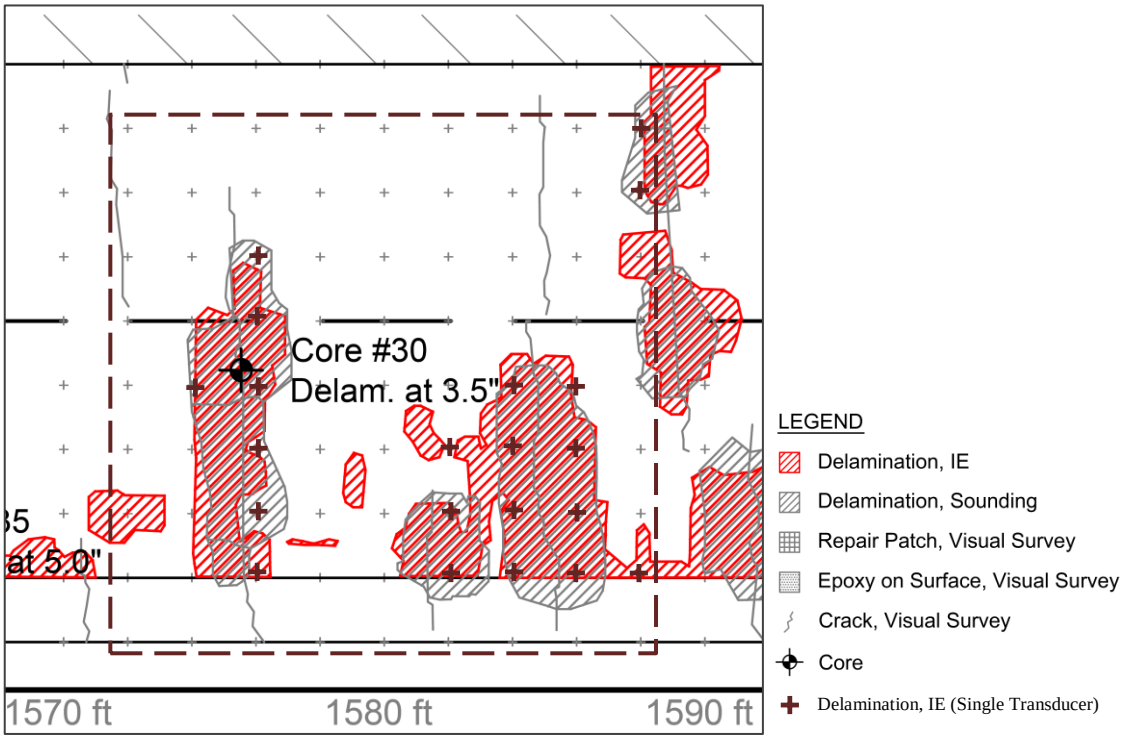

Figure 5.8. Results of single-transducer IE testing (delaminations identified at brown crosses) shown along with results of Scanning IE (hatched red) and sounding at Study Area EB-2 (Station 1572 to 1588).

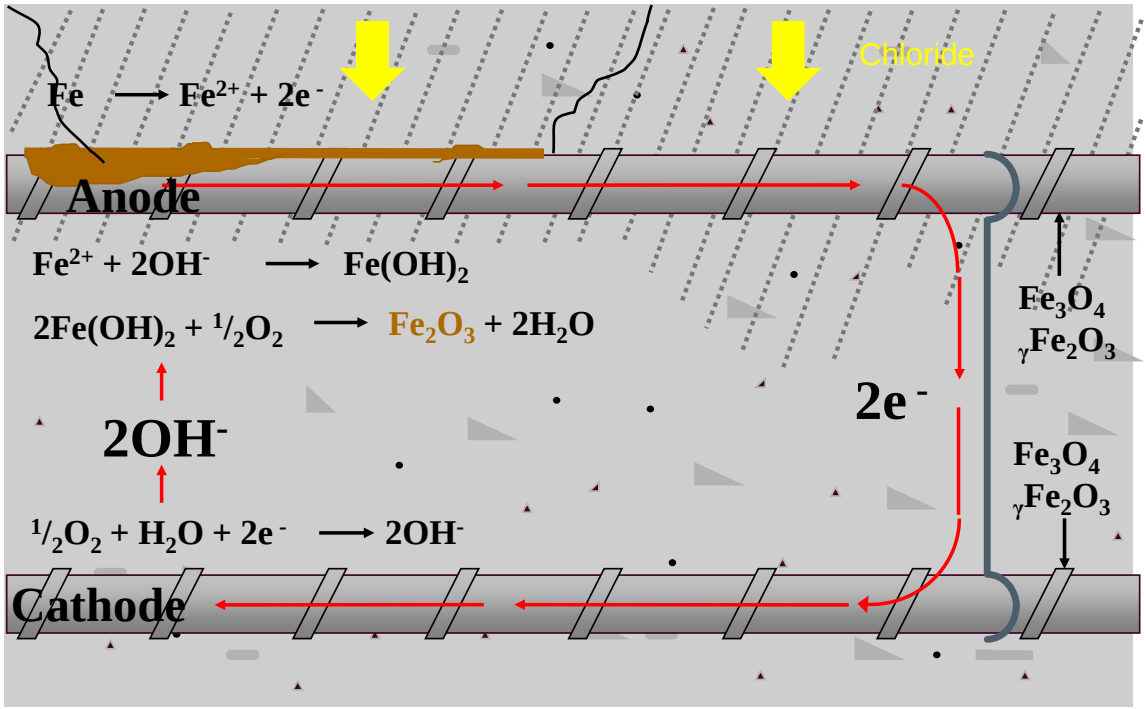

Figure 6.1. Sketch representing corrosion reaction in reinforced concrete.

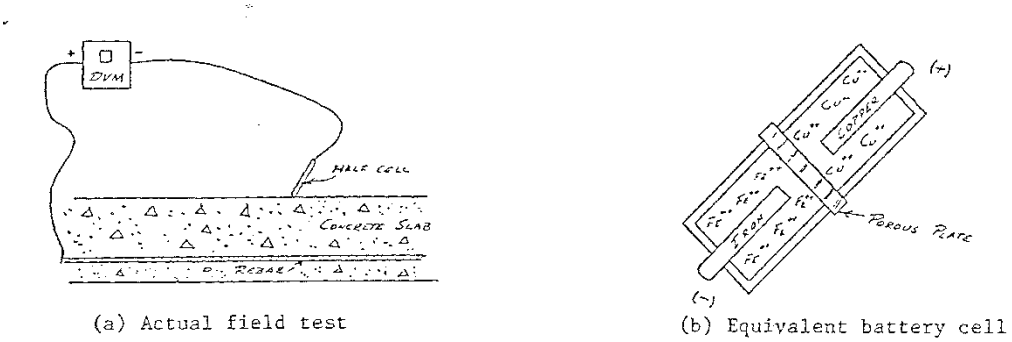

Figure 6.2. Representation of half-cell testing in concrete as equivalent battery cell.

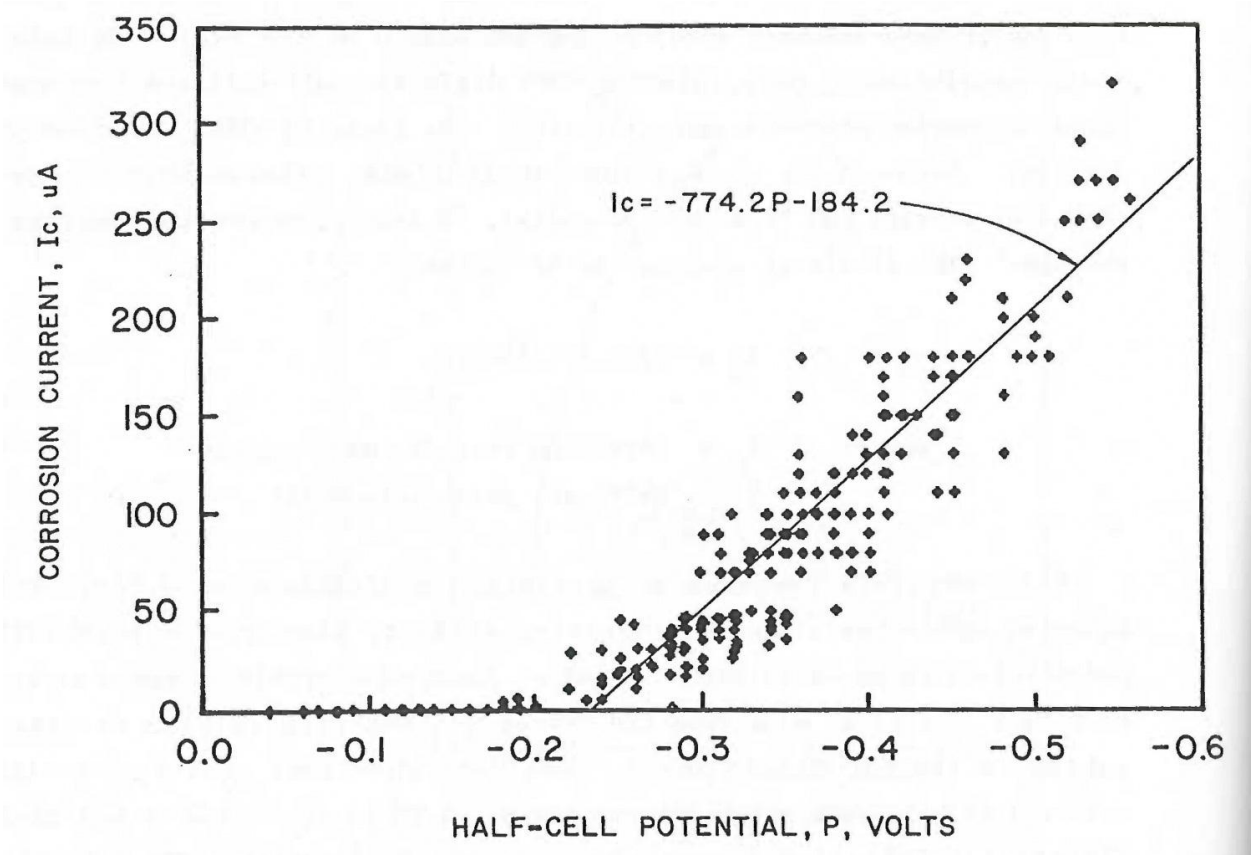

Figure 6.3. Relationship between corrosion current and half-cell potential for specimens with 1-in. cover and 0.50 w/c ratio. Reproduced from FHWA RD-86-93.

Figure 6.4. Rolling cart with five CSEs and datalogger, used for half-cell potential measurements.

Figure 6.5. Measuring half-cell potential using a CSE integrated with a rolling wheel.

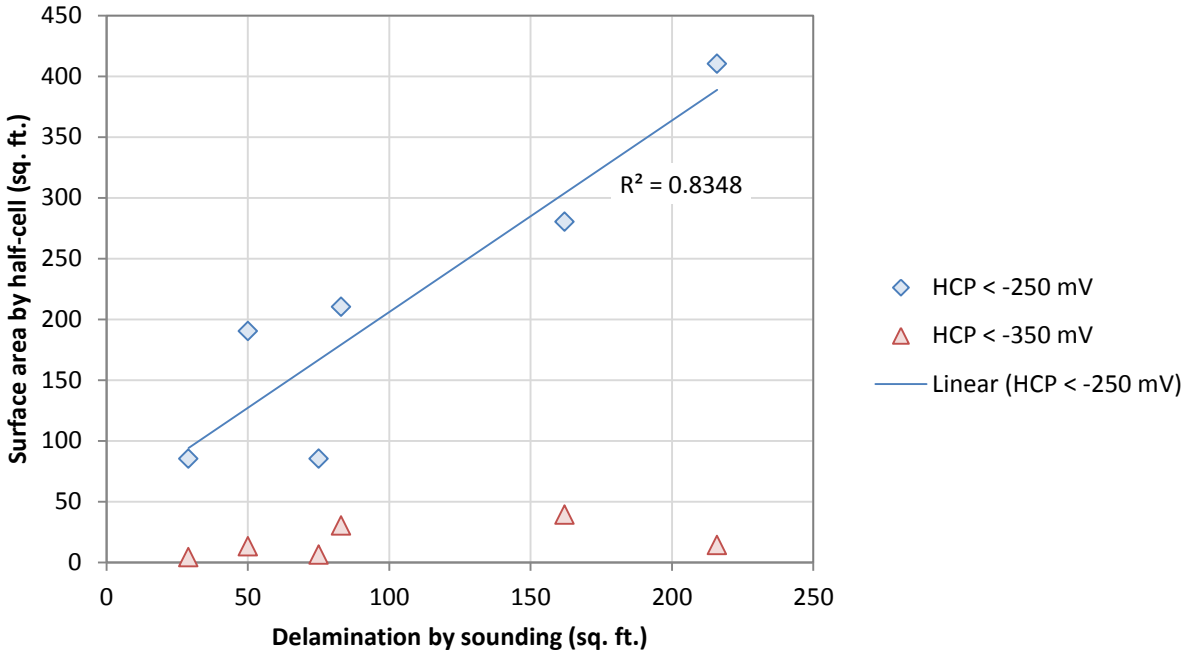

Figure 6.6. Plot of surface area measured by half-cell potential thresholds versus delaminated areas measured by sounding.

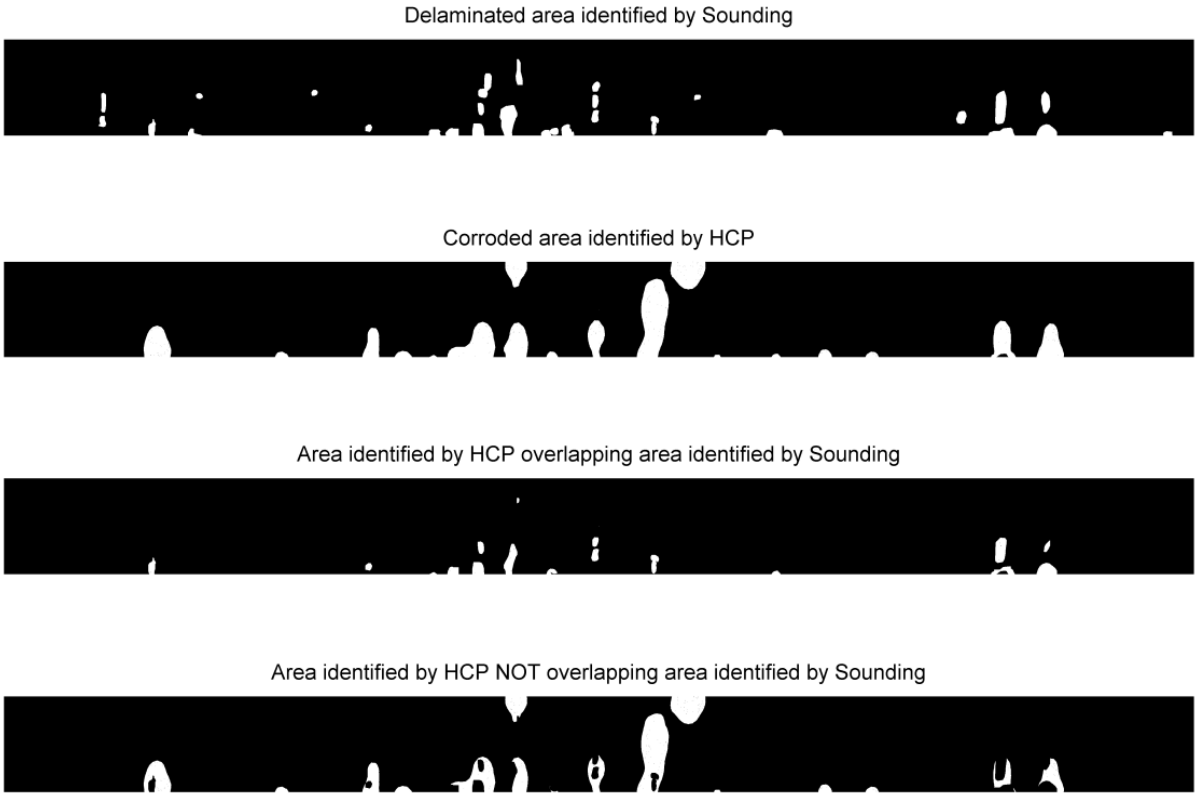

Figure 6.7. Images used to calculate the overlapped and not overlapped area between the delaminated areas identified by sounding and the areas identified by half-cell potential survey threshold of -250 mV vs CSE (example from Study Area EB-1).

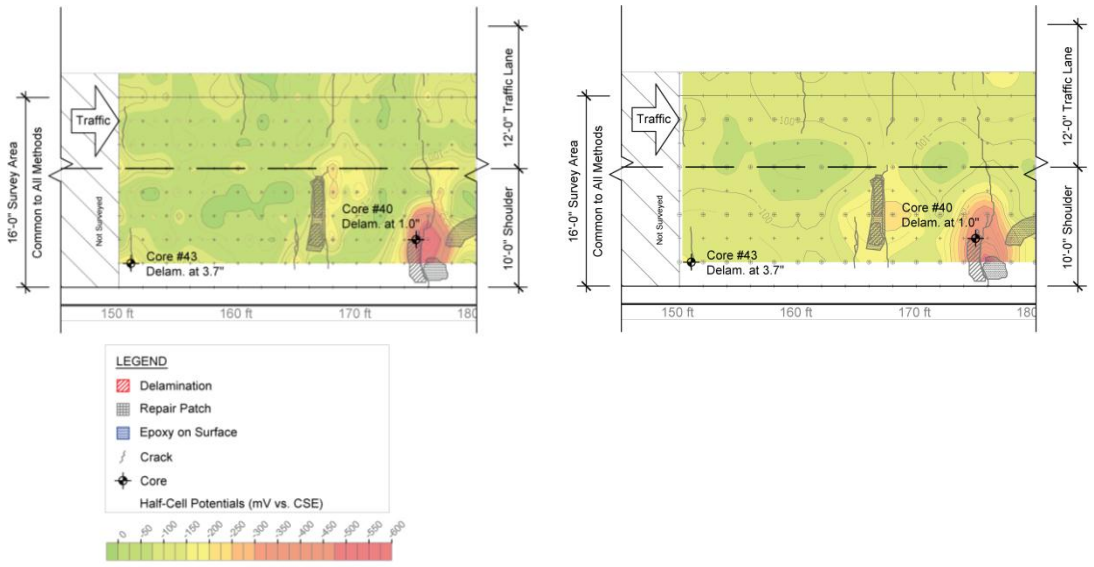

a) Single rolling wheel equipment *b) Rolling cart equipment*

Figure 6.8. Comparison between a) single rolling wheel and b) rolling cart equipment. Note that the elevated corrosion potential at Core #40 is shown in both a) and b), but that the elevated corrosion potential at Core #43 is only resolved in data collected with the single rolling wheel shown in a).

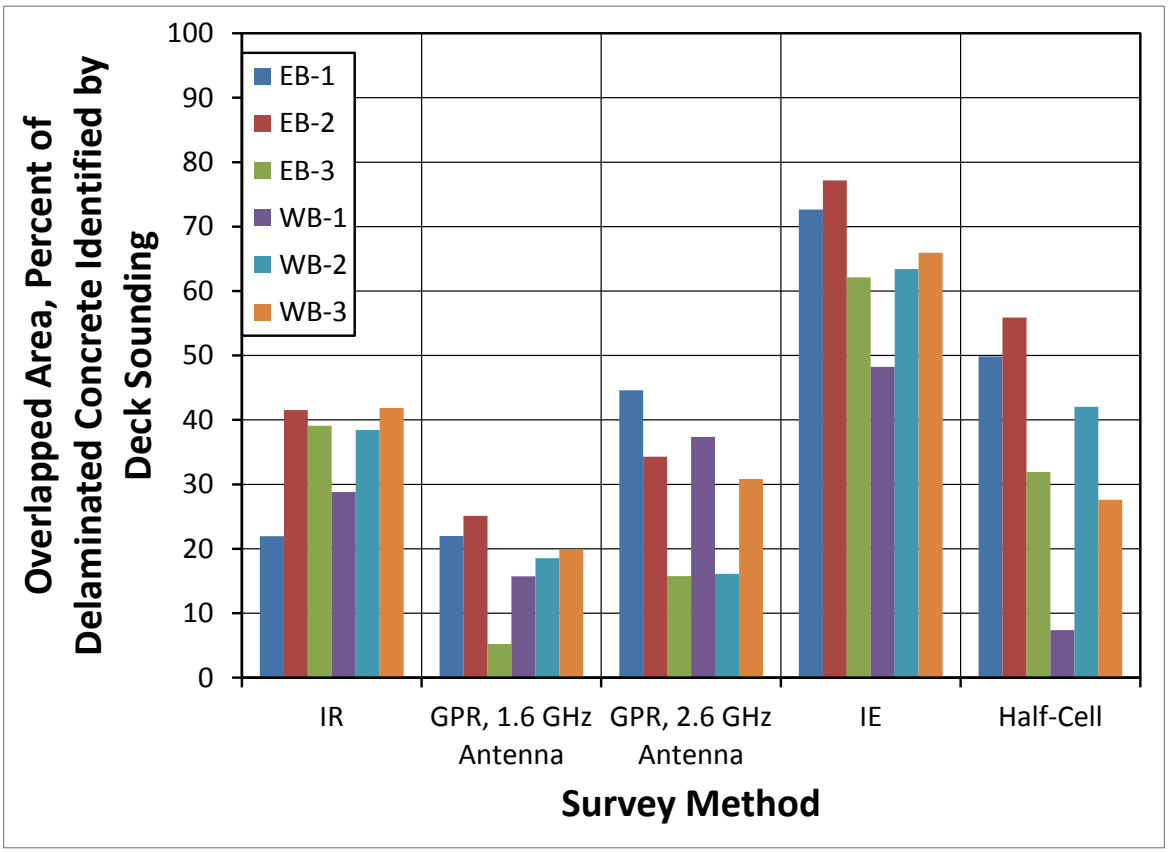

Figure 7.1. Overlap between the areas identified as delaminated by the NDT methods and by sounding for each in-depth study area, as a percentage of total delaminated area. Note that Study Area WB-2 was 12-ft wide, whereas all other study areas were 16-ft wide.

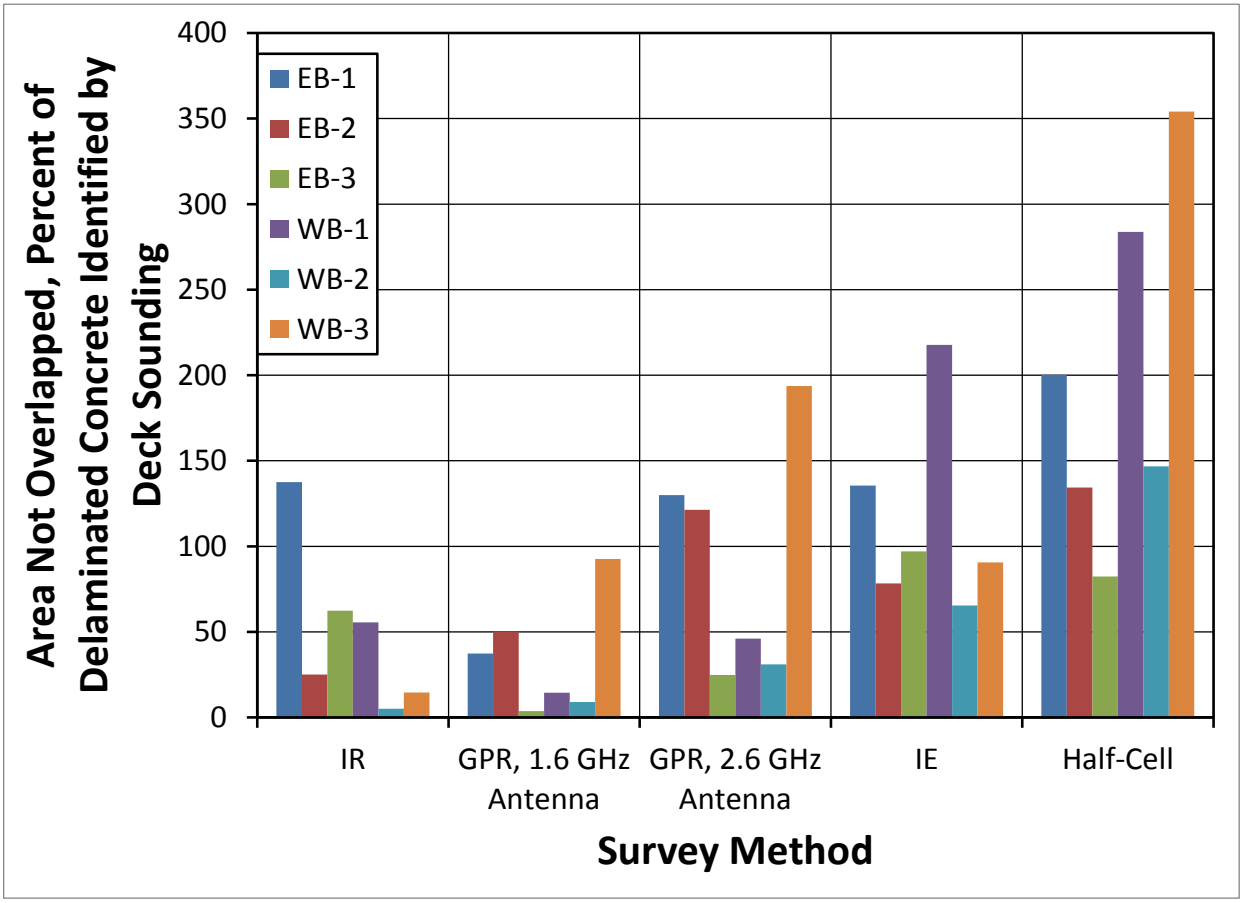

Figure 7.2. Not overlapped areas identified as delaminated by the NDT method, but not by sounding for each in-depth study area, as a percentage of total delaminated area. Note that Study Area WB-2 was 12-ft wide, whereas all other study areas were 16-ft wide.

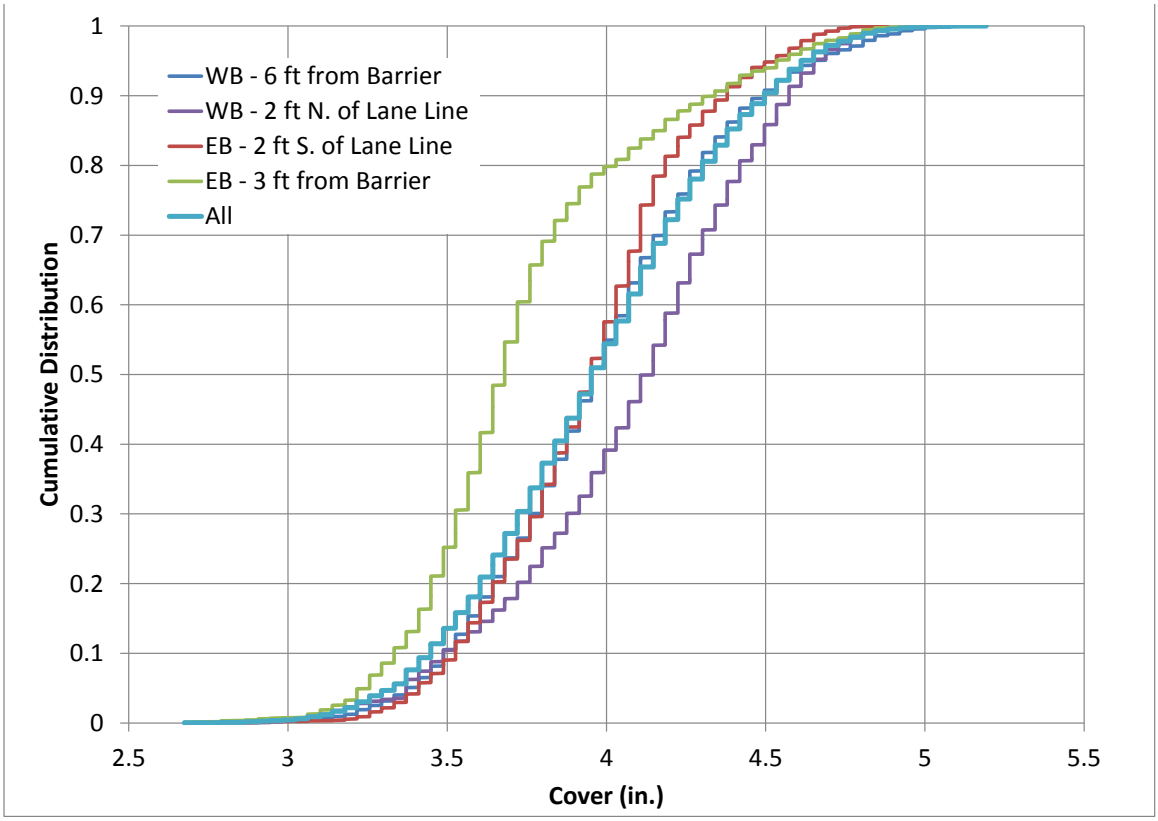

Figure 8.1. Cumulative Distribution of Cover

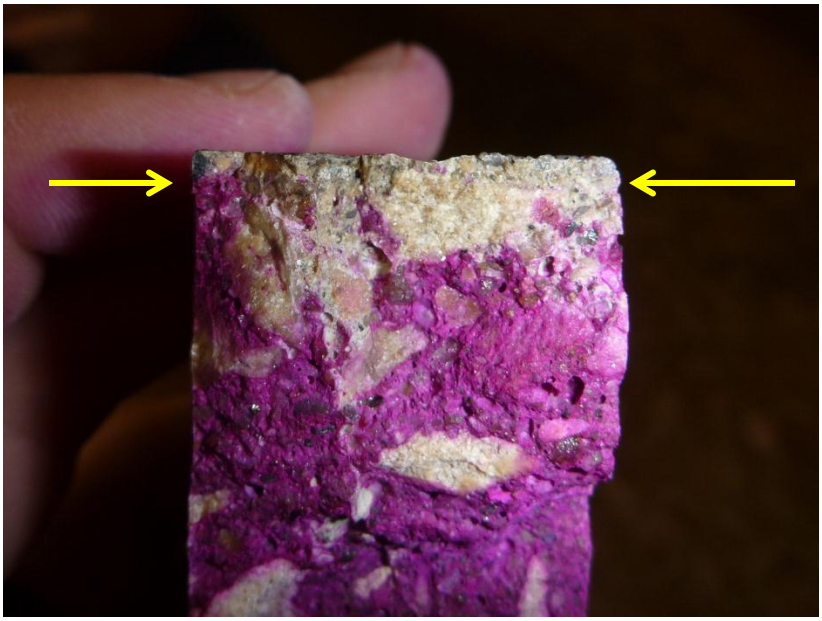

Figure 8.2. Phenolphthalein indicator on a freshly cracked surface of a core. The depth of carbonation is indicated by the arrow (pink color indicates pH > 9).

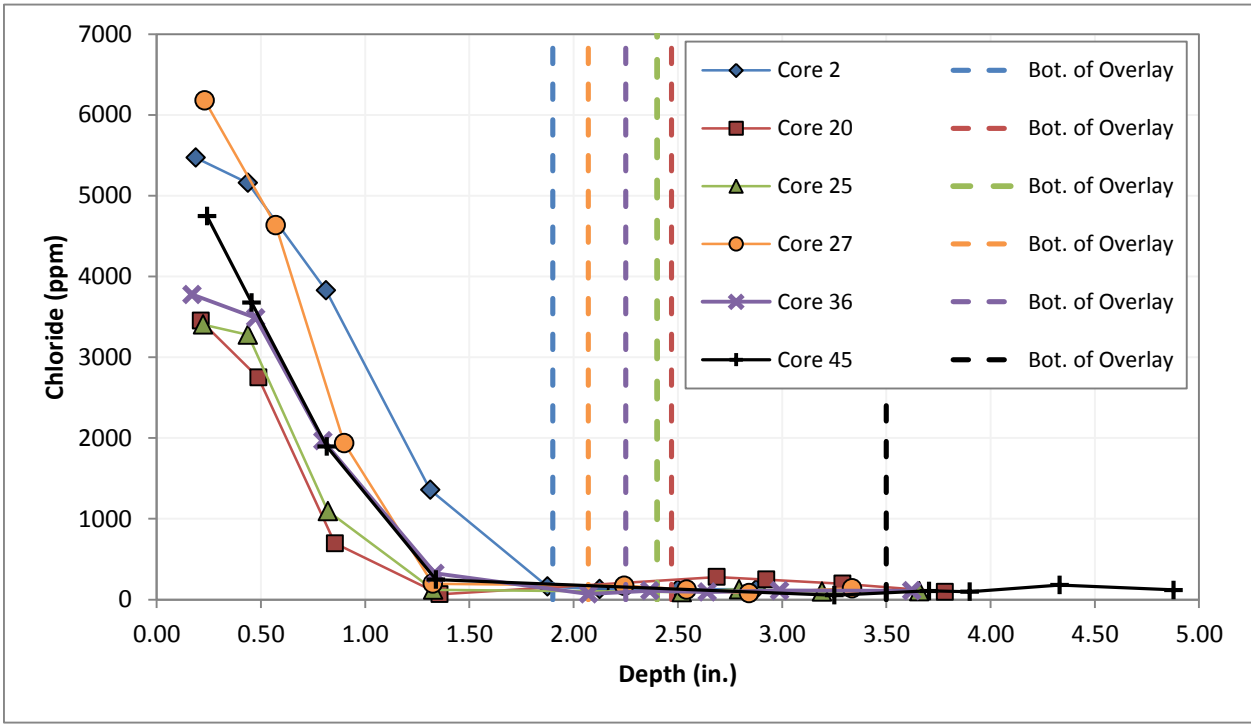

Figure 8.3. Cores from sound concrete (uncracked and no delaminations). Measured chloride contents and overlay thickness, measured as distance from the top surface of the overlay.

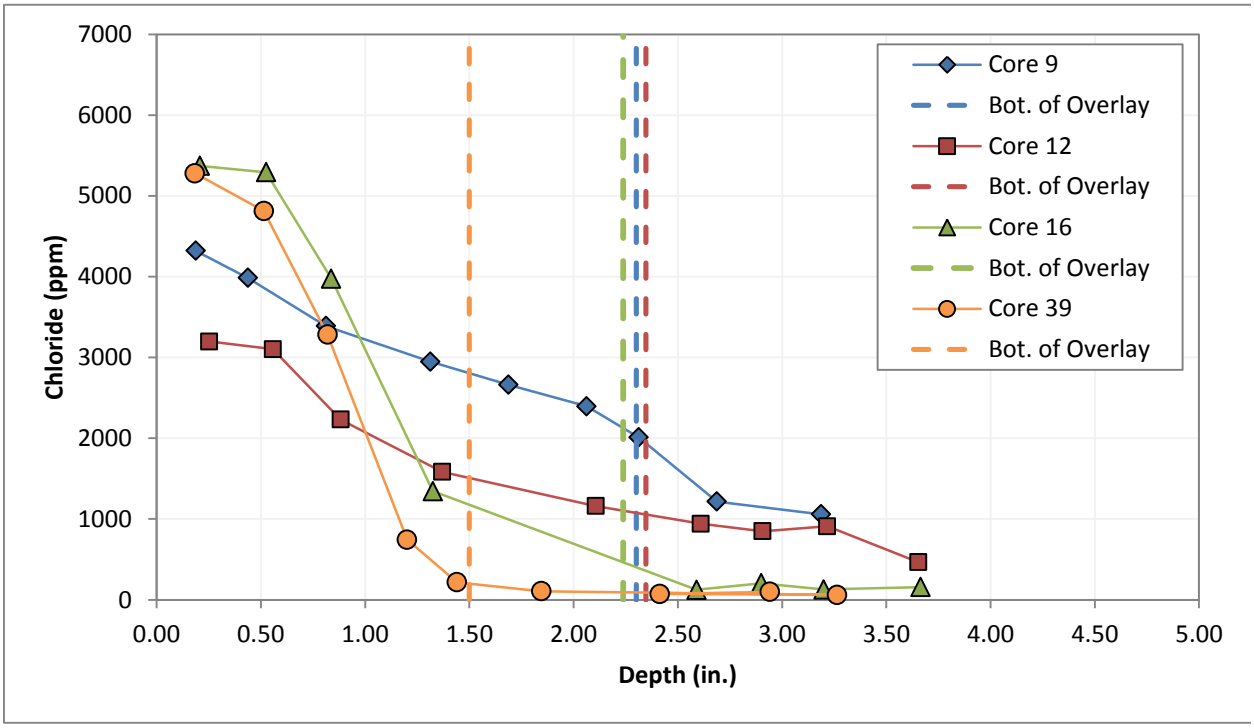

Figure 8.4. Cores with delaminations. Measured chloride contents and overlay thickness, measured as distance from the top surface of the overlay.

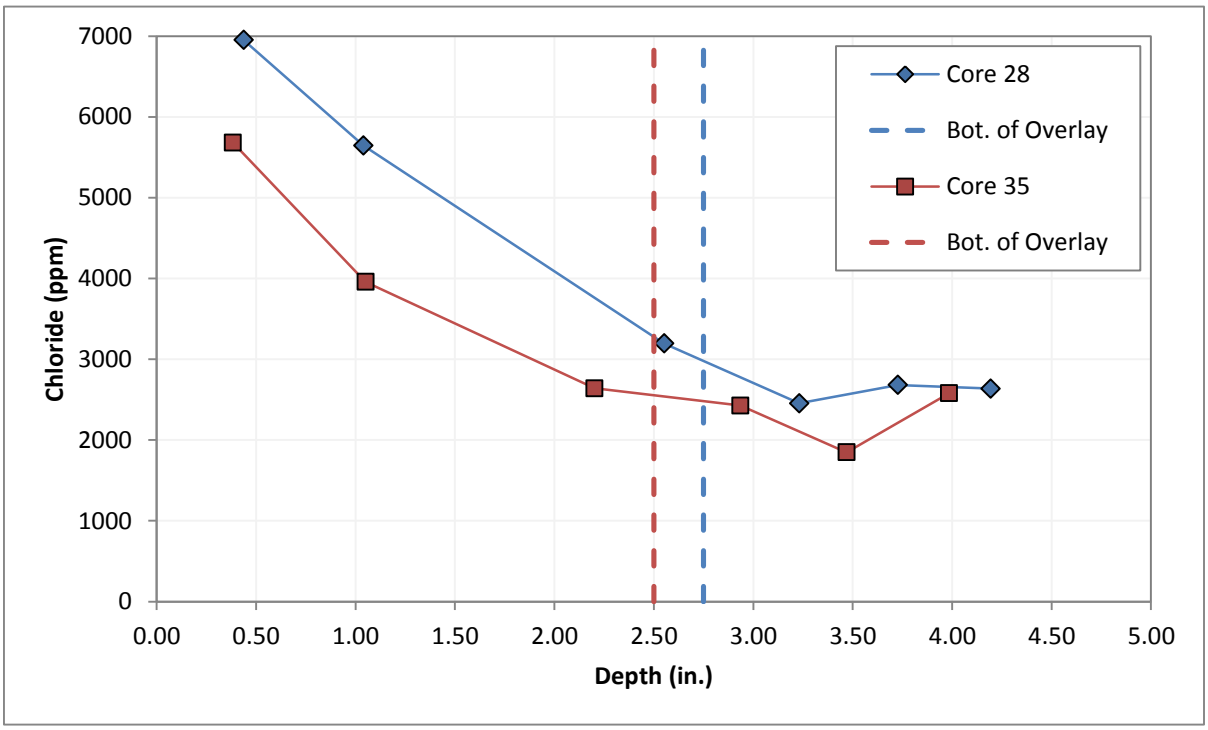

Figure 8.5. Cores with through-thickness vertical cracks. Measured chloride contents and overlay thickness, measured as distance from the top surface of the overlay.

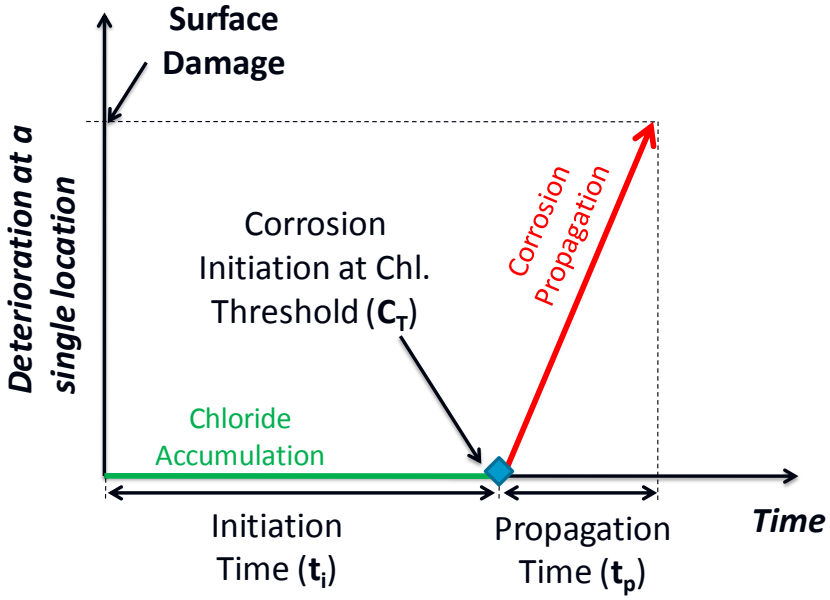

Figure 8.6. Corrosion sequence (adapted from Tuutti 1982).

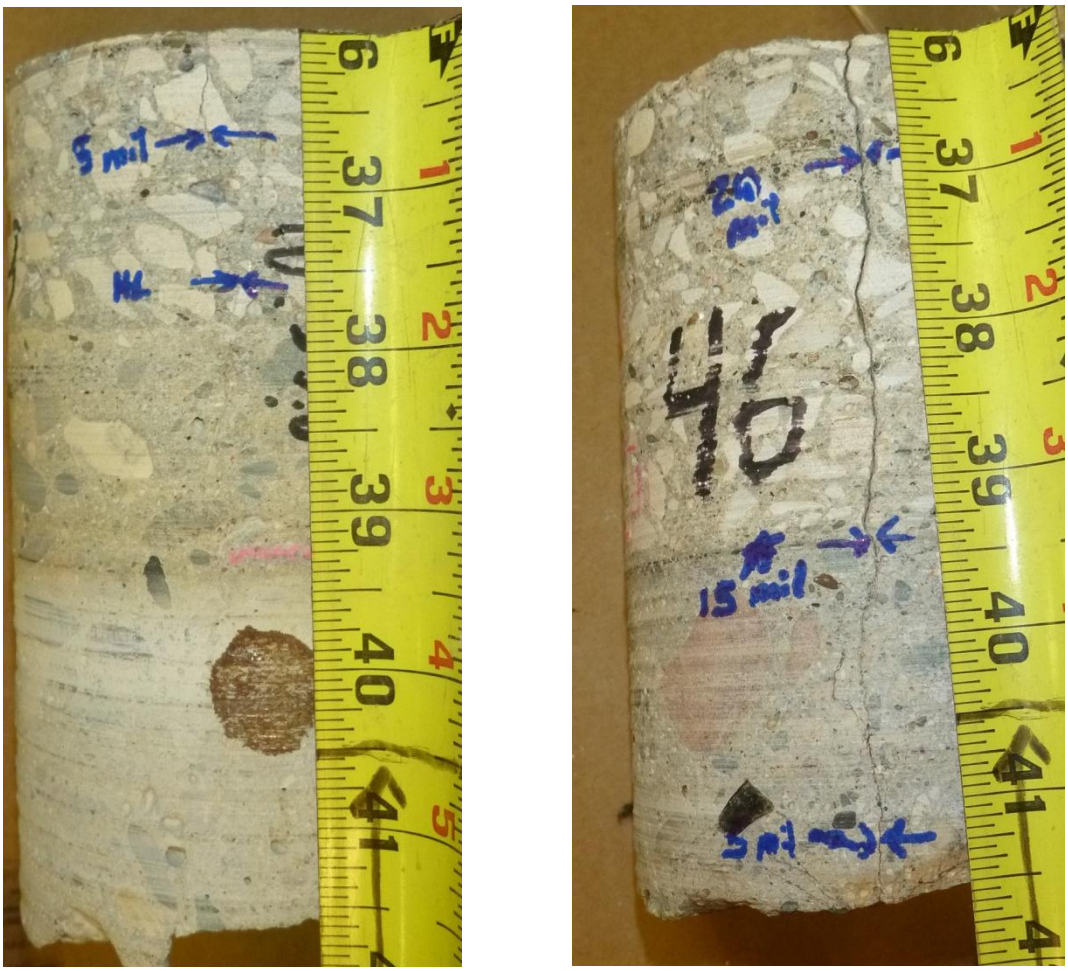

Figure 8.7. Comparison of crack width versus depth for Cores 33 and 46.

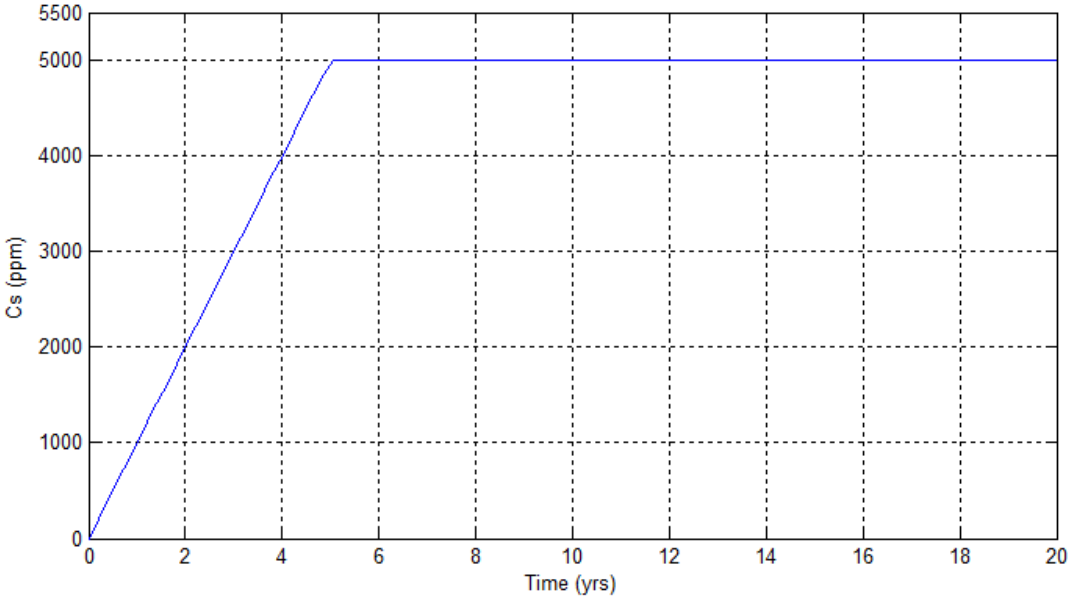

Figure 8.8. Representative plot of surface chloride concentration versus time used for model.

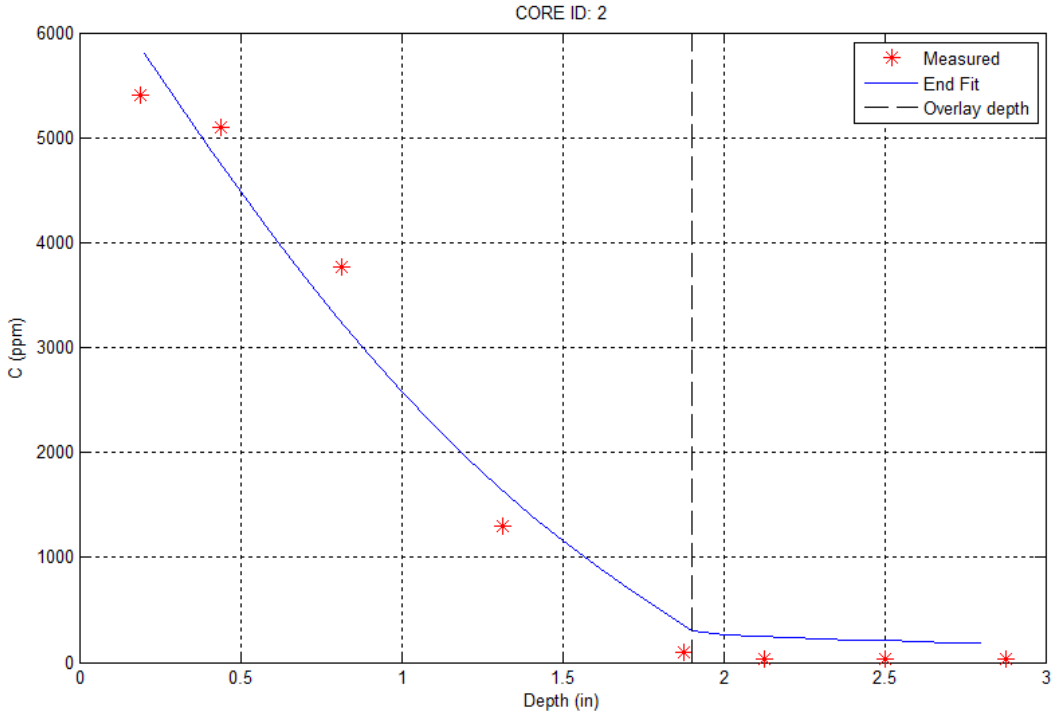

Figure 8.9. Example of least-squares fit to measured chloride content using finite difference solution.

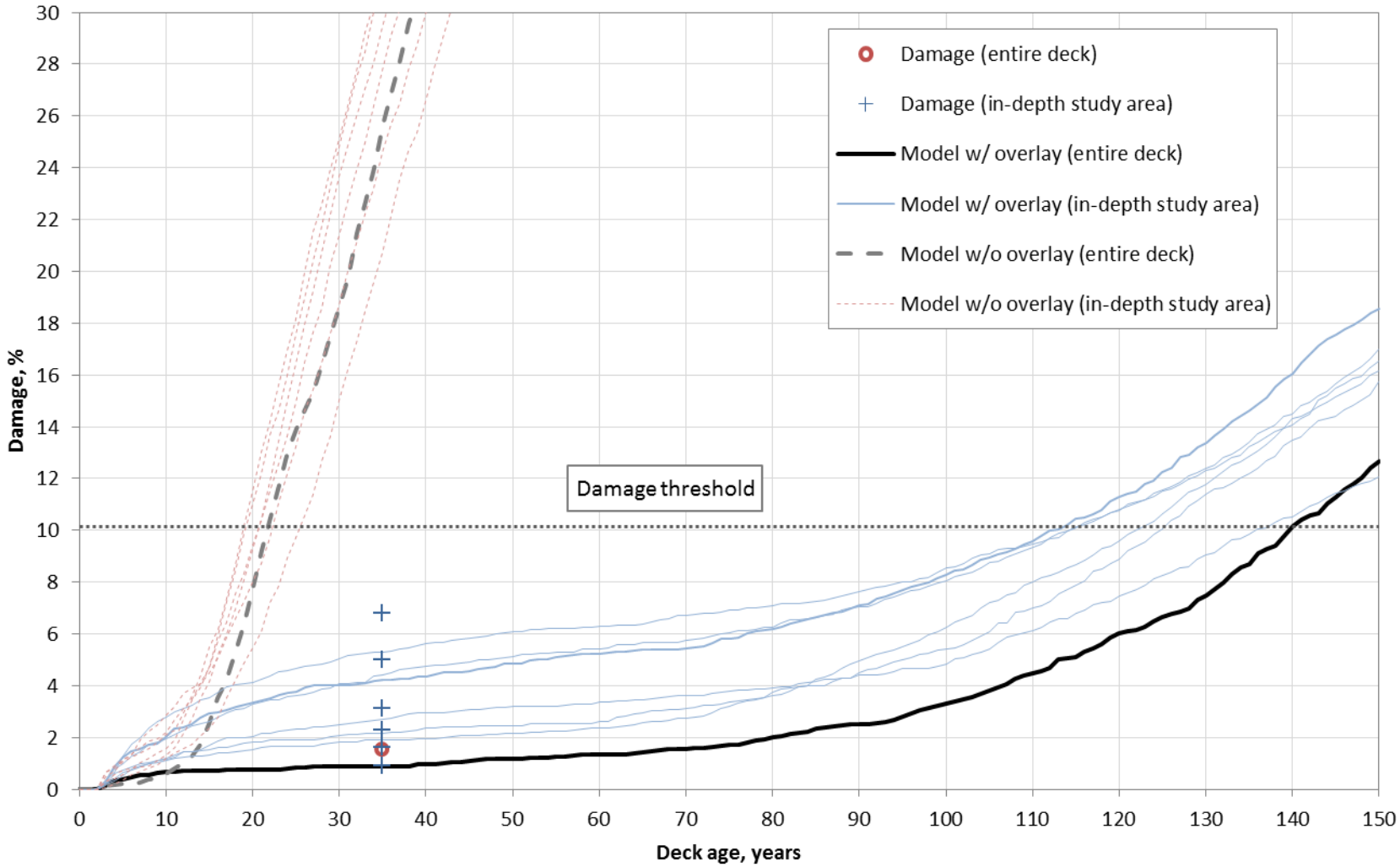

Figure 8.10. Service life model results: Plot of damage versus deck age for both the in-depth study areas and the entire deck.

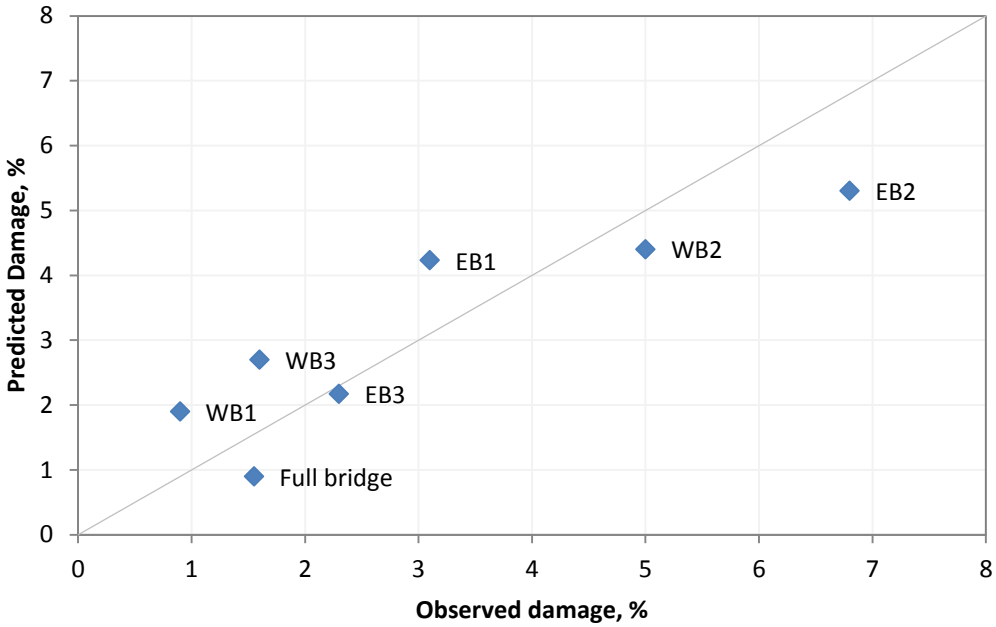

Figure 8.11. Plot of predicted damage versus observed damage at 35 years. Data includes both in-depth study areas and entire deck. Line represents perfect agreement between prediction and observed conditions.

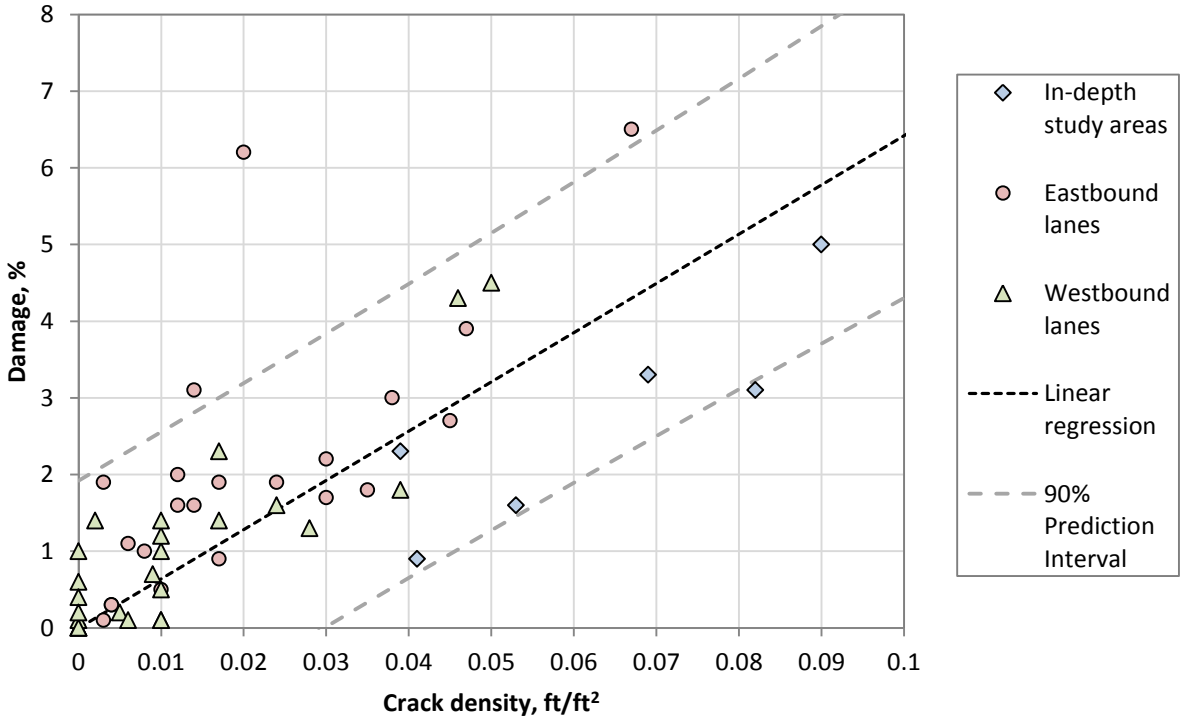

Figure 8.12. Relationship between crack density and observed damage.

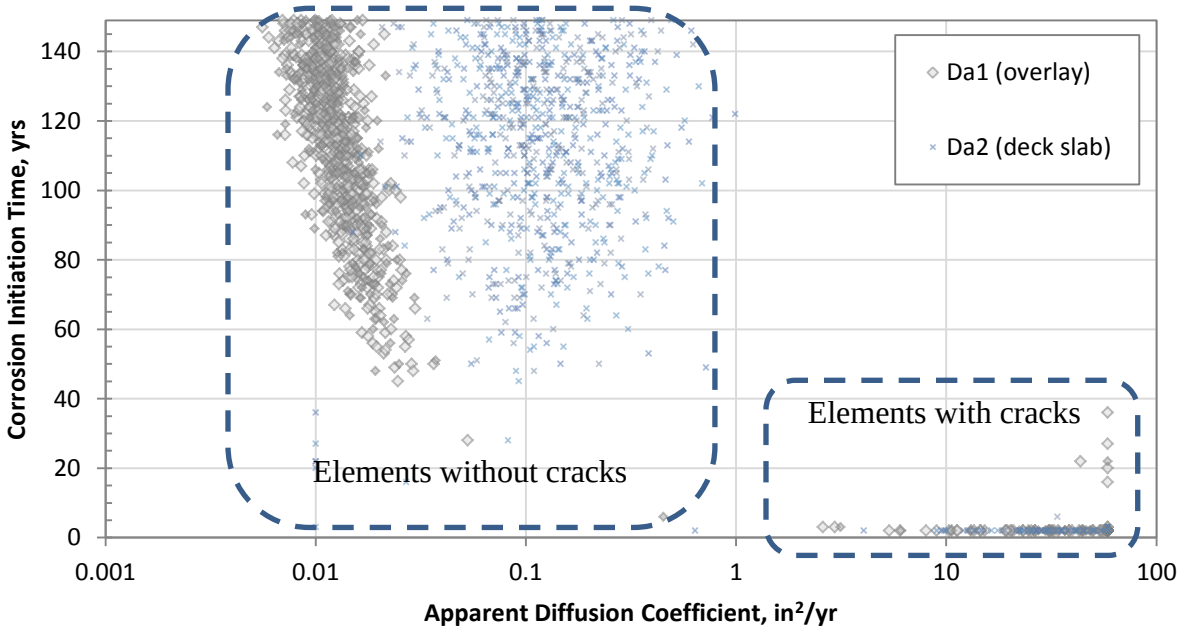

Figure 8.13. Relationship between apparent diffusion coefficient and corrosion initiation time, plotted for Study Area EB-1, as-built conditions.

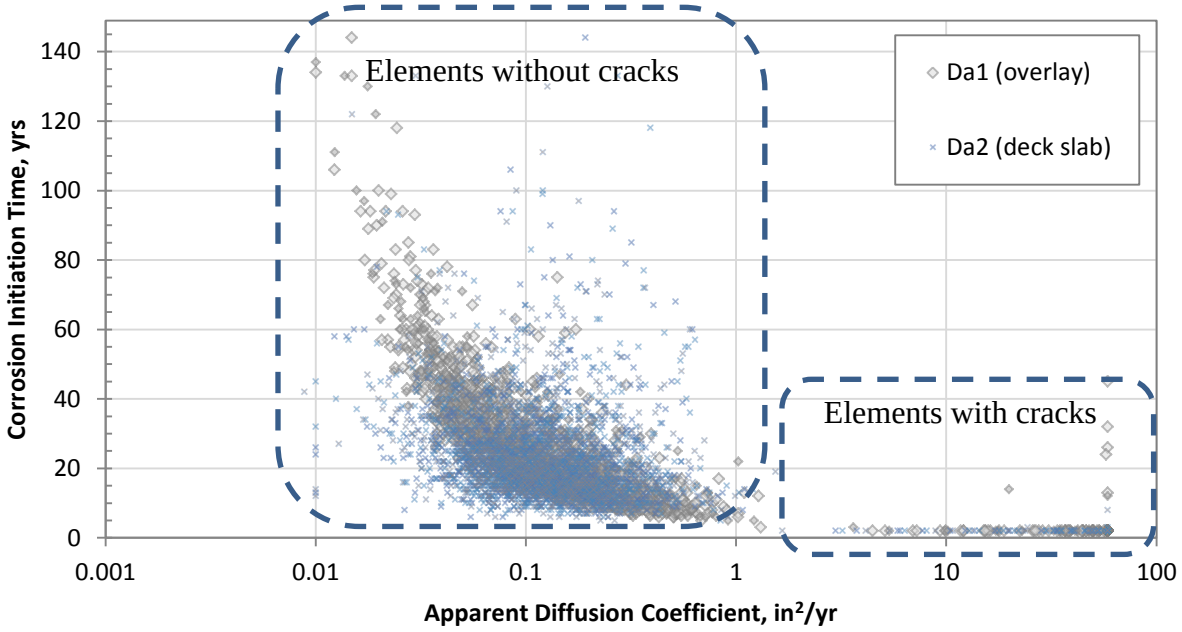

Figure 8.14. Relationship between apparent diffusion coefficient and corrosion initiation time, plotted for Study Area EB-1, calculated without the benefits of a low-permeable overlay.

Appendix A

Findings of Survey of In-Depth Study Areas
Visual Survey and Mechanical Sounding

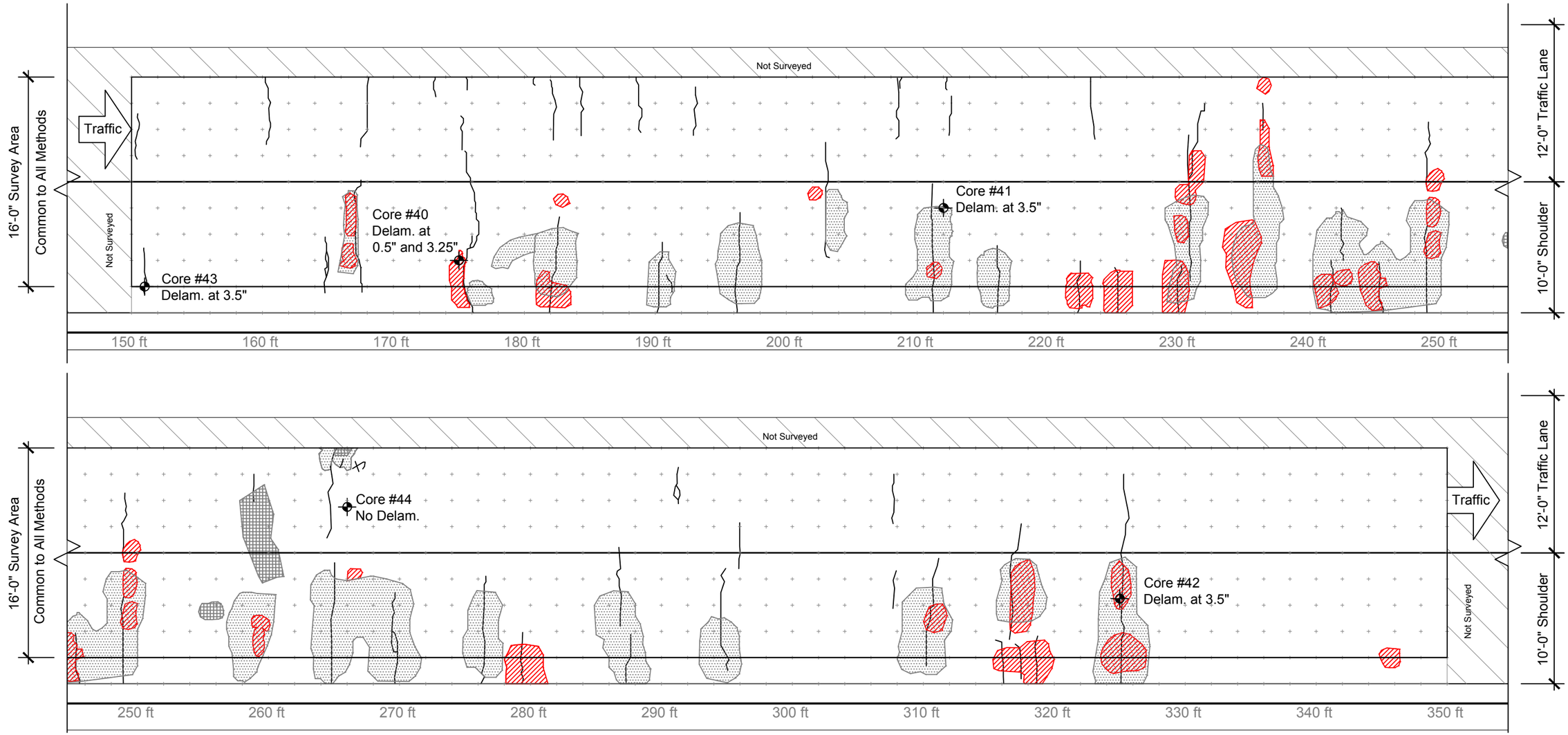

LEGEND

- Delamination, Sounding Survey
- Repair Patch, Visual Survey
- Evidence of Epoxy Repair, Visual Survey
- Crack, Visual Survey
- Construction Joint, Visual Survey
- Core

Study Area EB-1, Visual Survey/Sounding

SCALE: 1/8" = 1'-0"

N

0 1/2" 1"

THIS SHEET PLOTS FULL SCALE AT 11x17 (INCHES)

WJE ENGINEERS ARCHITECTS MATERIALS SCIENTISTS

Wiss, Janney, Elstner Associates, Inc.
330 Pfingsten Road
Northbrook, Illinois 60062
847.272.7400 tel | 847.291.9599 fax
www.wje.com

Project: I-129 Missouri River Bridge (No. 9700.05129)
Deck Condition Evaluation

Sheet Title: Findings of Visual Survey/Sounding

Proj. No.	2010.2389.0
Survey Date	June 20-24, 2011
Drawn	RDL
Checked	JSL
Scale	1/8" = 1'-0"

Sheet No. **A.1**

Plotted: 4/12/2012 9:01 AM by Lequesne, Remy File Name: \\wjenbfp.wje.com\projects\2010\2301-2400\2010.2389-JPD-Iowa NDE\.0_I-129 Sioux City\Drawings\Report Figures\combined study areas.dwg

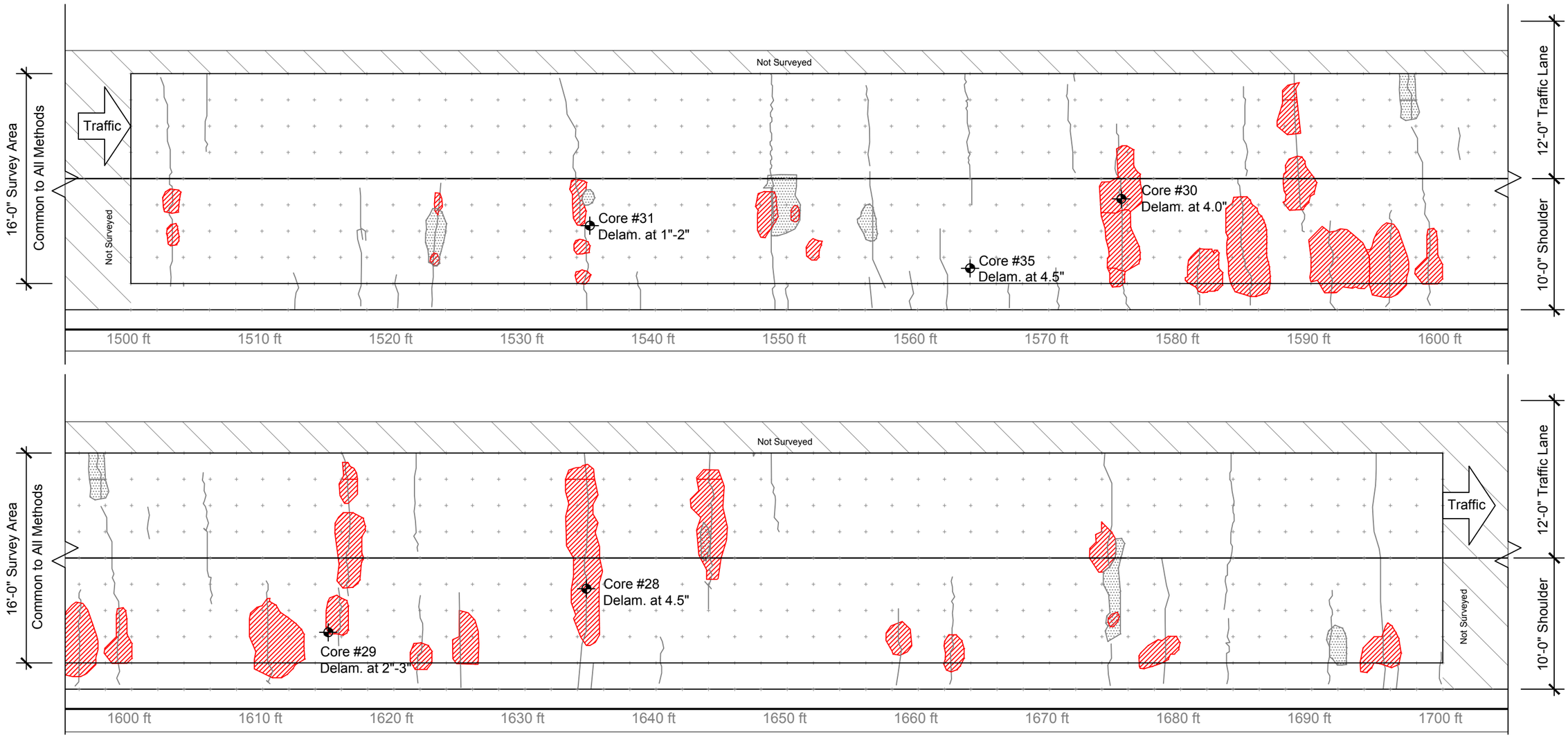

LEGEND

- Delamination, Sounding Survey
- Repair Patch, Visual Survey
- Evidence of Epoxy Repair, Visual Survey
- Crack, Visual Survey
- Construction Joint, Visual Survey
- Core

Study Area EB-2, Visual Survey/Sounding

SCALE: 1/8" = 1'-0"

N

0 1/2" 1"

THIS SHEET PLOTS FULL SCALE AT 11x17 (INCHES)

WJE ENGINEERS ARCHITECTS MATERIALS SCIENTISTS

Wiss, Janney, Elstner Associates, Inc.
330 Pfingsten Road
Northbrook, Illinois 60062
847.272.7400 tel | 847.291.9599 fax
www.wje.com

Project: I-129 Missouri River Bridge (No. 9700.05129)
Deck Condition Evaluation

Sheet Title: Findings of Visual Survey/Sounding

Proj. No.	2010.2389.0
Survey Date	June 20-24, 2011
Drawn	RDL
Checked	JSL
Scale	1/8" = 1'-0"

Sheet No. **A.2**

Plotted: 4/12/2012 9:01 AM by Lequesne, Remy File Name: \\wjenbfp.wje.com\projects\2010\2301-2400\2010.2389-JPD-Iowa NDE\.0_I-129 Sioux City\Drawings\Report Figures\combined study areas.dwg

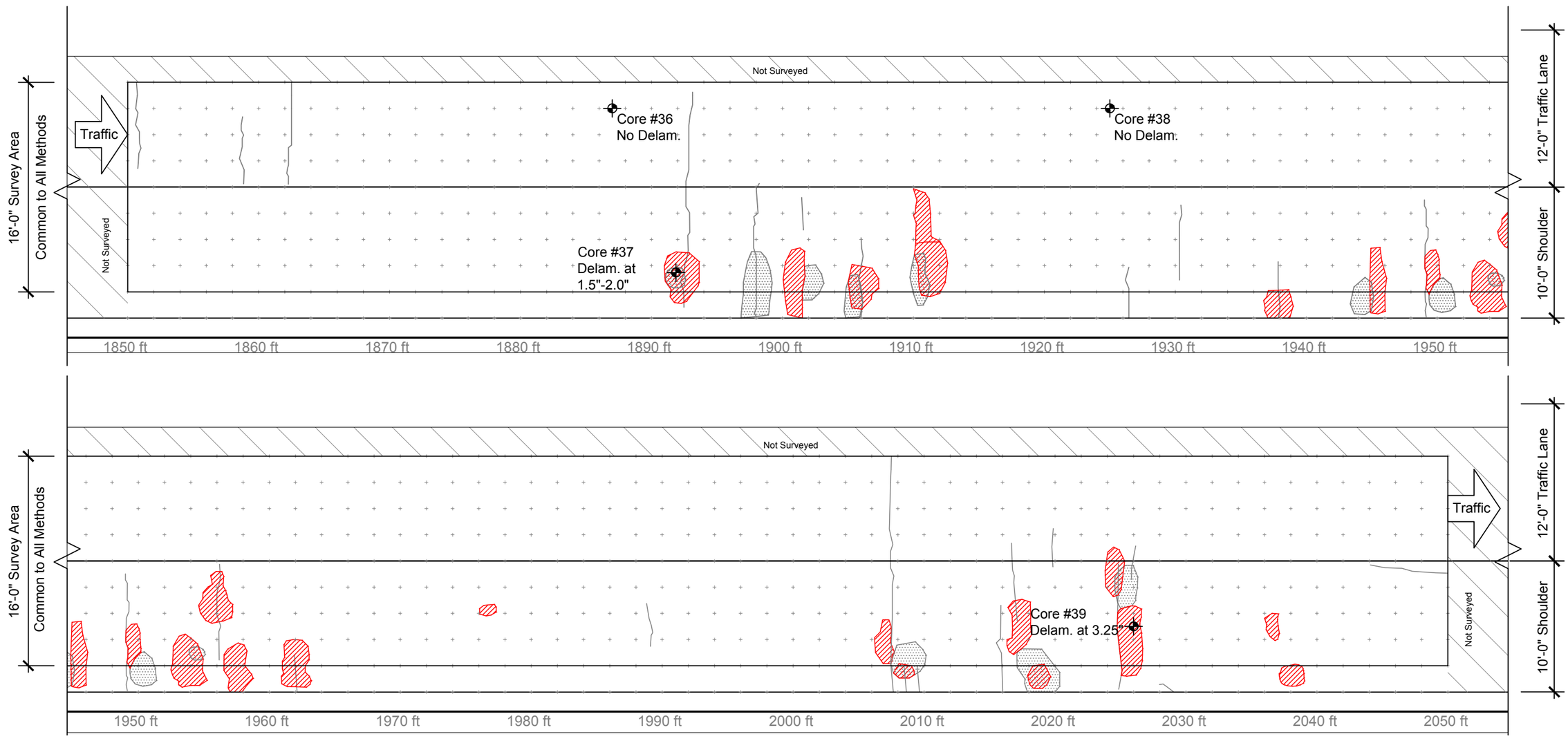

LEGEND

- Delamination, Sounding Survey
- Repair Patch, Visual Survey
- Evidence of Epoxy Repair, Visual Survey
- Crack, Visual Survey
- Construction Joint, Visual Survey
- Core

Study Area EB-3, Visual Survey/Sounding

SCALE: 1/8" = 1'-0"

N

0 1/2" 1"

THIS SHEET PLOTS FULL SCALE AT 11x17 (INCHES)

WJE ENGINEERS ARCHITECTS MATERIALS SCIENTISTS

Wiss, Janney, Elstner Associates, Inc.
330 Pfingsten Road
Northbrook, Illinois 60062
847.272.7400 tel | 847.291.9599 fax
www.wje.com

Project: I-129 Missouri River Bridge (No. 9700.05129)
Deck Condition Evaluation

Sheet Title: Findings of Visual Survey/Sounding

Proj. No.	2010.2389.0
Survey Date	June 20-24, 2011
Drawn	RDL
Checked	JSL
Scale	1/8" = 1'-0"

Sheet No. **A.3**

Plotted: 4/12/2012 9:01 AM by Lequesne, Remy File Name: \\wjenbfp.wje.com\projects\2010\2301-2400\2010.2389-JPD-Iowa NDE\.0_I-129 Sioux City\Drawings\Report Figures\combined study areas.dwg

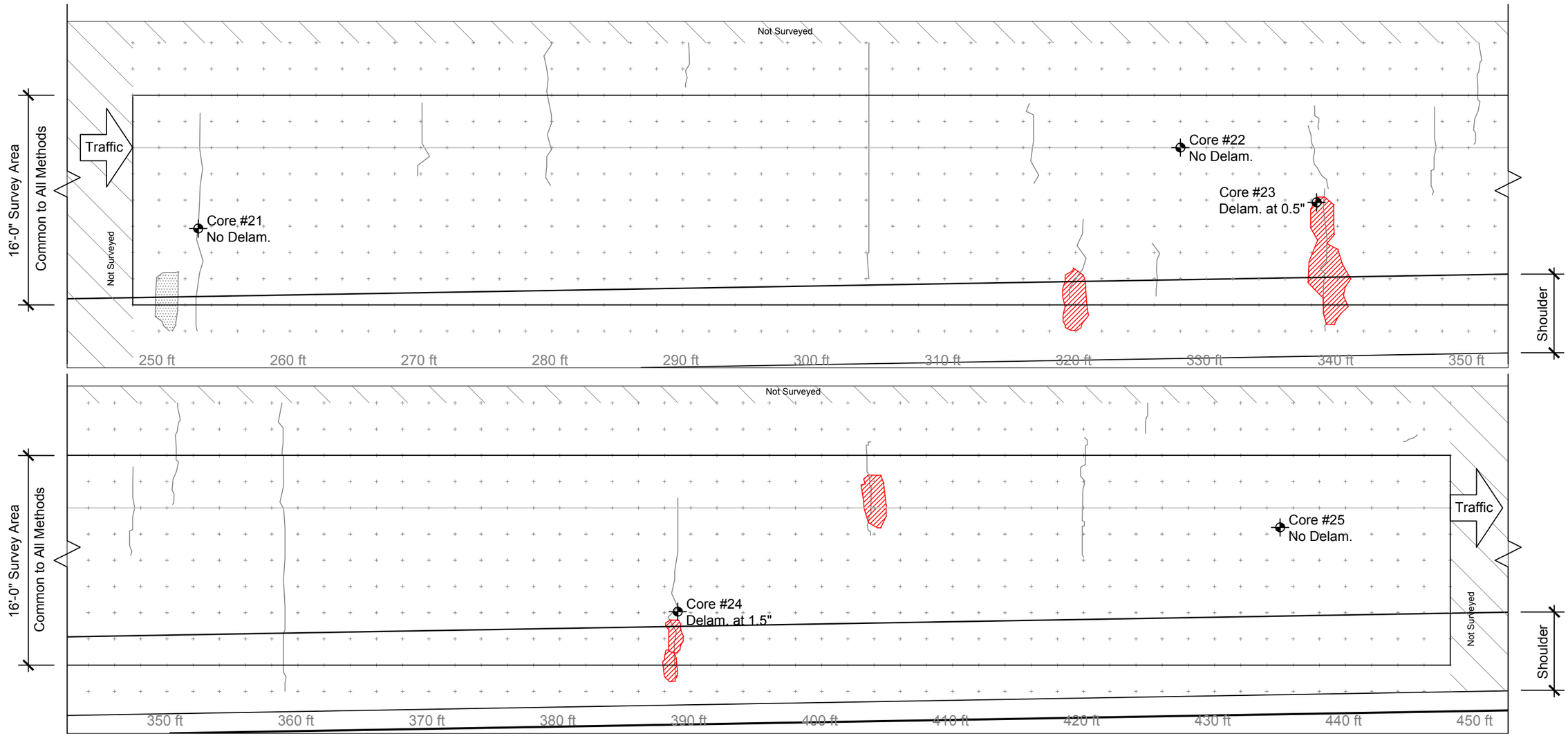

LEGEND

- Delamination, Sounding Survey
- Repair Patch, Visual Survey
- Evidence of Epoxy Repair, Visual Survey
- Crack, Visual Survey
- Construction Joint, Visual Survey
- Core

Study Area WB-1, Visual Survey/Sounding

SCALE: 1/8" = 1'-0"

N

0 1/2" 1"

THIS SHEET PLOTS FULL SCALE AT 11x17 (INCHES)

WJE ENGINEERS ARCHITECTS MATERIALS SCIENTISTS

Wiss, Janney, Elstner Associates, Inc.
330 Pfingsten Road
Northbrook, Illinois 60062
847.272.7400 tel | 847.291.9599 fax
www.wje.com

Project	I-129 Missouri River Bridge (No. 9700.05129) Deck Condition Evaluation
Sheet Title	Findings of Visual Survey/Sounding
Proj. No.	2010.2389.0
Survey Date	June 20-24, 2011
Drawn	RDL
Checked	JSL
Scale	1/8" = 1'-0"
Sheet No.	A.4

Plotted: 4/12/2012 9:01 AM by Lequesne, Remy File Name: \\wjenbfp.wje.com\projects\2010\2301-2400\2010.2389-JPD-Iowa NDE\.0_I-129 Sioux City\Drawings\Report Figures\combined study areas.dwg

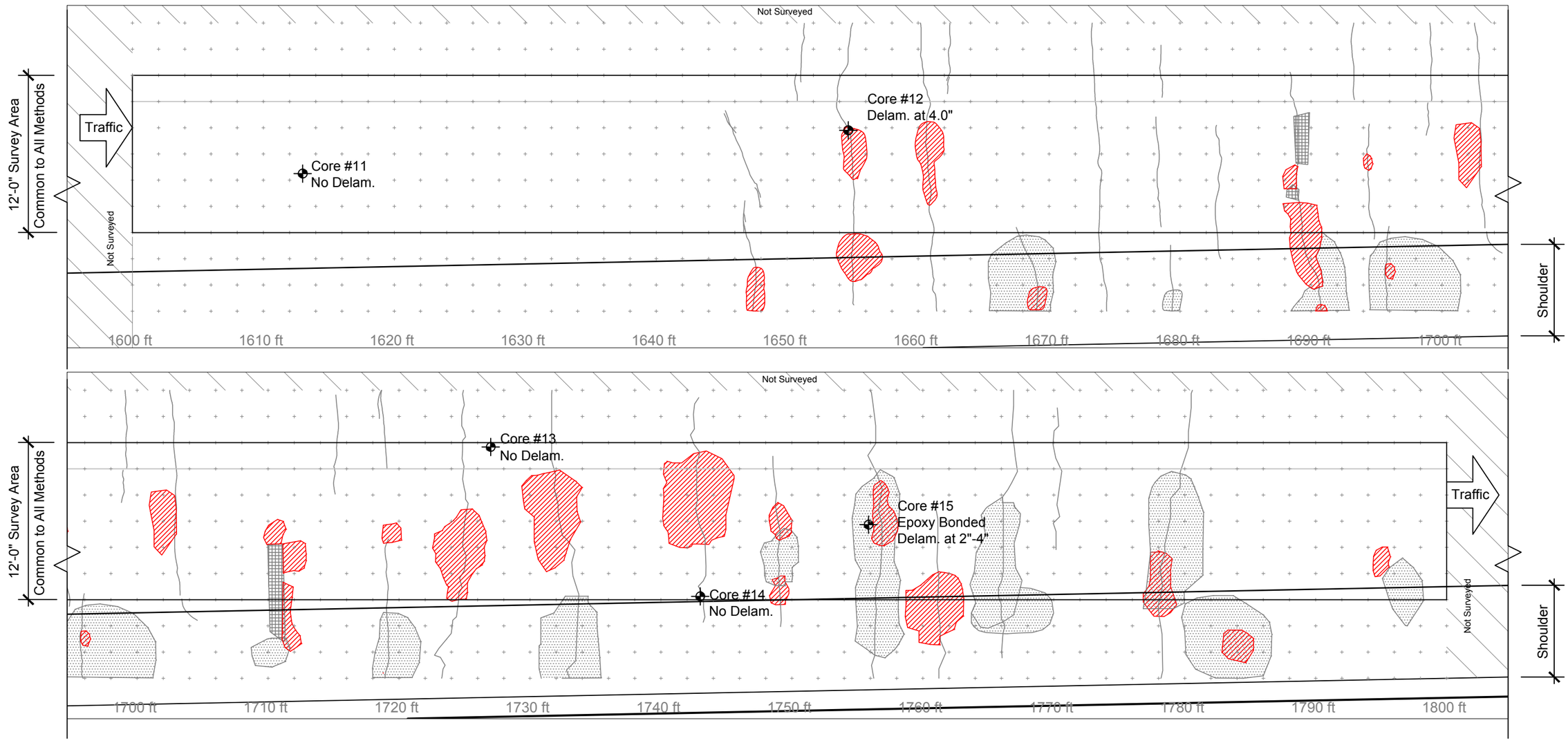

LEGEND

- Delamination, Sounding Survey
- Repair Patch, Visual Survey
- Evidence of Epoxy Repair, Visual Survey
- Crack, Visual Survey
- Construction Joint, Visual Survey
- Core

Study Area WB-2, Visual Survey/Sounding

SCALE: 1/8" = 1'-0"

N

0 1/2" 1"

THIS SHEET PLOTS FULL SCALE AT 11x17 (INCHES)

WJE ENGINEERS ARCHITECTS MATERIALS SCIENTISTS

Wiss, Janney, Elstner Associates, Inc.
330 Pfingsten Road
Northbrook, Illinois 60062
847.272.7400 tel | 847.291.9599 fax
www.wje.com

Project: I-129 Missouri River Bridge (No. 9700.05129)
Deck Condition Evaluation

Sheet Title: Findings of Visual Survey/Sounding

Proj. No.	2010.2389.0
Survey Date	June 20-24, 2011
Drawn	RDL
Checked	JSL
Scale	1/8" = 1'-0"

Sheet No. **A.5**

Plotted: 4/12/2012 9:01 AM by Lequesne, Remy File Name: \\wjenbfp.wje.com\projects\2010\2301-2400\2010.2389-JPD-Iowa NDE\.0_I-129 Sioux City\Drawings\Report Figures\combined study areas.dwg

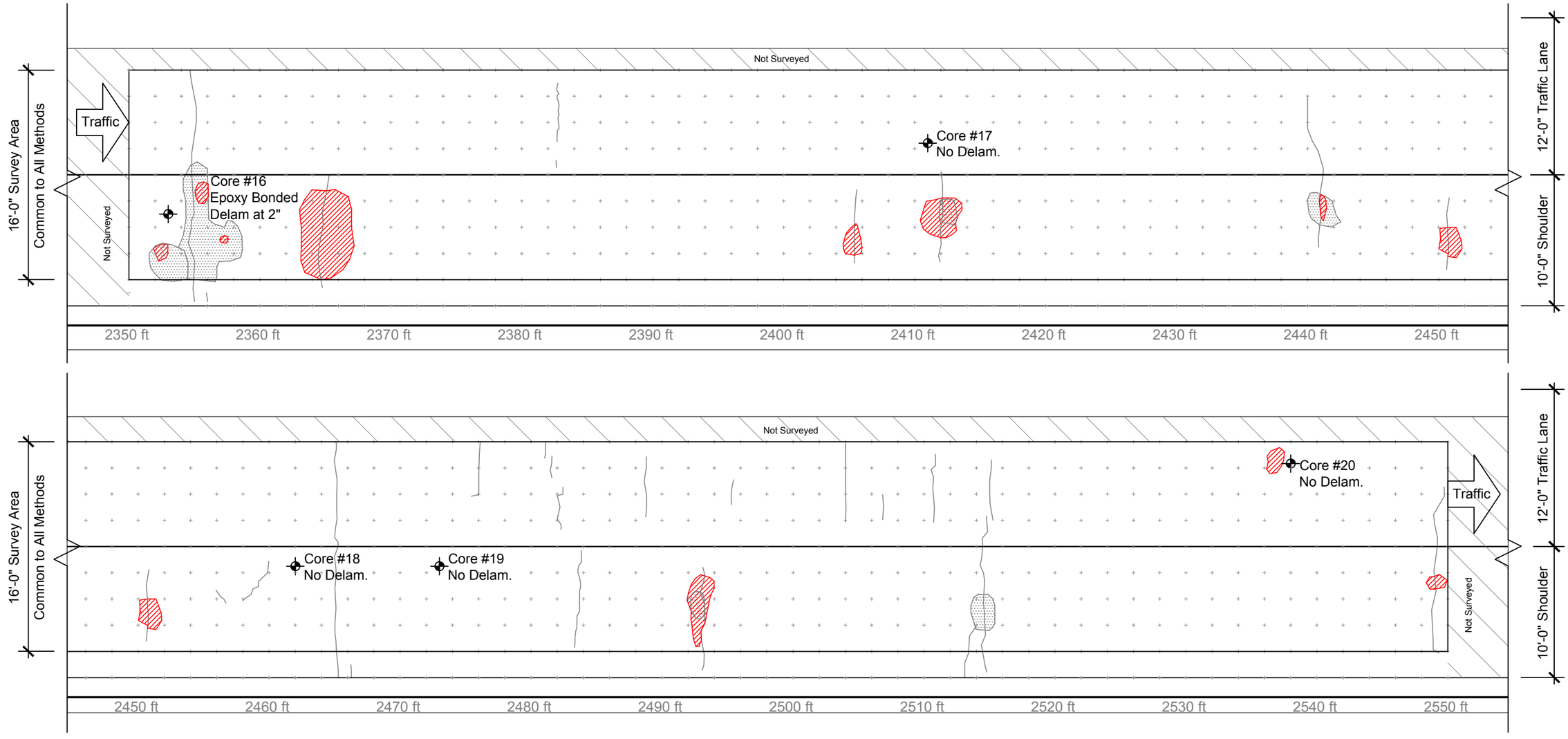

LEGEND

- Delamination, Sounding Survey
- Repair Patch, Visual Survey
- Evidence of Epoxy Repair, Visual Survey
- Crack, Visual Survey
- Construction Joint, Visual Survey
- Core

Study Area WB-3, Visual Survey/Sounding

SCALE: 1/8" = 1'-0"

N

0 1/2" 1"

THIS SHEET PLOTS FULL SCALE AT 11x17 (INCHES)

WJE ENGINEERS ARCHITECTS MATERIALS SCIENTISTS

Wiss, Janney, Elstner Associates, Inc.
330 Pfingsten Road
Northbrook, Illinois 60062
847.272.7400 tel | 847.291.9599 fax
www.wje.com

Project: I-129 Missouri River Bridge (No. 9700.05129)
Deck Condition Evaluation

Sheet Title: Findings of Visual Survey/Sounding

Proj. No.	2010.2389.0
Survey Date	June 20-24, 2011
Drawn	RDL
Checked	JSL
Scale	1/8" = 1'-0"

Sheet No. **A.6**

Plotted: 4/12/2012 9:01 AM by Lequesne, Remy File Name: \\wjenbfp.wje.com\projects\2010\2301-2400\2010.2389-JPD-Iowa NDE\.0_I-129 Sioux City\Drawings\Report Figures\combined study areas.dwg

Appendix B

Findings of Survey of In-Depth Study Areas
Infrared Thermography

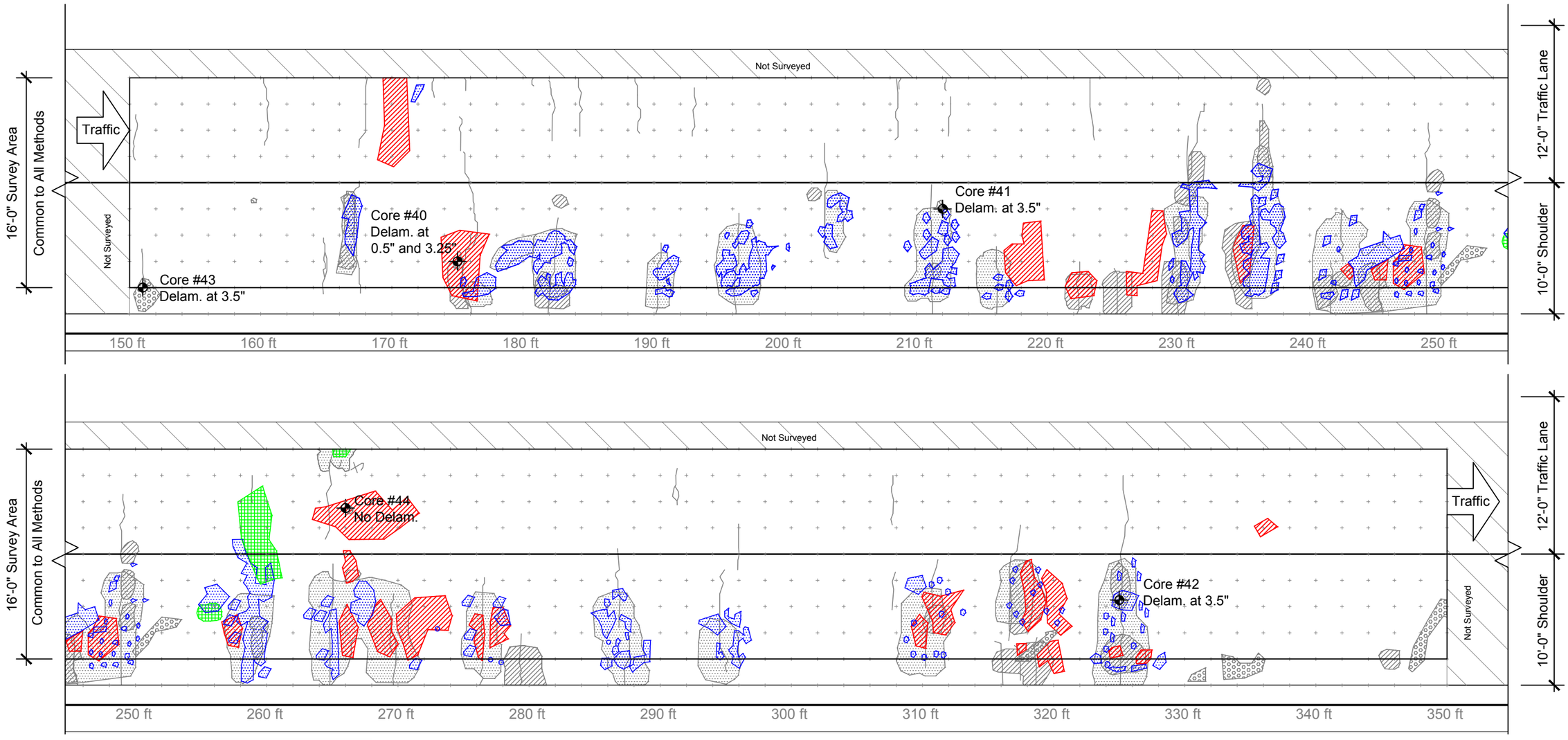

LEGEND

- Delamination, IR Survey
- Delamination, Sounding Survey
- Repair Patch, IR Survey
- Epoxy on Surface, IR Survey
- Evidence of Epoxy Repair, Visual Survey
- Surface Discoloration, IR Survey
- Crack, Visual Survey
- Construction Joint, Visual Survey
- Core

Study Area EB-1, IR Thermography

SCALE: 1/8" = 1'-0"

N

0 1/2" 1"

THIS SHEET PLOTS FULL SCALE AT 11x17 (INCHES)

WJE ENGINEERS ARCHITECTS MATERIALS SCIENTISTS

Wiss, Janney, Elstner Associates, Inc.
330 Pfingsten Road
Northbrook, Illinois 60062
847.272.7400 tel | 847.291.9599 fax
www.wje.com

Project: I-129 Missouri River Bridge (No. 9700.05129)
Deck Condition Evaluation

Sheet Title: Findings of IR Thermography

Proj. No.	2010.2389.0
Survey Date	June 20-24, 2011
Drawn	RDL
Checked	JSL
Scale	1/8" = 1'-0"

Sheet No. **B.1**

Plotted: 4/12/2012 9:03 AM by Lequesne, Remy File Name: \\wjenbfp.wje.com\projects\2010\2301-2400\2010.2389-JPD-Iowa NDE\.0_I-129 Sioux City\Drawings\Report Figures\combined study areas.dwg

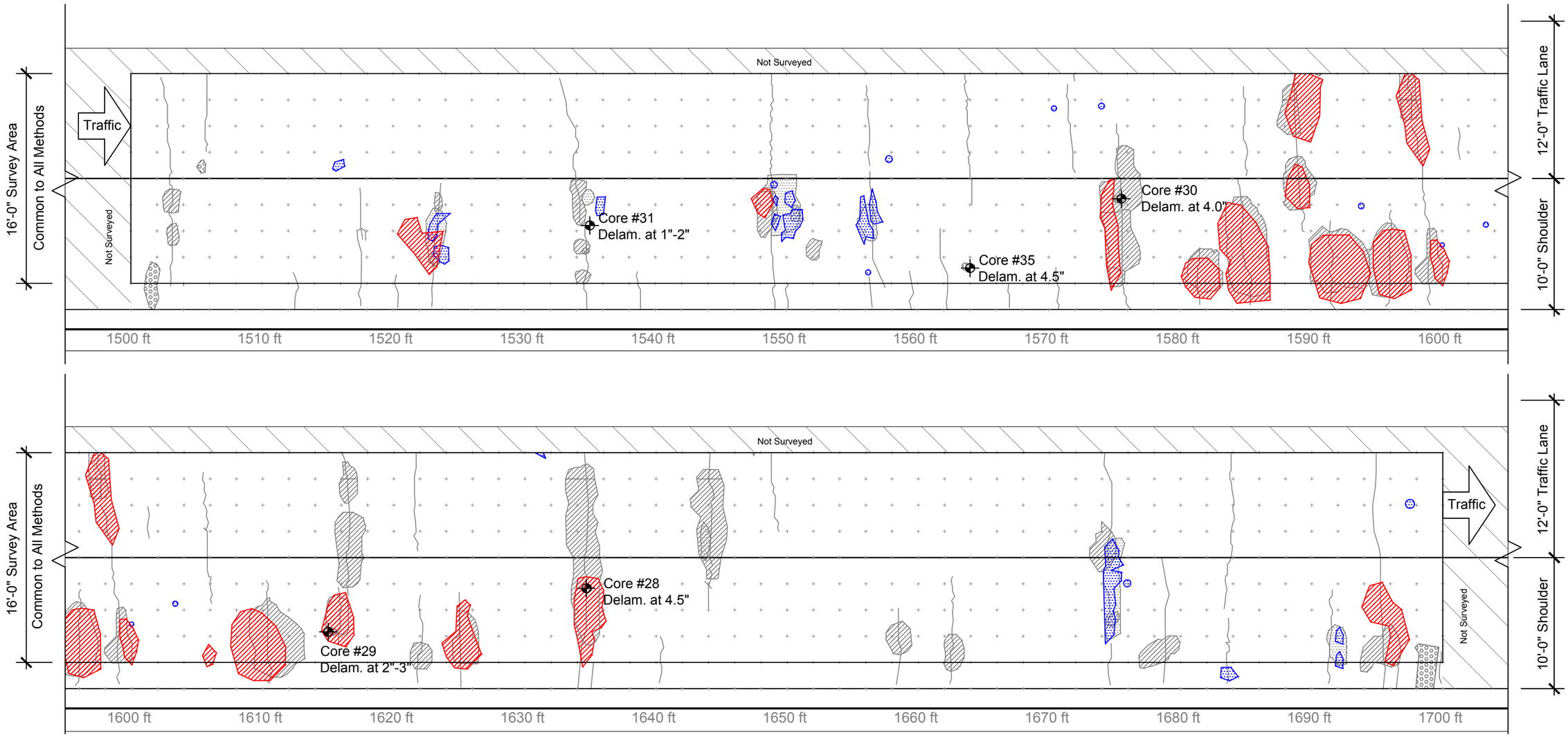

LEGEND

- Delamination, IR Survey
- Delamination, Sounding Survey
- Repair Patch, IR Survey
- Epoxy on Surface, IR Survey
- Evidence of Epoxy Repair, Visual Survey
- Surface Discoloration, IR Survey
- Crack, Visual Survey
- Construction Joint, Visual Survey
- Core

Study Area EB-2, IR Thermography

SCALE: 1/8" = 1'-0"

N

0 1/2" 1"

THIS SHEET PLOTS FULL SCALE AT 11x17 (INCHES)

WJE ENGINEERS ARCHITECTS MATERIALS SCIENTISTS
Wiss, Janney, Elstner Associates, Inc.
330 Pfingsten Road
Northbrook, Illinois 60062
847.272.7400 tel | 847.291.9599 fax
www.wje.com

Project: I-129 Missouri River Bridge (No. 9700.05129)
Deck Condition Evaluation

Sheet Title: Findings of IR Thermography

Proj. No.	2010.2389.0
Survey Date	June 20-24, 2011
Drawn	RDL
Checked	JSL
Scale	1/8" = 1'-0"

Sheet No. **B.2**

Plotted: 4/12/2012 9:03 AM by Lequesne, Remy File Name: \\wjenbfp.wje.com\projects\2010\2301-2400\2010.2389-JPD-Iowa NDE\.0_I-129 Sioux City\Drawings\Report Figures\combined study areas.dwg

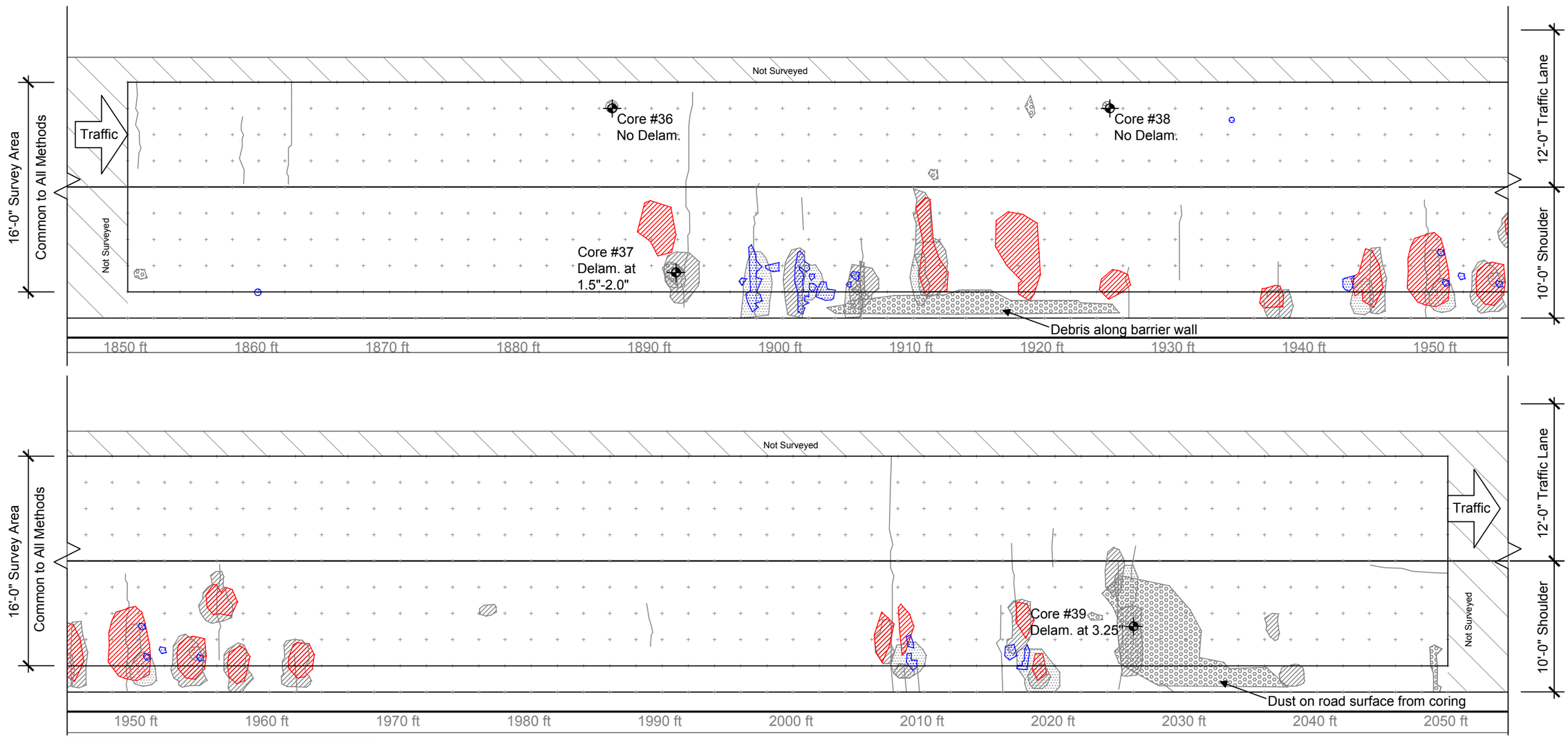

LEGEND

- Delamination, IR Survey
- Delamination, Sounding Survey
- Repair Patch, IR Survey
- Epoxy on Surface, IR Survey
- Evidence of Epoxy Repair, Visual Survey
- Surface Discoloration, IR Survey
- Crack, Visual Survey
- Construction Joint, Visual Survey
- Core

Study Area EB-3, IR Thermography

SCALE: 1/8" = 1'-0"

N

0 1/2" 1"

THIS SHEET PLOTS FULL SCALE AT 11x17 (INCHES)

WJE ENGINEERS ARCHITECTS MATERIALS SCIENTISTS

Wiss, Janney, Elstner Associates, Inc.
330 Pfingsten Road
Northbrook, Illinois 60062
847.272.7400 tel | 847.291.9599 fax
www.wje.com

Project: I-129 Missouri River Bridge (No. 9700.05129)
Deck Condition Evaluation

Sheet Title: Findings of IR Thermography

Proj. No.	2010.2389.0
Survey Date	June 20-24, 2011
Drawn	RDL
Checked	JSL
Scale	1/8" = 1'-0"

Sheet No. **B.3**

Plotted: 4/12/2012 9:03 AM by Lequesne, Remy File Name: \\wjenbfp.wje.com\projects\2010\2301-2400\2010.2389-JPD-Iowa NDE\.0_I-129 Sioux City\Drawings\Report Figures\combined study areas.dwg

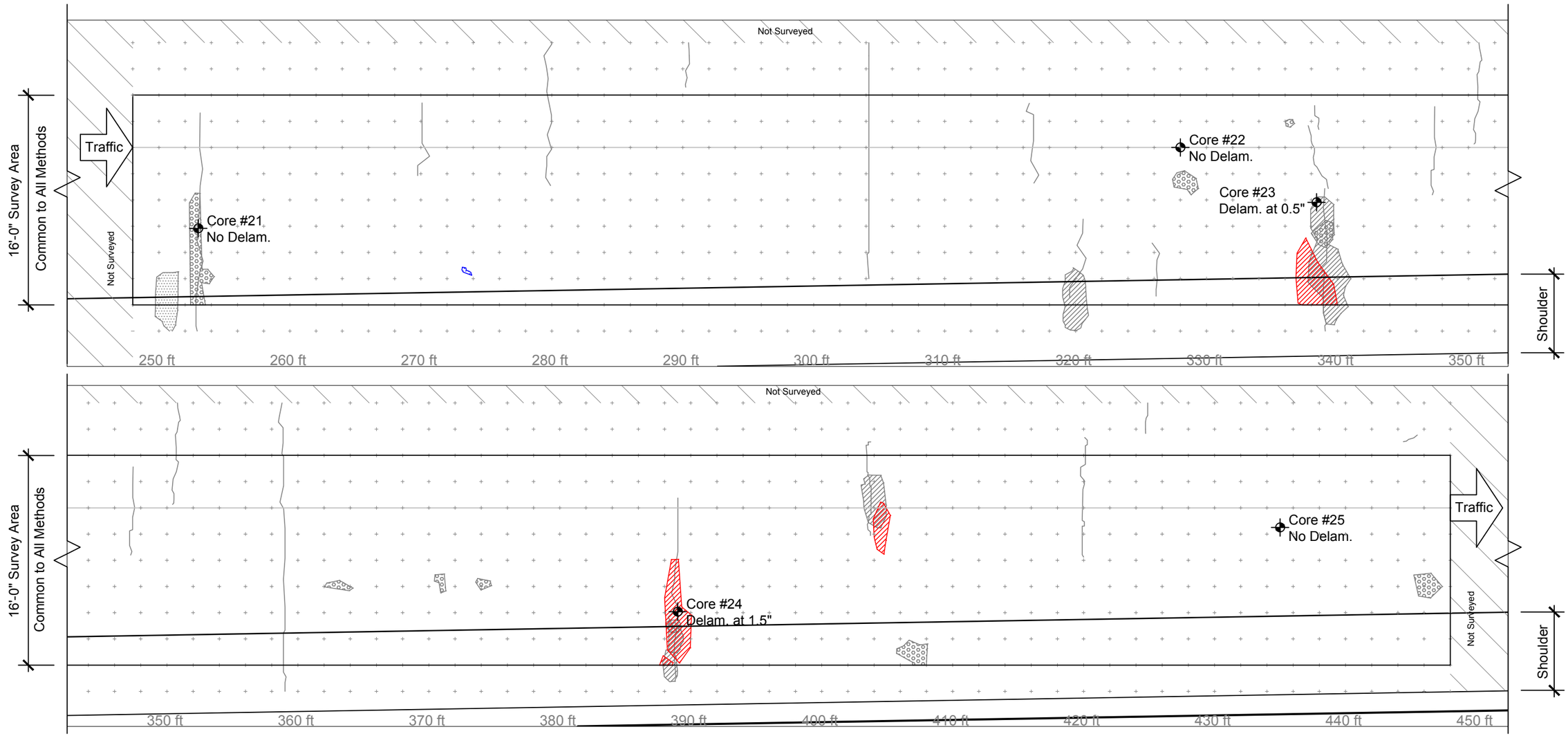

LEGEND

- Delamination, IR Survey
- Delamination, Sounding Survey
- Repair Patch, IR Survey
- Epoxy on Surface, IR Survey
- Evidence of Epoxy Repair, Visual Survey
- Surface Discoloration, IR Survey
- Crack, Visual Survey
- Construction Joint, Visual Survey
- Core

Study Area WB-1, IR Thermography

SCALE: 1/8" = 1'-0"

N

0 1/2" 1"

THIS SHEET PLOTS FULL SCALE AT 11x17 (INCHES)

WJE ENGINEERS ARCHITECTS MATERIALS SCIENTISTS
Wiss, Janney, Elstner Associates, Inc.
330 Pfingsten Road
Northbrook, Illinois 60062
847.272.7400 tel | 847.291.9599 fax
www.wje.com

Project: I-129 Missouri River Bridge (No. 9700.05129)
Deck Condition Evaluation

Sheet Title: Findings of IR Thermography

Proj. No.	2010.2389.0
Survey Date	June 20-24, 2011
Drawn	RDL
Checked	JSL
Scale	1/8" = 1'-0"

Sheet No. **B.4**

Plotted: 4/12/2012 9:03 AM by Lequesne, Remy File Name: \\wjenbfp.wje.com\projects\2010\2301-2400\2010.2389-JPD-Iowa NDE\.0_I-129 Sioux City\Drawings\Report Figures\combined study areas.dwg

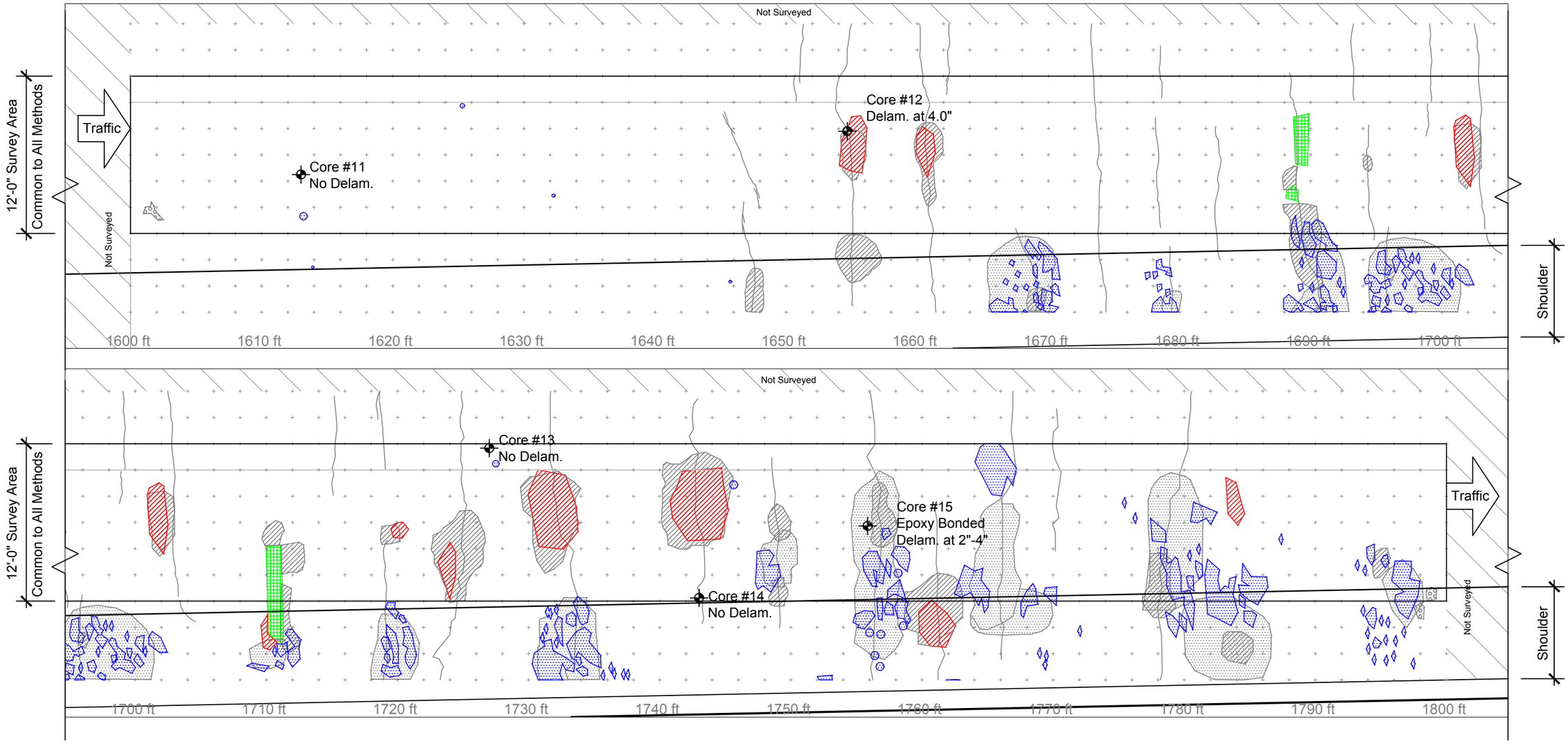

LEGEND

- Delamination, IR Survey
- Delamination, Sounding Survey
- Repair Patch, IR Survey
- Epoxy on Surface, IR Survey
- Evidence of Epoxy Repair, Visual Survey
- Surface Discoloration, IR Survey
- Crack, Visual Survey
- Construction Joint, Visual Survey
- Core

Study Area WB-2, IR Thermography

SCALE: 1/8" = 1'-0"

N

0 1/2" 1"

THIS SHEET PLOTS FULL SCALE AT 11x17 (INCHES)

WJE ENGINEERS ARCHITECTS MATERIALS SCIENTISTS

Wiss, Janney, Elstner Associates, Inc.
330 Pfingsten Road
Northbrook, Illinois 60062
847.272.7400 tel | 847.291.9599 fax
www.wje.com

Project: I-129 Missouri River Bridge (No. 9700.05129)
Deck Condition Evaluation

Sheet Title: Findings of IR Thermography

Proj. No.	2010.2389.0
Survey Date	June 20-24, 2011
Drawn	RDL
Checked	JSL
Scale	1/8" = 1'-0"

Sheet No. **B.5**

Plotted: 4/12/2012 9:03 AM by Lequesne, Remy File Name: \\wjenbfp.wje.com\projects\2010\2301-2400\2010.2389-JPD-Iowa NDE\.0_I-129 Sioux City\Drawings\Report Figures\combined study areas.dwg

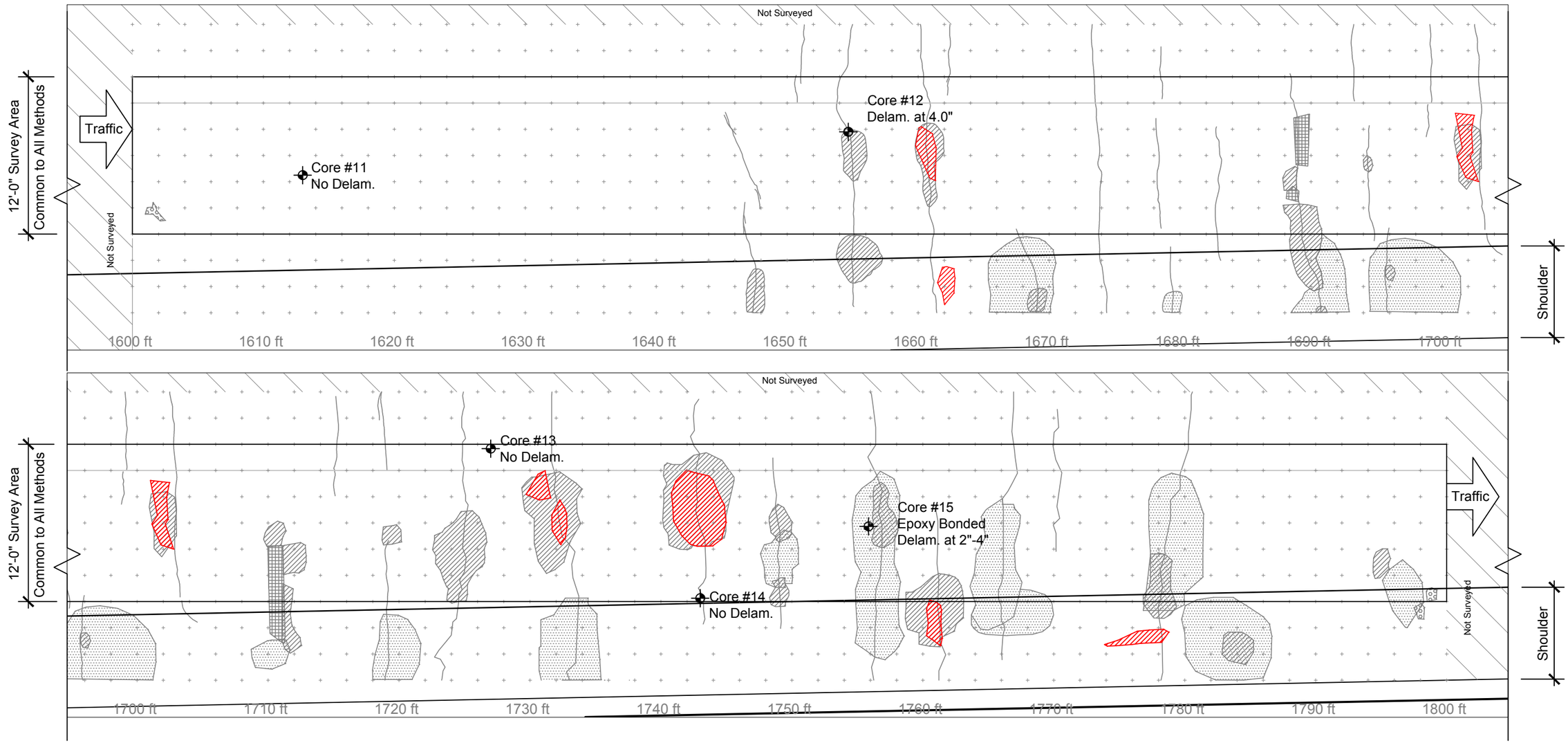

LEGEND

- Delamination, IR Survey
- Delamination, Sounding Survey
- Repair Patch, IR Survey
- Evidence of Epoxy Repair, Visual Survey
- Surface Discoloration, IR Survey
- Crack, Visual Survey
- Construction Joint, Visual Survey
- Core

Study Area WB-2, Evening Scan, IR Thermography

SCALE: 1/8" = 1'-0"

N

0 1/2" 1"

THIS SHEET PLOTS FULL SCALE AT 11x17 (INCHES)

WJE ENGINEERS ARCHITECTS MATERIALS SCIENTISTS

Wiss, Janney, Elstner Associates, Inc.
330 Pfingsten Road
Northbrook, Illinois 60062
847.272.7400 tel | 847.291.9599 fax
www.wje.com

Project: I-129 Missouri River Bridge (No. 9700.05129)
Deck Condition Evaluation

Sheet Title: Findings of IR Thermography

Proj. No.	2010.2389.0
Survey Date	June 20-24, 2011
Drawn	RDL
Checked	JSL
Scale	1/8" = 1'-0"

Sheet No. **B.6**

Plotted: 4/12/2012 9:04 AM by Lequesne, Remy File Name: \\wjenbfp.wje.com\projects\2010\2301-2400\2010.2389-JPD-Iowa NDE\.0_I-129 Sioux City\Drawings\Report Figures\combined study areas.dwg

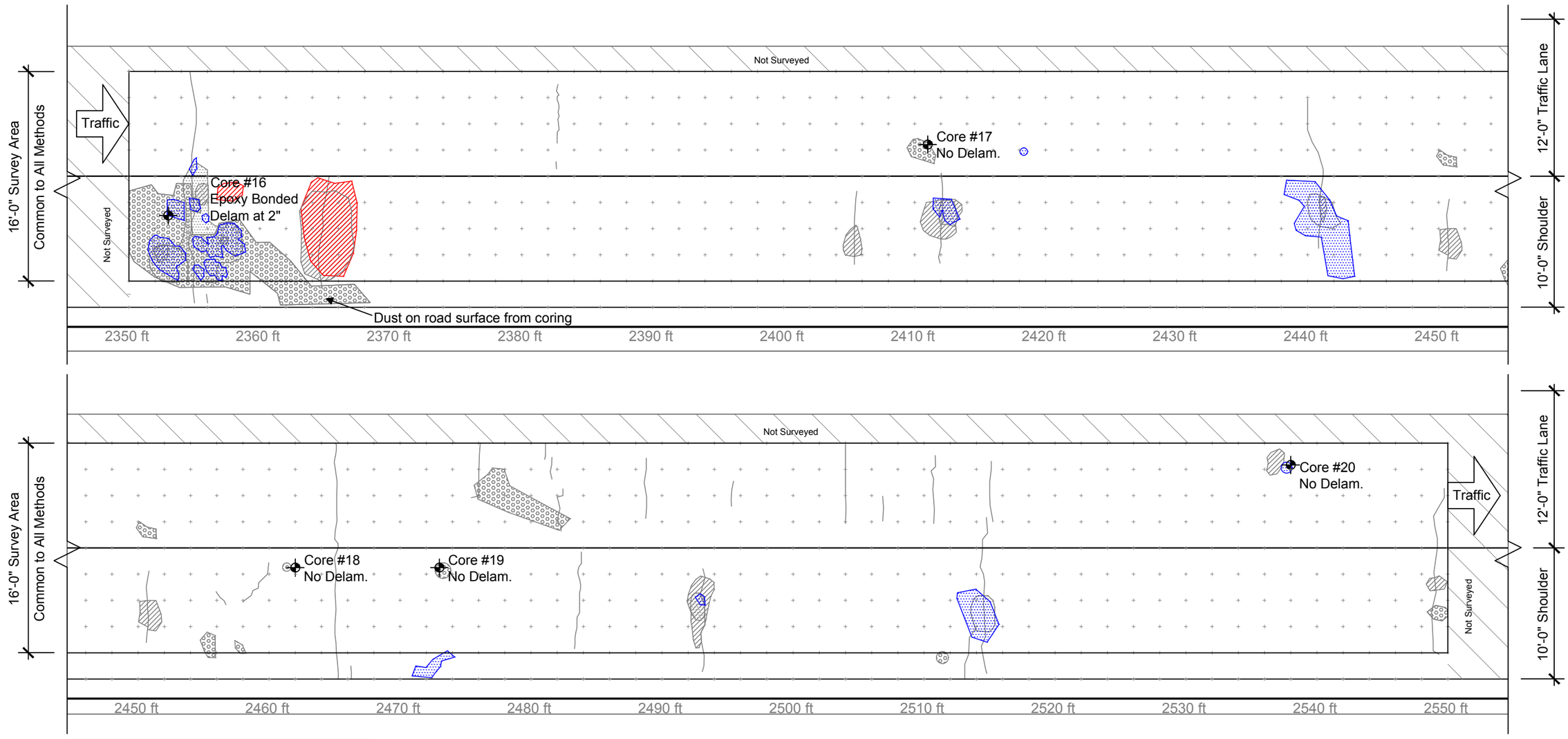

LEGEND

- Delamination, IR Survey
- Delamination, Sounding Survey
- Repair Patch, IR Survey
- Epoxy on Surface, IR Survey
- Evidence of Epoxy Repair, Visual Survey
- Surface Discoloration, IR Survey
- Crack, Visual Survey
- Construction Joint, Visual Survey
- Core

Study Area WB-3, IR Thermography

SCALE: 1/8" = 1'-0"

N

0 1/2" 1"

THIS SHEET PLOTS FULL SCALE AT 11x17 (INCHES)

WJE ENGINEERS ARCHITECTS MATERIALS SCIENTISTS

Wiss, Janney, Elstner Associates, Inc.
330 Pfingsten Road
Northbrook, Illinois 60062
847.272.7400 tel | 847.291.9599 fax
www.wje.com

Project: I-129 Missouri River Bridge (No. 9700.05129)
Deck Condition Evaluation

Sheet Title: Findings of IR Thermography

Proj. No.	2010.2389.0
Survey Date	June 20-24, 2011
Drawn	RDL
Checked	JSL
Scale	1/8" = 1'-0"

Sheet No. **B.7**

Plotted: 4/12/2012 9:04 AM by Lequesne, Remy File Name: \\wjenbfp.wje.com\projects\2010\2301-2400\2010.2389-JPD-Iowa NDE\0_I-129 Sioux City\Drawings\Report Figures\combined study areas.dwg

Appendix C

Findings of Survey of In-Depth Study Areas
Ground Penetrating Radar

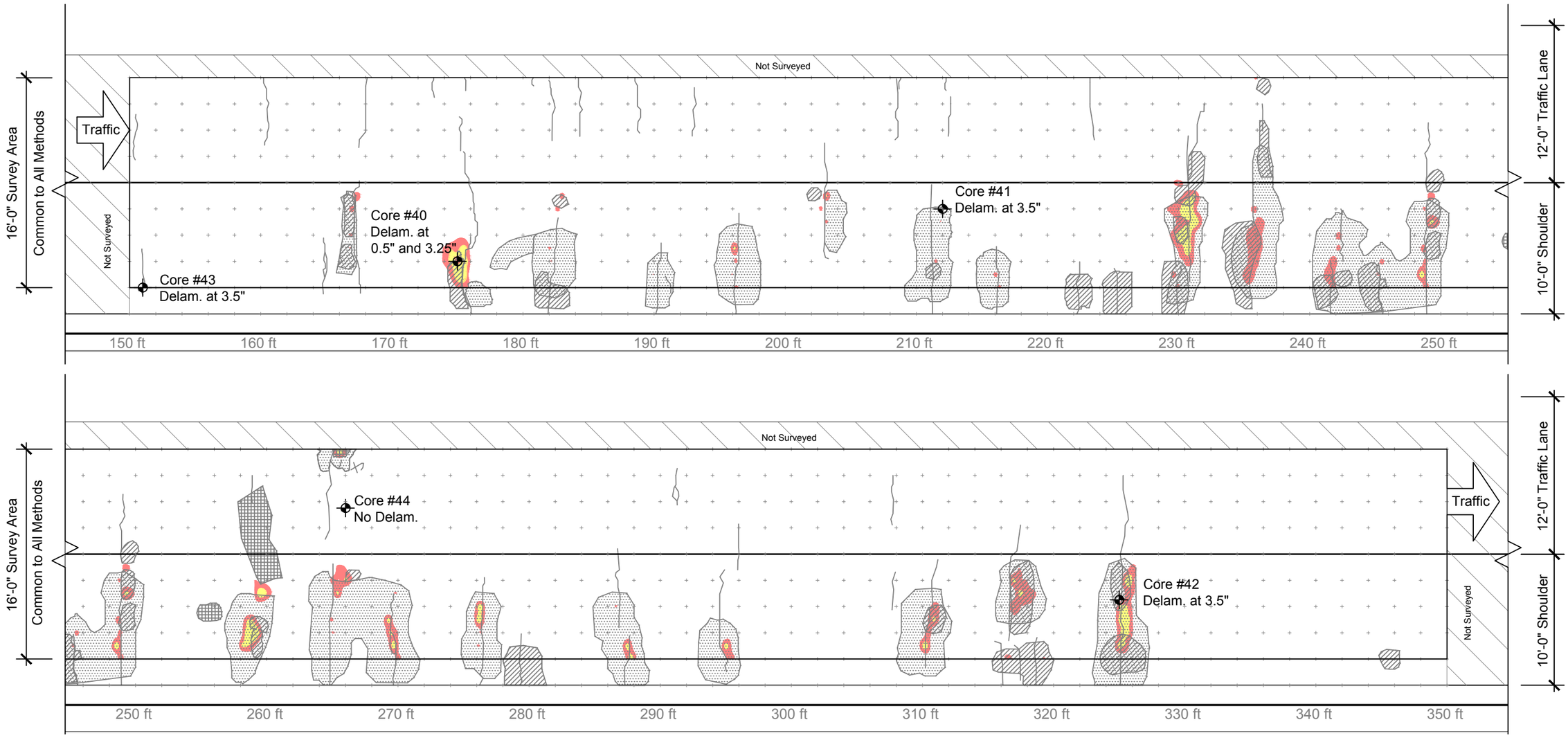

LEGEND

- Lower Delamination Threshold, GPR Survey
- Upper Delamination Threshold, GPR Survey
- Delamination, Sounding Survey
- Repair Patch, Visual Survey
- Evidence of Epoxy Repair, Visual Survey
- Crack, Visual Survey
- Construction Joint, Visual Survey
- Core

Study Area EB-1, GPR 1.6GHz

SCALE: 1/8" = 1'-0"

N

0 1/2" 1"

THIS SHEET PLOTS FULL SCALE AT 11x17 (INCHES)

WJE ENGINEERS ARCHITECTS MATERIALS SCIENTISTS

Wiss, Janney, Elstner Associates, Inc.
330 Pfingsten Road
Northbrook, Illinois 60062
847.272.7400 tel | 847.291.9599 fax
www.wje.com

Project	I-129 Missouri River Bridge (No. 9700.05129) Deck Condition Evaluation
Sheet Title	Findings of Ground Penetrating Radar Survey
Proj. No.	2010.2389.0
Survey Date	June 20-24, 2011
Drawn	RDL
Checked	JSL
Scale	1/8" = 1'-0"
Sheet No.	**C.1**

Plotted: 4/12/2012 9:04 AM by Lequesne, Remy File Name: \\wjenbfp.wje.com\projects\2010\2301-2400\2010.2389-JPD-Iowa NDE\.0_I-129 Sioux City\Drawings\Report Figures\combined study areas.dwg

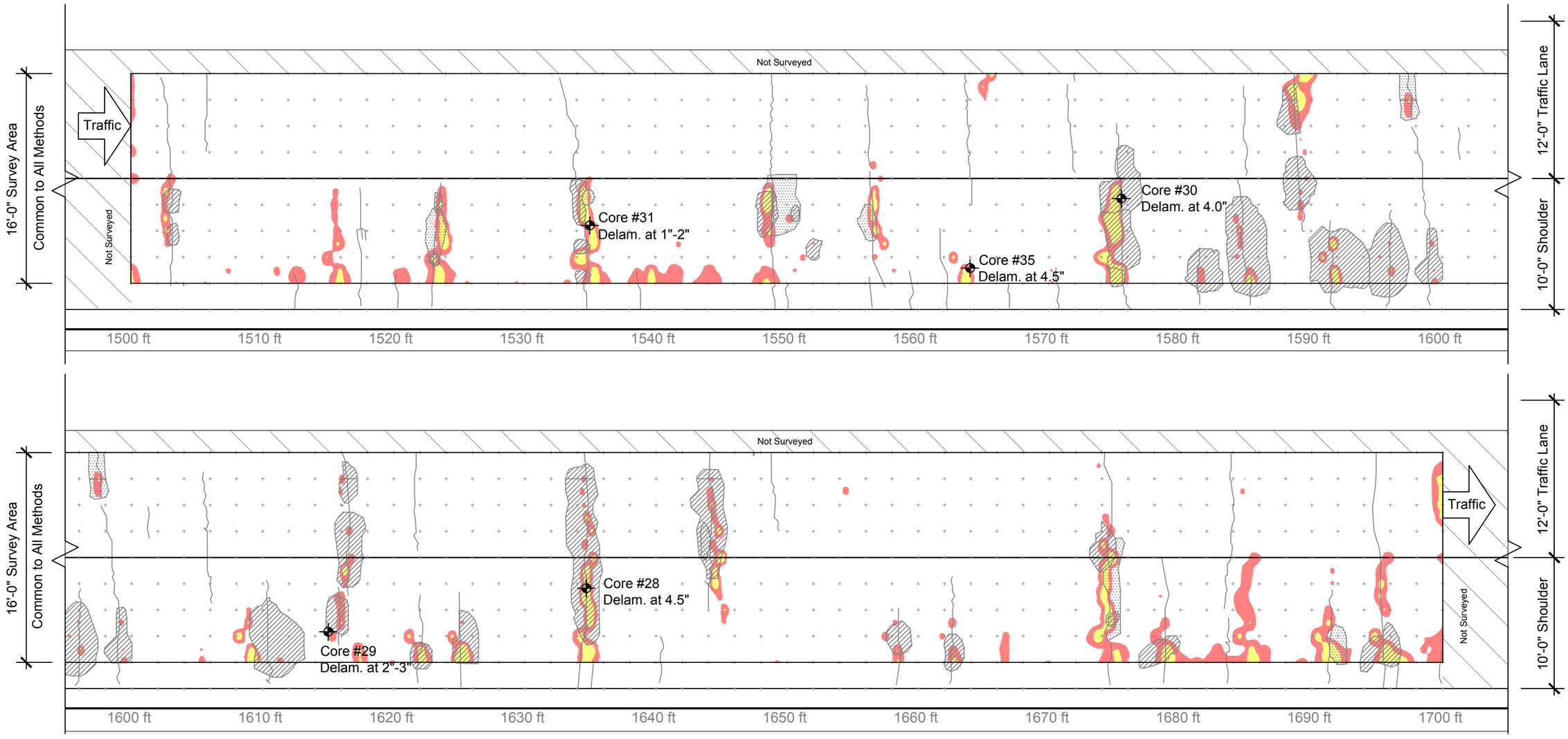

LEGEND

- Lower Delamination Threshold, GPR Survey
- Upper Delamination Threshold, GPR Survey
- Delamination, Sounding Survey
- Repair Patch, Visual Survey
- Evidence of Epoxy Repair, Visual Survey
- Crack, Visual Survey
- Construction Joint, Visual Survey
- Core

Study Area EB-2, GPR 1.6GHz

SCALE: 1/8" = 1'-0"

N

0 1/2" 1"

THIS SHEET PLOTS FULL SCALE AT 11x17 (INCHES)

WJE ENGINEERS ARCHITECTS MATERIALS SCIENTISTS

Wiss, Janney, Elstner Associates, Inc.
330 Pfingsten Road
Northbrook, Illinois 60062
847.272.7400 tel | 847.291.9599 fax
www.wje.com

Project: I-129 Missouri River Bridge (No. 9700.05129)
Deck Condition Evaluation

Sheet Title: Findings of Ground Penetrating Radar Survey

Proj. No.	2010.2389.0
Survey Date	June 20-24, 2011
Drawn	RDL
Checked	JSL
Scale	1/8" = 1'-0"

Sheet No. **C.2**

Plotted: 4/12/2012 9:04 AM by Lequesne, Remy File Name: \\wjenbfp.wje.com\projects\2010\2301-2400\2010.2389-JPD-Iowa NDE\.0_I-129 Sioux City\Drawings\Report Figures\combined study areas.dwg

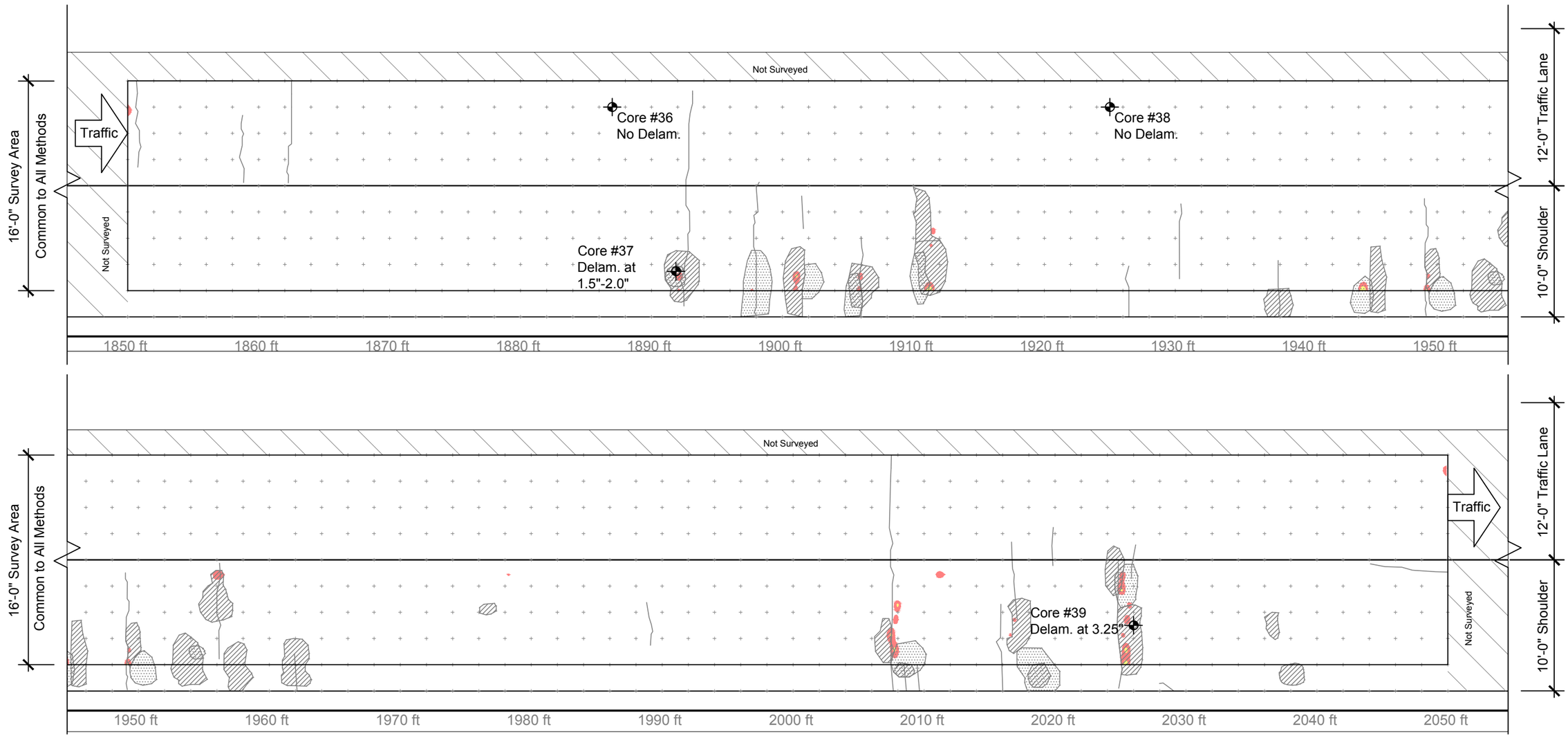

LEGEND

- Lower Delamination Threshold, GPR Survey
- Upper Delamination Threshold, GPR Survey
- Delamination, Sounding Survey
- Repair Patch, Visual Survey
- Evidence of Epoxy Repair, Visual Survey
- Crack, Visual Survey
- Construction Joint, Visual Survey
- Core

Study Area EB-3, GPR 1.6GHz

SCALE: 1/8" = 1'-0"

N

0 1/2" 1"

THIS SHEET PLOTS FULL SCALE AT 11x17 (INCHES)

WJE ENGINEERS ARCHITECTS MATERIALS SCIENTISTS

Wiss, Janney, Elstner Associates, Inc.
330 Pfingsten Road
Northbrook, Illinois 60062
847.272.7400 tel | 847.291.9599 fax
www.wje.com

Project: I-129 Missouri River Bridge (No. 9700.05129)
Deck Condition Evaluation

Sheet Title: Findings of Ground Penetrating Radar Survey

Proj. No.	2010.2389.0
Survey Date	June 20-24, 2011
Drawn	RDL
Checked	JSL
Scale	1/8" = 1'-0"

Sheet No. **C.3**

Plotted: 4/12/2012 9:04 AM by Lequesne, Remy File Name: \\wjenbfp.wje.com\projects\2010\2301-2400\2010.2389-JPD-Iowa NDE\.0_I-129 Sioux City\Drawings\Report Figures\combined study areas.dwg

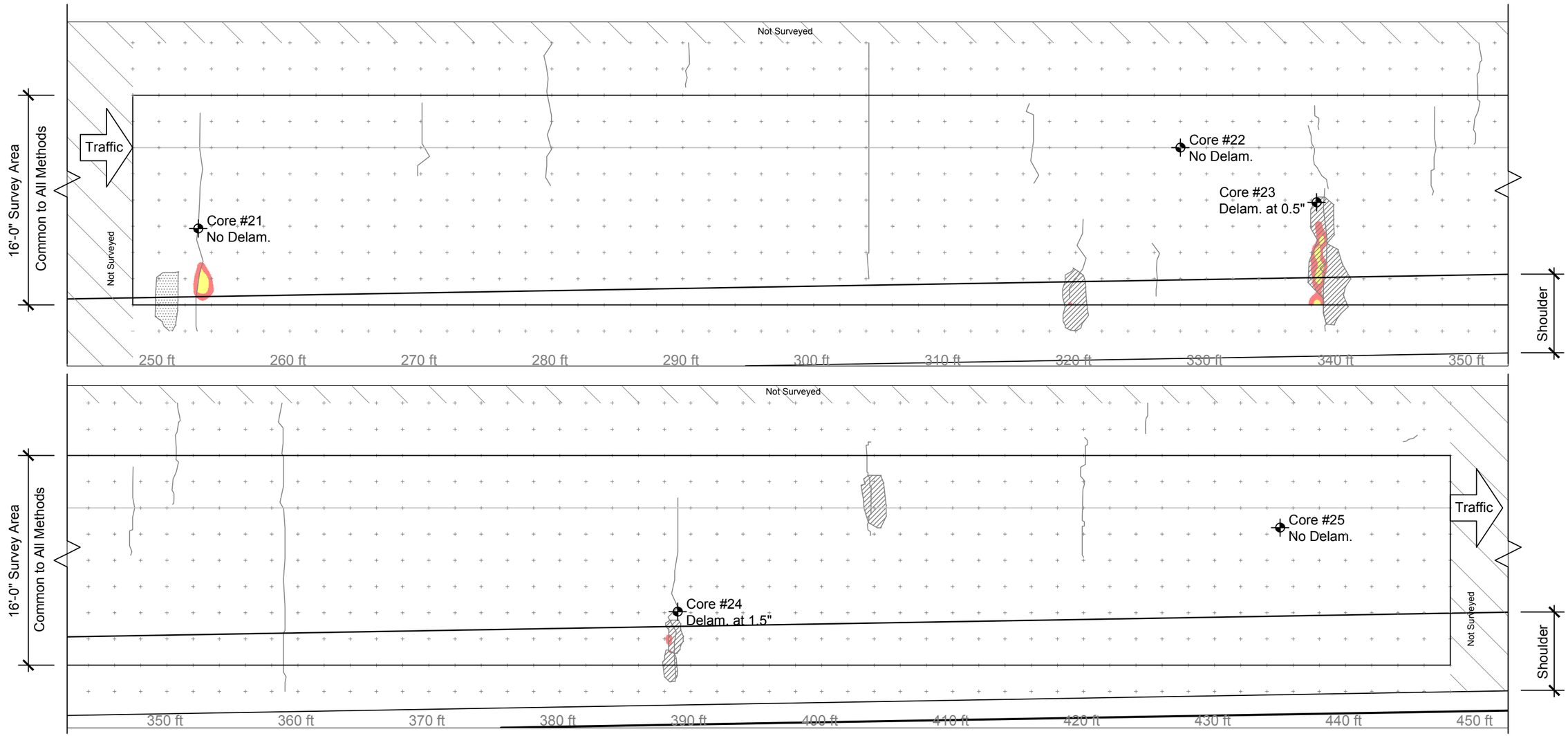

LEGEND

- Lower Delamination Threshold, GPR Survey
- Upper Delamination Threshold, GPR Survey
- Delamination, Sounding Survey
- Repair Patch, Visual Survey
- Evidence of Epoxy Repair, Visual Survey
- Crack, Visual Survey
- Construction Joint, Visual Survey
- Core

Study Area WB-1, GPR 1.6GHz

SCALE: 1/8" = 1'-0"

N

0 1/2" 1"

THIS SHEET PLOTS FULL SCALE AT 11x17 (INCHES)

WJE ENGINEERS ARCHITECTS MATERIALS SCIENTISTS

Wiss, Janney, Elstner Associates, Inc.
330 Pfingsten Road
Northbrook, Illinois 60062
847.272.7400 tel | 847.291.9599 fax
www.wje.com

Project: I-129 Missouri River Bridge (No. 9700.05129)
Deck Condition Evaluation

Sheet Title: Findings of Ground Penetrating Radar Survey

Proj. No.	2010.2389.0
Survey Date	June 20-24, 2011
Drawn	RDL
Checked	JSL
Scale	1/8" = 1'-0"
Sheet No.	C.4

Plotted: 4/12/2012 9:04 AM by Lequesne, Remy File Name: \\wjenbfp.wje.com\projects\2010\2301-2400\2010.2389-JPD-Iowa NDE\.0_I-129 Sioux City\Drawings\Report Figures\combined study areas.dwg

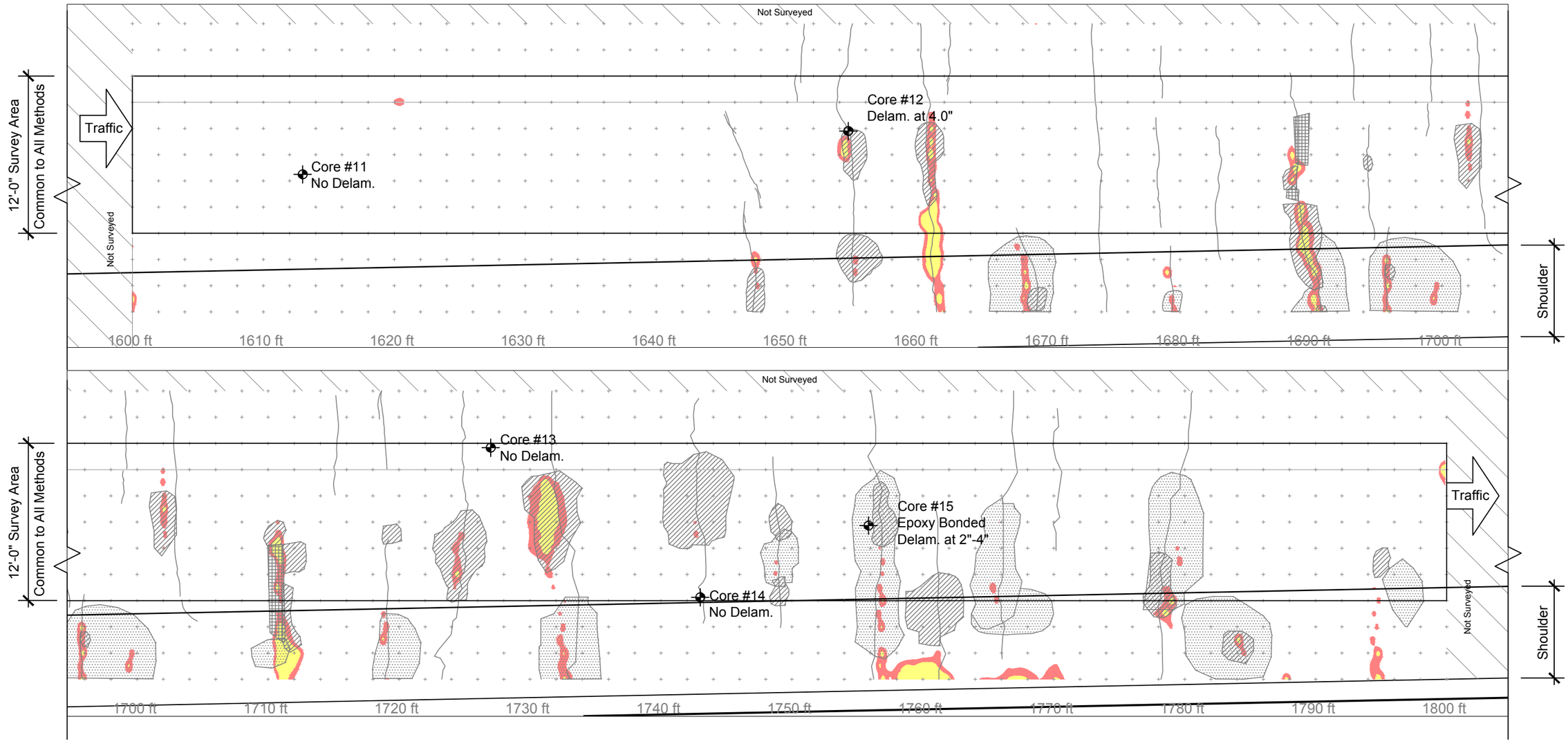

LEGEND

- Lower Delamination Threshold, GPR Survey
- Upper Delamination Threshold, GPR Survey
- Delamination, Sounding Survey
- Repair Patch, Visual Survey
- Evidence of Epoxy Repair, Visual Survey
- Crack, Visual Survey
- Construction Joint, Visual Survey
- Core

Study Area WB-2, GPR 1.6GHz

SCALE: 1/8" = 1'-0"

N

0 1/2" 1"

THIS SHEET PLOTS FULL SCALE AT 11x17 (INCHES)

WJE ENGINEERS ARCHITECTS MATERIALS SCIENTISTS

Wiss, Janney, Elstner Associates, Inc.
330 Pfingsten Road
Northbrook, Illinois 60062
847.272.7400 tel | 847.291.9599 fax
www.wje.com

Project: I-129 Missouri River Bridge (No. 9700.05129)
Deck Condition Evaluation

Sheet Title: Findings of Ground Penetrating Radar Survey

Proj. No.	2010.2389.0
Survey Date	June 20-24, 2011
Drawn	RDL
Checked	JSL
Scale	1/8" = 1'-0"

Sheet No. **C.5**

Plotted: 4/12/2012 9:04 AM by Lequesne, Remy File Name: \\wjenbfp.wje.com\projects\2010\2301-2400\2010.2389-JPD-Iowa NDE\.0_I-129 Sioux City\Drawings\Report Figures\combined study areas.dwg

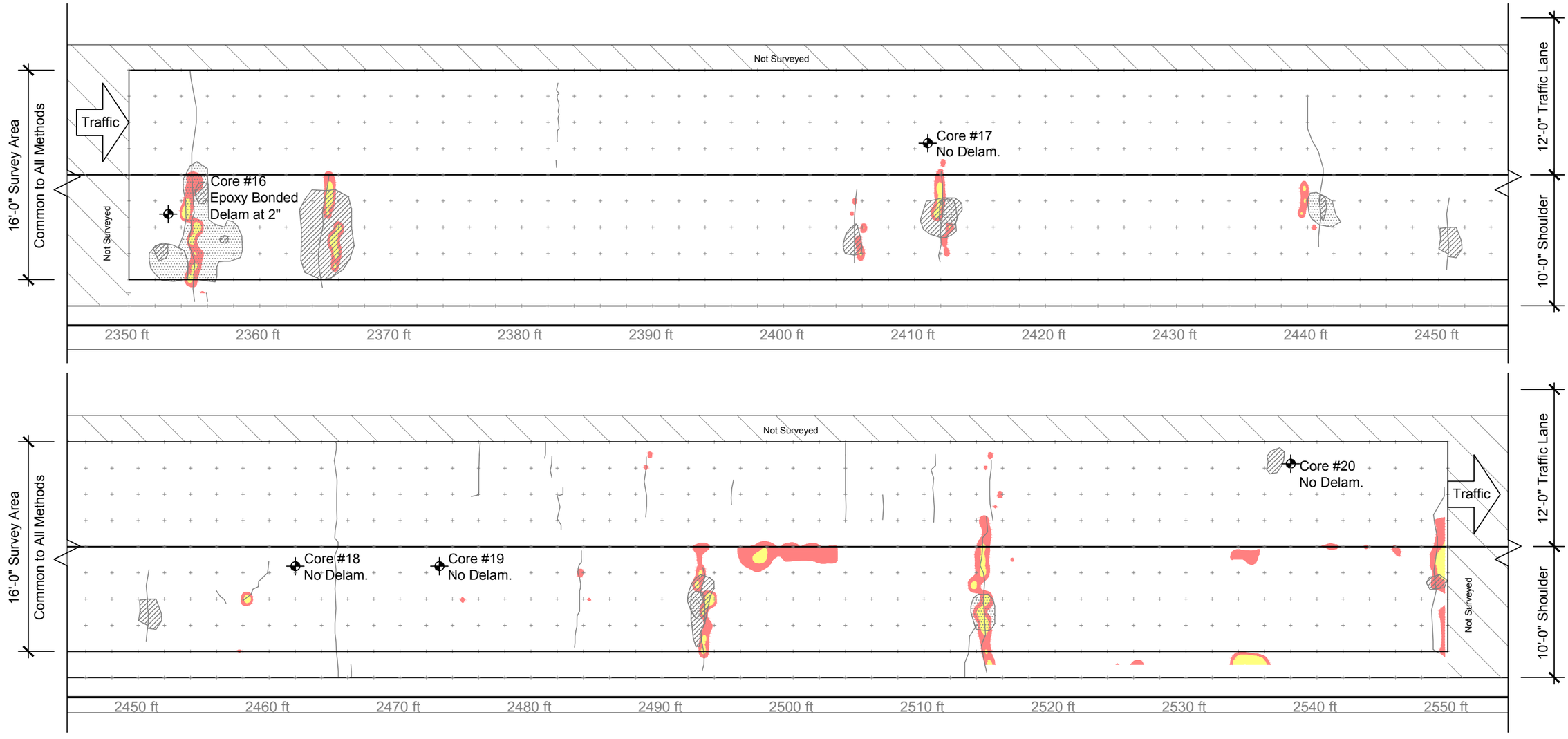

LEGEND

- Lower Delamination Threshold, GPR Survey
- Upper Delamination Threshold, GPR Survey
- Delamination, Sounding Survey
- Repair Patch, Visual Survey
- Evidence of Epoxy Repair, Visual Survey
- Crack, Visual Survey
- Construction Joint, Visual Survey
- Core

Study Area WB-3, GPR 1.6GHz

SCALE: 1/8" = 1'-0"

N

0 1/2" 1"

THIS SHEET PLOTS FULL SCALE AT 11x17 (INCHES)

WJE ENGINEERS ARCHITECTS MATERIALS SCIENTISTS

Wiss, Janney, Elstner Associates, Inc.
330 Pfingsten Road
Northbrook, Illinois 60062
847.272.7400 tel | 847.291.9599 fax
www.wje.com

Project: I-129 Missouri River Bridge (No. 9700.05129)
Deck Condition Evaluation

Sheet Title: Findings of Ground Penetrating Radar Survey

Proj. No.	2010.2389.0
Survey Date	June 20-24, 2011
Drawn	RDL
Checked	JSL
Scale	1/8" = 1'-0"

Sheet No. C.6

Plotted: 4/12/2012 9:04 AM by Lequesne, Remy File Name: \\wjenbfp.wje.com\projects\2010\2301-2400\2010.2389-JPD-Iowa NDE\.0_I-129 Sioux City\Drawings\Report Figures\combined study areas.dwg

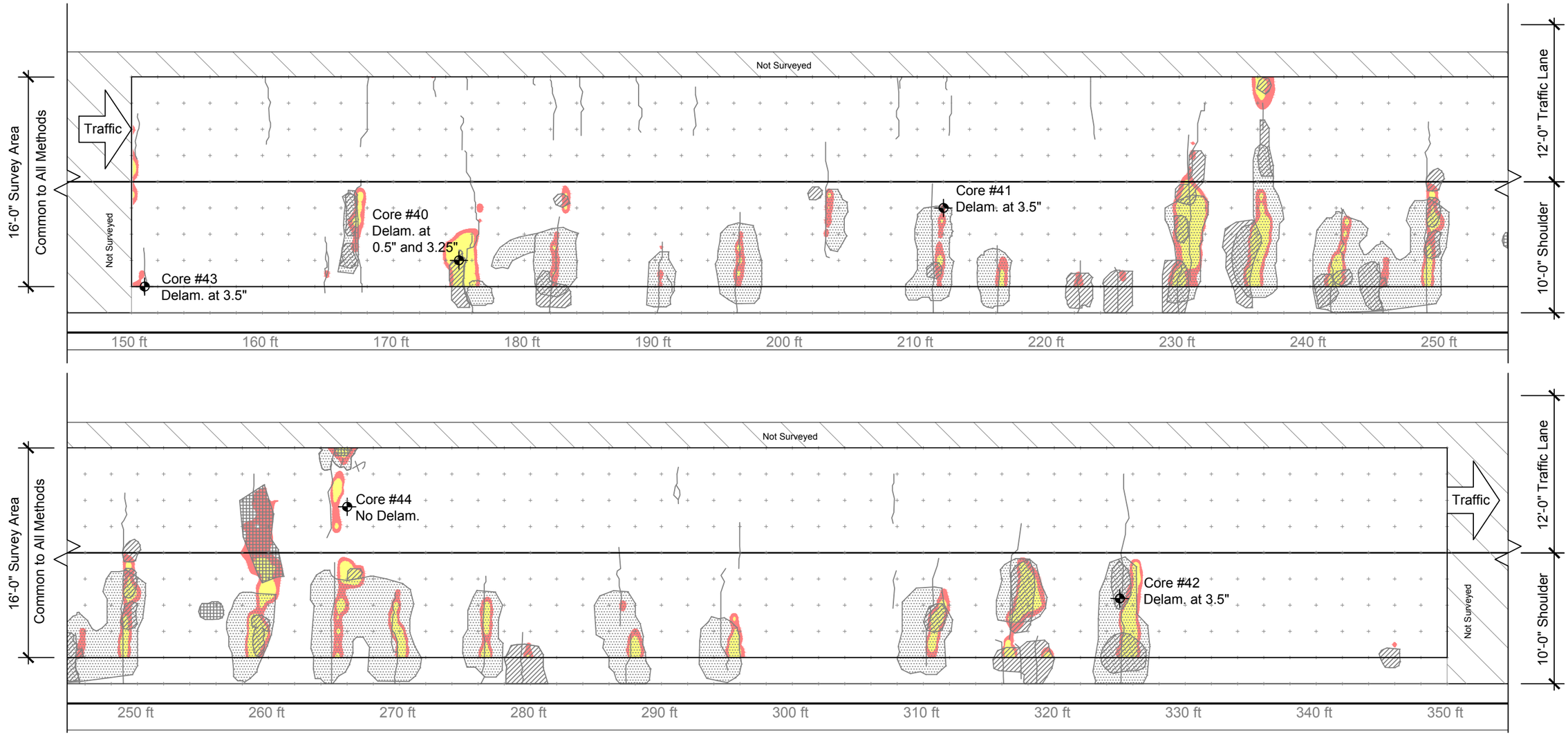

LEGEND

- Lower Delamination Threshold, GPR Survey
- Upper Delamination Threshold, GPR Survey
- Delamination, Sounding Survey
- Repair Patch, Visual Survey
- Evidence of Epoxy Repair, Visual Survey
- Crack, Visual Survey
- Construction Joint, Visual Survey
- Core

Study Area EB-1, GPR 2.6GHz

SCALE: 1/8" = 1'-0"

N

0 1/2" 1"

THIS SHEET PLOTS FULL SCALE AT 11x17 (INCHES)

WJE ENGINEERS ARCHITECTS MATERIALS SCIENTISTS

Wiss, Janney, Elstner Associates, Inc.
330 Pfingsten Road
Northbrook, Illinois 60062
847.272.7400 tel | 847.291.9599 fax
www.wje.com

Project: I-129 Missouri River Bridge (No. 9700.05129)
Deck Condition Evaluation

Sheet Title: Findings of Ground Penetrating Radar Survey

Proj. No.	2010.2389.0
Survey Date	June 20-24, 2011
Drawn	RDL
Checked	JSL
Scale	1/8" = 1'-0"

Sheet No. C.7

Plotted: 4/12/2012 9:04 AM by Lequesne, Remy File Name: \\wjenbfp.wje.com\projects\2010\2301-2400\2010.2389-JPD-Iowa NDE\.0_I-129 Sioux City\Drawings\Report Figures\combined study areas.dwg

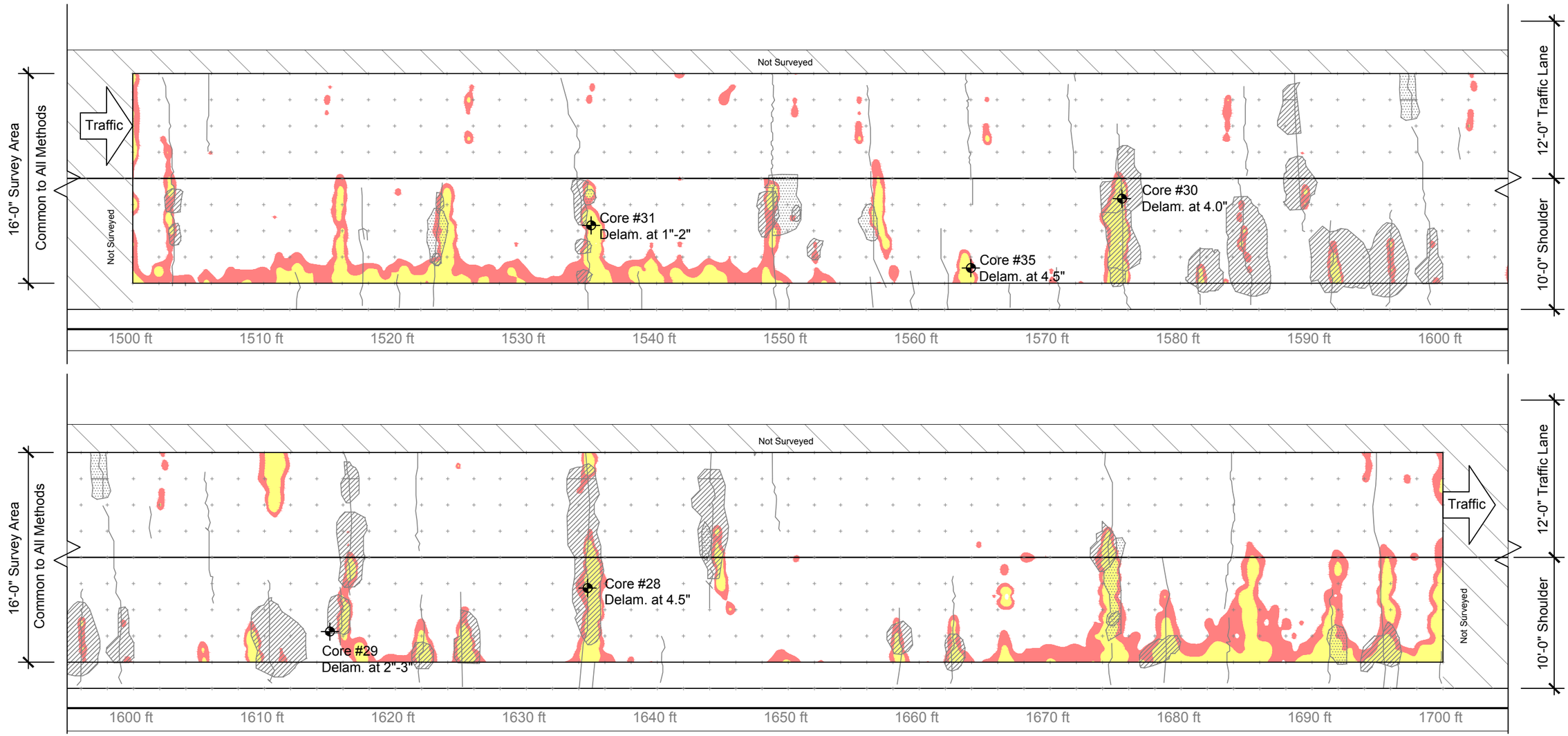

LEGEND

- Lower Delamination Threshold, GPR Survey
- Upper Delamination Threshold, GPR Survey
- Delamination, Sounding Survey
- Repair Patch, Visual Survey
- Evidence of Epoxy Repair, Visual Survey
- Crack, Visual Survey
- Construction Joint, Visual Survey
- Core

Study Area EB-2, GPR 2.6GHz

SCALE: 1/8" = 1'-0"

N

0 1/2" 1"

THIS SHEET PLOTS FULL SCALE AT 11x17 (INCHES)

WJE ENGINEERS ARCHITECTS MATERIALS SCIENTISTS

Wiss, Janney, Elstner Associates, Inc.
330 Pfingsten Road
Northbrook, Illinois 60062
847.272.7400 tel | 847.291.9599 fax
www.wje.com

Project: I-129 Missouri River Bridge (No. 9700.05129)
Deck Condition Evaluation

Sheet Title: Findings of Ground Penetrating Radar Survey

Proj. No.	2010.2389.0
Survey Date	June 20-24, 2011
Drawn	RDL
Checked	JSL
Scale	1/8" = 1'-0"

Sheet No. **C.8**

Plotted: 4/12/2012 9:04 AM by Lequesne, Remy File Name: \\wjenbfp.wje.com\projects\2010\2301-2400\2010.2389-JPD-Iowa NDE\.0_I-129 Sioux City\Drawings\Report Figures\combined study areas.dwg

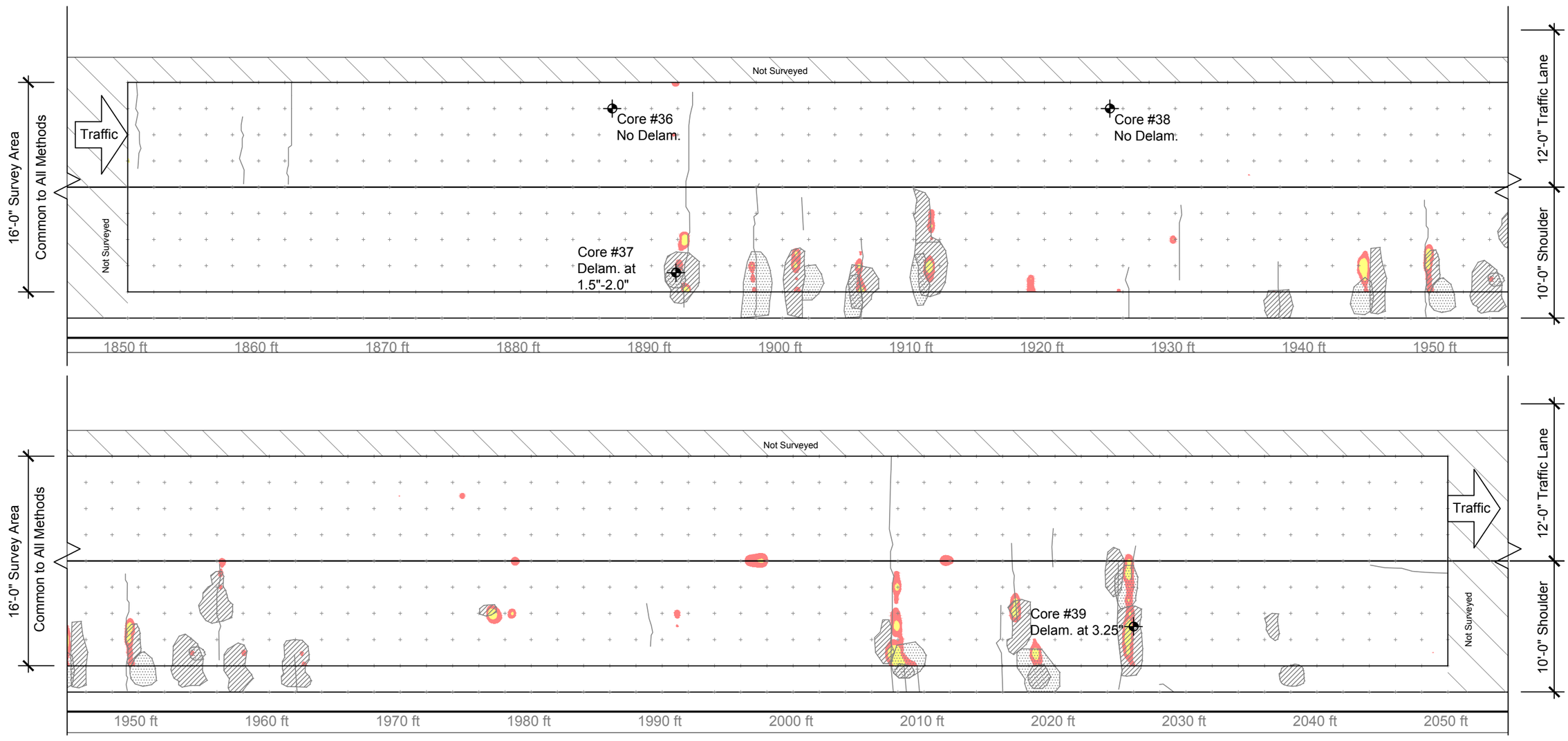

LEGEND

- Lower Delamination Threshold, GPR Survey
- Upper Delamination Threshold, GPR Survey
- Delamination, Sounding Survey
- Repair Patch, Visual Survey
- Evidence of Epoxy Repair, Visual Survey
- Crack, Visual Survey
- Construction Joint, Visual Survey
- Core

Study Area EB-3, GPR 2.6GHz

SCALE: 1/8" = 1'-0"

N

0 1/2" 1"

THIS SHEET PLOTS FULL SCALE AT 11x17 (INCHES)

WJE ENGINEERS ARCHITECTS MATERIALS SCIENTISTS

Wiss, Janney, Elstner Associates, Inc.
330 Pfingsten Road
Northbrook, Illinois 60062
847.272.7400 tel | 847.291.9599 fax
www.wje.com

Project: I-129 Missouri River Bridge (No. 9700.05129)
Deck Condition Evaluation

Sheet Title: Findings of Ground Penetrating Radar Survey

Proj. No.	2010.2389.0
Survey Date	June 20-24, 2011
Drawn	RDL
Checked	JSL
Scale	1/8" = 1'-0"

Sheet No. **C.9**

Plotted: 4/12/2012 9:04 AM by Lequesne, Remy File Name: \\wjenbfp.wje.com\projects\2010\2301-2400\2010.2389-JPD-Iowa NDE\.0_I-129 Sioux City\Drawings\Report Figures\combined study areas.dwg

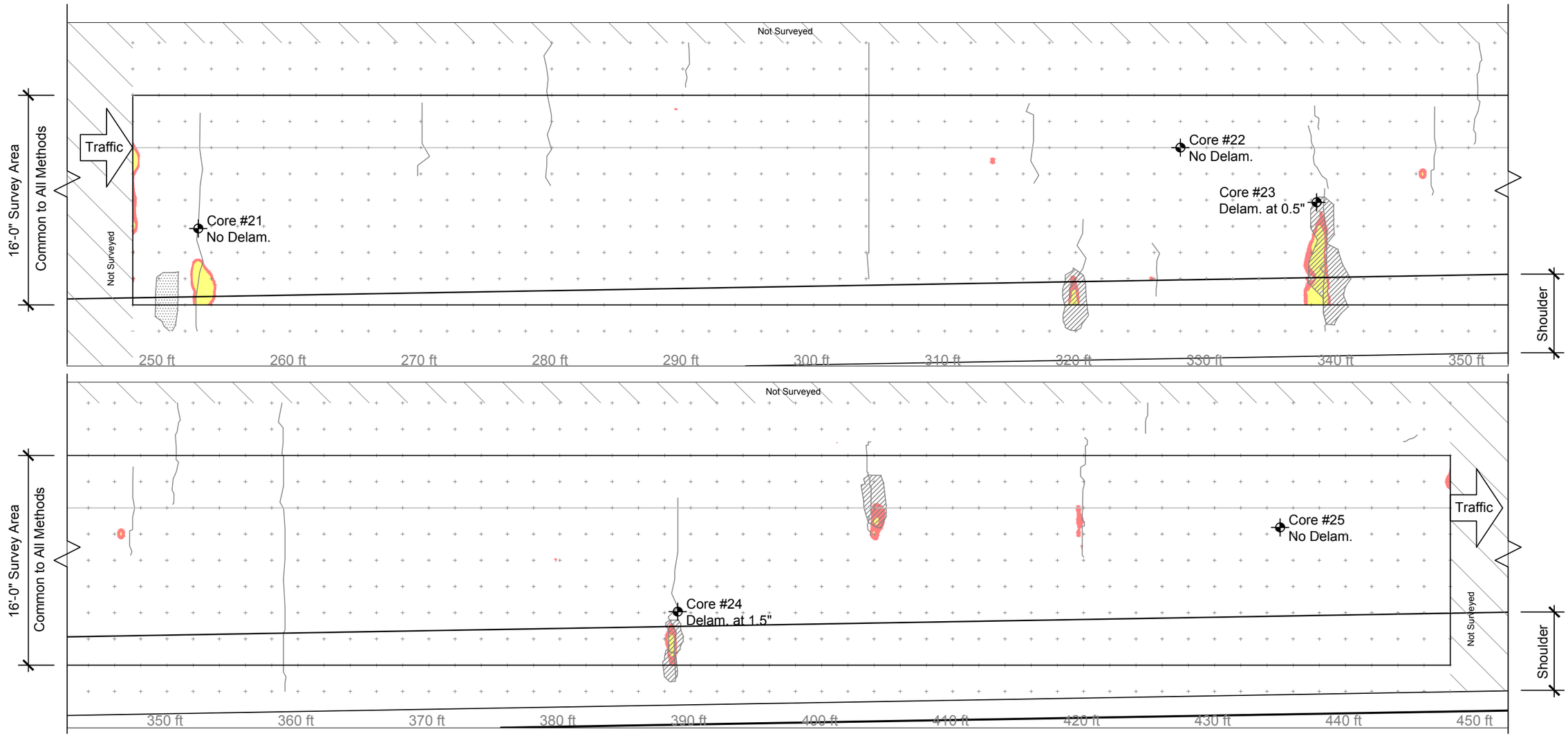

LEGEND

- Lower Delamination Threshold, GPR Survey
- Upper Delamination Threshold, GPR Survey
- Delamination, Sounding Survey
- Repair Patch, Visual Survey
- Evidence of Epoxy Repair, Visual Survey
- Crack, Visual Survey
- Construction Joint, Visual Survey
- Core

Study Area WB-1, GPR 2.6GHz

SCALE: 1/8" = 1'-0"

N

0 1/2" 1"

THIS SHEET PLOTS FULL SCALE AT 11x17 (INCHES)

WJE ENGINEERS ARCHITECTS MATERIALS SCIENTISTS

Wiss, Janney, Elstner Associates, Inc.
330 Pfingsten Road
Northbrook, Illinois 60062
847.272.7400 tel | 847.291.9599 fax
www.wje.com

Project: I-129 Missouri River Bridge (No. 9700.05129)
Deck Condition Evaluation

Sheet Title: Findings of Ground Penetrating Radar Survey

Proj. No.	2010.2389.0
Survey Date	June 20-24, 2011
Drawn	RDL
Checked	JSL
Scale	1/8" = 1'-0"
Sheet No.	C.10

Plotted: 4/12/2012 9:04 AM by Lequesne, Remy File Name: \\wjenbfp.wje.com\projects\2010\2301-2400\2010.2389-JPD-Iowa NDE\.0_I-129 Sioux City\Drawings\Report Figures\combined study areas.dwg

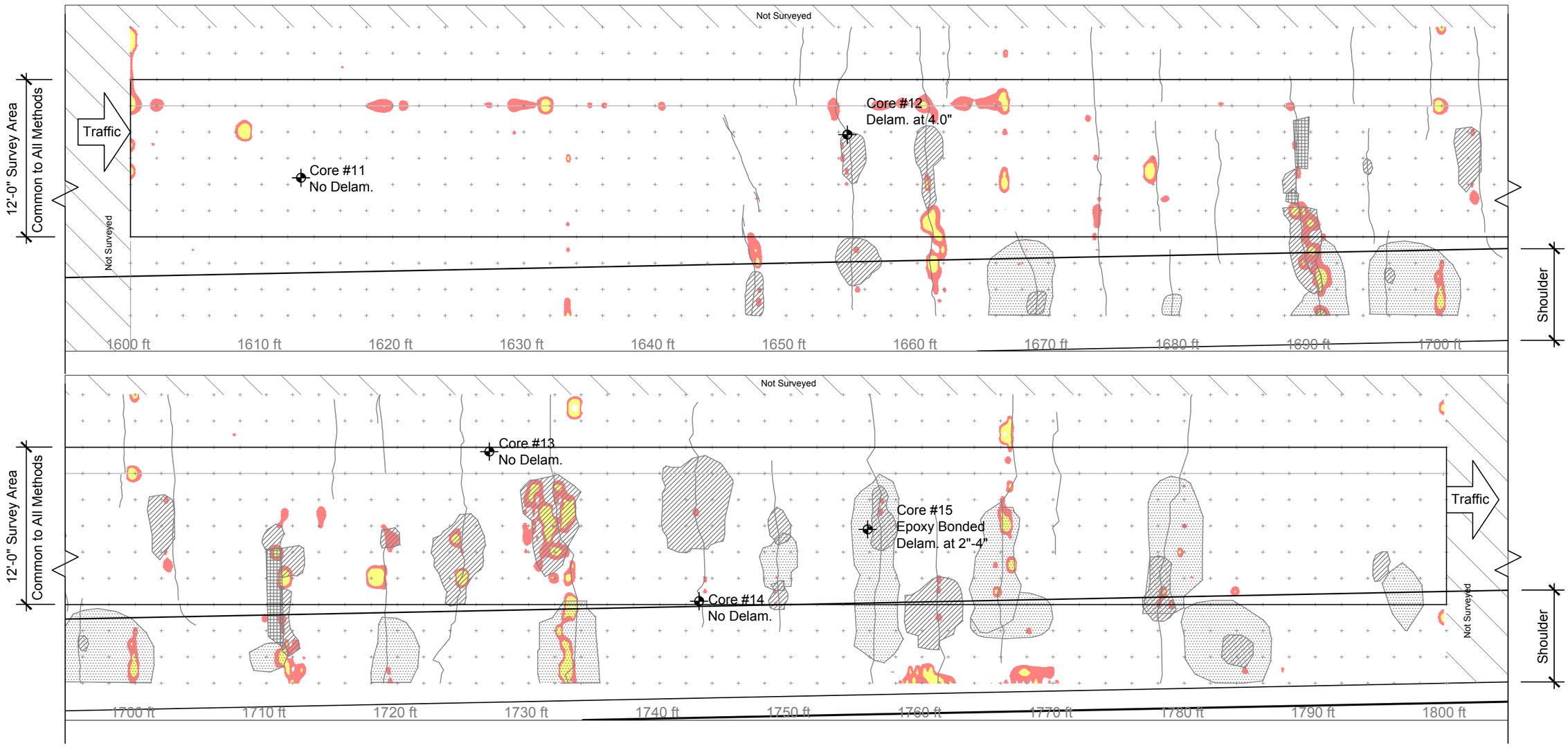

LEGEND

- Lower Delamination Threshold, GPR Survey
- Upper Delamination Threshold, GPR Survey
- Delamination, Sounding Survey
- Repair Patch, Visual Survey
- Evidence of Epoxy Repair, Visual Survey
- Crack, Visual Survey
- Construction Joint, Visual Survey
- Core

Study Area WB-2, GPR 2.6GHz

SCALE: 1/8" = 1'-0"

N

0 1/2" 1"

THIS SHEET PLOTS FULL SCALE AT 11x17 (INCHES)

WJE ENGINEERS ARCHITECTS MATERIALS SCIENTISTS

Wiss, Janney, Elstner Associates, Inc.
330 Pfingsten Road
Northbrook, Illinois 60062
847.272.7400 tel | 847.291.9599 fax
www.wje.com

Project: I-129 Missouri River Bridge (No. 9700.05129)
Deck Condition Evaluation

Sheet Title: Findings of Ground Penetrating Radar Survey

Proj. No.	2010.2389.0
Survey Date	June 20-24, 2011
Drawn	RDL
Checked	JSL
Scale	1/8" = 1'-0"
Sheet No.	C.11

Plotted: 4/12/2012 9:04 AM by Lequesne, Remy File Name: \\wjenbfp.wje.com\projects\2010\2301-2400\2010.2389-JPD-Iowa NDE\.0_I-129 Sioux City\Drawings\Report Figures\combined study areas.dwg

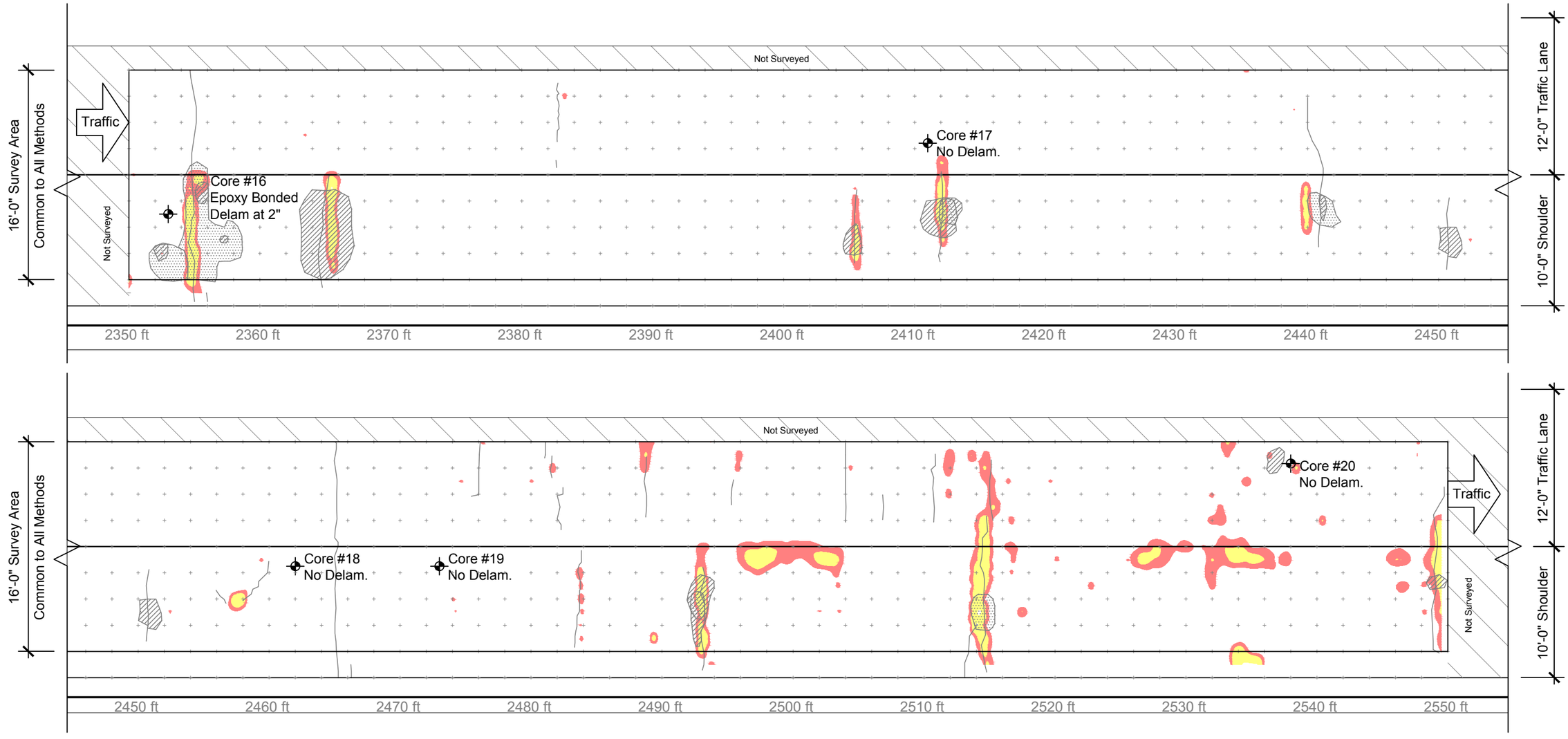

LEGEND

- Lower Delamination Threshold, GPR Survey
- Upper Delamination Threshold, GPR Survey
- Delamination, Sounding Survey
- Repair Patch, Visual Survey
- Evidence of Epoxy Repair, Visual Survey
- Crack, Visual Survey
- Construction Joint, Visual Survey
- Core

Study Area WB-3, GPR 2.6GHz

SCALE: 1/8" = 1'-0"

N

0 1/2" 1"

THIS SHEET PLOTS FULL SCALE AT 11x17 (INCHES)

WJE ENGINEERS ARCHITECTS MATERIALS SCIENTISTS

Wiss, Janney, Elstner Associates, Inc.
330 Pfingsten Road
Northbrook, Illinois 60062
847.272.7400 tel | 847.291.9599 fax
www.wje.com

Project: I-129 Missouri River Bridge (No. 9700.05129)
Deck Condition Evaluation

Sheet Title: Findings of Ground Penetrating Radar Survey

Proj. No.	2010.2389.0
Survey Date	June 20-24, 2011
Drawn	RDL
Checked	JSL
Scale	1/8" = 1'-0"

Sheet No. **C.12**

Plotted: 4/12/2012 9:05 AM by Lequesne, Remy File Name: \\wjenbfp.wje.com\projects\2010\2301-2400\2010.2389-JPD-Iowa NDE\.0_I-129 Sioux City\Drawings\Report Figures\combined study areas.dwg

Appendix D

Findings of Survey of In-Depth Study Areas
Impact Echo

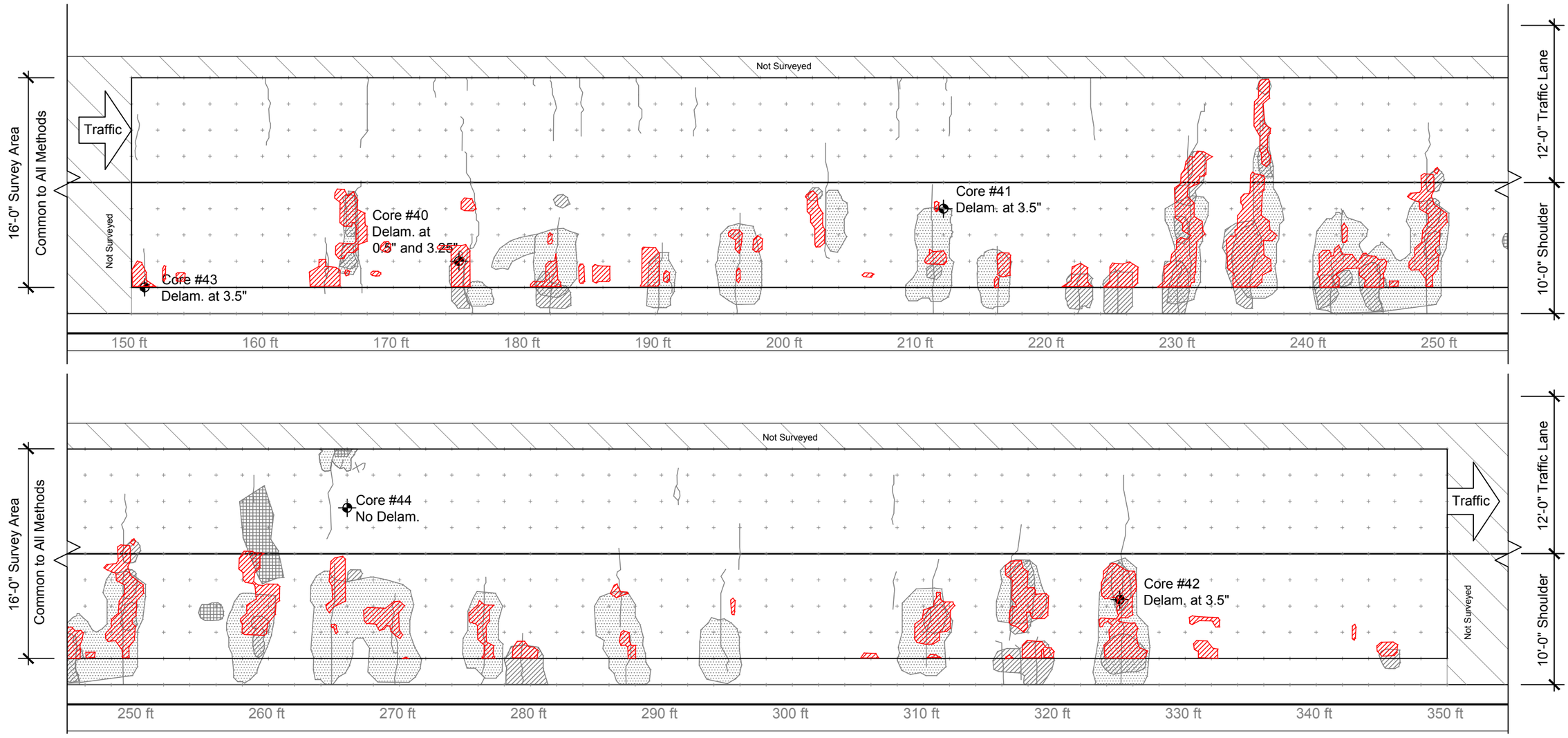

LEGEND

- Delamination, IE Survey
- Delamination, Sounding Survey
- Repair Patch, Visual Survey
- Evidence of Epoxy Repair, Visual Survey
- Crack, Visual Survey
- Construction Joint, Visual Survey
- Core

Study Area EB-1, IE (Olson)

SCALE: 1/8" = 1'-0"

N

0 1/2" 1"

THIS SHEET PLOTS FULL SCALE AT 11x17 (INCHES)

WJE ENGINEERS ARCHITECTS MATERIALS SCIENTISTS

Wiss, Janney, Elstner Associates, Inc.
330 Pfingsten Road
Northbrook, Illinois 60062
847.272.7400 tel | 847.291.9599 fax
www.wje.com

Project: I-129 Missouri River Bridge (No. 9700.05129)
Deck Condition Evaluation

Sheet Title: Findings of Impact-Echo Survey by Olson Engineering

Proj. No.	2010.2389.0
Survey Date	June 20-24, 2011
Drawn	RDL
Checked	JSL
Scale	1/8" = 1'-0"

Sheet No. **D.1**

Plotted: 4/12/2012 9:03 AM by Lequesne, Remy File Name: \\wjenbfp.wje.com\projects\2010\2301-2400\2010.2389-JPD-Iowa NDE\.0_I-129 Sioux City\Drawings\Report Figures\combined study areas.dwg

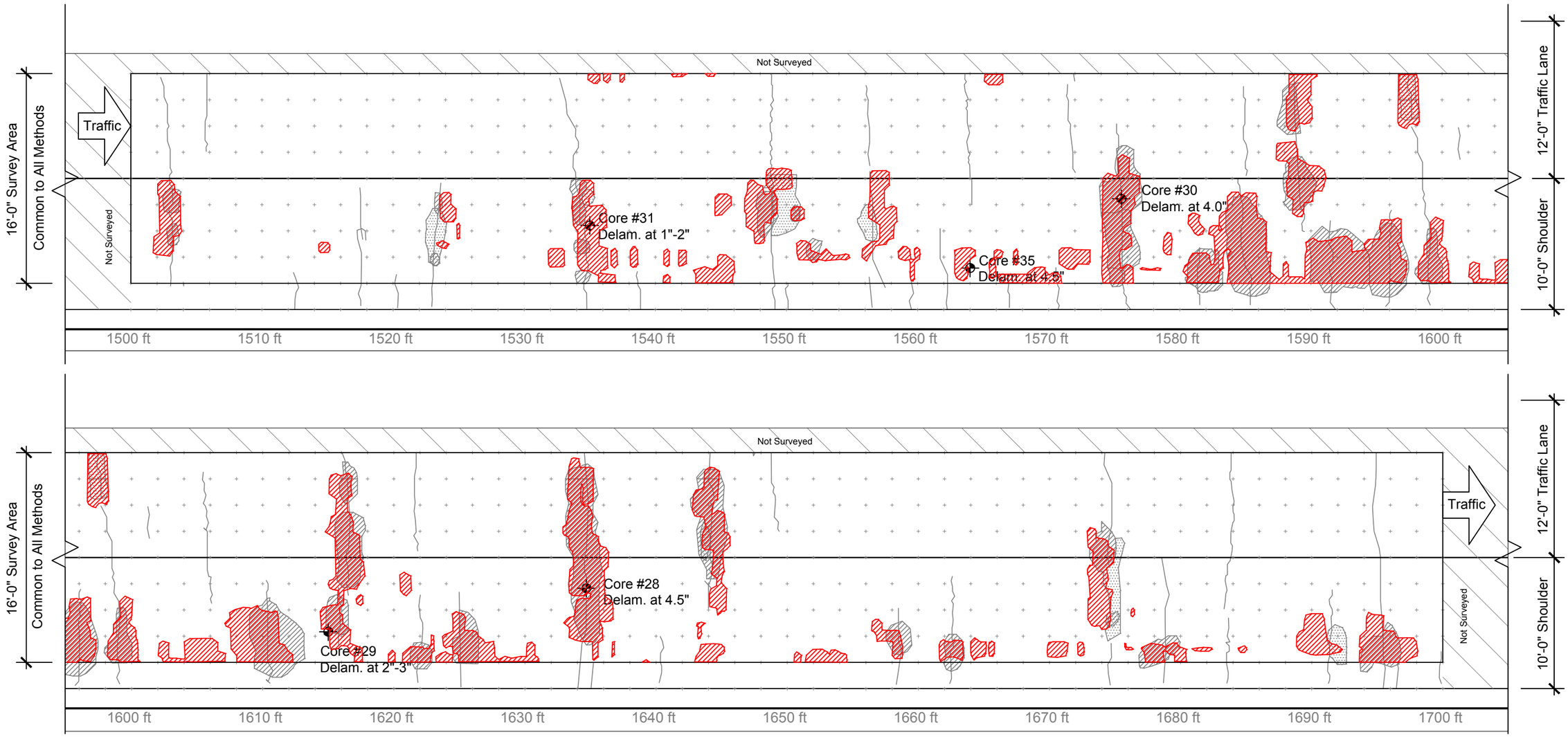

LEGEND

- Delamination, IE Survey
- Delamination, Sounding Survey
- Repair Patch, Visual Survey
- Evidence of Epoxy Repair, Visual Survey
- Crack, Visual Survey
- Construction Joint, Visual Survey
- Core

Study Area EB-2, IE (Olson)

SCALE: 1/8" = 1'-0"

N

0 1/2" 1"

THIS SHEET PLOTS FULL SCALE AT 11x17 (INCHES)

WJE ENGINEERS ARCHITECTS MATERIALS SCIENTISTS

Wiss, Janney, Elstner Associates, Inc.
330 Pfingsten Road
Northbrook, Illinois 60062
847.272.7400 tel | 847.291.9599 fax
www.wje.com

Project: I-129 Missouri River Bridge (No. 9700.05129)
Deck Condition Evaluation

Sheet Title: Findings of Impact-Echo Survey by Olson Engineering

Proj. No.	2010.2389.0
Survey Date	June 20-24, 2011
Drawn	RDL
Checked	JSL
Scale	1/8" = 1'-0"

Sheet No. **D.2**

Plotted: 4/12/2012 9:03 AM by Lequesne, Remy File Name: \\wjenbfp.wje.com\projects\2010\2301-2400\2010.2389-JPD-Iowa NDE\.0_I-129 Sioux City\Drawings\Report Figures\combined study areas.dwg

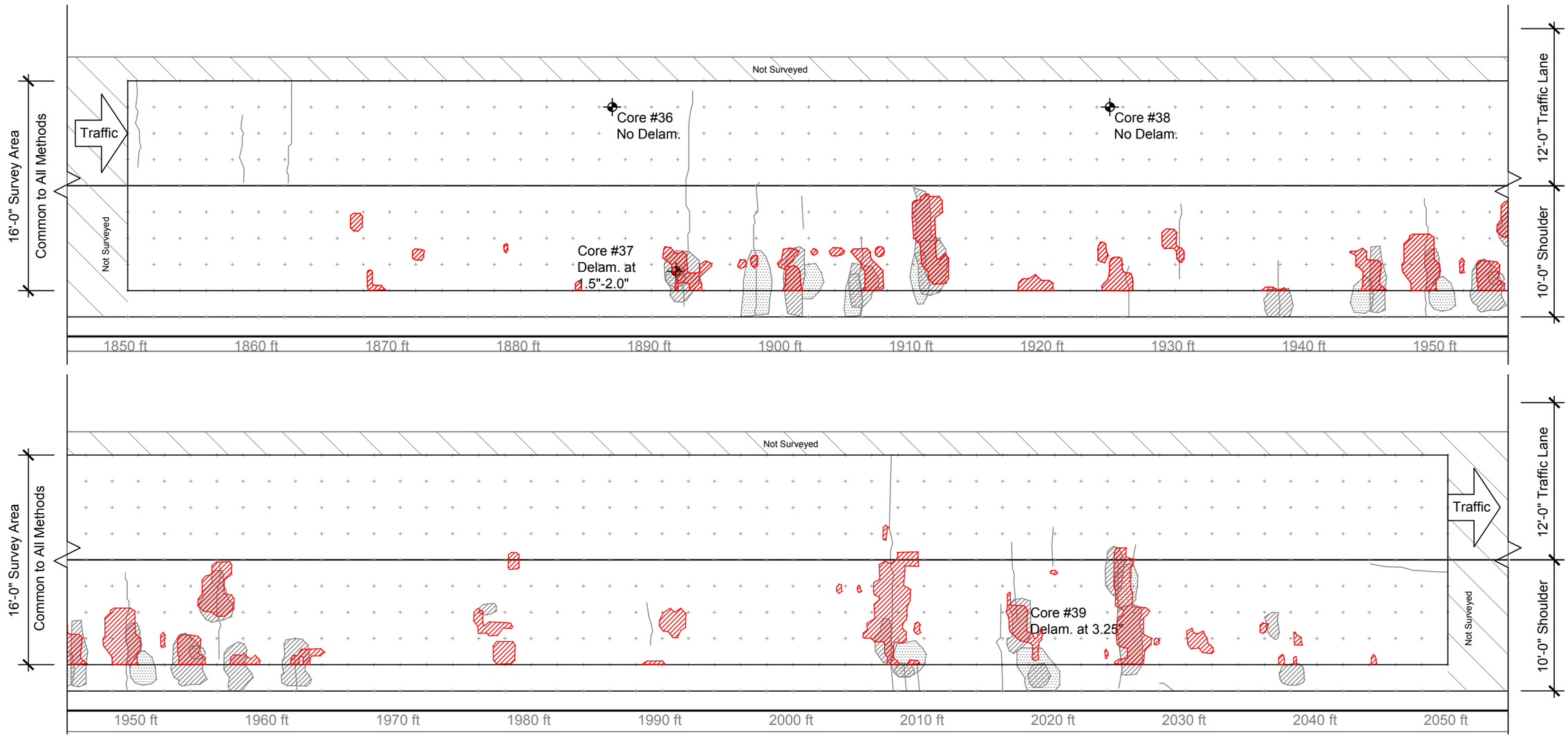

LEGEND

- Delamination, IE Survey
- Delamination, Sounding Survey
- Repair Patch, Visual Survey
- Evidence of Epoxy Repair, Visual Survey
- Crack, Visual Survey
- Construction Joint, Visual Survey
- Core

Study Area EB-3, IE (Olson)

SCALE: 1/8" = 1'-0"

N

0 1/2" 1"

THIS SHEET PLOTS FULL SCALE AT 11x17 (INCHES)

WJE ENGINEERS ARCHITECTS MATERIALS SCIENTISTS

Wiss, Janney, Elstner Associates, Inc.
330 Pfingsten Road
Northbrook, Illinois 60062
847.272.7400 tel | 847.291.9599 fax
www.wje.com

Project: I-129 Missouri River Bridge (No. 9700.05129)
Deck Condition Evaluation

Sheet Title: Findings of Impact-Echo Survey by Olson Engineering

Proj. No.	2010.2389.0
Survey Date	June 20-24, 2011
Drawn	RDL
Checked	JSL
Scale	1/8" = 1'-0"

Sheet No. **D.3**

Plotted: 4/12/2012 9:03 AM by Lequesne, Remy File Name: \\wjenbfp.wje.com\projects\2010\2301-2400\2010.2389-JPD-Iowa NDE\.0_I-129 Sioux City\Drawings\Report Figures\combined study areas.dwg

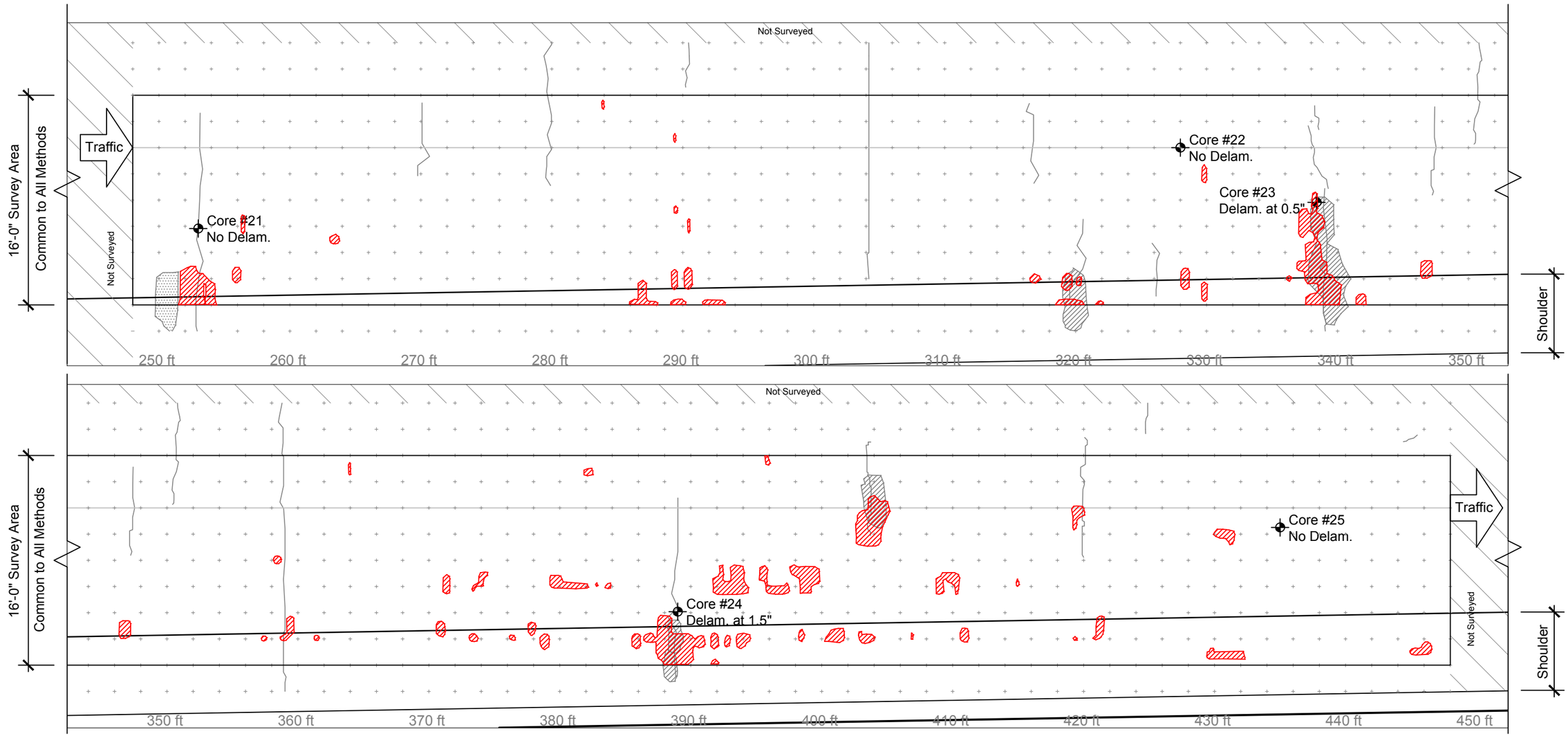

LEGEND

- Delamination, IE Survey
- Delamination, Sounding Survey
- Repair Patch, Visual Survey
- Evidence of Epoxy Repair, Visual Survey
- Crack, Visual Survey
- Construction Joint, Visual Survey
- Core

Study Area WB-1, IE (Olson)

SCALE: 1/8" = 1'-0"

N

0 1/2" 1"

THIS SHEET PLOTS FULL SCALE AT 11x17 (INCHES)

WJE ENGINEERS ARCHITECTS MATERIALS SCIENTISTS

Wiss, Janney, Elstner Associates, Inc.
330 Pfingsten Road
Northbrook, Illinois 60062
847.272.7400 tel | 847.291.9599 fax
www.wje.com

Project: I-129 Missouri River Bridge (No. 9700.05129)
Deck Condition Evaluation

Sheet Title: Findings of Impact-Echo Survey by Olson Engineering

Proj. No.	2010.2389.0
Survey Date	June 20-24, 2011
Drawn	RDL
Checked	JSL
Scale	1/8" = 1'-0"
Sheet No.	D.4

Plotted: 4/12/2012 9:03 AM by Lequesne, Remy File Name: \\wjenbfp.wje.com\projects\2010\2301-2400\2010.2389-JPD-Iowa NDE\.0_I-129 Sioux City\Drawings\Report Figures\combined study areas.dwg

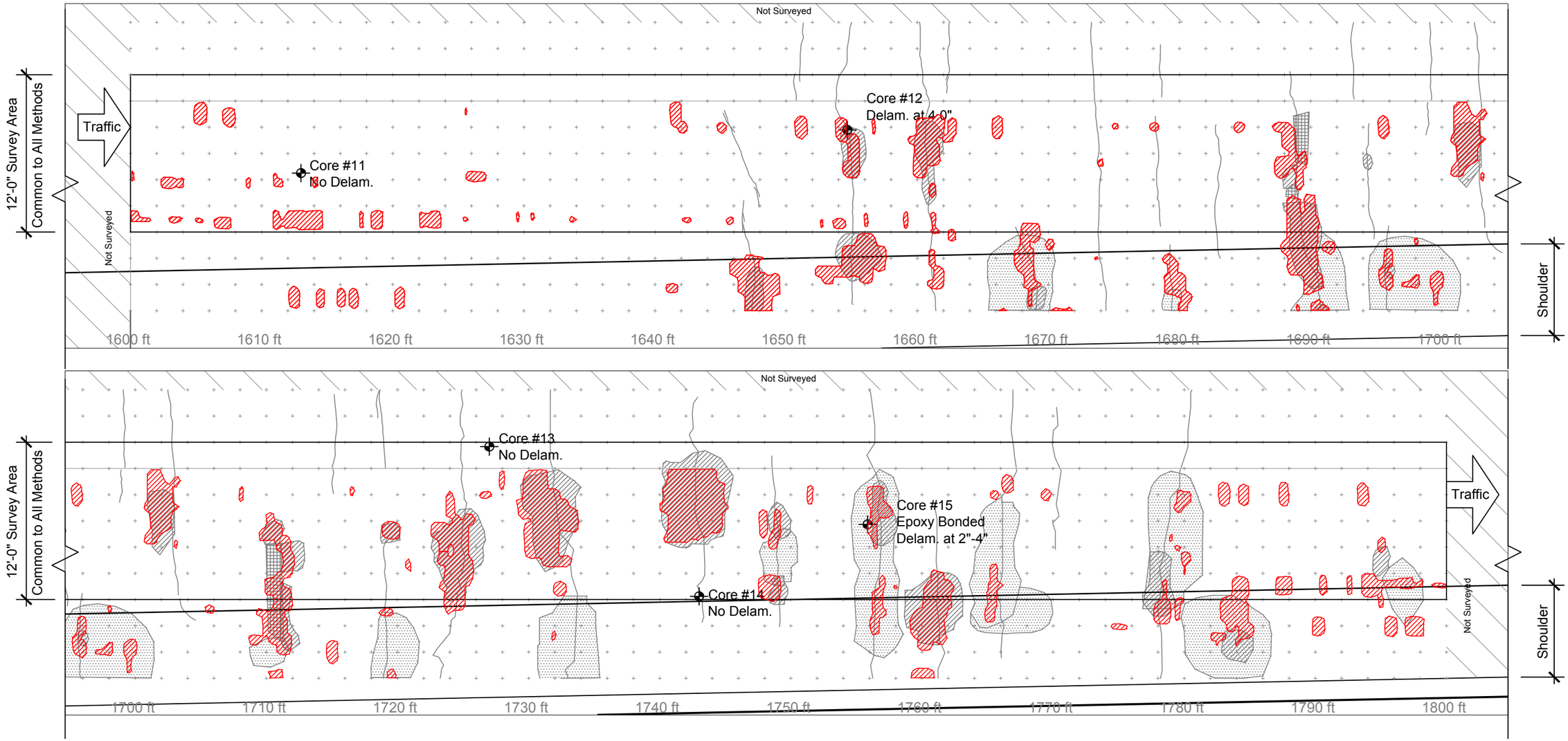

LEGEND

- Delamination, IE Survey
- Delamination, Sounding Survey
- Repair Patch, Visual Survey
- Evidence of Epoxy Repair, Visual Survey
- Crack, Visual Survey
- Construction Joint, Visual Survey
- Core

Study Area WB-2, IE (Olson)

SCALE: 1/8" = 1'-0"

N

0 1/2" 1"

THIS SHEET PLOTS FULL SCALE AT 11x17 (INCHES)

WJE ENGINEERS ARCHITECTS MATERIALS SCIENTISTS

Wiss, Janney, Elstner Associates, Inc.
330 Pfingsten Road
Northbrook, Illinois 60062
847.272.7400 tel | 847.291.9599 fax
www.wje.com

Project: I-129 Missouri River Bridge (No. 9700.05129)
Deck Condition Evaluation

Sheet Title: Findings of Impact-Echo Survey by Olson Engineering

Proj. No.	2010.2389.0
Survey Date	June 20-24, 2011
Drawn	RDL
Checked	JSL
Scale	1/8" = 1'-0"

Sheet No. **D.5**

Plotted: 4/12/2012 9:03 AM by Lequesne, Remy File Name: \\wjenbfp.wje.com\projects\2010\2301-2400\2010.2389-JPD-Iowa NDE\.0_I-129 Sioux City\Drawings\Report Figures\combined study areas.dwg

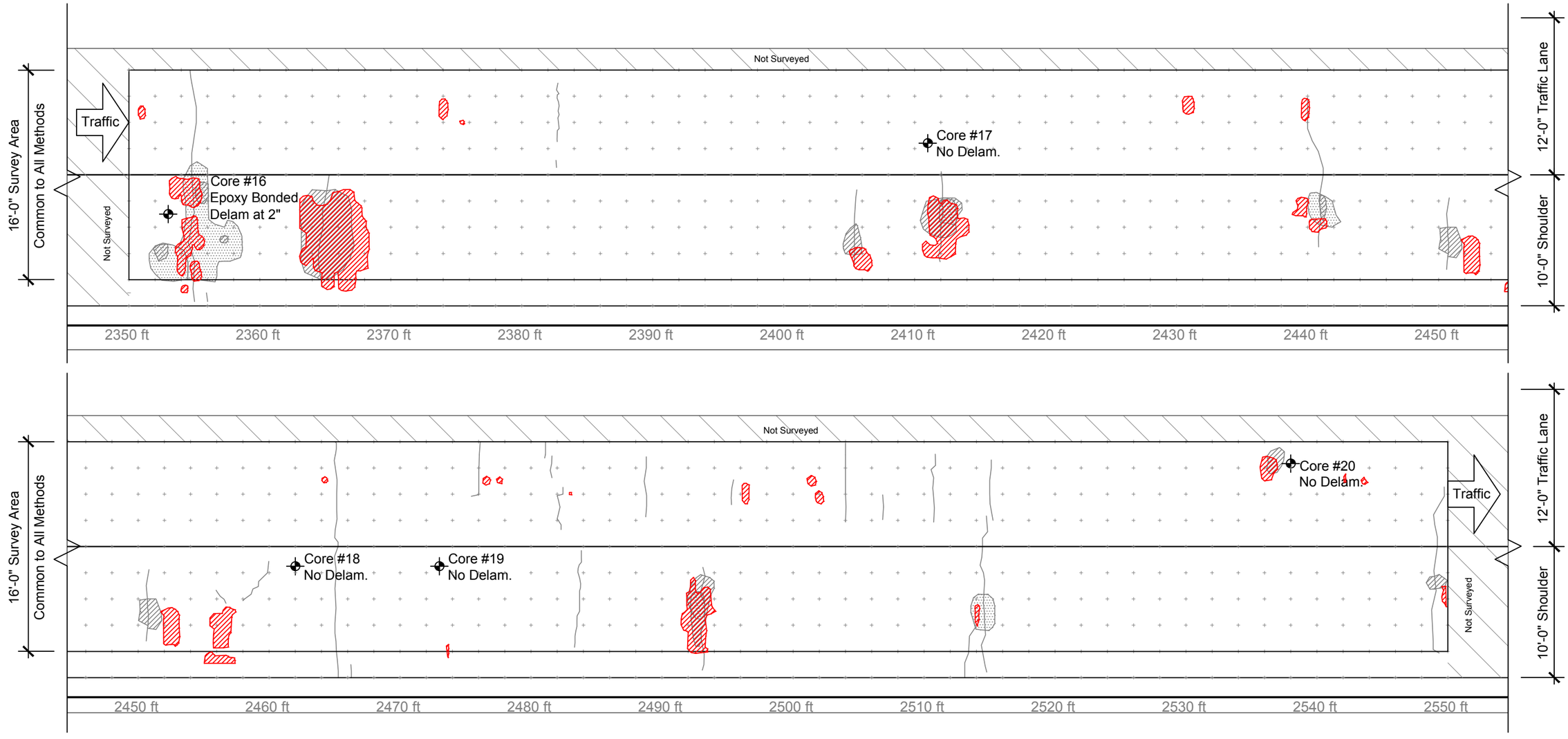

LEGEND

- Delamination, IE Survey
- Delamination, Sounding Survey
- Repair Patch, Visual Survey
- Evidence of Epoxy Repair, Visual Survey
- Crack, Visual Survey
- Construction Joint, Visual Survey
- Core

Study Area WB-3, IE (Olson)

SCALE: 1/8" = 1'-0"

N

0 1/2" 1"

THIS SHEET PLOTS FULL SCALE AT 11x17 (INCHES)

WJE ENGINEERS ARCHITECTS MATERIALS SCIENTISTS

Wiss, Janney, Elstner Associates, Inc.
330 Pfingsten Road
Northbrook, Illinois 60062
847.272.7400 tel | 847.291.9599 fax
www.wje.com

Project: I-129 Missouri River Bridge (No. 9700.05129)
Deck Condition Evaluation

Sheet Title: Findings of Impact-Echo Survey by Olson Engineering

Proj. No.	2010.2389.0
Survey Date	June 20-24, 2011
Drawn	RDL
Checked	JSL
Scale	1/8" = 1'-0"

Sheet No. **D.6**

Plotted: 4/12/2012 9:03 AM by Lequesne, Remy File Name: \\wjenbfp.wje.com\projects\2010\2301-2400\2010.2389-JPD-Iowa NDE\.0_I-129 Sioux City\Drawings\Report Figures\combined study areas.dwg

Appendix E

Findings of Survey of In-Depth Study Areas
Half-Cell Potential

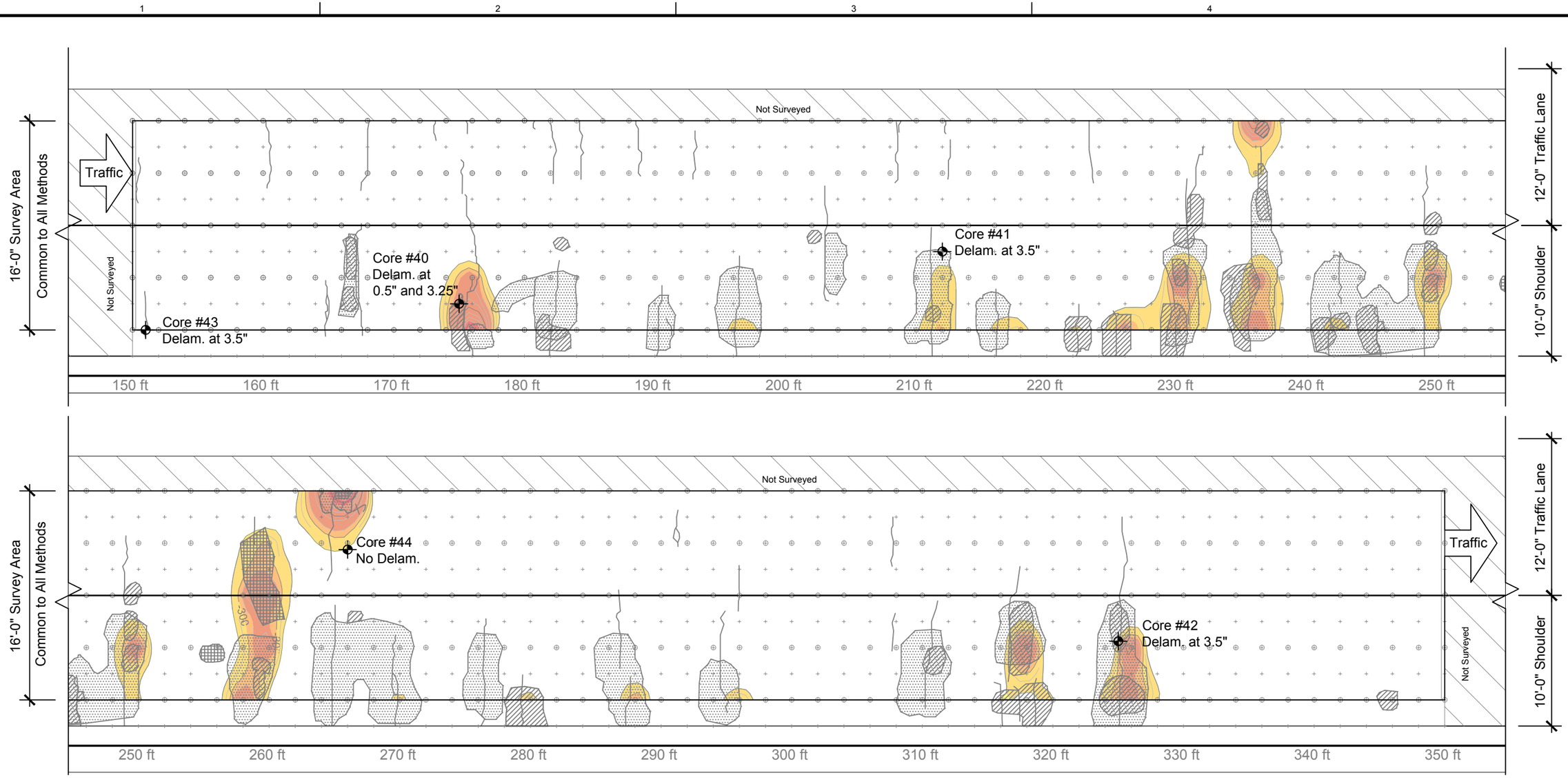

LEGEND

- Delamination, Sounding Survey
- Repair Patch, Visual Survey
- Evidence of Epoxy Repair, Visual Survey
- Crack, Visual Survey
- Construction Joint, Visual Survey
- Core
- Half-Cell Potentials (mV vs. CSE)

-250 -300 -350 -400 -450 -500 -550 -600

Study Area EB-1, Half-Cell

SCALE: 1/8" = 1'-0"

N

0 1/2" 1"

THIS SHEET PLOTS FULL SCALE AT 11x17 (INCHES)

WJE ENGINEERS ARCHITECTS MATERIALS SCIENTISTS

Wiss, Janney, Elstner Associates, Inc.
330 Pfingsten Road
Northbrook, Illinois 60062
847.272.7400 tel | 847.291.9599 fax
www.wje.com

Project	I-129 Missouri River Bridge (No. 9700.05129) Deck Condition Evaluation
Sheet Title	Findings of Half-Cell
Proj. No.	2010.2389.0
Survey Date	June 20-24, 2011
Drawn	RDL
Checked	JSL
Scale	1/8" = 1'-0"
Sheet No.	E.1

Plotted: 4/12/2012 9:02 AM by Lequesne, Remy File Name: \\wjenbfp.wje.com\projects\2010\2301-2400\2010.2389-JPD-Iowa NDE\.0_I-129 Sioux City\Drawings\Report Figures\combined study areas.dwg

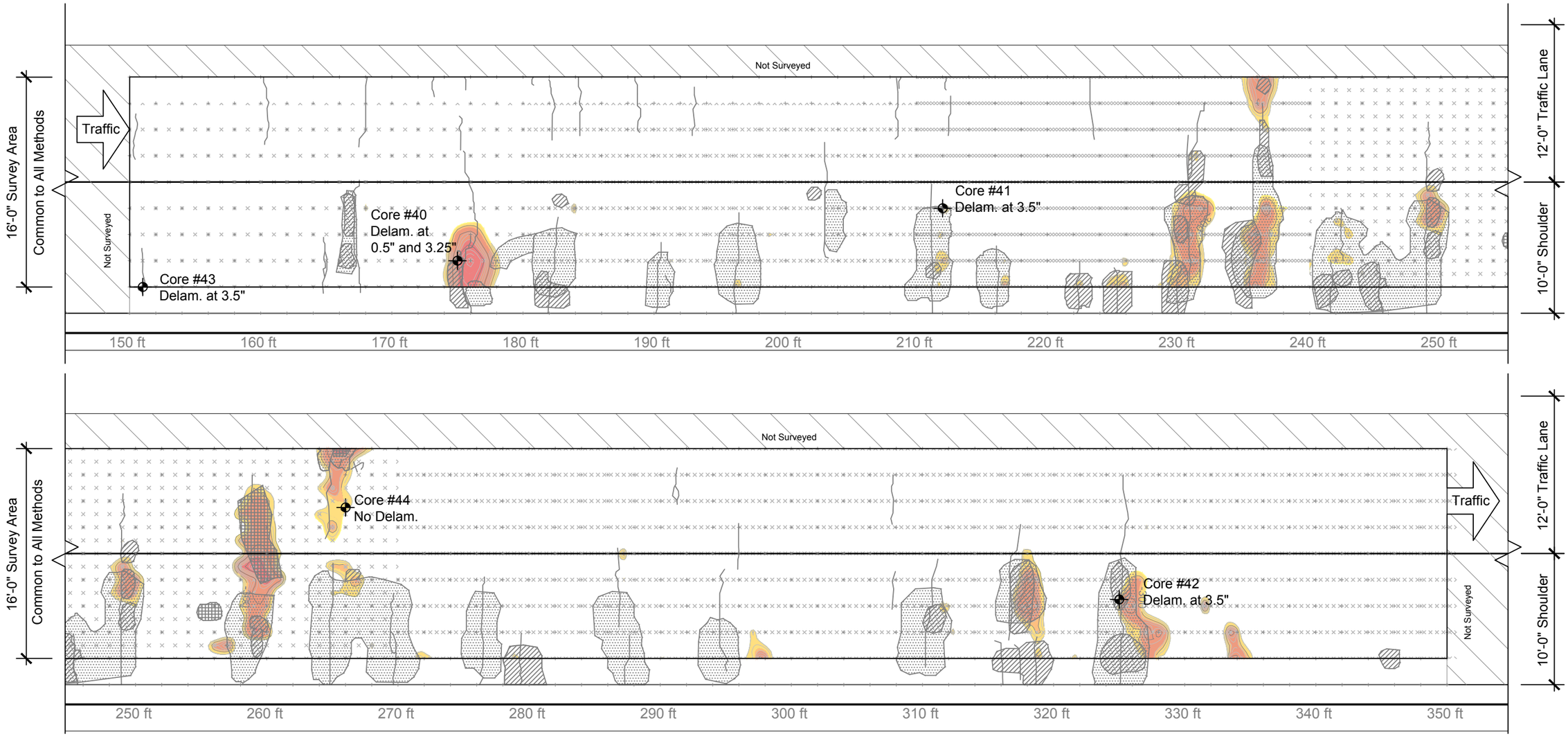

LEGEND

- Delamination, Sounding Survey
- Repair Patch, Visual Survey
- Evidence of Epoxy Repair, Visual Survey
- Crack, Visual Survey
- Construction Joint, Visual Survey
- Core

Half-Cell Potentials (mV vs. CSE)

-250 -300 -350 -400 -450 -500 -550 -600

Study Area EB-1, Half-Cell (Single Rolling Wheel)

SCALE: 1/8" = 1'-0"

N

0 1/2" 1"

THIS SHEET PLOTS FULL SCALE AT 11x17 (INCHES)

WJE ENGINEERS ARCHITECTS MATERIALS SCIENTISTS

Wiss, Janney, Elstner Associates, Inc.
330 Pfingsten Road
Northbrook, Illinois 60062
847.272.7400 tel | 847.291.9599 fax
www.wje.com

Project: I-129 Missouri River Bridge (No. 9700.05129)
Deck Condition Evaluation

Sheet Title: Findings of Half-Cell

Proj. No.	2010.2389.0
Survey Date	June 20-24, 2011
Drawn	RDL
Checked	JSL
Scale	1/8" = 1'-0"

Sheet No. **E.1b**

Plotted: 4/12/2012 9:02 AM by Lequesne, Remy File Name: \\wjenbfp.wje.com\projects\2010\2301-2400\2010.2389-JPD-Iowa NDE\.0_I-129 Sioux City\Drawings\Report Figures\combined study areas.dwg

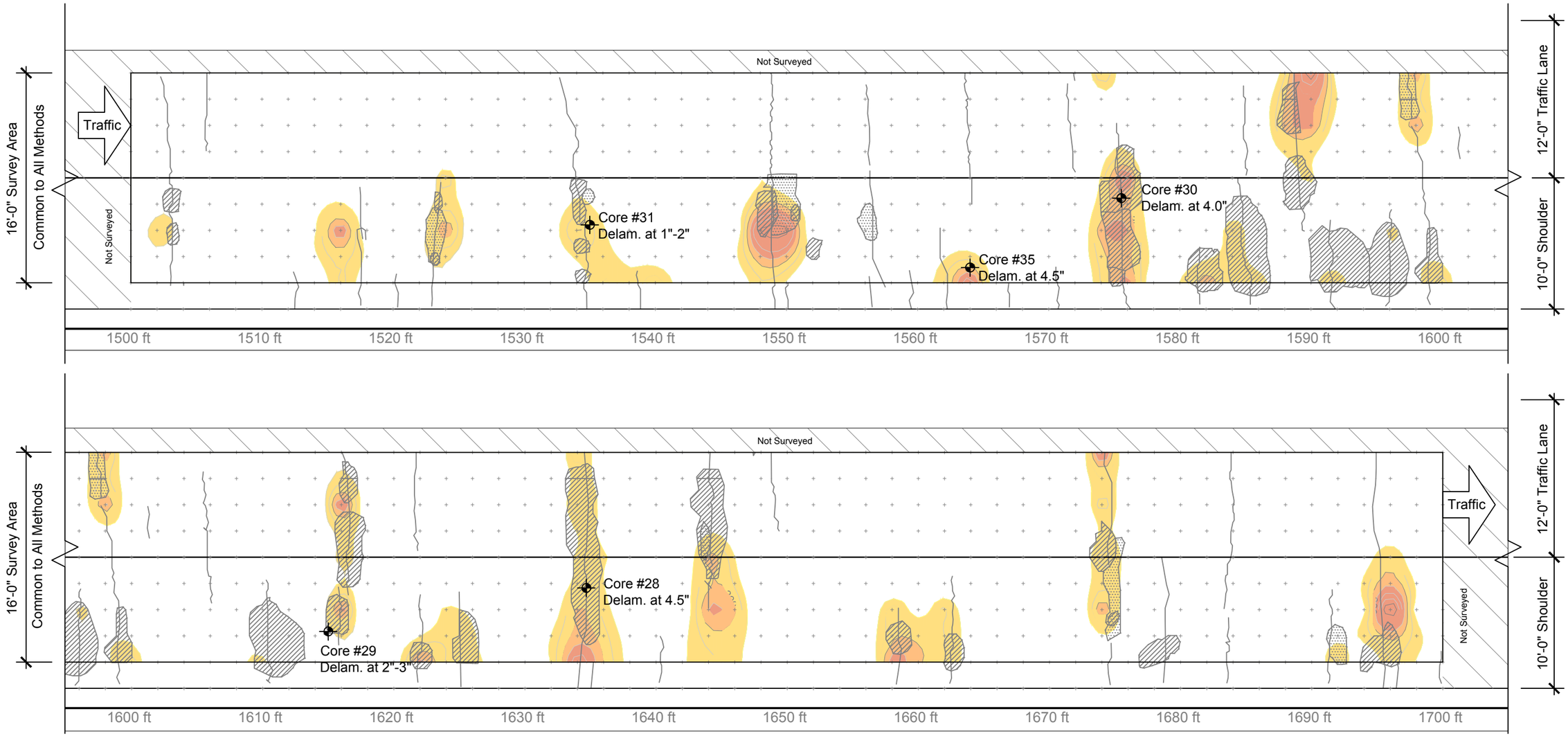

LEGEND

- Delamination, Sounding Survey
- Repair Patch, Visual Survey
- Evidence of Epoxy Repair, Visual Survey
- Crack, Visual Survey
- Construction Joint, Visual Survey
- Core
- Half-Cell Potentials (mV vs. CSE)

-250 -300 -350 -400 -450 -500 -550 -600

Study Area EB-2, Half-Cell

SCALE: 1/8" = 1'-0"

N

0 1/2" 1"

THIS SHEET PLOTS FULL SCALE AT 11x17 (INCHES)

WJE ENGINEERS ARCHITECTS MATERIALS SCIENTISTS

Wiss, Janney, Elstner Associates, Inc.
330 Pfingsten Road
Northbrook, Illinois 60062
847.272.7400 tel | 847.291.9599 fax
www.wje.com

Project: I-129 Missouri River Bridge (No. 9700.05129)
Deck Condition Evaluation

Sheet Title: Findings of Half-Cell

Proj. No.	2010.2389.0
Survey Date	June 20-24, 2011
Drawn	RDL
Checked	JSL
Scale	1/8" = 1'-0"

Sheet No. **E.2**

Plotted: 4/12/2012 9:02 AM by Lequesne, Remy File Name: \\wjenbfp.wje.com\projects\2010\2301-2400\2010.2389-JPD-Iowa NDE\0_I-129 Sioux City\Drawings\Report Figures\combined study areas.dwg

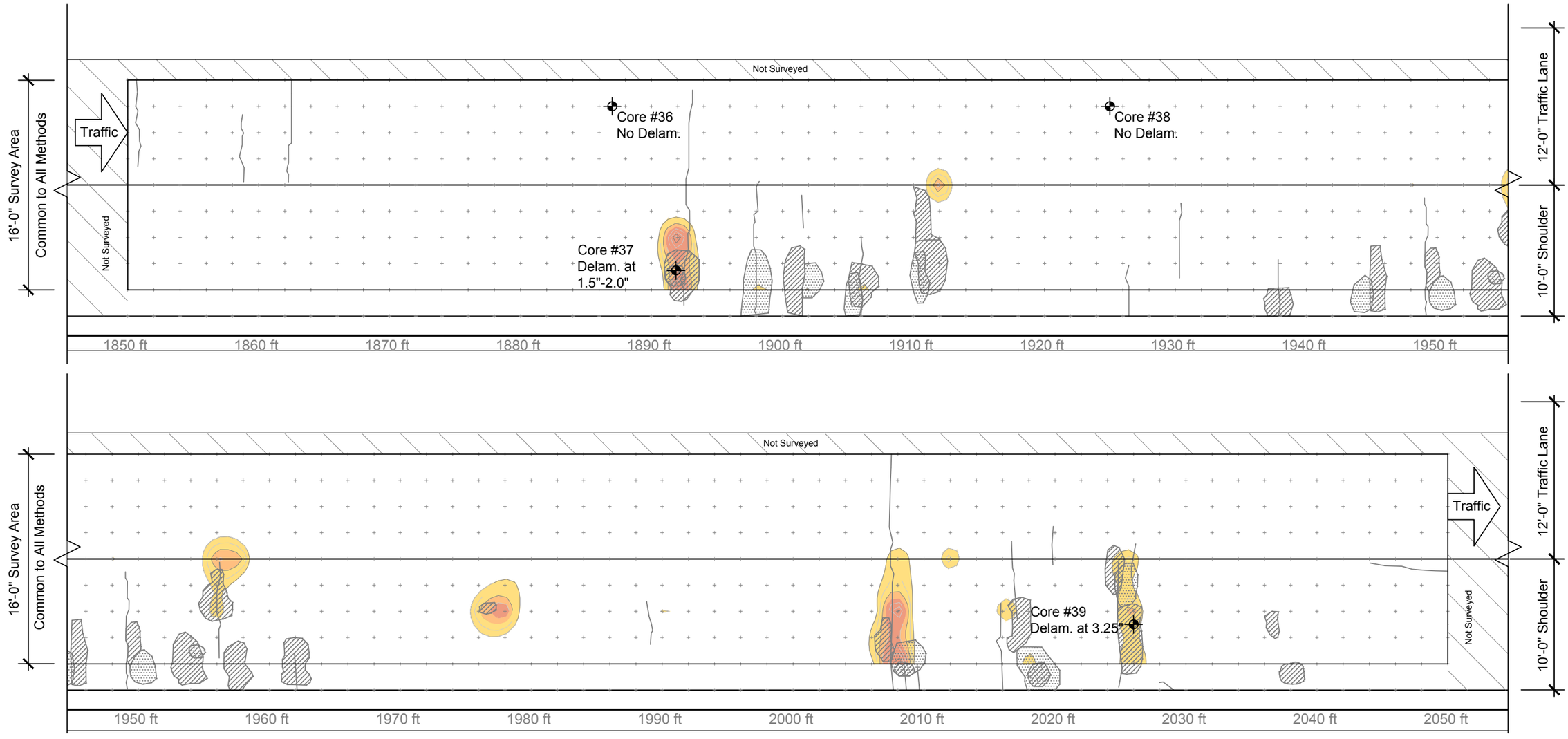

LEGEND

- Delamination, Sounding Survey
- Repair Patch, Visual Survey
- Evidence of Epoxy Repair, Visual Survey
- Crack, Visual Survey
- Construction Joint, Visual Survey
- Core
- Half-Cell Potentials (mV vs. CSE)

-250 -300 -350 -400 -450 -500 -550 -600

Study Area EB-3, Half-Cell

SCALE: 1/8" = 1'-0"

N

0 1/2" 1"

THIS SHEET PLOTS FULL SCALE AT 11x17 (INCHES)

WJE ENGINEERS ARCHITECTS MATERIALS SCIENTISTS

Wiss, Janney, Elstner Associates, Inc.
330 Pfingsten Road
Northbrook, Illinois 60062
847.272.7400 tel | 847.291.9599 fax
www.wje.com

Project: I-129 Missouri River Bridge (No. 9700.05129)
Deck Condition Evaluation

Sheet Title: Findings of Half-Cell

Proj. No.	2010.2389.0
Survey Date	June 20-24, 2011
Drawn	RDL
Checked	JSL
Scale	1/8" = 1'-0"

Sheet No. **E.3**

Plotted: 4/12/2012 9:02 AM by Lequesne, Remy File Name: \\wjenbfp.wje.com\projects\2010\2301-2400\2010.2389-JPD-Iowa NDE\.0_I-129 Sioux City\Drawings\Report Figures\combined study areas.dwg

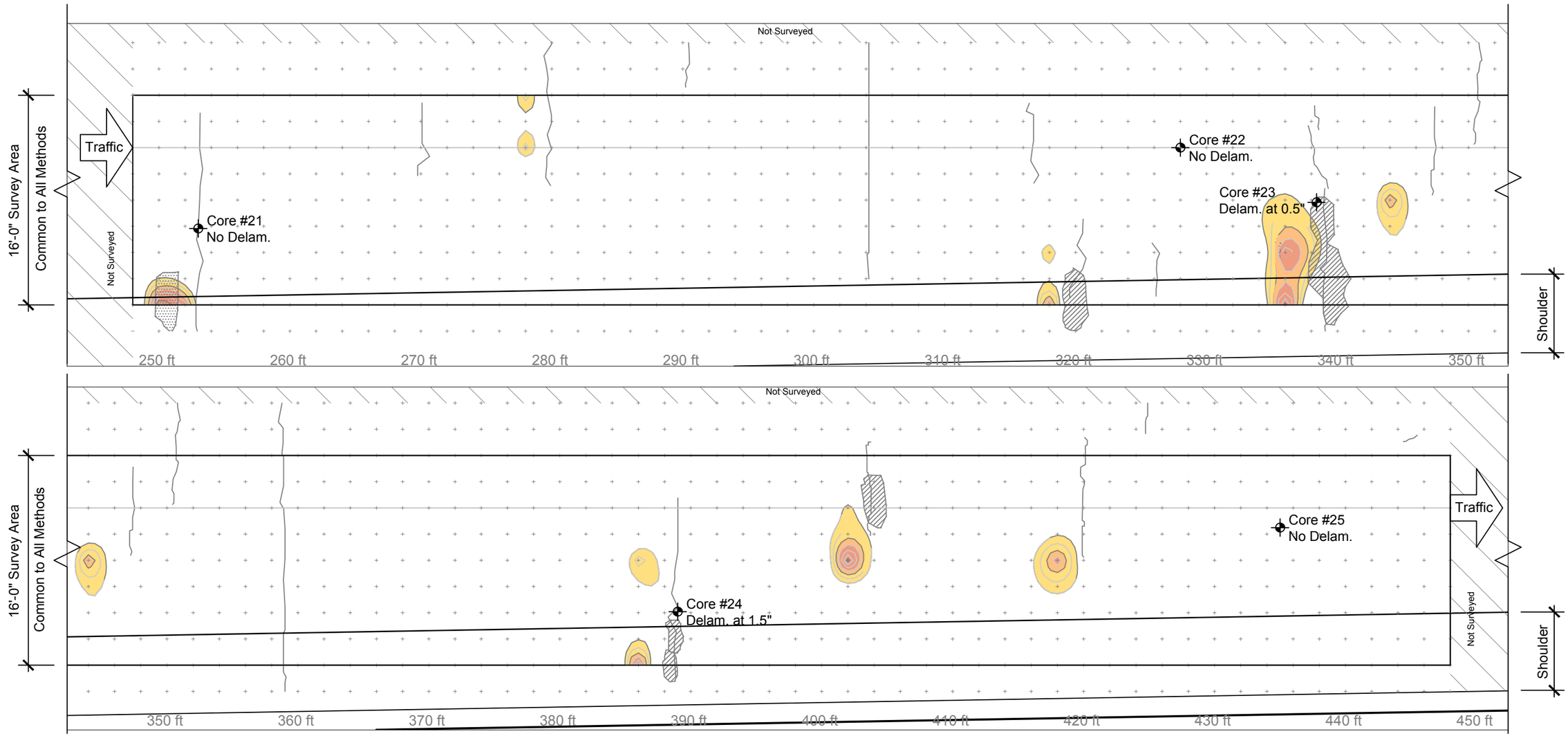

LEGEND

- Delamination, Sounding Survey
- Repair Patch, Visual Survey
- Evidence of Epoxy Repair, Visual Survey
- Crack, Visual Survey
- Construction Joint, Visual Survey
- Core
- Half-Cell Potentials (mV vs. CSE)

-250 -300 -350 -400 -450 -500 -550 -600

Study Area WB-1, Half-Cell

SCALE: 1/8" = 1'-0"

N

0 1/2" 1"

THIS SHEET PLOTS FULL SCALE AT 11x17 (INCHES)

WJE ENGINEERS ARCHITECTS MATERIALS SCIENTISTS
Wiss, Janney, Elstner Associates, Inc.
330 Pfingsten Road
Northbrook, Illinois 60062
847.272.7400 tel | 847.291.9599 fax
www.wje.com

Project: I-129 Missouri River Bridge (No. 9700.05129)
Deck Condition Evaluation

Sheet Title: Findings of Half-Cell

Proj. No.	2010.2389.0
Survey Date	June 20-24, 2011
Drawn	RDL
Checked	JSL
Scale	1/8" = 1'-0"

Sheet No. **E.4**

Plotted: 4/12/2012 9:02 AM by Lequesne, Remy File Name: \\wjenbfp.wje.com\projects\2010\2301-2400\2010.2389-JPD-Iowa NDE\.0_I-129 Sioux City\Drawings\Report Figures\combined study areas.dwg

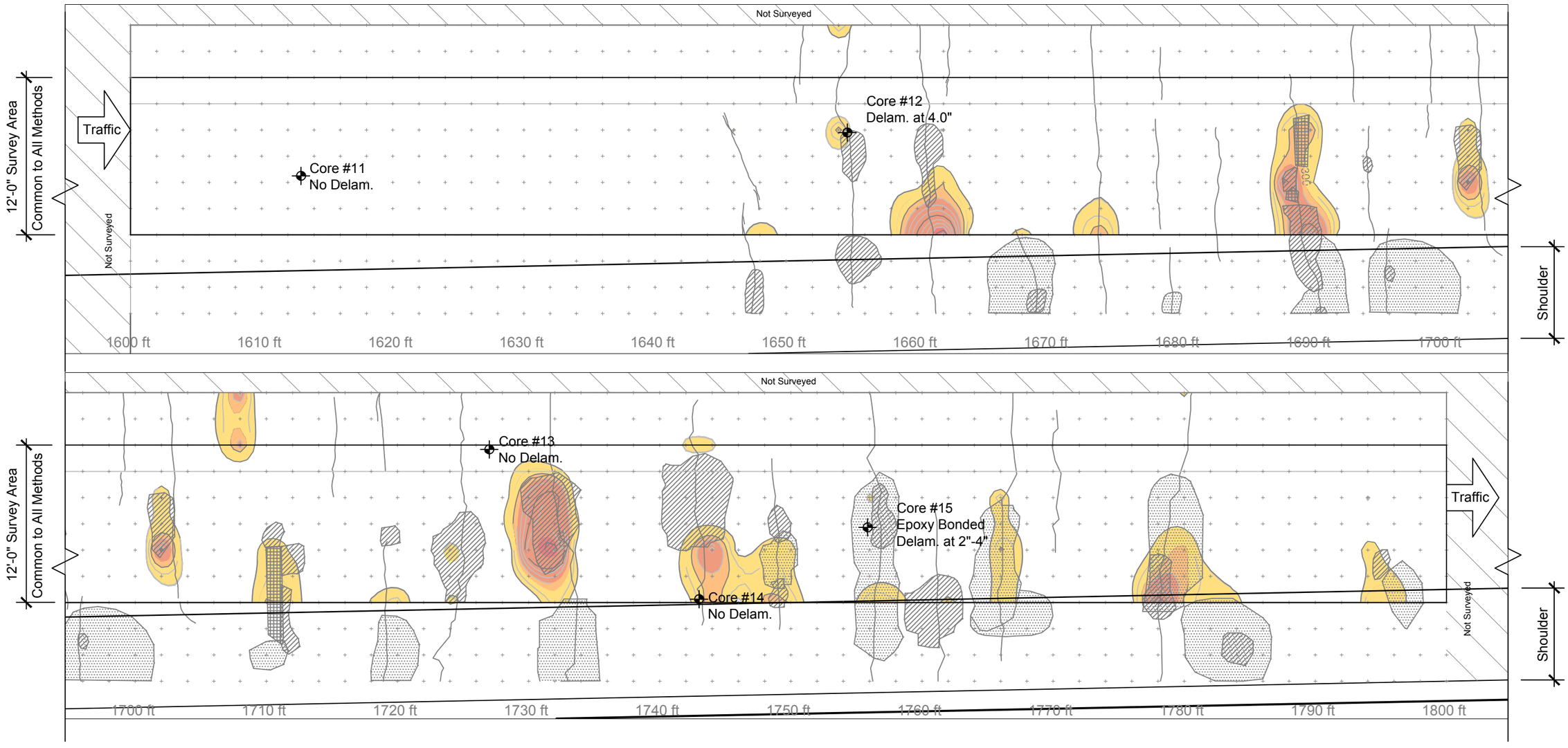

LEGEND

- Delamination, Sounding Survey
- Repair Patch, Visual Survey
- Evidence of Epoxy Repair, Visual Survey
- Crack, Visual Survey
- Construction Joint, Visual Survey
- Core

Half-Cell Potentials (mV vs. CSE)

-250 -300 -350 -400 -450 -500 -550 -600

Study Area WB-2, Half-Cell

SCALE: 1/8" = 1'-0"

N

0 1/2" 1"

THIS SHEET PLOTS FULL SCALE AT 11x17 (INCHES)

WJE ENGINEERS ARCHITECTS MATERIALS SCIENTISTS

Wiss, Janney, Elstner Associates, Inc.
330 Pfingsten Road
Northbrook, Illinois 60062
847.272.7400 tel | 847.291.9599 fax
www.wje.com

Project: I-129 Missouri River Bridge (No. 9700.05129)
Deck Condition Evaluation

Sheet Title: Findings of Half-Cell

Proj. No.	2010.2389.0
Survey Date	June 20-24, 2011
Drawn	RDL
Checked	JSL
Scale	1/8" = 1'-0"

Sheet No. **E.5**

Plotted: 4/12/2012 9:02 AM by Lequesne, Remy File Name: \\wjenbfp.wje.com\projects\2010\2301-2400\2010.2389-JPD-Iowa NDE\.0_I-129 Sioux City\Drawings\Report Figures\combined study areas.dwg

LEGEND

- Delamination, Sounding Survey
- Repair Patch, Visual Survey
- Evidence of Epoxy Repair, Visual Survey
- Crack, Visual Survey
- Construction Joint, Visual Survey
- Core
- Half-Cell Potentials (mV vs. CSE)

-250 -300 -350 -400 -450 -500 -550 -600

Study Area WB-3, Half-Cell

SCALE: 1/8" = 1'-0"

N

0 1/2" 1"

THIS SHEET PLOTS FULL SCALE AT 11x17 (INCHES)

WJE ENGINEERS ARCHITECTS MATERIALS SCIENTISTS
Wiss, Janney, Elstner Associates, Inc.
330 Pfingsten Road
Northbrook, Illinois 60062
847.272.7400 tel | 847.291.9599 fax
www.wje.com

Project: I-129 Missouri River Bridge (No. 9700.05129)
Deck Condition Evaluation

Sheet Title: Findings of Half-Cell

Proj. No.	2010.2389.0
Survey Date	June 20-24, 2011
Drawn	RDL
Checked	JSL
Scale	1/8" = 1'-0"

Sheet No. E.6

Plotted: 4/12/2012 9:02 AM by Lequesne, Remy File Name: \\wjenbfp.wje.com\projects\2010\2301-2400\2010.2389-JPD-Iowa NDE\.0_I-129 Sioux City\Drawings\Report Figures\combined study areas.dwg

Appendix F

Report of Petrographic Studies

WJE ENGINEERS ARCHITECTS MATERIALS SCIENTISTS

Wiss, Janney, Elstner Associates, Inc.
330 Pfingsten Road
Northbrook, Illinois 60062
847.272.7400 tel | 847.291.5189 fax
www.wje.com

INTEROFFICE MEMORANDUM

Via: E-mail

To: Paul Krauss, WJE

From: Uznanski, Lidia L.

Date: September 23, 2011

Project: Iowa Bridge I-129
WJE No. 2010.2389

Subject: Concrete Petrography

Two concrete cores identified as Nos. 6 and 42 (Figure 1) were examined using methods of ASTM C856, *Standard Practice for Petrographic Examination of Hardened Concrete*." The examination was performed using stereoscopic and petrographic microscopes at magnifications ranging from 10x to 600x. Powder mounts were employed in the examination using the polarized-light microscope. The purpose of the petrographic examination was to determine the characteristics and condition of the concrete and the embedded steel reinforcement, and to measure the depth of carbonation of the cement paste.

Core 6

Observations

Core 6 was 6-3/4 inches long and 3-3/4 inches in diameter. The core consisted of two different concrete mixes; a topping mix constituting the top 2-1/4 inches of the core, and a base mix constituting the bottom 4-1/2 inches of the core. The top surface of the core had shallow grooves spaced 1/2 inch apart. The bottom end of the core was a fractured surface.

As received, the topping was separated from the concrete substrate. The separation occurred at the interface between the two layers. Most of the top surface of the base substrate exhibited light scratches that appeared to be due to scarification by rotary cutters, but also had some smooth, shiny areas that might have been polished by the detached topping spinning during coring. The adjacent underside of the topping contained impressions of the top surface of the concrete substrate. Some areas of the underside were smooth and shiny and exhibited faint concentric scratches that were most likely due to spinning of the detached topping during coring. No steel reinforcement was present within this core.

Cracks were detected in both the topping and the substrate concretes. The topping layer had two microcracks; one horizontal, located mid-depth of the layer, and the other vertical. Secondary deposits of salt were present within the pores of the cement paste in localized areas of the top 1 inch of the overlay concrete. (Figures 2, 3, and 4). Because the core was taken adjacent to a delamination, it is possible the horizontal crack is an extension of the delamination plane that has not yet penetrated to the surface.

The base concrete had two vertical microcracks. One microcrack was visible on the top surface of the layer and extended to a depth of 1 inch, exiting from the side of the core. The other microcrack extended

from the bottom surface and terminated 1/2 inch below the top of the substrate. The vertical cracks in the base concrete appeared to be due to shrinkage and restraint from the bridge girders.

Topping Concrete

Aggregate - The coarse aggregate was crushed calcareous rock with a maximum nominal size of 3/8 inch (pea size). The main component of the aggregate was limestone; some was oolitic (composed of small spherical and sub-spherical calcareous bodies). The particles were light beige, moderately hard, firm, relatively dense, sub-angular to angular, and mostly equant.

The fine aggregate was natural siliceous and calcareous sand composed of a variety of rocks and minerals including quartz, granite, limestone, feldspar, shale, chert, and coal particles. Except for the particles of shale, coal, and some soft chert, most of the particles were moderately hard to hard, firm, and dense. Occasional particles of shale contained reactive elements as indicated by the presence of microcracks within those particles and associated gel. Some of these were found in the vicinity of the intercepting microcracks in topping layer, and secondary deposits of alkali-silica reactive (ASR) gel were detected in association with some of those particles. (Figure 5).

Cement Paste

- Cement paste within the topping layer was medium gray, moderately hard, relatively dense, and had a dull to sub-vitreous luster typical of moderate and lower water-cement ratio paste.
- The cement content was estimated at 6 ± 1/2 bags per cubic yard of concrete. No pozzolans were detected.
- The water-cement ratio was estimated at approximately 0.42±0.05. The estimate was based on the optical and physical characteristics of the cement paste.
- Hydration of the cement was moderately advanced. Residual (mostly unhydrated) cement particles were moderately frequent, and relict (mostly hydrated) cement particles were frequent.
- The depth of carbonation of the cement paste varied from the surface only to a maximum of 1/16 inch. The carbonation was deeper on the crack surfaces, extending from the top surface to a depth of 1-1/4 inch. At the bottom of the layer the paste was carbonated only at the debonded surface.

Air-void System

The concrete was air-entrained, and the total air content was estimated at 5 percent. The air occurred as small, medium size spherical voids that are typical of entrained air, and as larger, irregularly shaped voids that are typical of entrapped air. The entrapped air voids constituted approximately one third of the total air content. The air-voids were randomly distributed within the core. No freeze-thaw related damage was evident.

Base Concrete

Aggregate - The coarse aggregate was siliceous gravel that had a maximum nominal size of 3/4 inch. It was composed of a variety of igneous rocks such as granite, quartzite, and gabbro, as well as occasional calcareous particles such as limestone. The siliceous particles ranged in color from reddish/brown to dark gray. They were hard, firm, dense, mostly equant, and rounded to sub-rounded. The aggregates were well graded and uniformly distributed, but the content of the coarse aggregate was lower than in an average concrete.

The fine aggregate was natural siliceous and calcareous sand that had composition similar to the fine aggregate in the topping layer. A particle of shale containing reactive elements and associated ASR gel was detected on the lapped section of the core. However, there were no cracks in the surrounding cement paste (Figure 6).

Cement Paste

- Cement paste within the base layer was medium to dark gray, moderately hard, relatively dense, and had dull to sub-vitreous luster typical of moderate and lower water-cement ratio paste.
- The cement content was estimated at 5-1/2 ± 1/2 bags per cubic yard of concrete. No pozzolans were detected.
- The water-cement ratio was estimated at 0.42±0.03. The estimate was based on the optical and physical characteristics of the cement paste.
- The degree of hydration of the cement was moderately advanced. Residual (mostly unhydrated) cement particles were moderately frequent, and relict (mostly hydrated) cement particles were frequent.
- The cement paste was fully carbonated at the top surface and to a depth of 1/4 inch where a vertical microcrack was present.

Air-void System

The concrete was air-entrained, and the total air content was estimated at 5 percent. The air occurred as micro-air and small and medium size spherical and semi-spherical voids of entrained air, as well as some slightly larger voids of entrapped air. The entrained air voids comprised most of the total air content. The air voids were fairly uniformly distributed within the core with minor clustering. No freeze-thaw related damage was evident.

Core 42

Observations

The core was 5 to 6-3/4 inches long, and 3-3/4 inches in diameter. The core consisted of two different concrete mixes: a topping constituting the top 2-1/4 inch of the core; and base concrete constituting the bottom 2-3/4 to 4-1/2 inches of the core. The top surface of the core had shallow grooves as in Core 6, and the bottom end was a fractured surface. As received, the topping was bonded to the substrate concrete (Figure 7). A 3/4-inch diameter (No. 6) rebar was embedded in base concrete, 3-1/2 inches from the top of the core. The rebar was significantly corroded (Figures 8 and 9).

Cracking was not evident in the topping but numerous transverse cracks were present within the base concrete at the level of the corroded rebar. The cracks occurred in a 2-3/4-inch wide zone extending from just below the top of the base concrete to below the location of embedded rebar. The cracks transected the aggregate particles. The surfaces of the cracks nearest to the rebar were coated or filled with brown corrosion products and deposits of ASR gel.

Topping Concrete

Aggregate - The coarse and fine aggregate types in the topping were similar to the aggregate types in the topping of Core 6.

Cement Paste - The cement paste in the topping had the same characteristics as the topping of Core 6. The cement paste was fully carbonated within 1/32 to 3/32 inch of the top surface.

Air-void System - Unlike the topping layer of Core 6, the topping layer of Core 42 was non-air entrained. Its total air content was estimated at 3-1/2 percent. Some air content occurred as entrained air voids, but the majority of air content occurred as somewhat large, irregularly shaped voids of entrapped air. The air voids were randomly distributed. No freeze-thaw related damage was evident.

Base Concrete

Aggregates - The coarse aggregates in the base concrete were similar to Core 6. However, the coarse aggregates also contained reactive particles not detected in Core 6. The source of most of the ASR gel in cracks appeared to be a large, dark lump that was embedded at the fractured bottom end of the core. The lump appeared to be an industrial waste product and was composed mainly of siliceous glassy material, similar to silica fume. The approximate dimensions of the lump were 1 inch by 3/4 inch. The lump was most likely a contaminant within the aggregate (Figures 10 and 11).

Also present in the cracked zone were two particles of sandstone; one was relatively large measuring 1/2 by 3/8 inch. Similar particles were not observed in any other location of either of the two cores (Figure 12). This particle contained reactive elements and was partially consumed in ASR.

The fine aggregates were similar to those in Core 6. Soft particles of shale contained major amounts of siliceous, glassy material. Some of these particles were associated with the presence of ASR gel (Figure 13).

Cement Paste - The cement paste in the base concrete had the same characteristics as Core 6. The cement paste in the base concrete was fully carbonated mainly at top surface and in localized areas to a maximum depth of 1/4 inch.

Air-void System - The base concrete was air entrained and the air void system was similar to the base concrete of Core 6. No freeze-thaw related damage was evident.

Summary and Conclusions

Cracking was detected in both topping and base layers of Core 6. This cracking appeared to be extending from areas outside the core, and is likely related to delaminations or overall shrinkage and restraint of the deck.

The topping layer of Core 42 did not exhibit any cracking, but the base layer exhibited major cracking throughout. Most of the cracks were transverse to the core length but some were also randomly oriented. One significantly corroded rebar was observed in the base concrete at the level of the transverse cracks, and corrosion staining was present on the cracked surfaces and within the surrounding cement paste.

The base layer also contained reactive sandstone particles within the coarse aggregate that had cracked the surrounding paste. A large reactive siliceous lump of industrial waste, probably a contaminant, was embedded in the bottom of the core. Abundant ASR gel was found on crack surfaces and in air voids of this layer.

The cracking within this core was judged to be due to two factors: corrosion of the embedded steel and to ASR. Most of the ASR was due to the presence of a reactive contaminant lump and some was attributed to reactive sandstone particles within the coarse aggregate. It was unknown which occurred first: corrosion-related cracking or ASR-related cracking.

Alkali-silica reactive particles were also detected within fine aggregates in all concrete. The particles were shale particles containing siliceous elements that reacted with alkalies within the cement paste. Most of these particles were fine-size, and therefore too weak to exert sufficient pressure on the surrounding paste to cause cracking.

The cement paste was of good quality in all layers of both cores. The water-cement ratios were estimated at 0.42±0.05 in the topping layers and at 0.42±0.03 in the base concrete layers. The cement contents were estimated at 6 ± 1/2 bags per cubic yard of concrete for the topping layers and 5-1/2 ± 1/2 bags for the base concrete layers. Pozzolans were not detected in any of the layers. The carbonation of the cement paste was minimal (3/32 inch maximum) in all layers.

Air entrainment was lacking in the topping layer of Core 42, but was adequate (approximately 5 percent) in the remaining layers of both cores. There was no evidence of freeze-thaw related damage in any of the layers.

Figure 1. Core 6 and 42 as received for petrographic studies. Topping layer in Core 6 as received was delaminated from the base concrete.

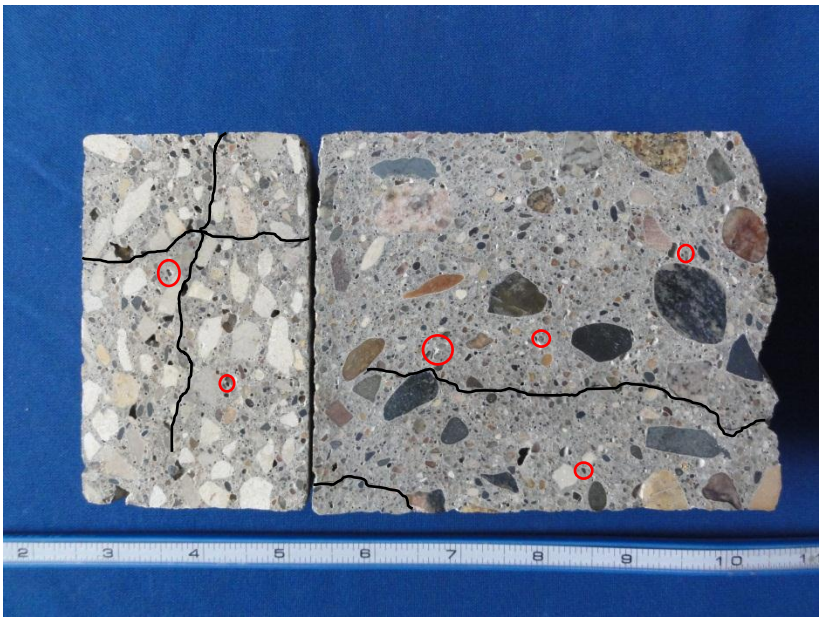

Figure 2. Lapped section of Core 6; top of the core is on the left of the photo. The locations of the microcracks are outlined. The largest reactive shale particles are encircled.

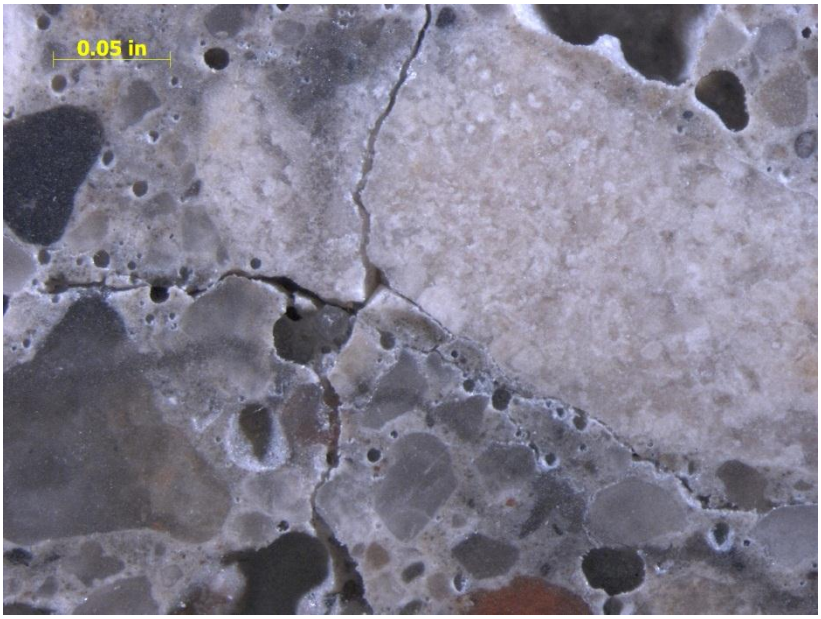

Figure 3. Core 6 topping; close up view of the area where the vertical and horizontal microcracks intercept.

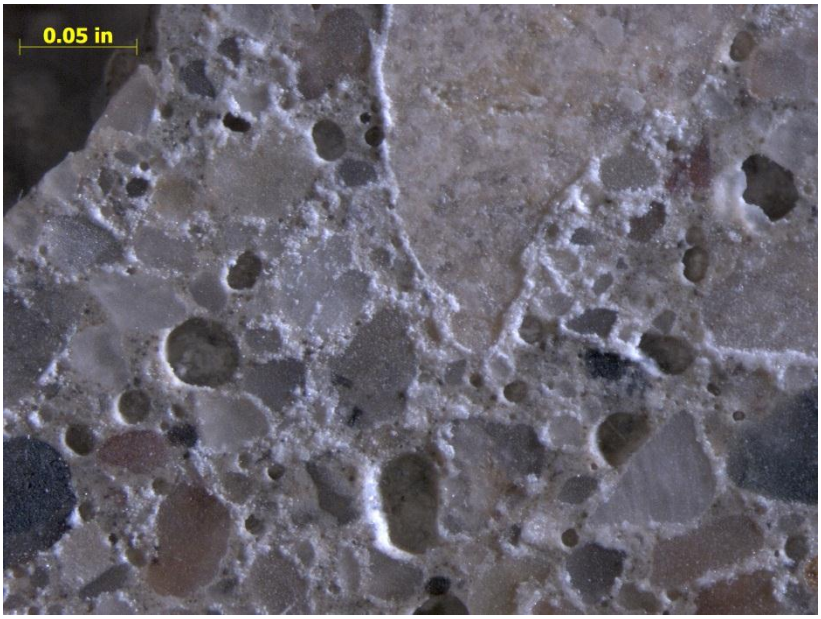

Figure 4. Core 6 topping; example of secondary salts deposits (most likely deicing compounds) precipitating from the pores of the cement paste in the top regions of topping layer.

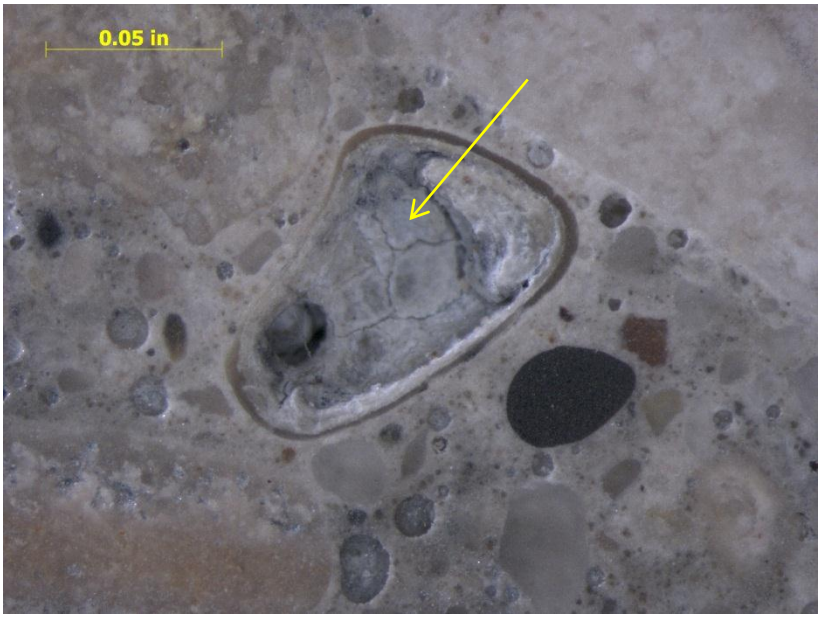

Figure 5. Core 6 topping; the largest reacted fine particle of shale (encircled in Figure 2) located in close proximity to the intercepting microcracks. Most of the interior of this particle has been consumed in the alkali-silica reaction; gel was found on the surfaces of the microcracks.

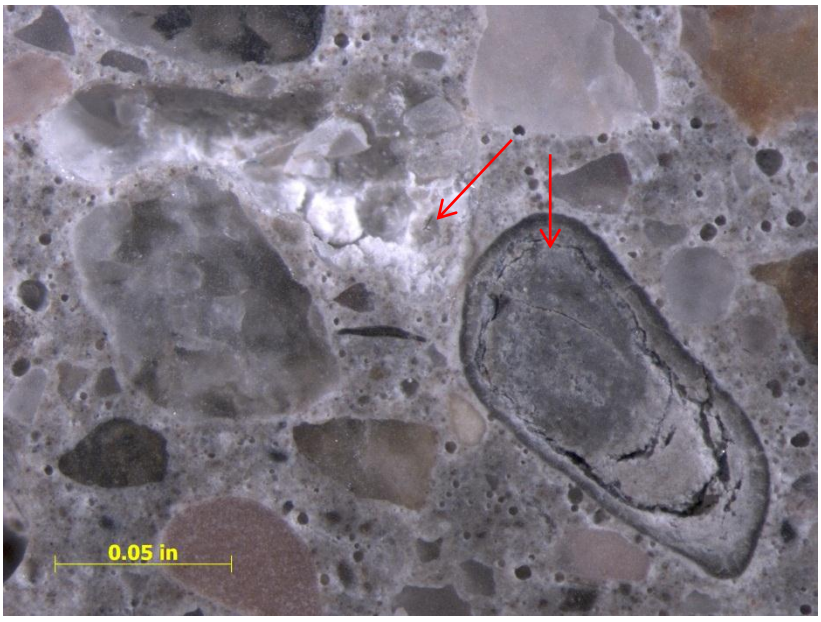

Figure 6. Core 6 base concrete; shown is the largest sand particle of reactive shale. White ASR gel partially fills large air void that is adjacent to the particle. Cracks are present within the shale particle but they do not extend to the surrounding cement paste.

Figure 7. Lapped section of Core 42; top end is on the left of the photo. Numerous cracks due to corrosion and ASR are present in the base concrete; no cracking was detected in the topping concrete.

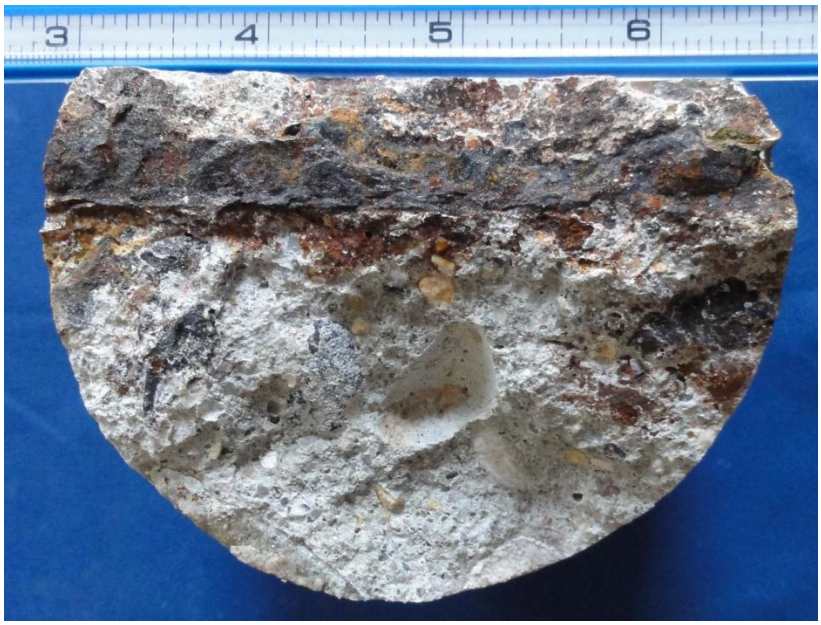

Figure 8. Core 42; corroded rebar in base concrete at one of the transverse cracks.

Figure 9. Core 42: corroded rebar taken out of base concrete at one of the cracks.

Figure 10. Core 42; large lump of industrial waste containing reactive glass embedded at the bottom of the base concrete.

Figure 11. Core 42; close up of the light color area of the bottom surface of the core from Figure 8 showing that the surface is coated with ASR gel.

Figure 12. Core 42 base concrete; reactive sandstone particle, partially consumed in ASR; cracks extending into the surrounding cement paste.

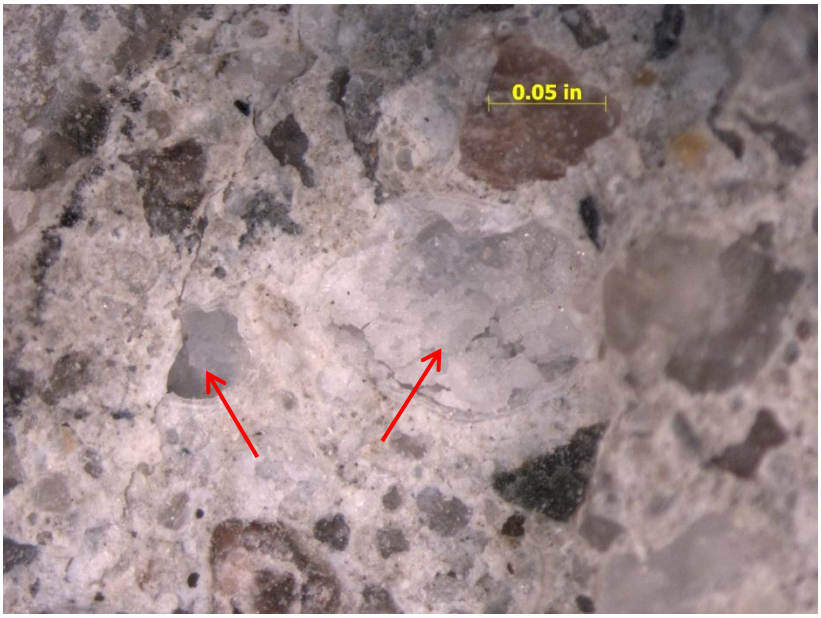

Figure 13. Core 42; air voids partially filled with ASR gel at one of the crack surfaces in the base concrete.

Appendix G

Chloride Testing Data

Chloride Test Data

Uncracked Cores											
Core No. 2		Core No. 20		Core No. 25		Core No. 27		Core No. 36		Core No. 45	
Depth (in.)	*Chloride (ppm)*	*Depth (in.)*	*Chloride (ppm)*	*Depth (in.)*	*Chloride (ppm)*	*Depth (in.)*	*Chloride (ppm)*	*Depth (in.)*	*Chloride (ppm)*	*Depth (in.)*	*Chloride (ppm)*
0.19	5470	0.21	3451	0.22	3404	0.23	6179	0.17	3778	0.24	4749
0.44	5158	0.49	2749	0.44	3278	0.57	4634	0.48	3487	0.45	3677
0.81	3829	0.86	697	0.82	1095	0.90	1936	0.80	1968	0.82	1895
1.31	1357	1.36	67	1.33	121	1.33	197	1.33	325	1.34	249
1.88	162	2.69	279	2.52	91	2.24	170	2.07	70	3.25	54
2.13	130	2.92	249	2.79	127	2.54	124	2.37	110	3.70	107
2.50	128	3.29	197	3.19	98	2.84	79	2.64	95	3.90	98
2.88	128	3.78	95	3.66	104	3.34	139	2.99	112	4.33	180
								3.62	109	4.88	119

Cores at Delaminations							
Core No. 9		Core No. 12		Core No. 16		Core No. 39	
Depth (in.)	*Chloride (ppm)*	*Depth (in.)*	*Chloride (ppm)*	*Depth (in.)*	*Chloride (ppm)*	*Depth (in.)*	*Chloride (ppm)*
0.19	4320	0.25	3198	0.21	5371	0.18	5278
0.44	3985	0.56	3103	0.53	5292	0.51	4812
0.81	3389	0.88	2231	0.84	3975	0.82	3282
1.31	2948	1.37	1583	1.33	1345	1.20	743
1.69	2661	2.11	1161	2.59	124	1.44	217
2.06	2394	2.61	941	2.90	205	1.85	107
2.31	2009	2.91	848	3.20	128	3.26	60
2.69	1217	3.22	911	3.66	156	2.41	72
3.19	1057	3.65	465			2.94	98

Cracked Cores			
Core No. 28		Core No. 35	
Depth (in.)	*Chloride (ppm)*	*Depth (in.)*	*Chloride (ppm)*
0.44	6951	0.38	5679
1.04	5645	1.05	3957
2.55	3194	2.20	2640
3.23	2455	2.94	2426
3.73	2681	3.47	1849
4.19	2635	3.98	2578

Appendix H

Olson Engineering Report

INFRASTRUCTURE IMAGING AND NDE
ASSESSMENT, MONITORING AND REPAIR

Olson ENGINEERING
Corporate Office:
12401 W. 49th Ave.
Wheat Ridge, CO 80033-1927 USA
phone: 303.423.1212
fax: 303.423.6071

NON-DESTRUCTIVE BRIDGE DECK EVALUATION
BRIDGE DECK SCANNER – IMPACT ECHO TESTING OF CONCRETE DECK
I-129 BRIDGE OVER MISSOURI RIVER
SIOUX CITY, IOWA

Prepared for:
Wiss, Janney, Elstner Associates, Inc.
330 Pfingsten Road
Northbrook, IL 60062

Attn: Mr. Paul Krauss, PE
Phone: 847.272.7400
Email: PKrauss@WJE.com

Olson Engineering Job No. 3641A
July 21st, 2011

Table of Contents

1.0 EXECUTIVE SUMMARY

A nondestructive evaluation (NDE) investigation and condition assessment was conducted for Wiss, Janney, Elstner Associates (WJE) on six sections of I-129 Bridge (concrete bridge deck) over the Missouri River in Sioux City, Iowa. The six sections are referred to herein as Eastbound# 1, Eastbound #2, Eastbound #3, Westbound #1, Westbound #2 and Westbound #3. The field investigation was performed using the Impact Echo (IE) nondestructive test method utilizing our newly developed concrete Bridge Deck Scanner (BDS) system. The investigation was performed in order to determine the condition of the concrete deck, specifically to locate areas of top delamination or any other notable defects.

Bridge Deck Scanner -Impact Echo (BDS-IE) Results. Table I summarizes the test results from the IE from all six tested sections in terms of top and bottom delaminations as well as incipient or "developing" delaminations on a square ft and percentage basis.

Table I – Summary of IE Test Results for the Six BDS-IE Test Areas

Section I.D.	Total Tested Areas (ft^2)	Areas with Shallow Top Delaminations (ft^2)	% of Areas with Shallow Top Delaminations	Areas with both Developing Delaminations and Shallow Top Delaminations (ft^2)	% Areas with both Developing Delaminations and Shallow Top Delaminations	Areas with Possible Bottom Delaminations (ft^2)	% of Areas with Possible Bottom Delaminations
Eastbound #1	3,201.8	186.8	5.8	286.6	9.0	17.9	0.6
Eastbound #2	3,201.0	342.5	10.7	521.1	16.3	24.7	0.8
Eastbound #3	3,404.4	129	3.8	228	6.7	18.4	0.5
Westbound #1	4,206.6	86.2	2.0	336	8.0	55.9	1.3
Westbound #2	4,603.8	285.5	6.2	528.7	11.5	136.5	3.0
Westbound #3	3,404.5	171.5	5.0	179.3	5.3	43.2	1.3

The IE testing indicates that the concrete bridge deck has significant areas of top delaminations. Eastbound #2 appears to have the most IE detected top shallow delaminations (10.7% of the total tested area). There are a few, very small and scattered areas that may indicate delamination on the bottom side of the concrete bridge deck. Some areas of the bridge deck appeared consistently thicker than the typical 10-12 inch deck thickness, and are understood to

be designed to be thicker, particularly on the Westbound side in the shoulder where the on-ramp merges onto the bridge. For this reason the Impact Echo results are presented as "normalized thickness" color images, where the actual measured thickness is divided by the expected thickness of the bridge deck at that location. Therefore, for presentation purpose, the differences in bridge deck thickness are accounted for and the percentage of variation from the design thickness can easily be observed. It is this change in frequency or apparent change in thickness that indicates near surface delaminations or other internal defects.

Approximately 45,800 Impact Echo test points were performed in 2 field days on a slow-rolling, scanning basis with the Olson Instruments Bridge Deck Scanner (BDS-IE) to provide an IE test on nominally every 0.5 sq ft of the deck. Six separate test areas were investigated. The overall IE test result maps from the BDS-IE scanning are included in Appendix A. Maps of shallow top steel delaminations and incipient delaminations (or developing delaminations) are presented in Appendix B. Maps of possible bottom steel delaminations and shallower, possible internal cracks are presented in Appendix C.

It should be noted that where a delamination is detected with the BDS-IE that no information can be determined on deeper portions of the bridge deck below the delamination depth. This is because the complete air gap of an open delamination blocks the compressional sound waves from penetrating any deeper.

2.0 PROJECT BACKGROUND AND INVESTIGATION OVERVIEW

The nondestructive evaluation (NDE) investigation and condition assessment of the concrete bridge deck of the I-129 Bridge over the Missouri River in Sioux City, Iowa was performed on June 21st – 22nd, 2011 by Dr. Yajai Tinkey and Mr. Patrick Miller, Associate Engineer and Senior Project Engineer of Olson Engineering, respectively. The results of all the BDS-IE scans are discussed in Section 3 below.

The Impact Echo testing was performed using an Olson Instruments Bridge Deck Scanner System (BDS-IE). The BDS-IE unit performs Impact Echo testing while slowly being rolled (~1 mph) along the top of the bridge deck (see Figure 1). The BDS-IE unit consists of multiple transducer wheels (approximately 1 ft in diameter) which measure the IE vibrations induced by an on-board automated solenoid impactor. The Olson Instruments Freedom Data PC based BDS-IE system performs an Impact Echo test at 6-inch intervals with each testing wheel. For this investigation the BDS-IE unit was set-up with two transducer wheels, therefore 2 lines of IE data were acquired simultaneously since the wheels are offset 30 degrees to provide for staggered testing every 3 inches by the left and right wheels. The resolution of IE testing is therefore every 6 inches in the longitudinal direction of the bridge with test lines spaced 1 foot apart across the width of the bridge. This test pattern provided for an IE test of every 0.5 sq ft of the nominally 10-12 inch thick bridge deck.

Note that for larger test areas in which the required field test time becomes more critical, an alternative BDS-IE set-up which utilizes six transducer wheels can be employed (see Figure 5 in Section 5). This expanded system is vehicle mounted and requires more equipment mobilization and was not used in this instance due to the comparatively small deck area of the tested bridge.

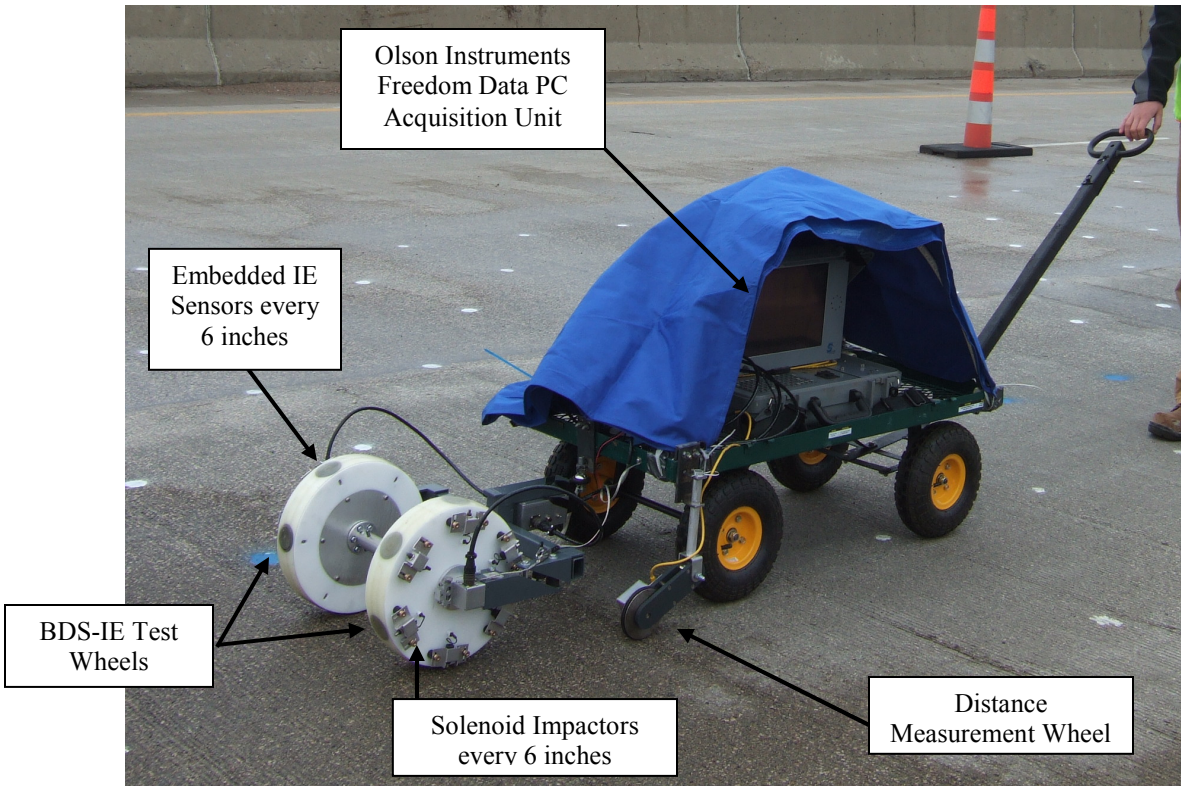

Figure 1: Photograph of Olson Instruments BDS-IE system (2 transducer wheels) on the I-129 Bridge. The computer acquisition system was covered with a tarp due to rain.

There were a total of six test areas investigated, three on the Eastbound side and three more on the Westbound side. The test areas are referred as Eastbound #1, Eastbound #2, Eastbound #3, Westbound #1, Westbound #2 and Westbound #3 in this report. The test areas were delineated on-site by WJE personnel by painting dots in a 2 x 2 foot grid. The test sections are considered straight and square. Each test section was 200 feet in length and varied between 16 – 23 feet wide. The BDS-IE testing was performed by towing the BDS-IE unit by hand with a cart (see Figures 1 and 2). For both the Eastbound and Westbound test areas the first test line (closest to the curb) was noted as the zero point for the Y-axis. The X-axis zero point was on the left when observing the test area from the curb. Therefore, for the Westbound test sections up is South, while on the Eastbound test sections up is North and for all test sections the X-axis increases in the direction of traffic. All BDS-OE deck condition image results discussed in Section 3.0 and presented in Appendix A are based upon this grid layout.

Figure 2: Photograph showing test grid layout for BDS-IEtesting on a 1 ft grid with impacts every 6 inches to provide 1 test every 0.5 sq ft

3.0 NONDESTRUCTIVE EVALUATION RESULTS FROM IMPACT ECHO TESTS

As discussed above, the Impact Echo test method was performed utilizing an Olson Instruments BDS-IE system. In total approximately 45,800 separate IE tests were performed on the I-129 / Missouri River Bridge deck in 2 field test days in rainy conditions. An impact echo concrete compression wave velocity of 12,500 ft/sec was used for all thickness calculations based on IE results in apparently sound deck areas. The impact echo data was analyzed by determining the resonant frequency of the concrete structure at each test point. The resonant echo frequency is directly related to the structure's thickness. Changes in the concrete condition of the structure are identified by shifts in the resonant frequency. For instance, a relatively lower resonant frequency, typically also with a high amplitude, indicates a shallow, top steel delamination within a few inches of the surface; the low frequency / high amplitude response is due to the audible flexural resonance response of a hollow-sounding, near-surface delaminations that can be heard during chain-dragging or with other acoustic sounding techniques. Other decreases in compressional wave resonant frequency (from a normal full-depth sound deck thickness echo) can indicate either thicker concrete or internal honeycomb/void while the presence of multiple resonant frequencies or a resonance higher than expected is indicative of internal cracking or possible bottom steel delamination.

The Impact Echo data was processed by applying a time domain rectangular window to remove any noise that may have occurred near the time of the impact. The data was then digitally filtered with a 4 pole Butterworth high-pass filter with a cut-off frequency of 1,500 Hz to remove low frequency rolling noise inherent to the system and the resonance of the IE displacement transducer. Note that the typical resonant echo frequency of the concrete bridge deck was approximately 7,000 Hz. These processing steps allow the resonant frequency of the concrete deck to be easily identified. Figure 3 displays example data from a test line performed with the BDS-IE system on the I-129 Bridge.

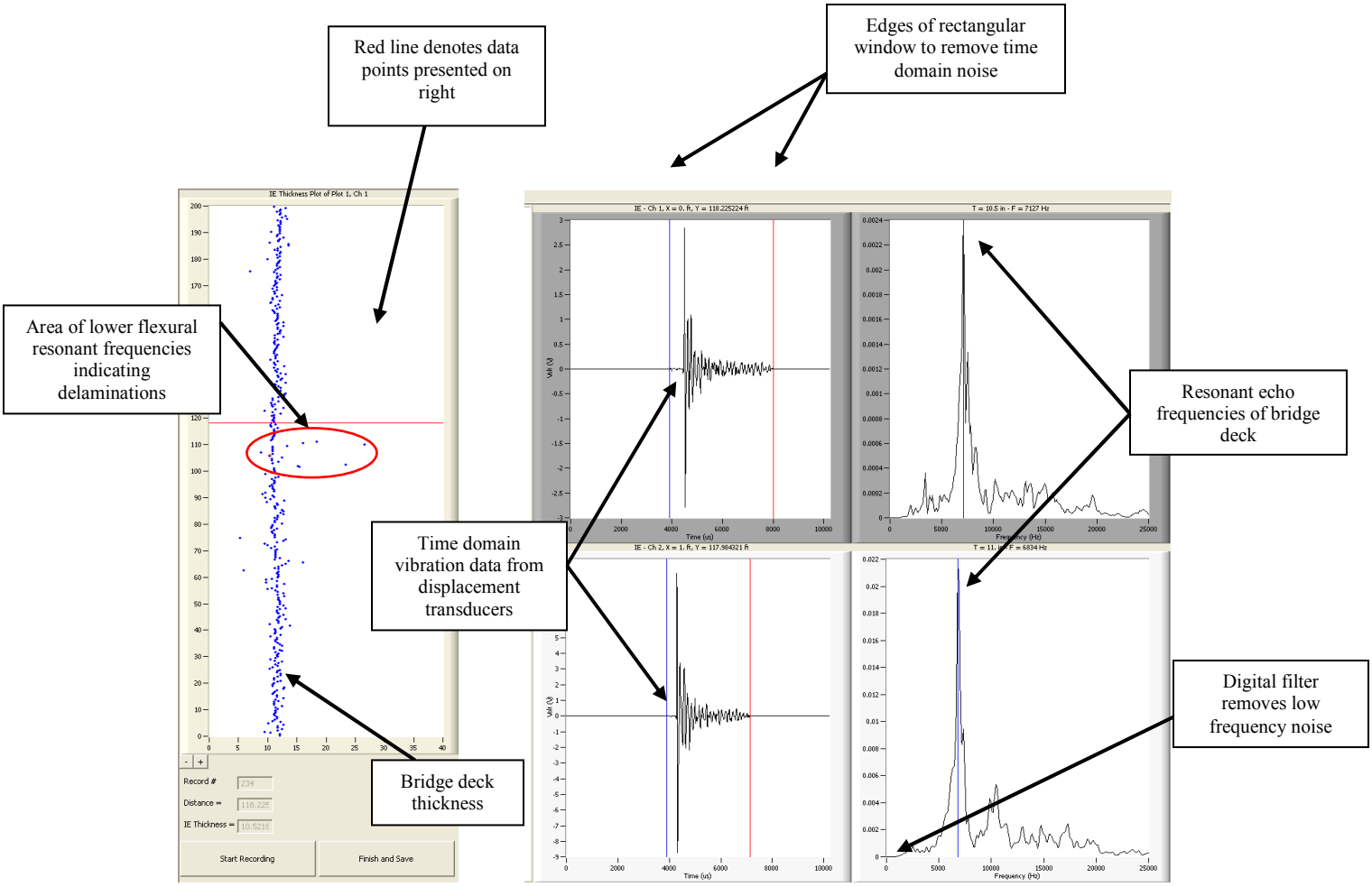

Figure 3: Example Impact Echo Results from a 50 ft long scan line for the Olson Instruments BDS-IE system.

Each BDS-IE test line acquired was analyzed as described above and combined to create a plan view image result of the I-129/Missouri River bridge deck conditions. For this application, due to the presence of some areas of the bridge deck which were significantly thicker by design, the normalized concrete thickness (measured thickness divided by design thickness) is plotted. This presentation removes designed variations in thickness and highlights defect areas. The variation in normalized concrete thickness from the impact echo results is displayed as different colors. Sound concrete conditions will appear as normalized thickness values near a value of 1.0, or near the design thickness. Areas with shallow, top reinforcing steel delaminations will have a lower resonant frequency and therefore a normalized thickness value greater than 1.0. Areas

with internal cracking resulting in shallower echoes than the deck thickness and possible bottom deck delamination will have a normalized thickness value of less than 1.0.

The plan view color plots of the results representing the general conditions of the test section are presented in Appendix A. Top delamination maps are presented in Appendix B. The top delamination maps (Appendix B) indicate that there are several areas of delamination within each of the six test areas. The areas with the most delaminations are Eastbound Area 2, Eastbound Area 1, and Westbound Area 2. Olson Engineering's experience has shown that top delaminations (where it is audible when sounding) typically have calculated thickness values that are 30% higher than the expected echo thickness (purple and red areas). The yellow areas (15 – 30% higher) produced questionable results and may be due to developing/incipient delaminations. The blue areas have resonant frequencies which are notably less than the expected full thickness echo. It is possible that these areas are due to cracking at the bottom layer of rebar steel and may emerge in the future as bottom delaminations. Areas with resonances within approximately 20% of the expected resonance from a full deck thickness echo are considered sound. The variations in resonant frequency are attributed to small variations in actual thickness due to cast in place construction and resurfacing, as well as slight, natural variations in the concrete velocity. Table I in Section 1.0 presents the summary of the BDS-IE test results of the 6 deck areas.

4.0 IMPACT ECHO TEST METHOD

The Impact Echo (IE) tests were performed during this investigation using Olson Instruments Bridge Deck Scanner Impact Echo testing system (BDS-IE). All test hardware was interfaced with the Olson Instruments Freedom Data PC, which is a nondestructive, battery powered system for data collection and storage. The IE test method is typically used for measuring the thickness and integrity of concrete slabs, beams, pavements, tunnel linings, walls, and other plate-like and columnar structural elements.

The IE tests involved impacting the top of the concrete deck with an impactor (solenoid or small hammer) and identifying the resonantly reflected compressional wave energy with a displacement transducer as shown in Figure 4 below for a point-by-point test head. The BDS-IE transducer wheels were rolled along the concrete surface while tests were performed with impacts at each test point. The resonant echoes of the displacement responses are generally not as apparent in the time domain, but are more easily identified in the frequency domain. Consequently, amplitude spectra of the displacement responses are calculated by performing a Fast Fourier Transform (FFT) analysis to determine the resonant echo peak(s). The relationship among the resonant echo depth frequency peak (f), the compression wave velocity (V_P) and the echo depth (D) is expressed in the following equation:

$$D = \beta V_p/(2*f)$$

where β is a geometric shape factor ranging from 0.87 for a square column to 0.96 for a slab/wall shape. An unflawed slab/wall shape has a single thickness resonance while unflawed beam and column shapes can have multiple resonances due to their cross-sectional shape. The IE compressional wave velocity was assumed to be 12,500 ft/s in this test based on typical thickness echoes on apparently sound concrete. When backside thickness echo resonant peaks shift downward from the normal pattern in slabs, and square and rectangular columns, this indicates poorer quality/flawed internal conditions such as void or honeycomb. If cracks or voids are parallel or subparallel to the test surface, shallow echoes may also be recorded from depths that correspond to the flaws. Distributed void/honeycomb may not result in such shallow echoes, but rather the false increase in backside echo depth due to the lower stiffness and associated resonant

echo frequency due to the void/honeycomb. Shallow delaminations produce low frequency, high amplitude flexural resonances that are much thicker than the concrete as discussed above.

The IE method can be used for measuring thicknesses, evaluating quality, and detecting hidden flaws such as delaminations, cracks, honeycombs, etc. The IE test data were recorded on the Freedom Data PC during the field NDT&E and initially analyzed in the field. The data was also saved for later detailed analysis at our office.

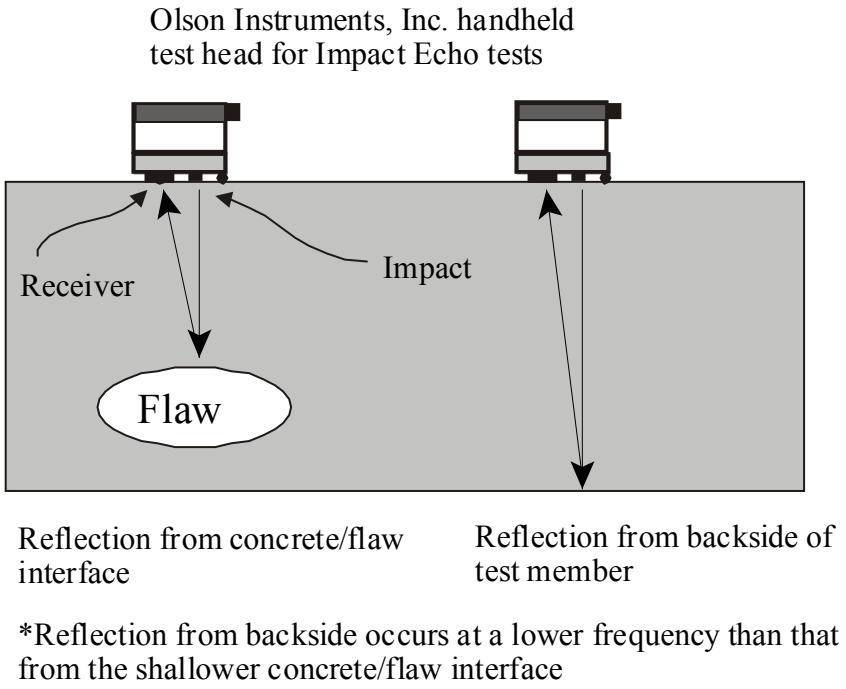

Figure 4: Schematic of Impact Echo (IE) method – point-by-point test head shown

5.0 APPLICATIONS OF BRIDGE DECK SCANNER

A Bridge Deck Scanner can be equipped with 2, 4 or 6 transducer wheels dependent on the quantity and time allowed for testing. The BDS system was designed to perform either:

1) Impact Echo testing on all transducer wheels

2) Impact Echo testing on the transducer wheel near the impactor solenoid and Spectral Analysis of Surface Waves (SASW) testing from adjacent pairs of transducer wheels

The first type of testing (IE) is best applied to condition assessment of concrete bridge or garage deck slabs without an asphalt overlay. Note that the first type of testing was used for condition assessment of I-129 Bridge over the Missouri River. The later type of testing (IE + SASW) works well with asphalt pavements, either full-depth or as an overlay, to detect delamination (debonding) between asphalt lift layers. To perform SASW testing, sensor elements in both transducer wheels (within a pair) are aligned and locked with a pin to prevent the slippage. The sensor elements are offset approximately 2 inches between each adjacent pair of transducer wheels (if all six transducer wheels are used). Figure 5 shows a typical test setup, including the transducer locations of all wheels for the IE-SASW setup.

Figure 5 – Vehicle Mounted BDS-IE-SASW Transducer Alignment for an IE test on one wheel and an SASW test between the wheel pair spaced at 6 inches apart for asphalt delamination (debonding) detection by velocity decreases. Note that for Bridge Deck Scanning the spacing can be increased to 1 ft or 2 ft between each pair of wheels to provide for ½ lane to a full lane scan per pass with tests ~ every 6 inches.

In the latter type of testing, the system was set so that only the solenoids of the left transducer wheel (of the pair) are used for generating impacts. The solenoids of the right transducer wheel (of the pair) are disabled for the duration of the testing. The impact sequence starts with firing the single solenoid used for the left pair of transducer wheels, followed by the solenoid for the middle pair of transducer wheels, and finally the solenoid for the right pair of transducer wheels.

6.0 CLOSURE

The field portion of this investigation was performed in accordance with generally accepted testing procedures. If additional information is developed that is pertinent to the findings of this investigation or we can provide any additional information, please contact our office. We also respectfully request feedback on how the BDS-IE Deck Condition Assessment results compare with other destructive/nondestructive tests byWJE.

Respectfully submitted,

OLSON ENGINEERING, INC.

Patrick K. Miller, P.E.
Senior Project Engineer

Yajai Tinkey, Ph.D., P.E.
Associate Engineer

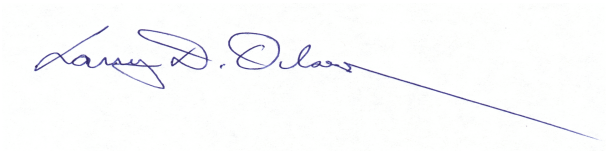

Larry D. Olson, P.E.
Principal Engineer

(1 copy emailed, 2 copies mailed)

APPENDIX A: BDS-IE TESTING RESULT IMAGES – OVERALL TEST RESULTS NORMALIZED TO DECK THICKNESS

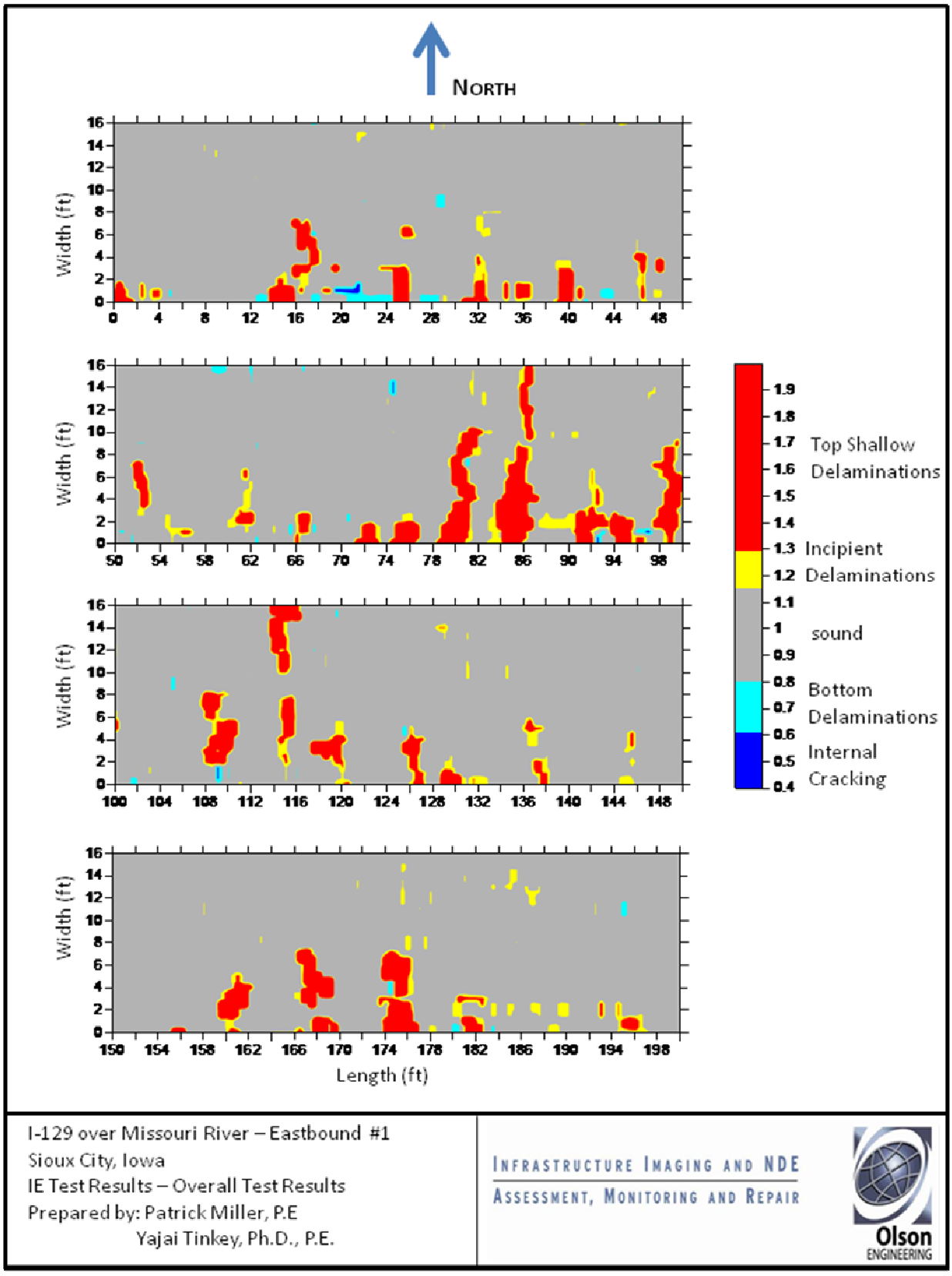

Figure A1: Eastbound Area 1, BDS-IE Results Image

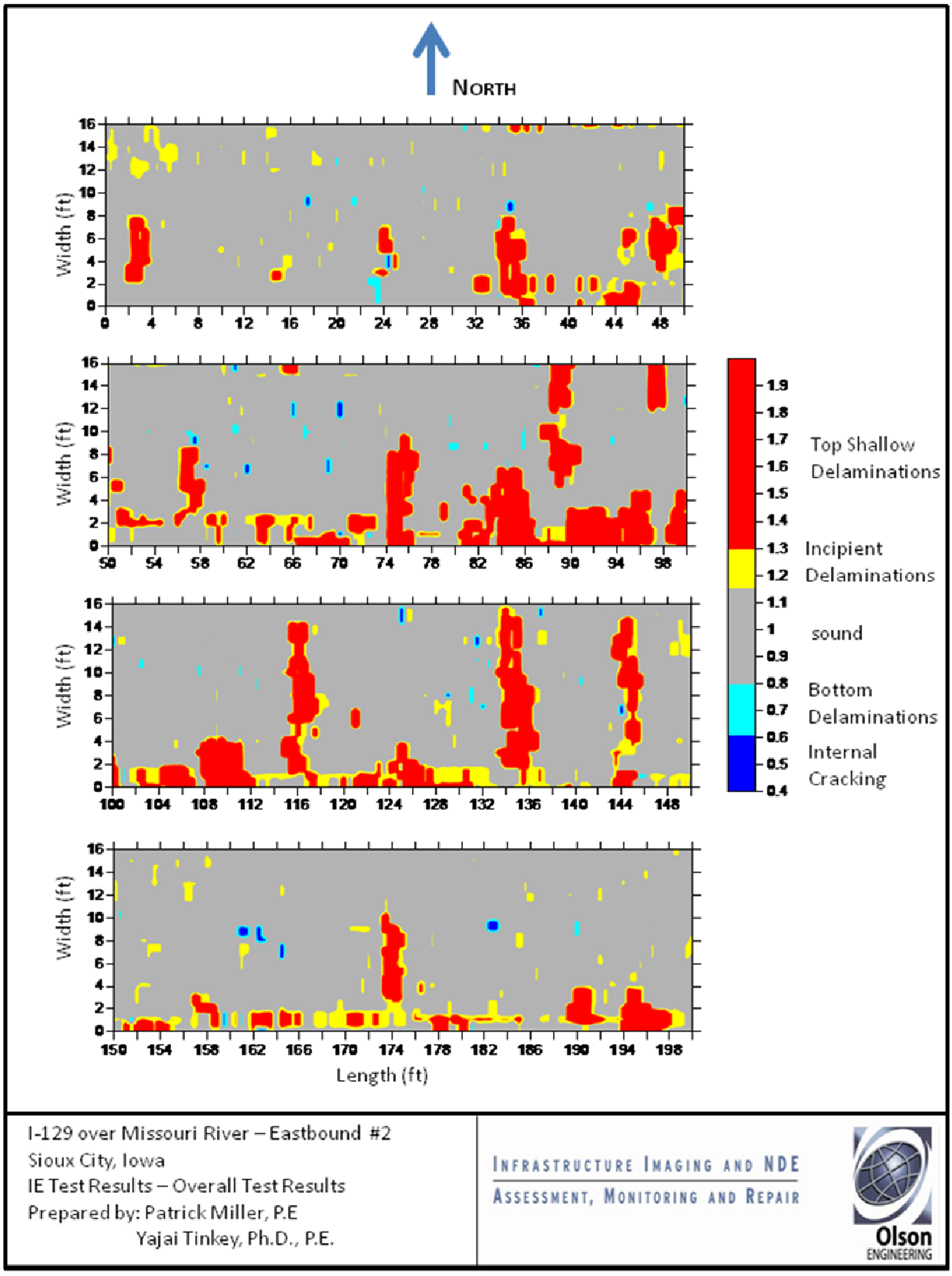

Figure A2: Eastbound Area 2, BDS-IE Results Image

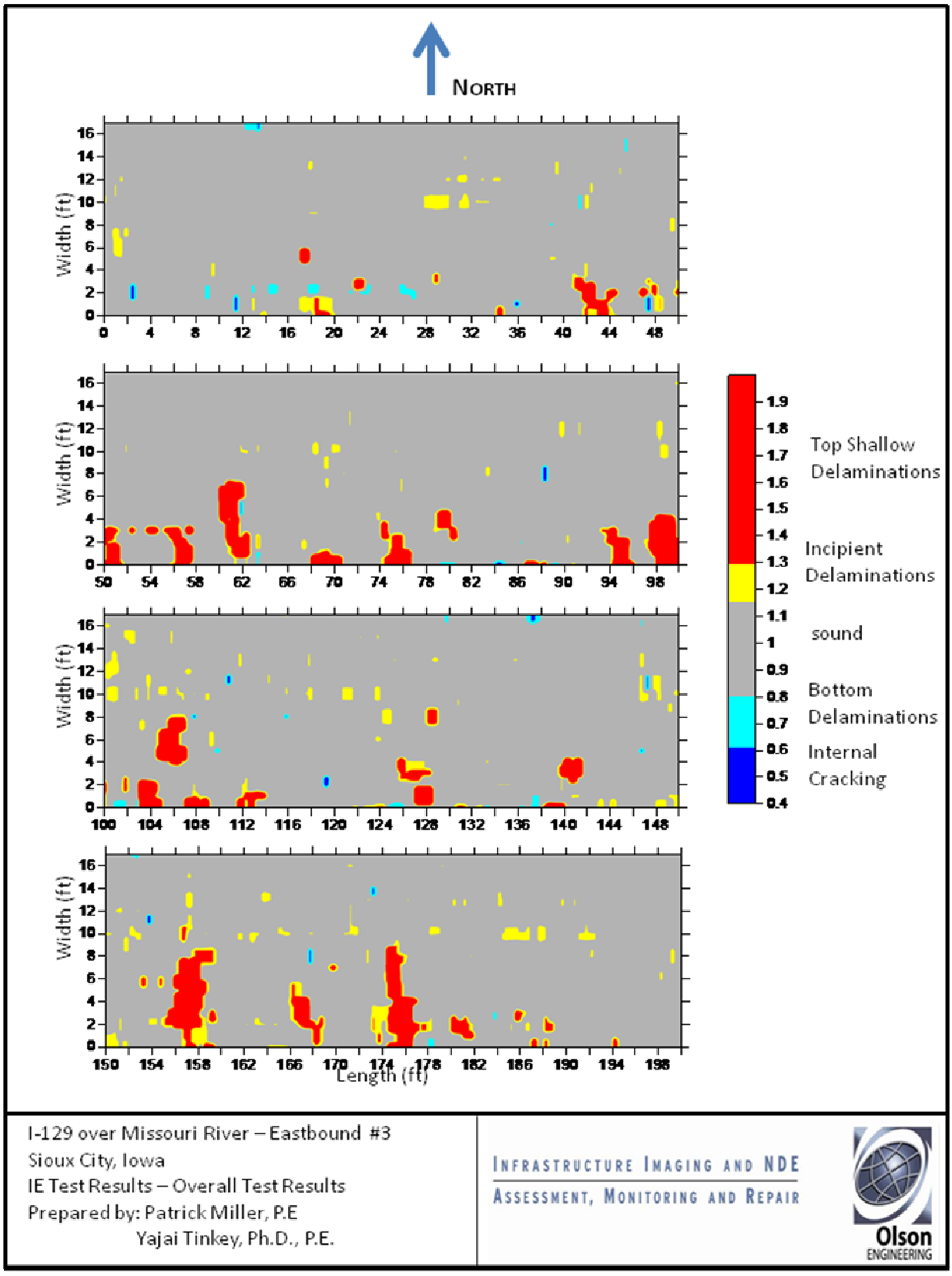

Figure A3: Eastbound Area 3, BDS-IE Results Image

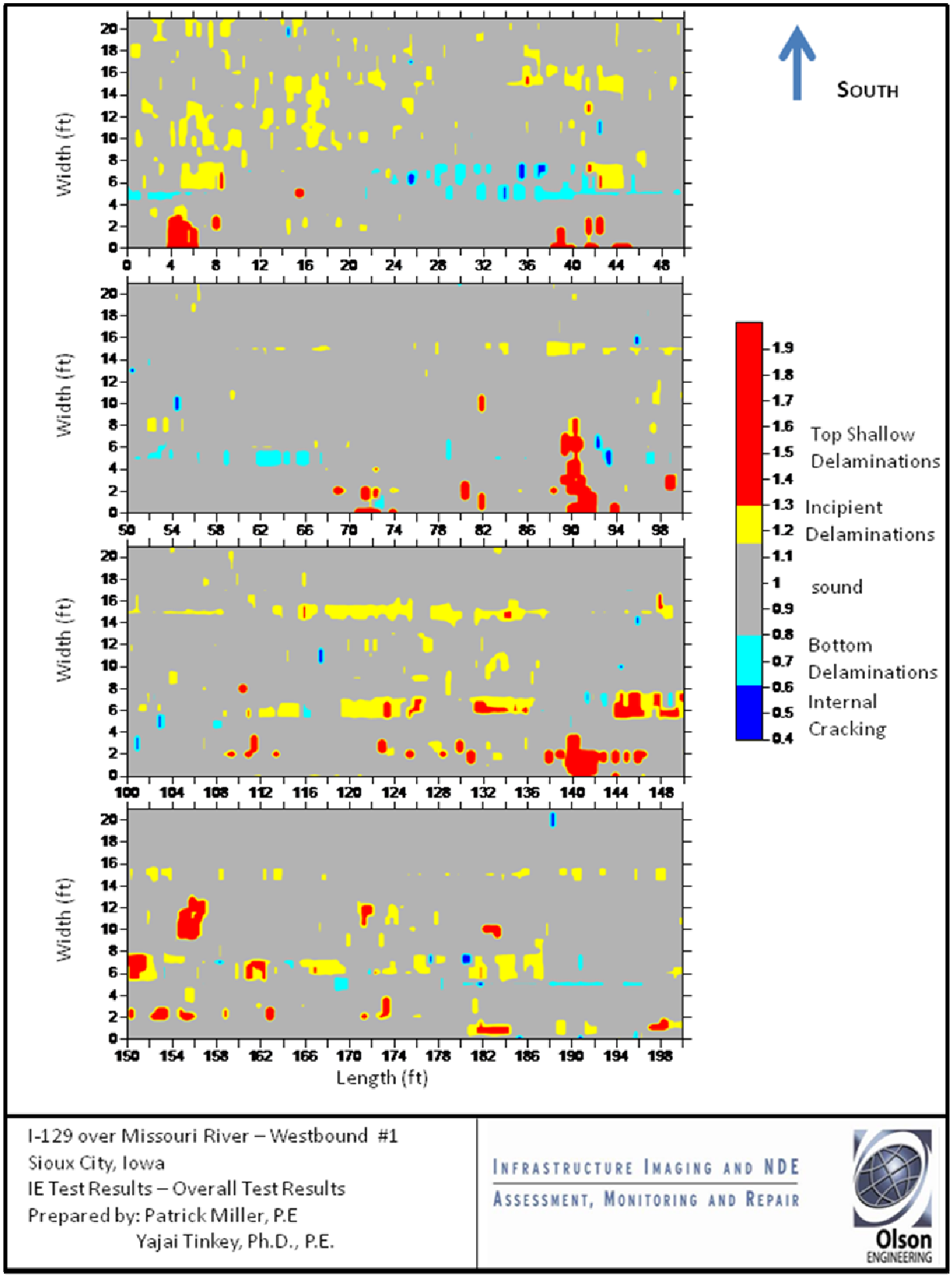

Figure A4: Westbound Area 1, BDS-IE Results Image

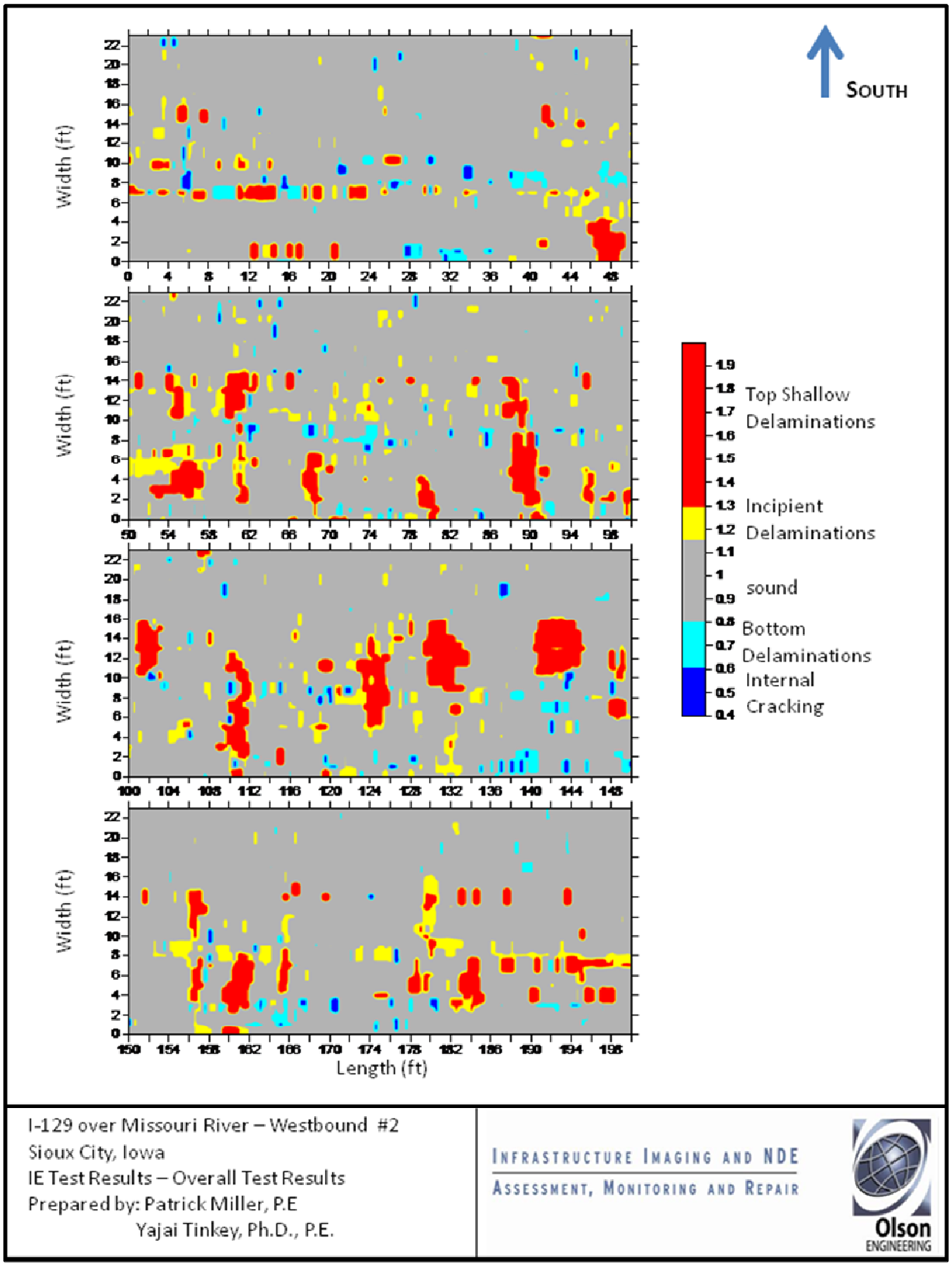

Figure A5: Westbound Area 2, BDS-IE Results Image

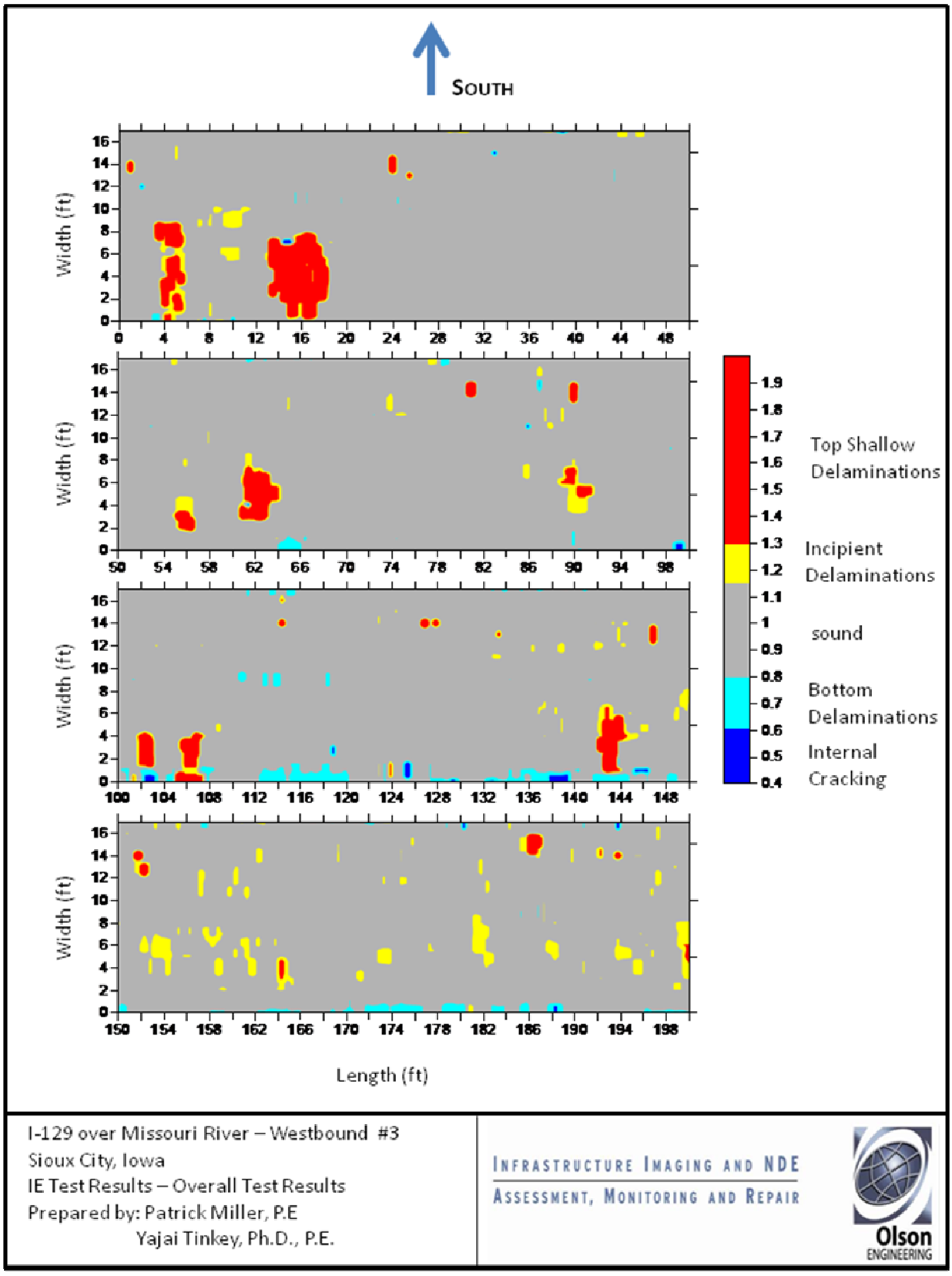

Figure A6: Westbound Area 3, BDS-IE Results Image

APPENDIX B: BDS-IE TOP STEEL DELAMINATION DECK CONDITION IMAGES

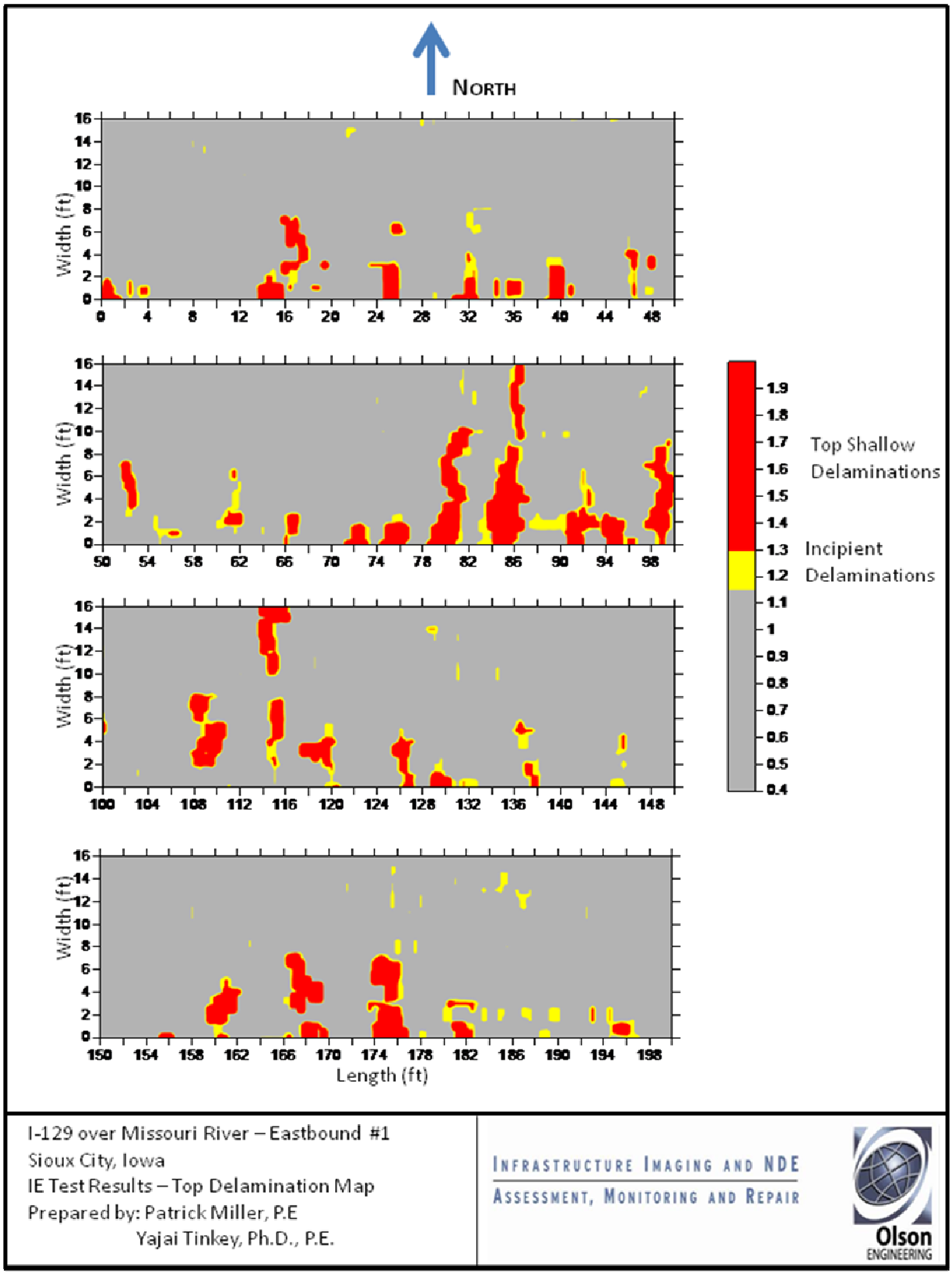

Figure B1 – Top Delamination Maps for Eastbound #1

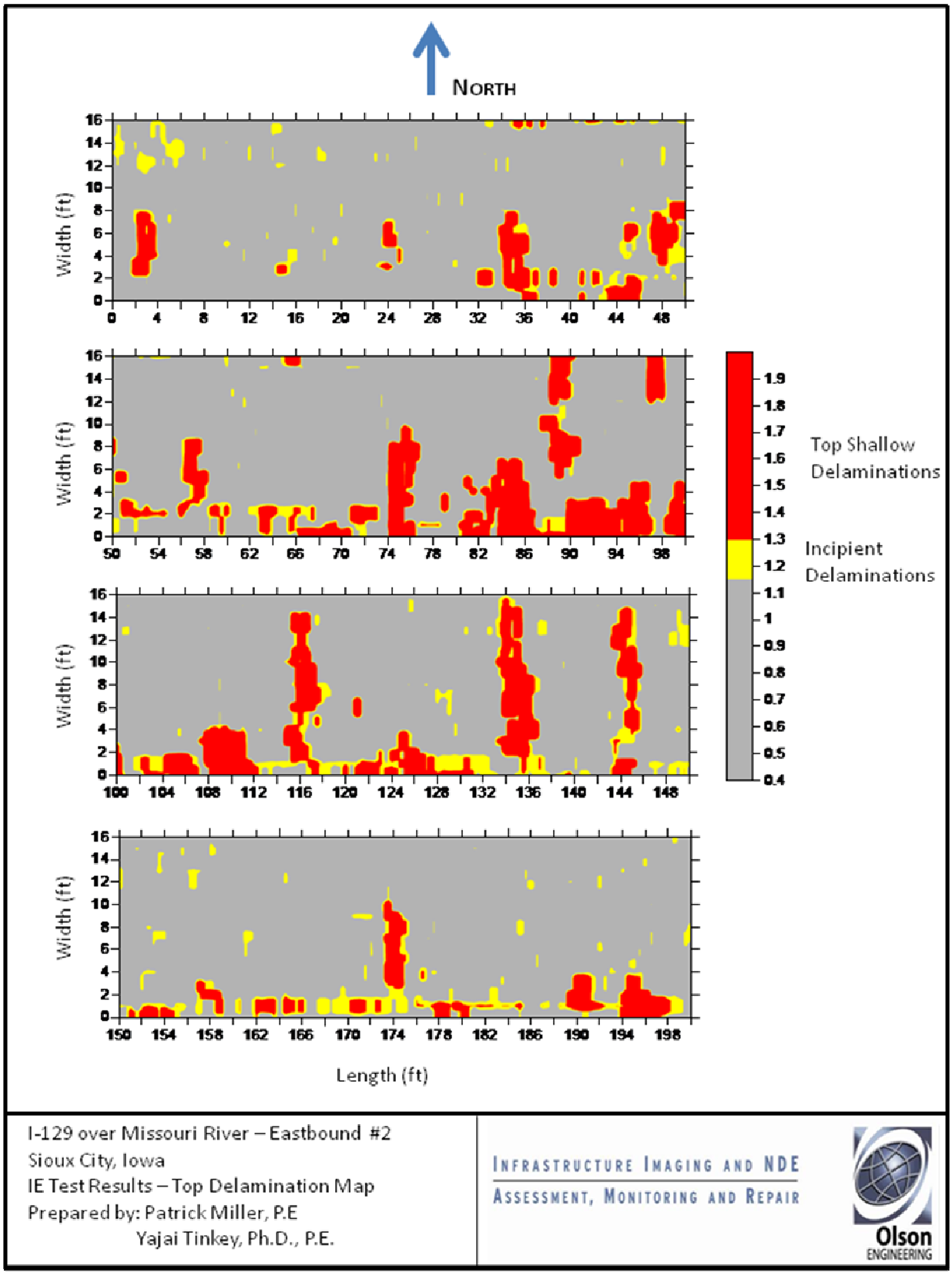

Figure B2 – Top Delamination Maps for Eastbound #2

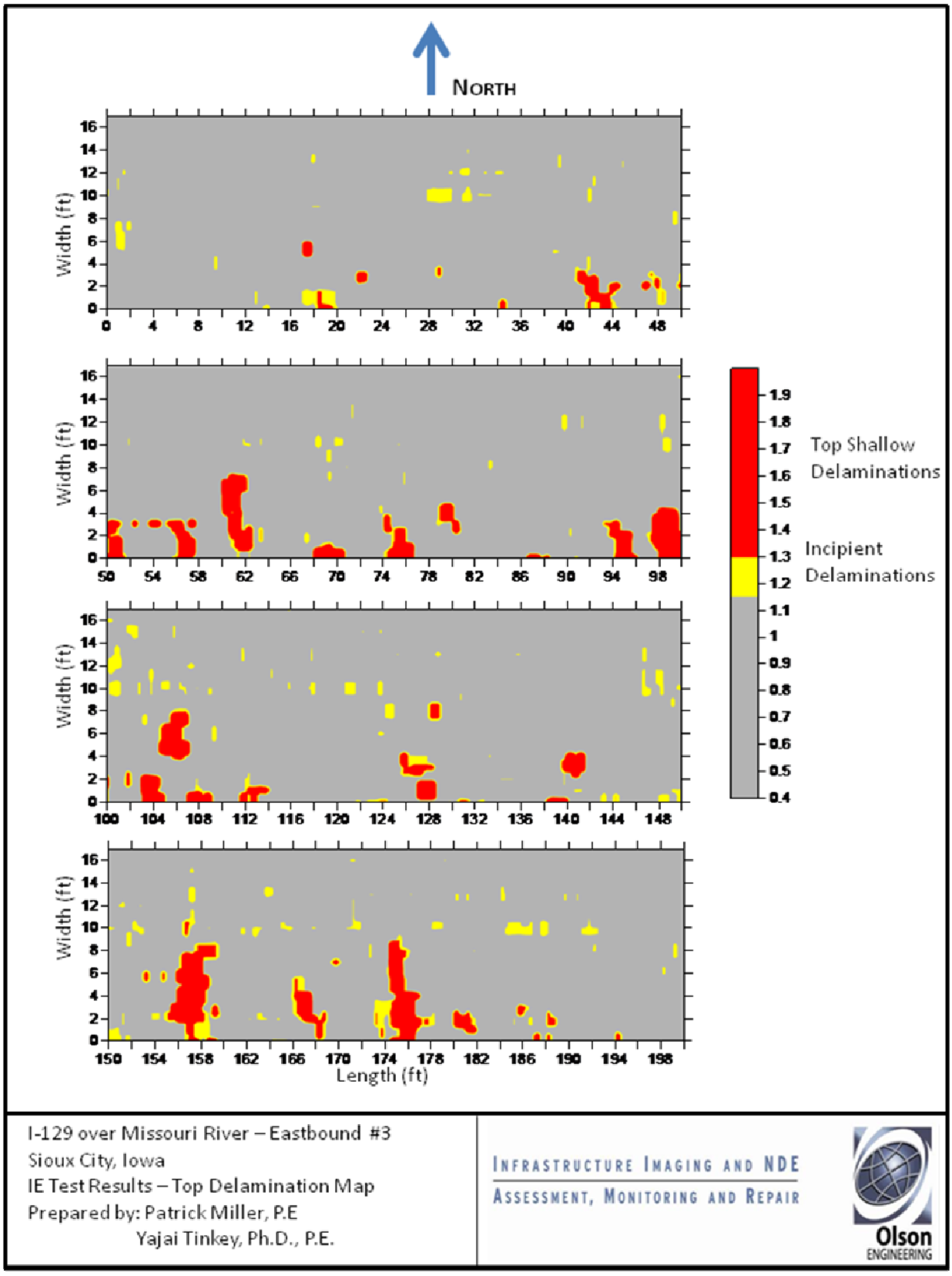

Figure B3 – Top Delamination Maps for Eastbound #3

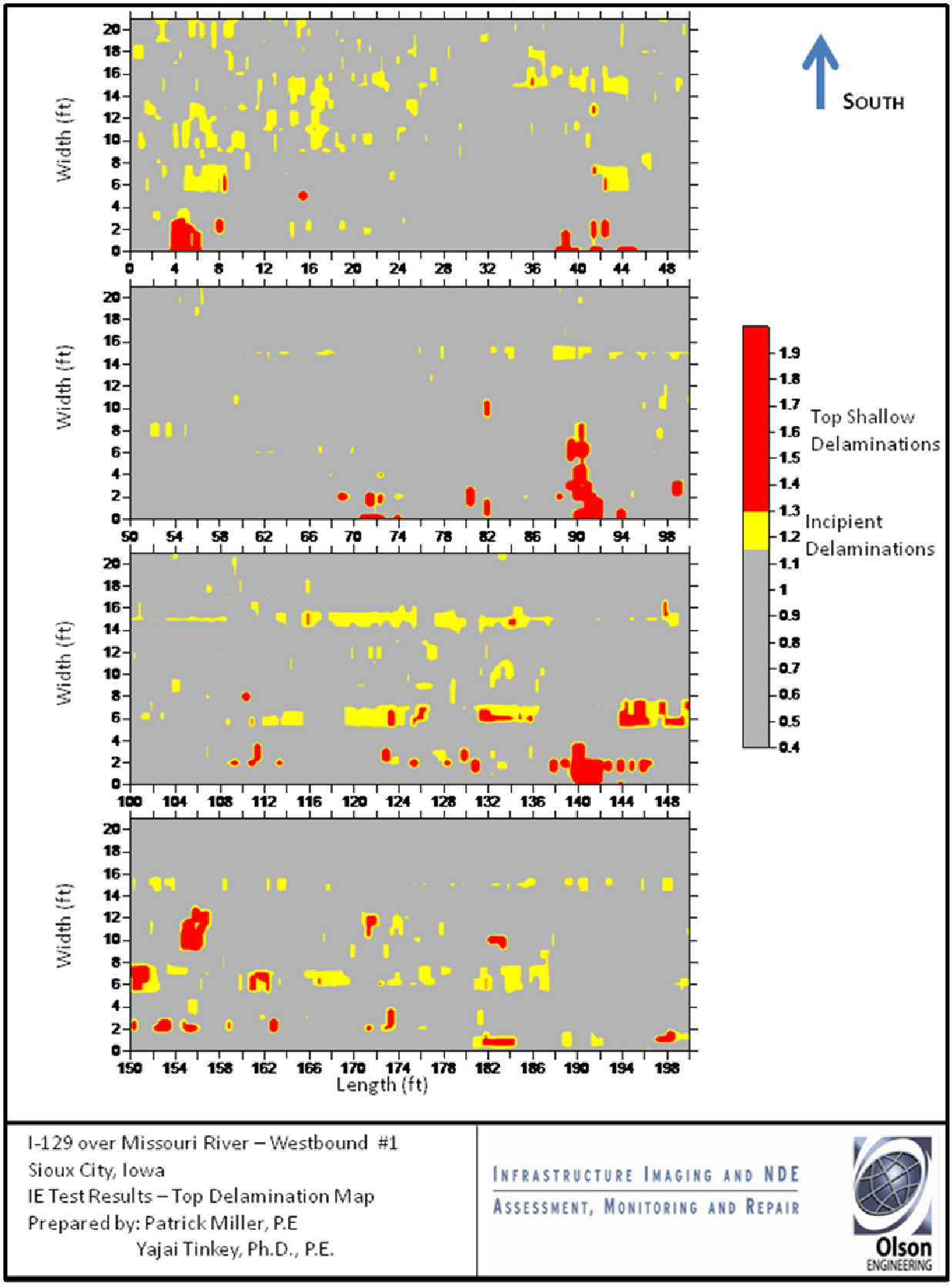

Figure B4 – Top Delamination Maps for Westbound #1

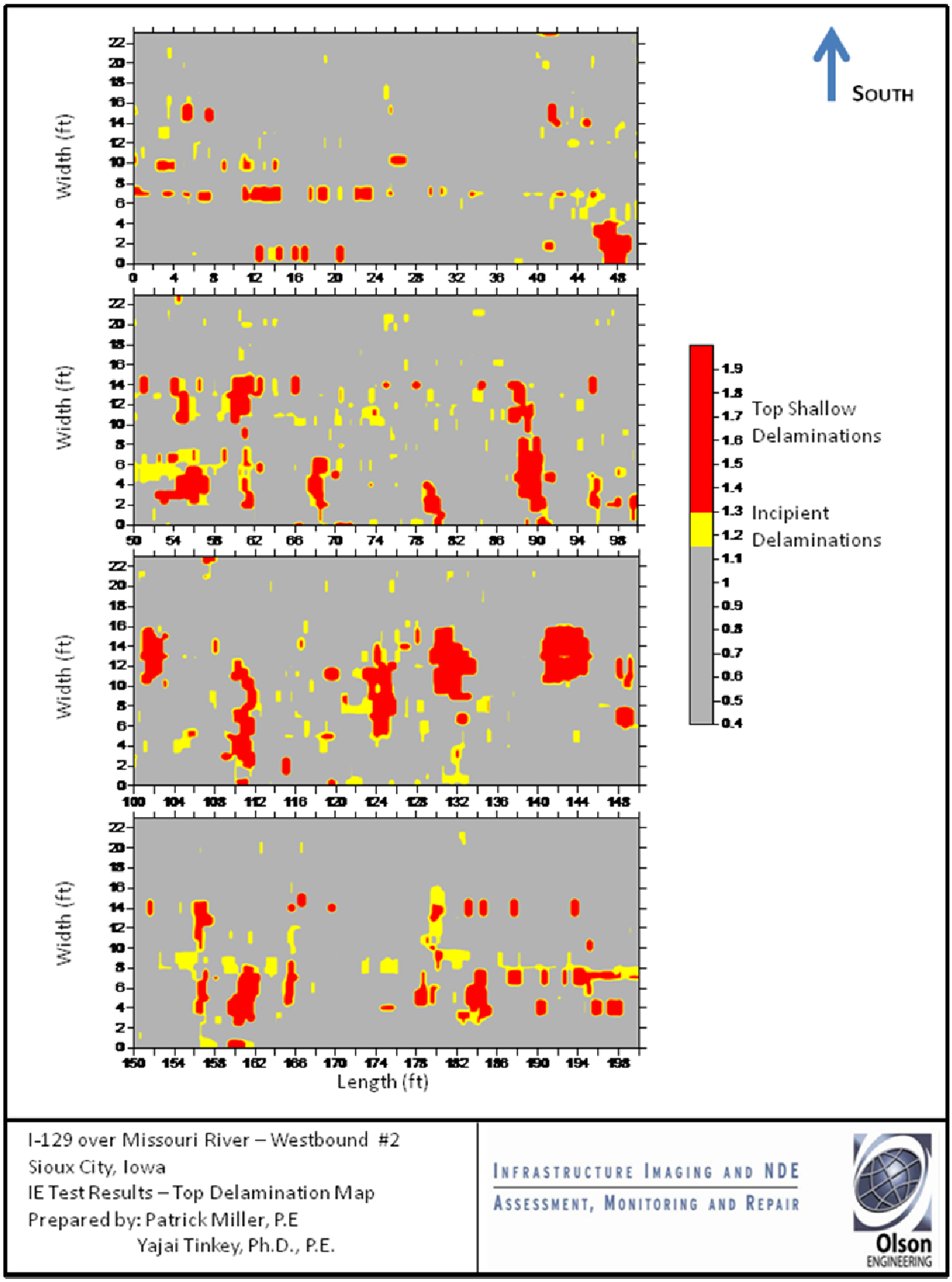

Figure B5 – Top Delamination Maps for Westbound #2

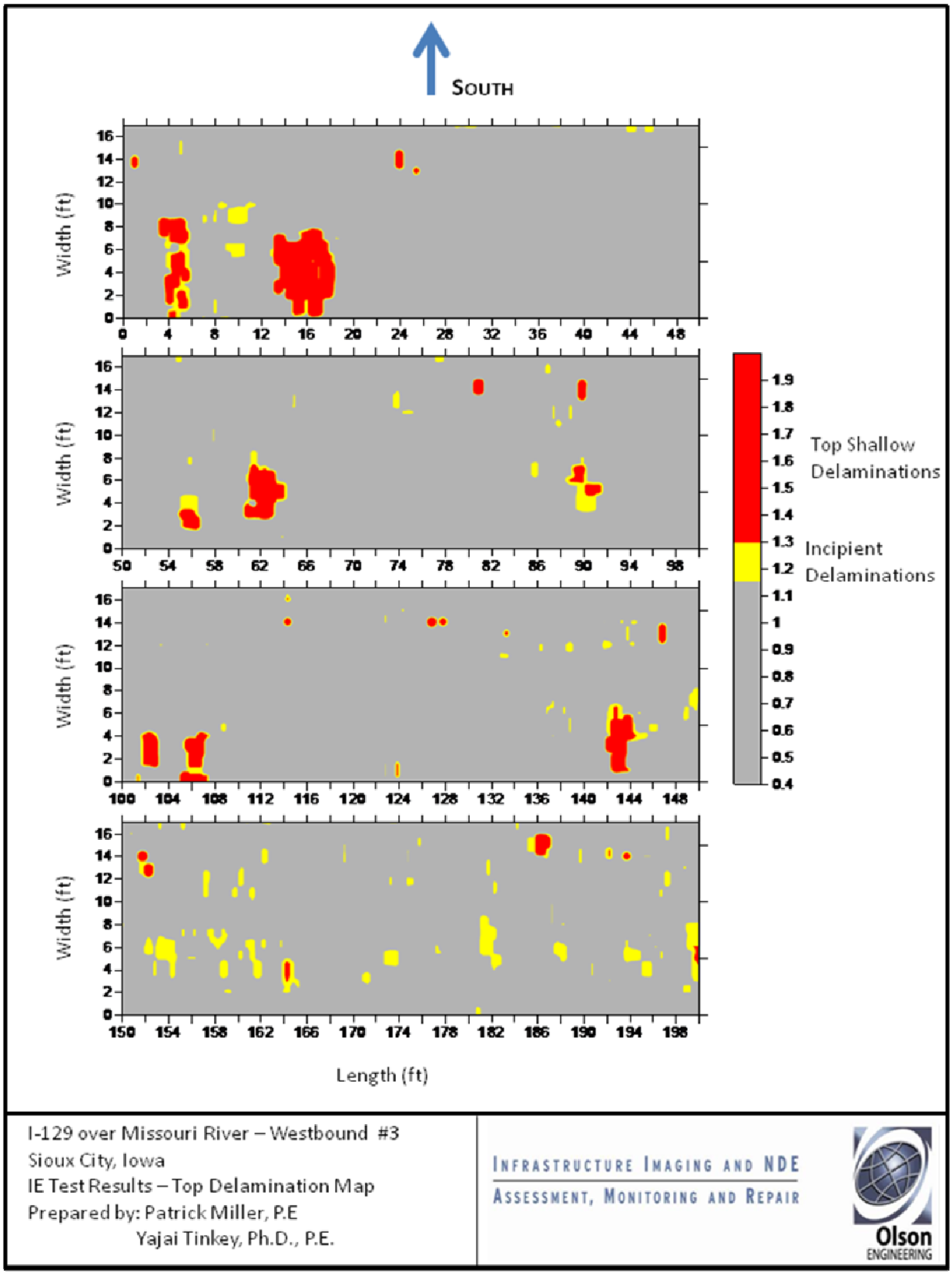

Figure B6 – Top Delamination Maps for Westbound #3

APPENDIX C: BDS-IE DECK CONDITION IMAGES FOR POSSIBLE BOTTOM DELAMINATION/INTERNAL CRACKING

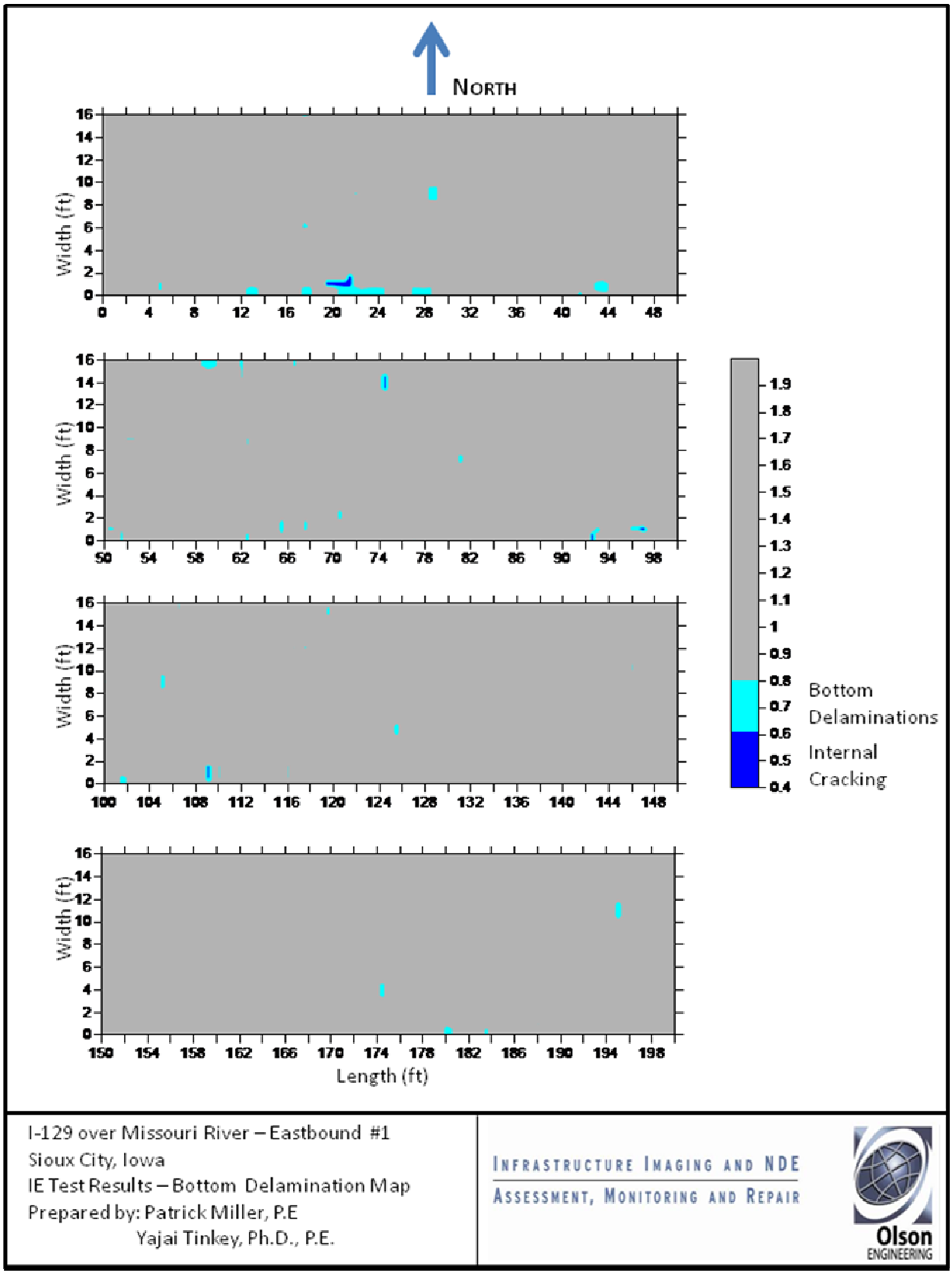

Figure C1 – Bottom Delamination Maps for Eastbound #1

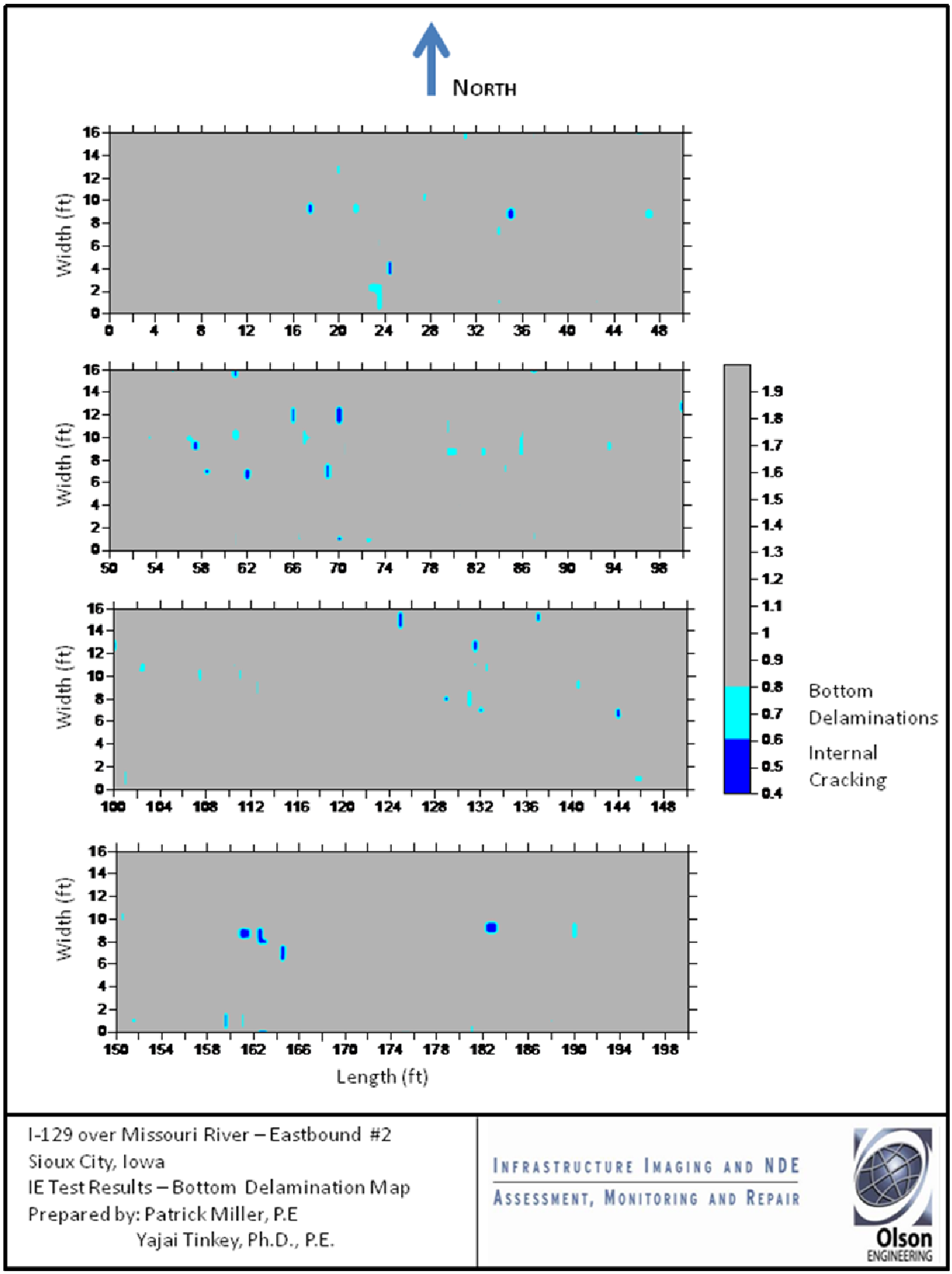

Figure C2 – Bottom Delamination Maps for Eastbound #2

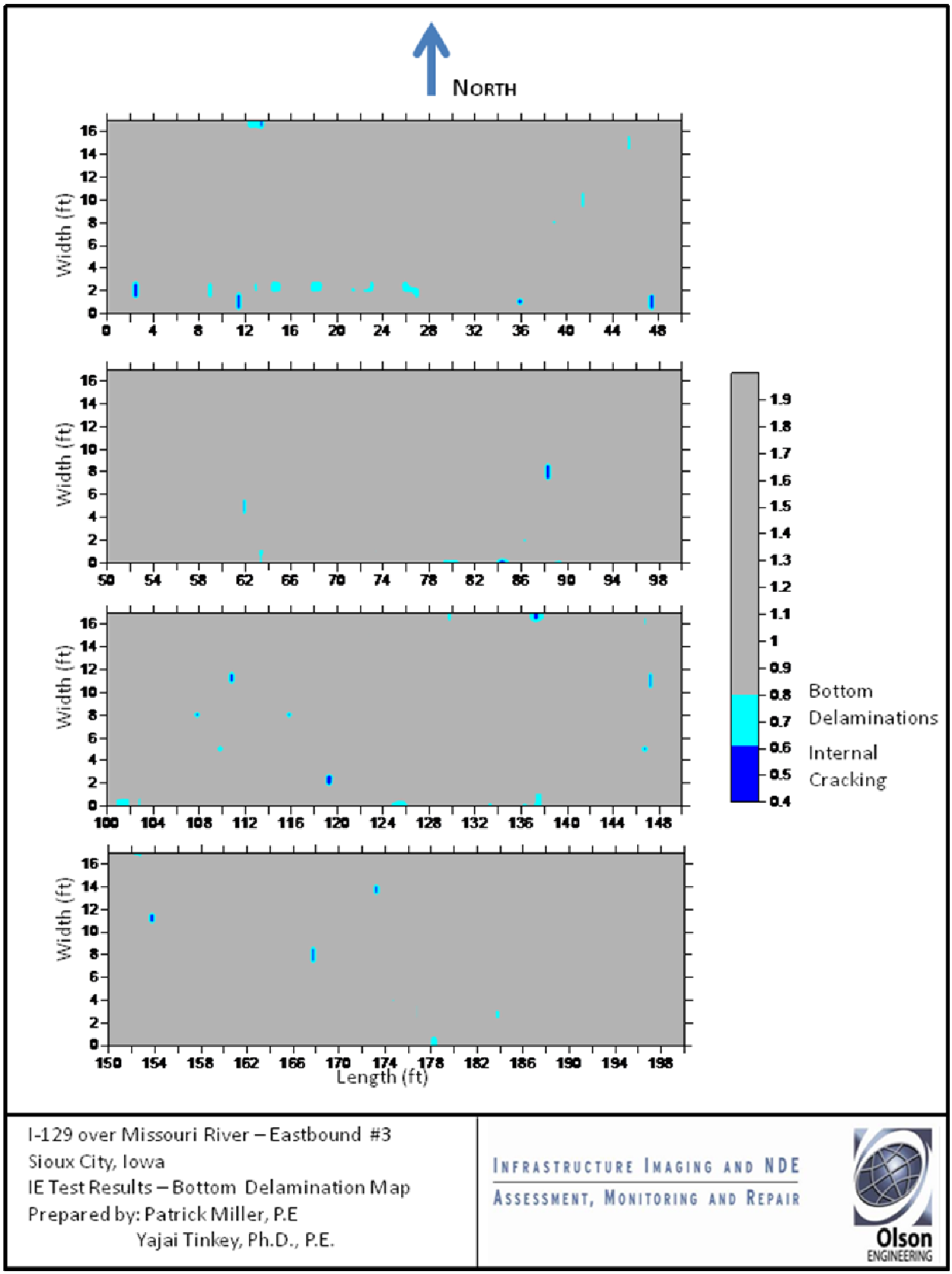

Figure C3 – Bottom Delamination Maps for Eastbound #3

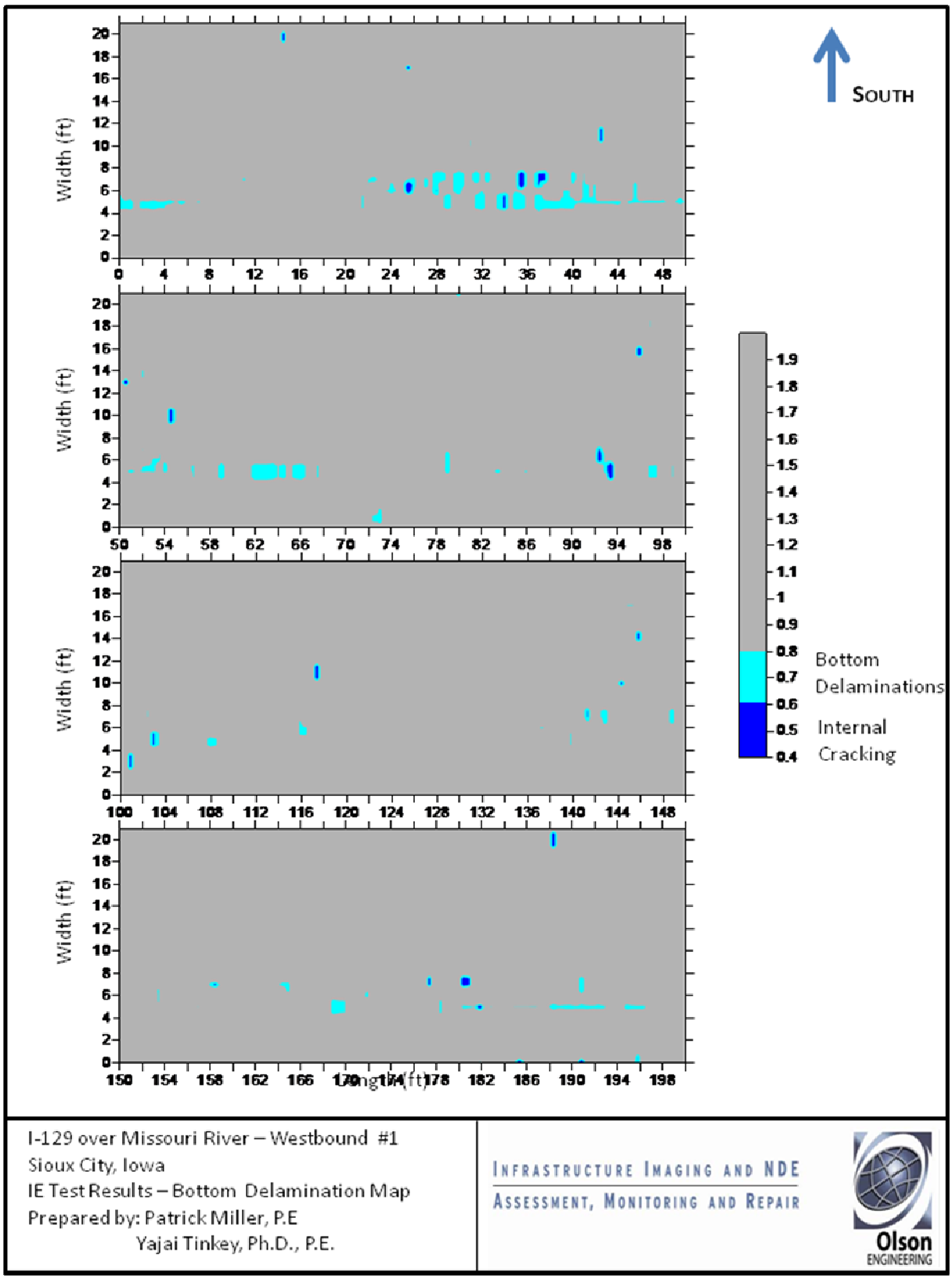

Figure C4 – Bottom Delamination Maps for Westbound #1

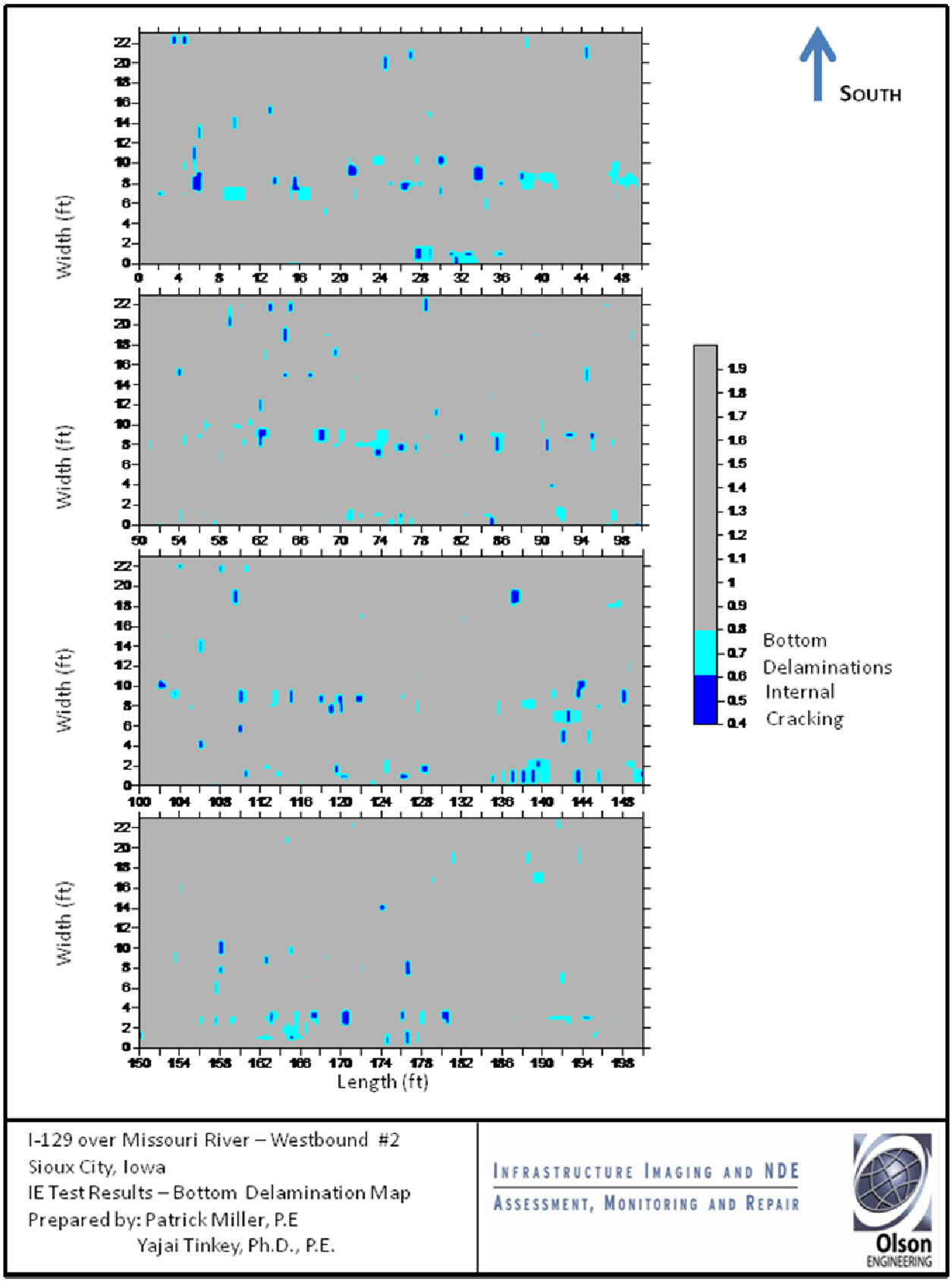

Figure C5 – Bottom Delamination Maps for Westbound #2

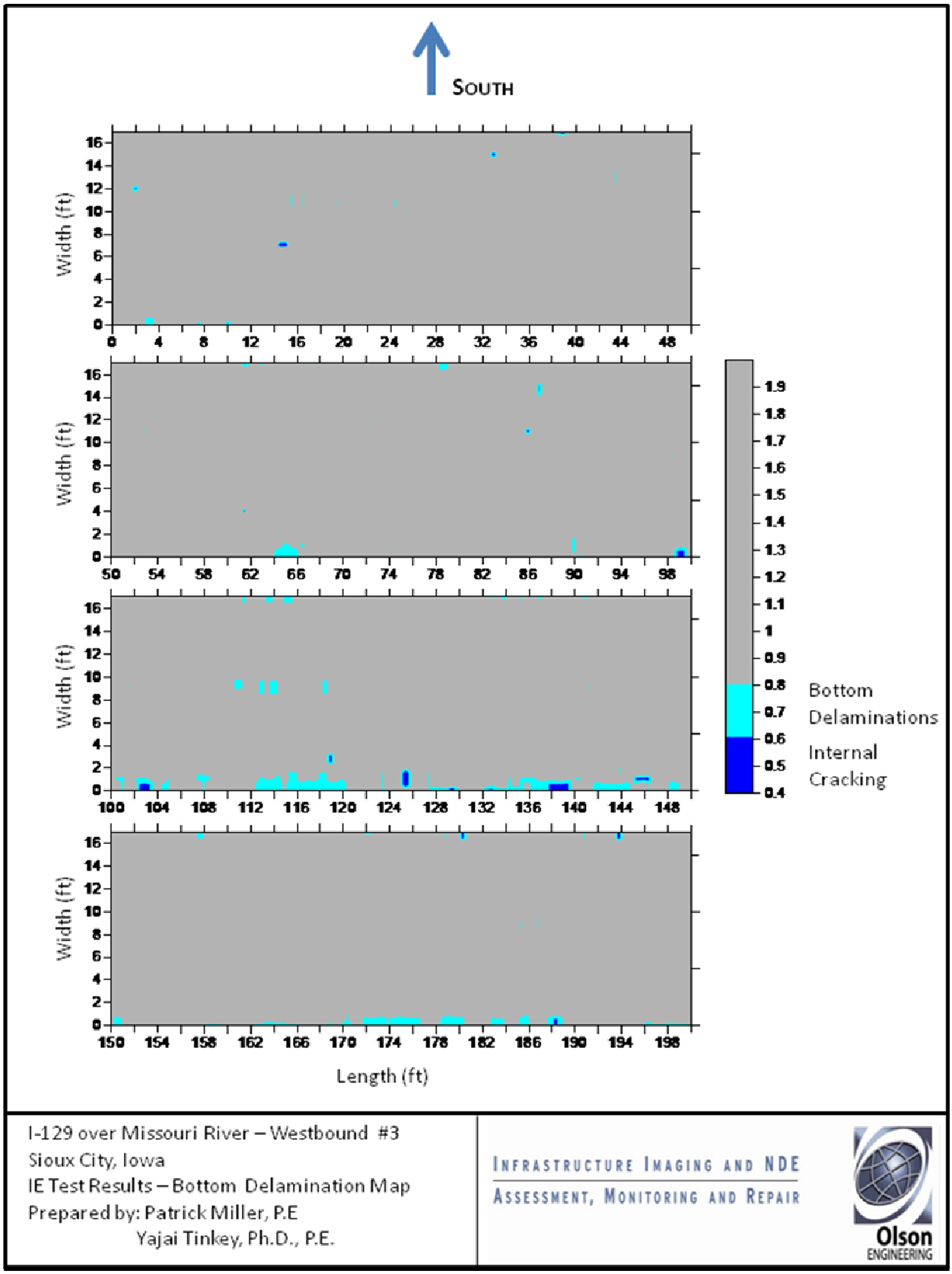

Figure C6 – Bottom Delamination Maps for Westbound #3

Appendix I

Finite Difference Solution for Diffusion in Two-Layer System

WJE	Wiss, Janney, Elstner Associates, Inc. 330 Pfingsten Rd., Northbrook, Illinois 60062	MADE BY JCK	SHEET NUMBER
Iowa I-129 Chloride Diffusion Transport Model		CHECKED BY JSL	PROJECT NUMBER 2010.2389
		DATE 2011.09.08	

Purpose

Model chloride transport through a two-layer system based on diffusion alone

Basis

Diffusion transport (Fick's 2nd law)

$$\frac{d}{dt}U = \frac{d^2}{dX^2}C$$

References

- Microstructural Development and Sulfate Attack Modeling in DBlended Cement-Based Materials (2000)
  R. Tixier, Ph.D. thesis, Arizona State University
- Numerical Methods for Engineers, 4th ed. (2002)
  Chapra, S. C., and Canale, R. P.

Model definition

Crank-Nicholson Discretization of equation above:

$$D\cdot\left[V_{i+1} - 2\cdot(D+K)\cdot V_i\right] + D\cdot V_{i-1} = -D\cdot U_{i+1} + (2\cdot D - 2\cdot K)\cdot U_i - D\cdot U_{i-1}$$

where:

i = current slice
D = apparent diffusion coefficient
U = concentration at timestep j
V = concentration at timestep j+1

$$K = \frac{(\Delta X)^2}{\Delta T}$$

The 2-layer system can be split into five different equations:

1. 1st slice below surface of 1st layer (i = 1)
2. 1st layer (i = 2 to i = S-1)
3. transition between layers (i = S)
4. 2nd layer (i = S+1 to N-1)
5. final slice in 2nd layer (i = N)

where:

S = slice located at transition between layers
N = last layer in slice

Define equations for each condition

1. For i = 1 (first layer, first slice below the surface boundary condition: fixed concentration above.)

Define variables:

$D = D_1$ diffusion coefficient for first layer

$U_{i-1} = U_0 = C_{s_j}$

$V_{i-1} = V_0 = C_{s_{j+1}}$

concentration above first layer is equal to surface concentration Cs at time = j or j+1

Substitute variables into discretized equation:

$$D_1 \cdot V_2 - 2 \cdot (D_1 + K) \cdot V_1 + D_1 \cdot C_{s_{j+1}} = -D_1 \cdot U_2 + 2(D_1 - K) \cdot U_1 - D_1 \cdot C_{s_j}$$

2. For i = 2 to i = S-1 (1st layer, no boundary conditions)

Define variables:

$D = D_1$ diffusion coefficient for first layer

Substitute variables into discretized equation:

$$D_1 \cdot V_{i+1} - 2 \cdot (D_1 + K) \cdot V_i + D_1 \cdot V_{i-1} = -D_1 \cdot U_{i+1} + (2 \cdot D_1 - 2 \cdot K) \cdot U_i - D_1 \cdot U_{i-1}$$

3. For i = S (slice at layer transition)

New definition of Crank-Nicholson discretization, based on Tixier (p. 196)

$$D_2 \cdot V_{i+1} - (D_1 + D_2 + 2K) \cdot V_i + D_1 \cdot V_{i-1} = -D_2 \cdot U_{i+1} + (D_1 + D_2 - 2 \cdot K) \cdot U_i - D_1 \cdot U_{i-1}$$

4. For i = S+1 to i = N-1 (2nd layer, no boundary conditions)

Defined variables:

$D = D_2$ diffusion coefficient for first layer

$$D_2 \cdot V_{i+1} - 2 \cdot (D_2 + K) \cdot V_i + D_2 \cdot V_{i-1} = -D_2 \cdot U_{i+1} + (2 \cdot D_2 - 2 \cdot K) \cdot U_i - D_2 \cdot U_{i-1}$$

5. For i = N (2nd layer, boundary condition: derivative of concentration = 0)

Discretize the derivative on the boundary and set it equal to zero:

$$\frac{d}{dX} U = \frac{U_{N-1} - U_{N+1}}{4 \cdot \Delta X} = 0$$

rearrange: $U_{N+1} = U_{N-1}$

similarly: $V_{N+1} = V_{N-1}$

Substiute variables into basic Crank-Nicholson discretization:

$$D_2 \cdot V_{N-1} - 2 \cdot (D_2 + K) \cdot V_N + D_2 \cdot V_{N-1} = -D_2 \cdot U_{N-1} + (2 \cdot D_2 - 2 \cdot K) \cdot U_N - D_2 \cdot U_{N-1}$$

Collect equations and rearrange into tri-diagonal matrix format:

$$-2\cdot\left(D_1+K\right)\cdot V_1 + D_1\cdot V_2 = 2\left(D_1-K\right)\cdot U_1 - D_1\cdot U_2 - D_1\cdot C_{s_j} - D_1\cdot C_{s_{j+1}}$$

$$D_1\cdot V_1 - 2\cdot\left(D_1+K\right)\cdot V_2 + D_1\cdot V_3 = -D_1\cdot U_1 + 2\left(D_1-K\right)\cdot U_2 - D_1\cdot U_3$$

$$D_1\cdot V_2 - \left(D_1+D_2+2K\right)\cdot V_3 + D_2\cdot V_4 = -D_1\cdot U_2 + \left(D_1+D_2-2\cdot K\right)\cdot U_3 - D_2\cdot U_4$$

$$D_2\cdot V_3 - 2\cdot\left(D_2+K\right)\cdot V_4 + D_2\cdot V_5 = -D_2\cdot U_3 + 2\left(D_2-K\right)\cdot U_4 - D_2\cdot U_5$$

$$2D_2\cdot V_4 - 2\cdot\left(D_2+K\right)\cdot V_5 = -2D_2\cdot U_4 + 2\left(D_2-K\right)\cdot U_5$$

Matrix Format

$$A\cdot V = B\cdot U + d$$

To solve equations:

$$V = A^{-1}\cdot(B\cdot U + d)$$

$$A = \begin{bmatrix} -2\cdot\left(D_1+K\right) & D_1 & 0 & 0 & 0 \\ D_1 & -2\cdot\left(D_1+K\right) & D_1 & 0 & 0 \\ 0 & D_1 & -\left(D_1+D_2+2K\right) & D_2 & 0 \\ 0 & 0 & D_2 & -2\cdot\left(D_2+K\right) & D_2 \\ 0 & 0 & 0 & 2\cdot D_2 & -2\cdot\left(D_2+K\right) \end{bmatrix}$$

$$B = \begin{bmatrix} 2\left(D_1-K\right) & -D_1 & 0 & 0 & 0 \\ -D_1 & 2\left(D_1-K\right) & -D_1 & 0 & 0 \\ 0 & -D_1 & \left(D_1+D_2+2K\right) & -D_2 & 0 \\ 0 & 0 & -D_2 & 2\left(D_2-K\right) & -D_2 \\ 0 & 0 & 0 & -2\cdot D_2 & 2\left(D_2-K\right) \end{bmatrix}$$

$$V = \begin{pmatrix} V_1 \\ V_2 \\ V_3 \\ V_4 \\ V_5 \end{pmatrix} \qquad U = \begin{pmatrix} U_1 \\ U_2 \\ U_3 \\ U_4 \\ U_5 \end{pmatrix}$$

i = 0, surface

i = 1 1st layer and boundary condition

i = 2 to i = S-1, 1st layer

i = S, transition

i = S+1 to i = N-1, 2nd layer

i = N, 2nd layer and boundary condition

$$d = \begin{bmatrix} -D_1\cdot\left(C_{s_j} + C_{s_{j+1}}\right) \\ 0 \\ 0 \\ 0 \\ 0 \end{bmatrix}$$